Dissecting the Molecular Mechanisms of *Drosophila* Border Cell Migration using Time-lapse Cell Imaging

Thesis submitted in accordance to the requirements of the University of Liverpool for the degree of Doctor in Philosophy

by

Lauren Michelle Dodgson

October 2013

Declaration

This thesis is a result of my own work unless stated otherwise. Results are based upon experimental and theoretical work performed as a PhD student between October 2009 and October 2013 within the Institute of Integrative Biology at the University of Liverpool. Neither this thesis nor any part of it has been submitted in support of an application for another degree or qualification at this or any other University or Institute of Learning.

Lauren Dodgson

October 2013

Abstract

Dissection of the cellular dynamics and molecular pathways that drive collective cell migration is necessary to better understand cellular rearrangements that underpin normal development, as well as disease states such as cancer metastasis. Border cell migration in the *Drosophila* ovary has proven to be a good model of invasive cell migration, because of its genetic tractability, and also because recent advances in culturing egg chambers *ex vivo* have facilitated live cell imaging in this system. The aim of this thesis was to further develop and implement live cell imaging approaches, and to apply these to characterise the role of Pico, the *Drosophila* Mig10/RIAM/Lpd (MRL) protein in border cell migration. MRL proteins are known to regulate actin dynamics, but their role in epithelial cell migration had not been established. Through careful optimisation, suitable approaches were developed for: medium preparation; dissection and mounting of egg chambers; acquisition of images by confocal microscopy. A fluorescently-labelled reporter strain with improved optical properties was generated to monitor actin dynamics, and a number of other reporters were characterised, either alone or in combination, to determine their behaviour and effect on migration. After trialling several analytical tools and quantitative methods, a streamlined approach to analysing the image data was developed allowing: tracking of border cell migration in four dimensions (XYZ and time) to obtain information about behaviour of the migratory cells; measurement of cellular protrusion dynamics to obtain mechanistic insight into why cellular dynamics might change in different genetic backgrounds. Finally, these approaches were applied to the characterisation of Pico and its interacting partner SCAR, demonstrating that *pico* affects border cell migration through the modulation of actin protrusion dynamics in a *SCAR*-dependent manner.

Table Of Contents

List of Figures

List of Tables

Abbreviations

2D	Two Dimensions
3D	Three Dimensions
Abi	Abl Interactor
Abl	Abelson tyrosine kinase
ADF	Actin Depolymerising Factor
ACF	As the Crow Flies
Arp	Actin-Related Proteins
bcp	Border Cell Position
CFP	Cyan fluorescent protein
DIA	Diaphanous
EcR	Ecdysone Receptor
EGF	Epidermal growth factor
eGFP	Enchanced Green fluorescent protein
EGFR	Epidermal growth factor receptor
en	Engrailed
Ena	Enabled
eYFP	Enchanced Yellow Fluorescent Protein
FA	Focal Adhesions
F-actin	Filamentous Actin
FBS	Fetal Bovine Serum
FCS	Fetal Calf Serum
FM4-64	N-(3-triethylammoniumpropyl)-4- (p-diethylaminophenyl-hexatrienyl) pyridinium dibromide
FRT	FLP recombinase target
G-Actin	Monomeric Actin
GAP	GTPase-Activating Protein
GFP	Green Fluorescent Protein
HCL	Hydrochloric Acid
JAK	Janus Kinase
JNK	Jun N-terminal Kinase
Lpd	Lamellipodin
LSFM	Light sheet fluorescence microscopy
LSM	Laser Scanning Microscope
Mig-10	Abnormal cell migration protein 10
MRL	Mig-10/RIAM/Lamellipodin
msn	Misshapen
mTFP	Monomeric Teal flourescent protein
NLS	Nuclear Localisation Sequence
OE	Over-expression
PAR	Partitioning defective
PBS	Phosphate Buffered Saline
PBS-T	Phosphate Buffered Saline - Tween 20
PDGF	Platelet-derived growth factor
PDGFR	Platelet-derived growth factor receptor 1

Pen/Strep	Penicillin/Streptomycin
PH	Pleckstin homology
PI	Phosphoinositide
PI3K	Phosphoinositide 3-kinase
Pvf1	Platelet derived growth factor (PDGF) and Vascular endothelial growth factor (VEGF) related factor 1
PVR	PDGF/VEGF receptor related
RA	Ras-association
RFP	Red fluorescent protein
RIAM	Rap1-GTP-interacting adapter molecule
RNAi	RNA interference
S2R+	S2 receptor +
S9	Stage 9
S10	Stage 10
SCAR	Suppressor of cAMP Receptor
slbo	slow border cell
SRE	Serum response element
SRF	Serum response factor
STAT	Signal transducer and activator of transcription
TAI	Taiman
TCF	Ternary complex factor
UAS	Upstream activating sequence
USP	Ultraspiricle
VASP	Vasodilator-stimulated phosphoprotein
VEGF	Vascular endothelial growth factor
WASP	Wiskott-Aldrich syndrome protein
WAVE	WASP family Verprolin-homologous protein
WRC	WAVE regulatory complex
WT	Wild type

1. General Introduction

1.1. Cell Migration

Cell migration provides a crucial role in many fundamental processes including embryonic growth and development, in the immune response and in wound healing, as well as in many others (Webb et al., 2005; Yilmaz and Christofori, 2010). Cell migration can also be involved in aberrant events including cancer metastasis and other diseases (Alberts *et al*, 2002). Whether migration is part of normal development or a capability that is acquired during disease development, a cell's ability to migrate is dependent on the local polymerisation of actin filaments in the plasma membrane, driving protrusions that propel the leading edge forward. In a choreographed manner, the cell adheres to the migration substrate at the leading edge with specific adhesion proteins, contractile elements retract the trailing end following adhesion release and the cell essentially crawls forwards (Lauffenburger and Horwitz, 1996; Mattila and Lappalainen, 2008). In events such as cancer, a cell's ability to metastasize depends on its ability to detach from the primary tumour, migrate and invade surrounding tissue (Bacac and Stamenkovic, 2008). This invasive cell migration requires changes in cell-cell and also cell-matrix adhesion, resulting in altered cell signalling and further changes in cell functioning, progressing to a secondary tumour site (Hanahan and Weinberg, 2000).

1.2. Mechanisms of Cellular Migration

Much is known about migration in single cells, with many experiments being performed *in vitro* using cultured cells migrating along a solid surface, or through an artificial matrix, that has been designed to resemble a cell's natural surroundings. Cell migration is driven by

reorganisation of the actin cytoskeleton framework, which involves cell polarization and formation of actin-based protrusions at the front of the cell, coupled with retraction at the rear of the cell illustrated in Figure 1.1 below (Bacac and Stamenkovic, 2008).

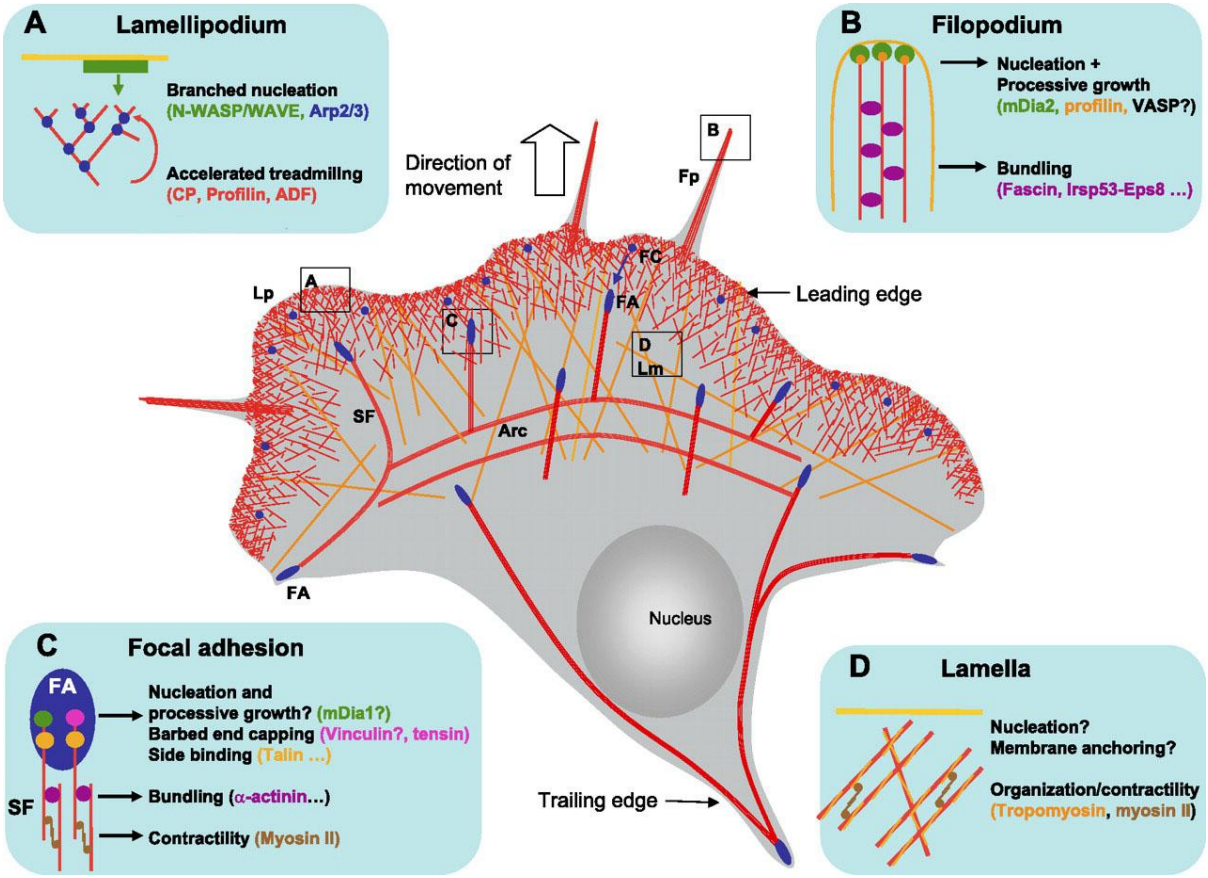

Figure 1.1 Schematic illustration of cellular migration. Actin assembly at the newly created cell front drives lamellipodia formation. Adhesions form at the leading edge to connect the extracellular matrix to the actin cytoskeleton enabling further extension of the protrusions. Finger-like filopodia protrusions extend beyond the leading edge of the lamellipodia to sense the environment. Finally, the cell combines actomyosin contractility and rear adhesion disassembly to retract its trailing edge. Figure taken from (Le Clainche and Carlier, 2008) and edited slightly.

Lamellipodia (flat, branched membrane protrusions) and filopodia (thin actin-rich plasma membrane protrusions) are essential for cell mobility (Mattila and Lappalainen, 2008; Small

et al., 2002). Following protrusion at the leading edge, the cell forms focal adhesions (FA) via extracellular adhesion receptors, which connect to the extracellular matrix; and link the substrate to the cytoskeleton. These act as an anchor, cementing the attachment of the leading edge of the cell and preventing its retraction. At the trailing (rear) end of the cell disassembly of actin bundles, loss of adhesion molecules and the contraction of the cytoskeleton de-adheres the cell from the substrate. Finally, the cell is pulled forwards due to contractile forces produced by myosin motors (Kaiser et al., 1999; Le Clainche and Carlier, 2008).

1.2.1. Actin Treadmilling and Protrusion Formation

Cellular actin exists as G-actin (monomeric) or F-actin (filamentous), with the majority of G-actin bound to proteins such as profilin. Newly polarised cells polymerize actin filaments at the barbed end through ATP hydrolysis and depolymerise at the pointed end at a similar rate (Lauffenburger and Horwitz, 1996; Theriot and Mitchison, 1991).

This instigates a 'treadmilling' mechanism, enabling the filaments to move forwards whilst maintaining the same length. This mechanism is influenced by several actin regulatory proteins such as ADF (cofillin), profillin and various capping proteins (Wang, 1985). The filaments push against the cellular membrane to form protrusions, resulting in the extension of the front of the cell in the direction of migration (Small et al., 2002).

ADF (Actin Depolymerising Factor) is located throughout lamellipodium (with the exception of the leading edge) and binds to ADP-actin filaments to induce pointed end depolymerisation , increasing the steady state levels of G-actin available. This promotes faster barbed end growth to compensate for the increased rate of pointed end depolymerisation (Carlier and Pantaloni, 1997; Svitkina and Borisy, 1999). Profilin enhances

the action of ADF by binding to G-actin and increasing the exchange rate of ADP to ATP (Yarmola and Bubb, 2006). Capping proteins facilitate the rapid growth of filaments by amplifying polymerisation, through the blocking of actin filaments at the barbed end and limiting their length. This therefore funnels actin monomers to the non-capped filament ends, resulting in quicker growth (Pantaloni et al., 2001; Wiesner et al., 2003).

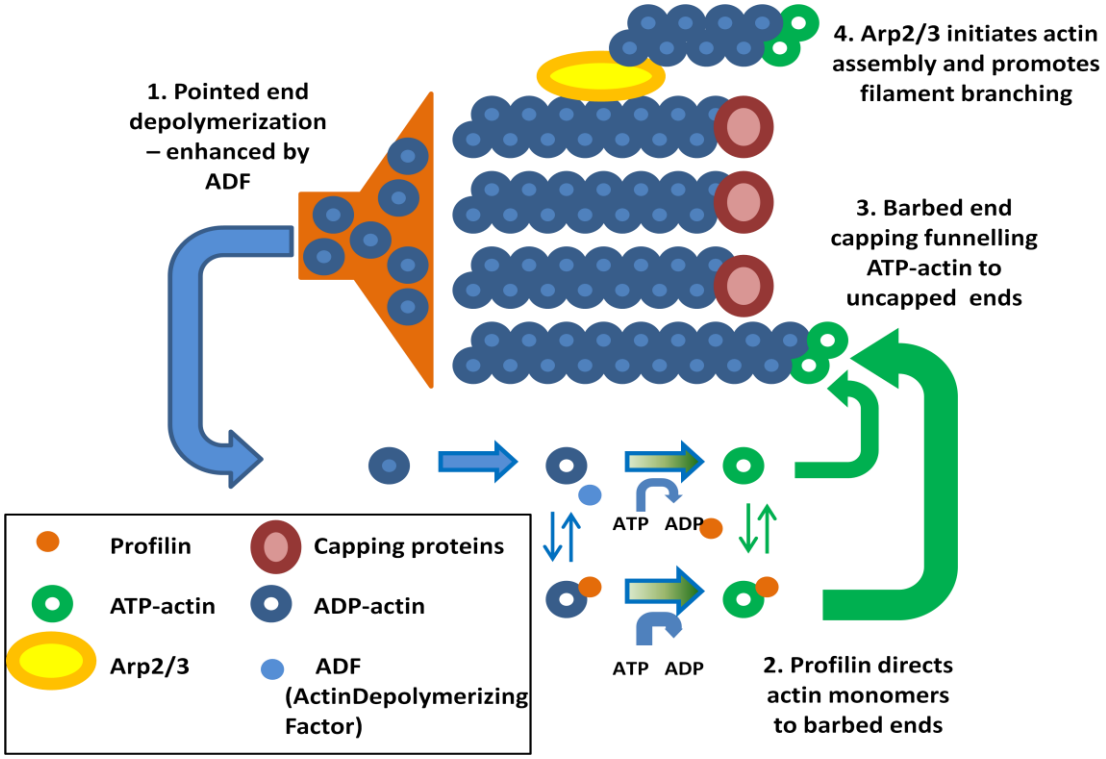

Figure 1.2. Regulation of actin treadmilling. Image adapted from (Le Clainche and Carlier, 2008) **(1)** ADF enhances pointed end depolymerisation, increasing the concentration of monomeric actin. **(2)** Profilin increases the rate of exchange of ATP for ADP. **(3)** Capping proteins funnel ATP-actin to uncapped barbed ends. **(4)** Arp2/3 promotes filament branching.

Changes in actin dynamics are driven by a whole host of cytoskeletal regulatory proteins. The Ena/VASP (Enabled/ Vasodilator-stimulated phosphoprotein) family of proteins are important regulators of the cytoskeleton and are recruited to sites of actin remodelling during cell adhesion, polarisation and migration (Ananthakrishnan and Ehrlicher, 2007). This

recruitment allows the Ena/VASP proteins to alter local actin dynamics through their interactions with profilin and actin and also through proteins that bind to their proline-rich protein interacting domain, EVH1. Ena/VASP proteins are recruited to the tips of lamellipodia; driven by actin assembly through polymerisation and play a role in preventing the capping of actin filaments. This action promotes the formation of longer, less branched filaments, which may influence the motile behaviour of migratory cells (Bear et al., 2002; Krause et al., 2004; Le Clainche and Carlier, 2008). The formation of branched actin filaments in lamellipodia formation involves assembly via the Arp2/3 complex, nucleating actin filaments which activates members of the WASP family (Wiskott-Aldrich syndrome protein) such as SCAR/WAVE (Suppressor of cAMP Receptor/WASP family Verprolin-homologous protein). The SCAR/WAVE complex is composed of five proteins (Sra1/Pir121, Nap1, Scar/WAVE1-3, Abi1-3, and HSPC300) and exists normally in an inactive conformation that cannot interact with the Arp2/3 complex. Activation is facilitated by interaction with Rac via Sra1/Pir121, by interaction with phospholipids at the leading edge and by phosphorylation of SCAR/WAVE (Campellone and Welch, 2010; Insall and Machesky, 2009). These proteins act as scaffolds to integrate signals from Ras GTPases to changes in actin polymerisation via Arp2/3 and assist in directionality of protrusion generation (Machesky and Cooper, 1999; Machesky and Insall, 1999; Suraneni et al., 2012). The generation of actin protrusions is directed by multiple signalling pathways, and is not a single linear relationship. Many signals and pathways cross to promote and inhibit filament elongation, each of the pathways are specific to the cell type and location and are susceptible to different guanine nucleotide exchange factors (GEFs). In addition to proteins playing a role in modifying actin structures, controlling monomer turnover and actin dynamics, lipids and other membrane based proteins have been found to play a role in protrusion elongation.

Regulating the Treadmilling Force

Cells control migration through the modulation of actin treadmilling, involving mechanical coupling between the actin cytoskeleton and the extracellular matrix. In addition to regulating the rate of actin treadmilling, cells control migration by modulating the extent of mechanical coupling between the actin cytoskeleton and the extracellular matrix. These cell matrix adhesions act as a 'molecular clutch', which when engaged, provide traction to the polymerising actin network. This force generated through treadmilling enables protrusion formation at the leading edge (Figure 1.3). When the clutch is disengaged, traction is lost and slippage occurs between the polymerising actin filaments and the extracellular matrix adhesions, resulting in retrograde flow and a decrease in protrusion rate (Hu et al., 2007; Macdonald et al., 2008). The clutch also controls the transmission of the actomyosin contractile force applied on focal adhesions which facilitates traction of the cell body and retraction of the rear (Webb et al., 2002).

Engagement of the molecular clutch is controlled through a variety of molecular interactions at different levels. One key interaction is through integrins, a large family of finely regulated heterodimeric transmembrane adhesion receptors, that connect the cell to the extracellular matrix (Humphries et al., 2006). A variety of actin binding proteins, such as talin, vinculin and α-actinin, interact either directly or indirectly with the cytoplasmic tails of the integrins to 'engage the clutch' and enable traction with the extracellular matrix (Vicente-Manzanares and Horwitz, 2011a, b).

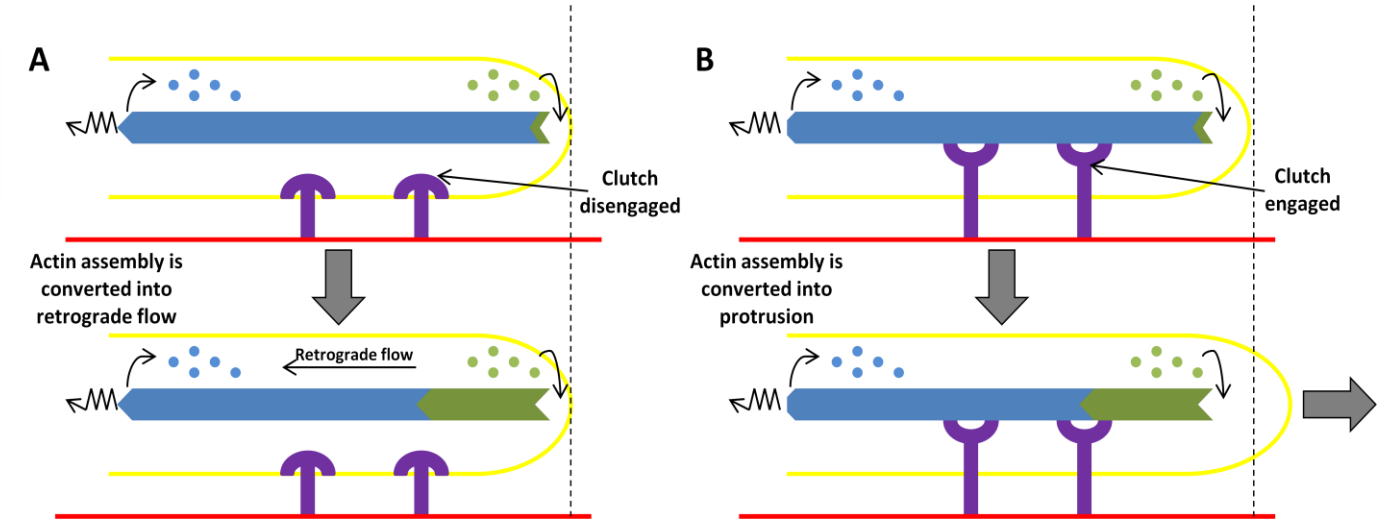

Figure 1.3. Regulating the treadmilling force. Image adapted from Le Claince and Carlier., 2008. Adhesion acts as a "molecular clutch" to convert the force generated by actin assembly into a protrusion. In this figure, the actin network is represented in blue, while newly polymerized actin is represented in green. **(A)** The molecular clutch is disengaged reducing traction between focal adhesions and the actin cytoskeleton preventing protrusion formation as actin treadmilling force is predominantly converted into retrograde flow. **(B)** The molecular clutch is engaged enabling traction between the polymerizing actin network and the substrate resulting in membrane protrusion. (Le Clainche and Carlier, 2008).

1.3. Modelling Cell Migration *in vivo*

While examining migration in cell culture has proven to be experimentally tractable, mimicking complex *in vivo* environments *in vitro* has proven to be more difficult. Therefore, there is a need to develop protocols to examine and explore the behaviour of motile cells *in vivo* to elucidate the endogenous mechanisms underpinning motile cell behaviours.

A cell's surroundings are usually part of a three-dimensional (3D) network and migration occurs in between or across other cells, not just a two dimensional (2D) matrix. In addition to cell-type specific regulation of lamellipodia and filopodia, migration in a 3D matrix also requires the control of non-actin based protrusions such as 'blebs' and pseudpods, which

play a key role in enabling cells to squeeze through small gaps in their surroundings (Wolf and Friedl, 2006).

In addition to migrating as single cells, groups of cells have the ability to migrate as a cohesive cluster in a mechanism known as collective cell migration. Collective cell migration requires cell-cell and cell-matrix dynamics to be controlled and coordinated for effective migration to occur (Rorth, 2012). The *Drosophila* border cell migration model is a good example of coordinated collective cell migration, in which its normal behaviour has been well characterised in fixed tissues and, more recently using live cell time-lapse imaging.

1.4. Border Cell Migration

Border cell migration is a part of normal cellular development of the *Drosophila* egg chamber. A *Drosophila* ovary consists of approximately 20 strands of egg chambers known as ovarioles, each containing a string of egg chambers at various stages of development, the most mature at the posterior end. Each egg chamber is derived from 16 germ line cells, one of these cells differentiates to form the oocyte at the posterior end; the other 15 form the polyploid nurse cells surrounded by an epithelial layer of somatic follicle cells. At the anterior and posterior ends of the egg chamber are specialised non-motile polar cells. During development the follicle cells rearrange and form a flat sheet over the nurse cells. During this rearrangement the anterior polar cells recruit 6-10 neighbouring follicle cells (rosette cells), which form the border cell cluster. At the beginning of stage 9, the border cell cluster delaminates from the follicle cells and migrates down the centre of the egg chamber, between the nurse cells, to the anterior oocyte border (nurse cell-oocyte boundary) shown in Figure 1.1 (Montell, 2003). Once the cluster reaches the oocyte it forms

a structure called the micropyle, which is an essential structure, since it allows sperm entry to fertilise the egg (Montell, 2003).

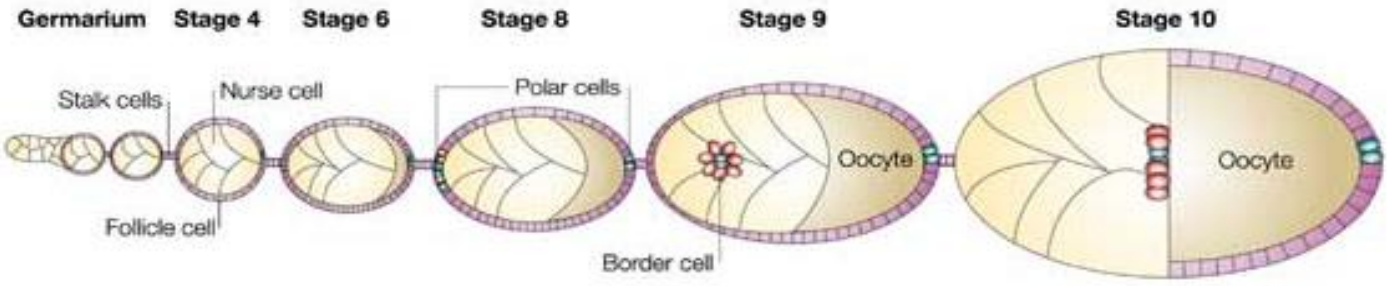

Figure 1.4. Image taken from Montell 2003, showing a string of *Drosophila* egg chambers at various stages in development. The egg chamber consists of 16 differentiated germline cells, the oocyte and 15 nurse cells surrounded by follicle cells. At stage 8 the polar cells are differentiated and during the late stage the anterior polar cell recruits 6-10 neighbouring follicle cells which form the border cell cluster. At stage 9 the BC cluster delaminates from the surrounding epithelium, invades the germ layer and migrates towards the oocyte, eventually reaching the nurse cell-oocyte boundary at stage 10. (Montell, 2003).

This migration is guided by the expression of specific chemotactic ligands and growth factors. Growth factors have been shown to be chemotactic factors in cancer cells, increasing invasion and metastasis (Naora and Montell, 2005; Xue et al., 2006).

Furthermore, border cell migration has also been shown to be controlled by genes and signalling pathways in which mammalian homologues have been found to promote ovarian cancer progression (Yoshida et al., 2004) so the analysis of border cell migration enables genes to be identified that are involved in ovarian cancer metastasis (Yoshida et al., 2005).

Drosophila is a tractable *in vivo* system in which to study the regulation of these migratory mechanisms, as there are numerous tools and resources which makes it easy to perturb gene function (Jang *et al*, 2007). For instance, heritable RNAi and the availability of complete

genome sequencing enables gene function to be determined using reverse genetics (Dietzl et al., 2007). In *Drosophila*, tissue-specific RNA-mediated knockdown is mediated by expression of inverted repeat constructs capable of producing dsRNA hairpins using the GAL4 UAS system (Dietzl et al., 2007; Kuttenkeuler and Boutros, 2004). The GAL4 UAS system is a bipartite system that enables ectopic expression of target genes that can be directed by different tissues or cell types by the definition of the GAL4 driver. GAL4 was identified in yeast as a gene regulator, which binds to and activates an upstream activator sequence (UAS) (Brand and Perrimon, 1993; Klueg et al., 2002). This system can be used to investigate genes affecting border cell migration using two independent fly lines, one containing a silent target gene without an activator, and one containing a border cell specific activator with no target gene. Only in the progeny once the two lines are crossed are the effects of the target gene or the fluorescent reporter observed in the border cell cluster.

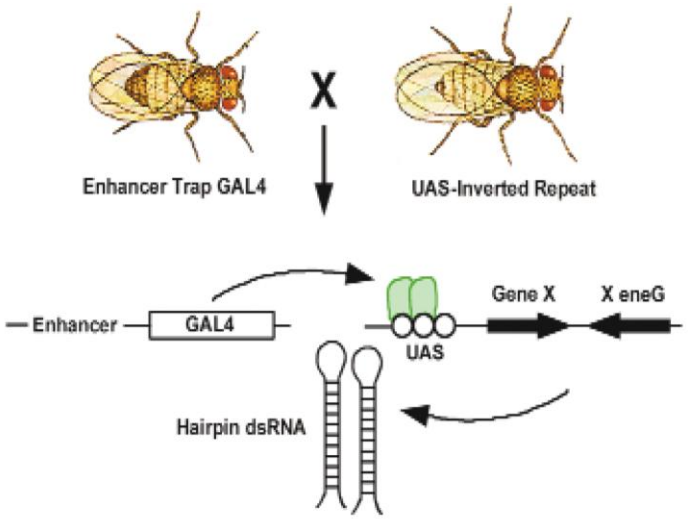

Figure 1.5. Gene knockout by RNAi *in vivo*, in a tissue specific manner. RNAi can be triggered by expression of long double-stranded hairpin RNA (dsRNA) from a stably inserted transgene containing a gene fragment cloned as an inverted repeat. When placed under control of the GAL4/UAS expression system, such RNAi transgenes can be used to target gene knockdown to specific cell types, such as the border cells.

1.5. Signalling pathways Controlling Border Cell Migration

Border cell specific expression can be targeted using *slbo* (slow border cells) a homologue of the C/EBP family of basic region-leucine zipper transcription factor (Montell et al., 1992). *slbo* is expressed in the follicle cells of the border cell cluster and the retracting centripetal cells, but not the polar cells. It has been shown to play a critical role in border cell migration, with mutants unable to migrate or generate protrusions (Rorth et al., 2000).

1.5.1. Specification

The border cell cluster consists of two distinct cell types, motile follicle cells and non-motile polar cells. Despite the presence of approximately 650 epithelial follicle cells, only 6-8 become specialised and form the motile cells of the border cell cluster. The specification of the cluster is the result of a multistep molecular pathway, initiated through the differentiated polar cells. The two anterior polar cells secrete the cytokine Unpaired (UPD), which binds to a transmembrane receptor Domeless, activates the tyrosine kinase JAK (Janus Kinase encoded by Hopscotch) and phosphorylates itself and the UPD receptor. STAT (Signal transducer and activator of transcription) then binds to JAK, becomes phosphorylated, dimerises and then translocates to the nucleus where it activates transcription of numerous downstream targets, including slbo and Apontic (Denef and Schupbach, 2003; Ghiglione et al., 2002; Silver and Montell, 2001). Apontic is a feedback inhibitor of STAT which carefully controls the level of STAT activity (Starz-Gaiano et al., 2008). JAK/STAT signalling components are essential for border cell migration, as mutants in any aspect of the pathway can result in failed migration. In addition to this, ectopic STAT activation can result in the migration of non motile cells and abrogation of STAT activity can stop migration part way (Silver et al., 2005; Silver and Montell, 2001). The 20 Ste-like kinase

Misshapen (encoded by *msn*) is also required for border cell migration and specification in a STAT and *slbo*-independent manner (Cobreros-Reguera et al., 2010). The number of cells in a border cell cluster is proportional to the percentage of clusters that reach the oocyte, and is controlled by STAT, therefore, the levels of STAT and the localisation of STAT activation needs to be tightly controlled. Exactly how STAT allows motile to non motile cells to be distinguished is unknown, however many genes required for border cell migration such as *shotgun* (E-cadherin) and *slbo* have been found to be expressed in cells with high levels of STAT activity (Borghese et al., 2006; Wang et al., 2006).

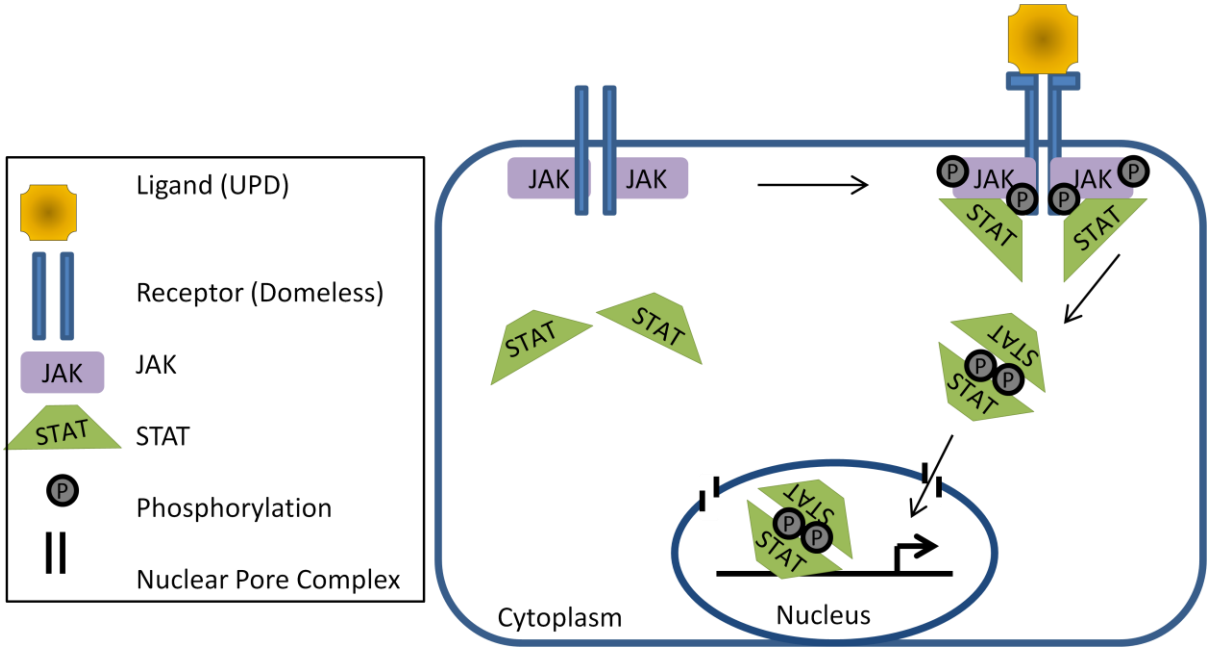

Figure 1.6 Image adapted from Arbouzova & Zeidler 2006 (Arbouzova and Zeidler, 2006). Showing the molecular pathway resulting in activation of STAT downstream targets and Border cell specification. The ligand UPD secreted by the anterior follicle cells binds to the transmembrane receptor Domeless, resulting in the phosphorylation of JAK and consequently STAT. STAT dimerises and translocates to the nucleus resulting in the transcription of border cell specific genes.

1.5.2. Timing

In addition to spatial signalling in the migratory group of cells, signals are required to determine when the cluster begins to migrate. This developmental timing cue has to cooperate with STAT signalling to ensure the cluster of cells is capable of migrating. The insect steroid hormone Ecdysone (the only steroid hormone in *Drosophila melanogaster*) initiates transcription of numerous genes required for border cell migration. Levels of Ecdysone rise in stages 8-10 (produced locally), and is required for the progression of development of the egg chamber through the various stages (Buszczak et al., 1999). The signalling pathway proceeds through the binding of a co-activator Taiman (TAI) to a heterodimer consisting of the Ecdysone receptor (EcR) and Ultraspiricle (USP), which binds to DNA (Yao et al., 1993; Yoshida et al., 2005). All three elements are necessary for migration to occur. In addition to STAT levels being higher in the anterior follicle cells and border cells, Ecdysone levels are also increased in these cells. Cooperation between the two signalling path ways is crucial and partially controlled by the zinc-finger domain-containing protein Abrupt. Abrupt attenuates Ecdysone signalling through binding to TAI localised in the nucleus. STAT activity excludes Abrupt from the nucleus during border cell migration thus antagonizing Abrupt activity and indirectly promoting the Ecdysone response (Jang et al., 2009). Mutants in target genes of both pathways controlled by Ecdysone and STAT have been shown to alter E-cadherin levels (Bai et al., 2000; Schober et al., 2005; Van Haastert and Devreotes, 2004), which plays a fundamental role in traction generation and cluster integrity (Niewiadomska et al., 1999), see also Section 1.2.1. This suggests there are convergent signalling pathways and cooperation between transcriptional regulators.

1.5.3. Guidance

In order for cells to migrate to a specific destination they need guidance of some sort. In single cells, chemoattractive gradients play a key role in directed migration, resulting in receptor activation at the front of the cell and dynamic changes in actin polymerisation and adhesion. In migrating cells, there is most often a clearly defined leading edge and trailing end as a result in elongation of actin filaments at the front, due to gradients of signalling molecules (Vicente-Manzanares et al., 2005). The migrating cell has to coordinate its front/back polarity enabling adhesion at the leading edge to generate traction, contraction of the rear of the cell and adhesion to enable the cell to move forwards. Cells that move as part of a collective such as in border cell migration need to coordinate cell-cell as well as cell-matrix adhesion (Rorth, 2011, 2012).

In 3D environments, such as in the border cell cluster, different distinct polarities, such as front-back, and inside-out, need to be maintained to enable efficient border cell migration to occur. In response to guidance cues, the cluster generates one or two long thin actin protrusions in the direction of migration at the forming leading edge, protrusions at the sides and back are fewer and less stable (Fulga and Rorth, 2002; Prasad and Montell, 2007). Front/back polarity in the border cell cluster is generated by the presence of two receptor kinases present on all follicle cells, which are activated in response to several chemo-attractant signals. Follicle cells and border cells express the tyrosine kinase receptor PVR, which binds Pvf1 (Platelet derived growth factor (PDGF) and Vascular endothelial growth factor (VEGF) related factor 1), and EGFR (epithelial growth factor receptor) which has shown to also bind the growth factors Spitz, Keren and Gurken, which are also partly

responsible for border cell migration guidance (Duchek et al., 2001; McDonald et al., 2006; McDonald et al., 2003).

Chemo-attractant guidance is provided by the oocyte. Gurken differs from the other ligands as it is responsible for late dorsal migration of the cluster once anterior posterior migration has completed (Duchek et al., 2001). Gurken, along with Spitz is a TGF-α like protein involved in egg chamber polarity establishment (Neuman-Silberberg and Schupbach, 1993). Loss of either PVR or EGFR results in impaired migration. PVR ligand binding has been shown to be responsible for the polarised quick migration observed in the first half of migration, whereas EGFR is responsible for later migration, prior to movement of the cluster dorsally. However, loss of both receptors results in a greatly enhanced phenotype suggesting they act in a redundant fashion and one can at least partially compensate for loss of the other (McDonald et al., 2006; McDonald et al., 2003; Poukkula et al., 2011). When dominant negative forms of both receptors are expressed, border cells maintain protrusion activity, but lose strong directed migration (Poukkula et al., 2011). Receptor cycling is believed to play a key role in directed migration resulting in high receptor activity at the front of the cluster than at the back (Janssens et al., 2010).

During the collective phase of migration, cells need to communicate and retain apical-basal polarity whilst interchanging positions in the cluster. This issue does not arise in individual migrating cells with basic front/back polarity (mesenchymal like). The cluster needs to maintain some epithelial characteristics such as elevated adhesion between cells and, with adhesion, maintain apical/basal polarity markers (Rorth, 2011, 2012). PAR3, PAR1 and PAR6 (partitioning defective) are located in the apical face of the border cell cluster prior to migration and remain in contact with nurse cells during migration, they also play a key role

in holding the cluster together (McDonald et al., 2008). Knocking down levels of PAR3 or PAR6 by RNAi has been shown to cause cluster disassembly (Goode et al., 2005; McDonald et al., 2008; Tanentzapf et al., 2000). Basal contacts are required to maintain the epithelium and must be remodelled to enable migration. The third type of polarity border cell clusters need to have is inside-out polarity. This is due to only some of the follicle cells being in contact with the surrounding nurse cells, as the cluster is a three dimensional shape. This polarity is important during directed migration as protrusions need to be directed on the correct face of each of the individual cells to be effective. This can be described as something similar to contact-inhibition of locomotion, where cells sense the presence of other cells in their path and have the ability to change cytoskeletal properties and polarity, and change direction (Desai et al., 2013). This can describe why protrusions are never observed at cell-cell contacts (between border cells or with the polar cells), resulting in collective chemotactic behaviour mediated by strong adhesion between cells.

The three types of polarity cooperate to enable the border cell cluster to maintain close contacts, whilst migrating between the nurse cells in a controlled directed manner.

1.6. Adhesion and Actin Polymerisation during Border Cell Migration

Migration of the border cell cluster proceeds by the formation of cellular protrusions that attach to the surrounding nurse cells via E-Cadherin (Fulga and Rorth, 2002). E-cadherin is critical for border cell migration, and its expression up regulated before and during migration. E-cadherin expression is also seen to be higher in ovarian carcinoma cells, compared to the cells from which they are derived (Naora and Montell, 2005; Niewiadomska et al., 1999). E-cadherin plays a key role in holding the migrating border cell cluster together and generating traction with the surface (Niewiadomska et al., 1999).

Myosins are best known for their role in muscle contraction, but also play a role in migrating cells. Myosins are a family of ATP dependent actin based motor proteins; non-muscle myosins bind or localise to cell membranes and play a role in force generation during migration (Oliver et al., 1999). Myosin VI is an unconventional myosin and has been shown to be expressed in follicle cells, including border cells and protrusions, throughout migration. Depletion of Myosin VI has been shown to severely inhibit border cell migration and results in the reduction of E-cadherin and β-catenin levels (Geisbrecht and Montell, 2002). The actin cytoskeleton also contributes to E-cadherin-mediated adhesion. Mutations in the Serum Response Factor (SRF), a transcription factor which normally stimulates F-actin production, results in the border cell cluster falling apart during migration (Somogyi and Rorth, 2004).

Given that a robust actin cytoskeleton is necessary to maintain cell shape and migration it is unsurprising that many genes that have been shown to play a role in actin regulation have been shown to be up-regulated in border cells (Wang et al., 2006). Profilin, which is encoded by chickadee in *Drosophila*, has been shown to promote protrusions in border cells and other cell types (Sokol and Cooley, 2003; Verheyen and Cooley, 1994). Diaphanous (DIA) a member of the formin family has been shown to promote linear rather than branched filaments during actin polymerisation and shown to be activated in border cells (Miralles et al., 2003; Somogyi and Rorth, 2004). It enables MAL-D translocation into the nucleus, most probably due to membrane tension, which in turn activates the transcription factor SRF. The actin binding protein cofillin (twinstar) has also shown to be required for border cell migration (Chen et al., 2001) and may partly explain the high ratio of actin protrusions at the front of a border cell cluster, compared to elsewhere. The low ratio of phosphorylated

(inactive) compared to un-phosphorylated (active) cofillin at the front of the border cell cluster suggests that it is somewhat guidance signal dependent (Zhang et al., 2011). Enabled (Ena) which can promote and inhibit cell motility in fibroblasts (Bear and Gertler, 2009; Bear et al., 2000). In border cells, sequestration of Ena from the leading edge and ectopic expression of Ena has been shown to impede migration (Gates et al., 2009), indicating that levels of actin regulatory proteins must be finely tuned to promote productive migration. Changes in Ena have been linked to increased metastatic behaviour in migratory invasive tumour cells (Gertler and Condeelis, 2011).

Recently, live imaging studies have extended our understanding of the behaviour of border cell clusters, showing that there are two phases of border cell migration: polarised behaviour in the first half of migration, followed by a more rounded cluster exhibiting a tumbling movement in the second half, where individual cells change their position within the cluster (Bianco et al., 2007; Poukkula et al., 2011; Prasad and Montell, 2007). Determining the behaviour of the cluster in its distinct stages has been facilitated by the advances in techniques to culture and image live egg chambers, *ex vivo*, enabling border cell migration to be well characterised.

1.7. The MIG-10/RIAM/Lamellipodin (MRL) Family of Adapter Proteins

MIG-10/RIAM/Lamellipodin (MRL) proteins link activated Ras-GTPases with actin regulator proteins including Ena/VASP to induce chances in actin dynamics, cell motility and the cytoskeleton (Krause et al., 2004; Lafuente et al., 2004).

The MRL proteins share common structural characteristics (Figure 1.6), including the

presence of a consecutive RA (Ras-association) and PH domain (Holt and Daly, 2005). The RA motif is a conserved region, which directly interacts with specific Ras-like GTPases. The PH domain is thought to play a role in membrane localisation (Holt and Daly, 2005). MRL proteins also possess several proline rich regions, which directly interact with the Ena/VASP proteins (Holt and Daly, 2005; Krause et al., 2004; Lafuente et al., 2004).

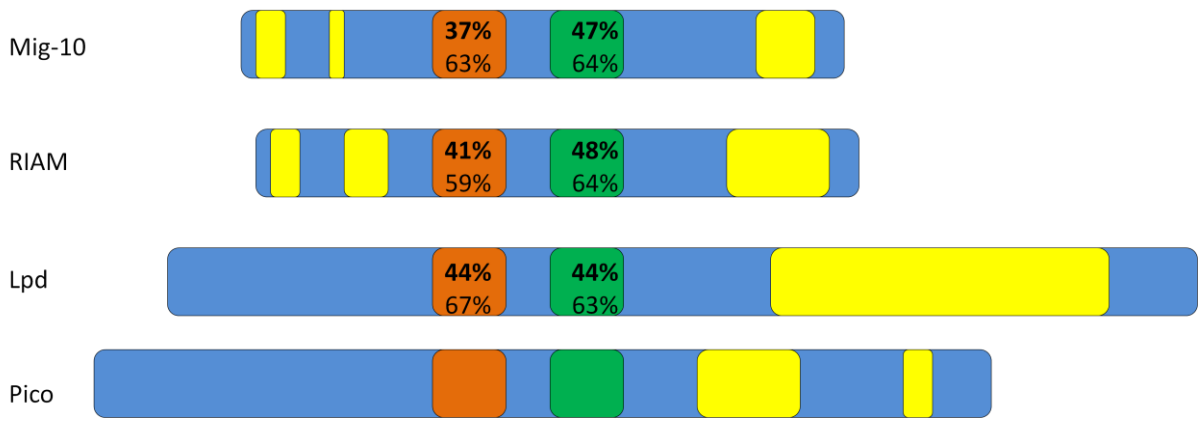

Figure 1.7. Image adapted from Holt, & Daly, 2005, showing the domain alignments of the MRL proteins of human RIAM and Lpd, also the C. elegans orthologue Mig-10. The figure also shows the domain structure of the different MRL proteins, their percentage identity (bold) and similarity to Pico (Lyulcheva et al., 2008). Yellow regions show proline rich regions, orange regions represent the RA domains and the green regions the PH domains. Sequences were taken from ensemble and domains annotated using information from Genbank. Several pair wise Blasts against the Mig-10, Lpd and RIAM domain sequences were performed using Pico as the query source.

RIAM acts with Profilin and Ena/VASP proteins to regulate actin dynamics. Over-expression of Lpd has been shown to increase lamellipodia protrusion velocity in fibroblasts in an Ena/VASP dependent manner; similarly knockdown of Lpd by RNA interference, impairs lamellipodia formation and reduced actin polymerization (Krause et al., 2004). RIAM and Lpd have overlapping functionality in humans, as over-expression of RIAM induces cell

spreading and lamellipodia formation, and also changes in actin polymerisation (Lafuente et al., 2004). Lpd and RIAM have been shown to alter the cellular ratio between monomeric (G) and filamentous (F) actin (Krause et al., 2004; Lafuente et al., 2004).

Recent reports suggest that the Lpd orthologue in *C.elegans*, MIG-10, may directly or indirectly bind to Abi-1 (part of the SCAR/WAVE complex) and both genetically interact to regulate axon guidance, synaptic vesicle clustering, and excretory canal outgrowth in *C.elegans* (McShea et al., 2013; Stavoe et al., 2012; Xu and Quinn, 2012).

Drosophila has been found to possess only one MRL homologue, encoded by *pico* (See Figure 1.6), (*CG11940*) which contains the characteristic RA, PH and proline-rich Ena/VASP binding domains (Krause et al., 2004; Lafuente et al., 2004; Lyulcheva et al., 2008). *pico* is required for tissue and organismal growth, as a reduction in pico level results in reduced cell division, growth retardation and increased G: F actin ratios. Conversely, over-expression of *pico* results in a reduced G: F actin ratio and promotion of tissue overgrowth. It was found that tissue overgrowth and increased F actin levels were epidermal growth factor receptor (EGFR)-dependent (Lyulcheva et al., 2008). Lyulcheva *et al* also showed that pico and Lpd both activate Serum Response Factor (SRF) and proposed that MRL proteins link EGFR activation to SRF-dependent gene expression via changes in actin dynamics.

1.8. Aims and Thesis Outline

The aim of this thesis was to develop and implement live cell imaging approaches for the study of *Drosophila* egg chambers, to better understand the mechanisms of invasive cell migration and border cell dynamics. In this respect, an important goal of the research was to

apply the techniques developed to characterise the role of *pico*, which encodes the *Drosophila* Mig10/RIAM/Lpd (MRL) protein, in border cell migration.

Chapter 3, describes the importance of medium composition and careful dissection, the optimisation of imaging settings, the properties of different imaging dishes as well as the behaviour and effect on migration of different border cell specific driver-reporter combinations. Chapter 4 describes analytical approaches to extract quantitative data from time-lapse images in a consistent and accurate manner. In this context, the use of ImageJ plugins to track the movement of the border cell cluster is reported, with emphasis on the differences between manual and semi-automated approaches. The strengths and weaknesses of different data extraction procedures are discussed and recommendations made for analysis of future experimental work. Finally, in Chapter 5, the knowledge and techniques developed to culture and image egg chambers is applied to determine the role of Pico and its interacting protein, SCAR in border cell migration.

2. Materials and Methods

2.1. Growth and Fly Maintenance

Fly stocks and crosses were kept at 25°C on standard yeast medium with dried yeast balls. Adults from the crosses were transferred to new vials every 2-3 days. Newly eclosed females with a few males were fattened with fresh yeast paste for approximately two days before dissection.

2.2. Immunostaining *Drosophila* Ovaries

Three day old flies kept with yeast paste were anaesthetised with CO_2 and females with the correct genotype selected by phenotype for dissection. Flies were dissected in cold 1x Phosphate Buffered Saline (PBS) (phosphate buffer concentration of 0.01M and a sodium chloride concentration of 0.154M, pH 7.4) using sharp forceps to remove the ovaries. Once removed, the ovaries were separated and the egg chambers spread out. Dissected ovaries were immediately fixed in 4 % (w/v) paraformaldehyde in PBST (1x PBS, 0.1 % (v/v) tween-20) for 20 minutes at room temperature. Following this samples were washed in 1 x PBST for 5 minutes then placed in blocking solution (PBST containing 5 mg/mL Bovine Serum Albumin (BSA)(Sigma 05470) for 2 hours minimum. Samples were then incubated overnight in blocking solution containing AF633-phalloidin (Sigma, 0.25 mg/mL) in the dark at 4°C. The following day samples were washed 4 x 20 minutes with PBST followed by 5 minutes in PBS at room temperature. Finally, ovaries were mounted on a slide and separated, in VectaShield mounting media (Vector Laboratories, H-1000), covered with a cover slip and the sides sealed with clear nail polish. Slides were kept at 4°C in the dark until imaged.

Images were taken using a 20x objective, 1024 x 1024 resolution. GFP, RFP and AF633 phalloidin were excited at 488 nm, 561 nm and 633 nm respectively.

2.2.1. Genotypes Used for Fixed Samples

Genotypes used to determine the role pico/SCAR plays in border cell migration (Chapter 5):

slbo-GAL4, UAS-GFP, his2A-RFP/+

slbo-GAL4, UAS-GFP, his2A-RFP/ UAS-pico RNAi (line 9); UAS-pico RNAi (line 4)/+

slbo-GAL4, UAS-GFP, his2A-RFP/+; UAS-pico/+

slbo-GAL4, UAS-GFP, his2A-RFP/UAS-SCAR RNAi (VDRC 21908)

slbo-GAL4, UAS-GFP, his2A-RFP/UAS-SCAR RNAi (VDRC 21908); UAS-pico/+

slbo-GAL4, UAS-GFP, his2A-RFP/+; UAS-Lpd/+

slbo-GAL4, UAS-GFP, his2A-RFP/ UAS-pico RNAi (line 9); UAS-Lpd/ UAS-pico RNAi (line 4)

2.2.2. Quantifying Fixed Samples

At stage 9, the distance between the centre of the border cell cluster and the anterior columnar follicle cells (border cell position) was measured in ImageJ (http://rsb.info.nih.gov/ij/). For stage 10 egg chambers, the percentage of the total migration was calculated using the distance from the anterior edge of the egg chamber to the centre of the cluster as a percentage of the total migration distance (to the anterior columnar follicle cells).

2.3. Live Imaging Techniques

2.3.1. Overview

Three day old flies kept with yeast paste were anaesthetised with CO_2 and females with the correct genotype selected by phenotype for dissection. Flies were dissected in cold

Schneider's Insect media (Sigma S0146) containing 15 % (v/v) Fetal Bovine Serum (Sigma F4135), 1 µg/mL Streptomycin and Penicillin (P4333) and Insulin (10 mg/ml) (Sigma I6634) as described in (Prasad et al., 2007). When preparing the media more than was needed (5 mL) was made to minimize contamination when adjusting the pH. It was important fresh solutions were used, in particular the insulin (avoid freeze thaw cycles) and that pH was in between 6.95 and 7.00. Using sharp forceps the ovaries were removed and single strands of egg chambers at variable stages removed. Extra care was taken not to touch the strands of egg chambers at any point including when transporting from the dissection plate to the imaging dish. To avoid this, the pipette tip was cut and care taken when positioning the tip in the medium to draw up and release the egg chambers. The amount of medium the egg chambers were left in was critical, for larger numbers of egg chambers (7-10) approximately 30 µL was needed, however excessive amounts resulted in egg chambers flowing out the side of the mounted cover-slip. Before imaging the edges of the cover-slips were surrounded by hydrocarbon oil 27 (Sigma H8773). Confocal stacks were taken at multiple positions using a Zeiss710 confocal microscope equipped with a 488 nm argon ion laser, fitted to an inverted microscope with 20x 0.75NA Fluar objective. Z sections, 2.5 µm thick (approximately 10-15 images/stack) were taken at each position at 2 minute intervals. If necessary, imaging was paused briefly during the time lapse to adjust the focus.

2.3.2. Imaging Medium

Fresh Schneider's medium was important in ensuring the success of border cell migration. One way that I enabled this was to make sterile measured aliquots of the medium components before storage and freezing where possible. During preparation, specifically for the dissecting and imaging process the antibiotics Penicillin and Streptomycin were added

to reduce bacterial growth promoted by increased temperature during imaging, and the presence of serum in the media. In the case of Schneider's, which needed to be stored at 4°C, measured aliquots were made and replenished on a monthly basis. Complete medium was made fresh using the aliquoted elements on the day of imaging and disposed of at the end of the experiments. It was decided through trial and error that 5 mL was the ideal amount to make on a daily basis, enough to accurately measure with the pH monitor (to allow submersion of the probe) and not too much that it was wasteful. Aliquots of FBS were also made and frozen to preserve the stability of elements of the serum such as growth factors. In addition, batches of FBS that were shown to be successful in the culturing of egg chambers were clearly labelled and only used for this purpose. As the initial powdered insulin was stored at -20 degrees, it was very important that measured aliquots were made to avoid freeze/thaw cycles and deterioration. Each aliquot of insulin was measured to generate a 10 mg/mL solution using a very weak acid (pH 5, HCL), the instructions directed a slightly acidic environment for stability, but did not specify pH.

2.3.3. Dissection

The different protocols suggest using females aged for 3-6 days (Bianco et al., 2007; Poukkula et al., 2011) or less than 4 days (Prasad et al., 2007; Prasad and Montell, 2007). On the day new females eclose they were placed with yeast paste and left for 48 hours before dissection. This was found to be an ideal time to dissect as the ovaries were suitably fattened and ovarioles contained egg chambers at the correct stage of development. All dissection took place at room temperature on the top part of a modified plastic petri-dish.

Dissection Surface

The modification of a petri dish entailed cutting off the outer rim producing a flat, clear circular piece of plastic. This was important, as the outer rim was difficult to manoeuvre around when trying to carefully dissect. Turning the dish upside down resulted in difficulty in focussing on the translucent ovarioles once they were separated from the ovary, due to the distance between the microscope platform and the dissecting surface containing the medium. Other protocols have suggested dissection on a glass surface (Prasad et al., 2007) or a glass slide with a depression (Bianco et al., 2007) to hold the dissection media. Dissecting on a glass slide produced problems, as it was too easy to blunt the sharp ends of the forceps during dissection. Sharp forceps were very important to ensure precision when dissecting, and although they can be sharpened using a sharpening stone (Norton) they cannot be guaranteed to be as sharp and accurate as they originally were. Using a plastic surface prevents damage to the forceps as the plastic tends to scratch when touched with the forceps and no damage occurs. The plastic surface was ideal for working within a medium sized droplet of imaging medium, which held its shape due to surface tension. However, it was noted that any slight abrasion to the plastic surface could damage the egg chambers when they fell to the bottom of the medium droplet.

Dissection Technique

Dissection of the ovaries from the adult fly was carried out as demonstrated above. The fattened female was grasped by the head with one set of forceps and the abdomen pulled with another, releasing the ovaries into the media. If on the rare occasion the ovaries did not easily come out along with the rear end of the abdomen, that fly was discarded and the procedure repeated on another fly. This is important as any further manipulation of the fly can result in damage to the egg chambers within the ovary. Once the ovaries were

separated from the fly the ovaries were transferred to another droplet of medium holding them by the interconnecting oviducts.

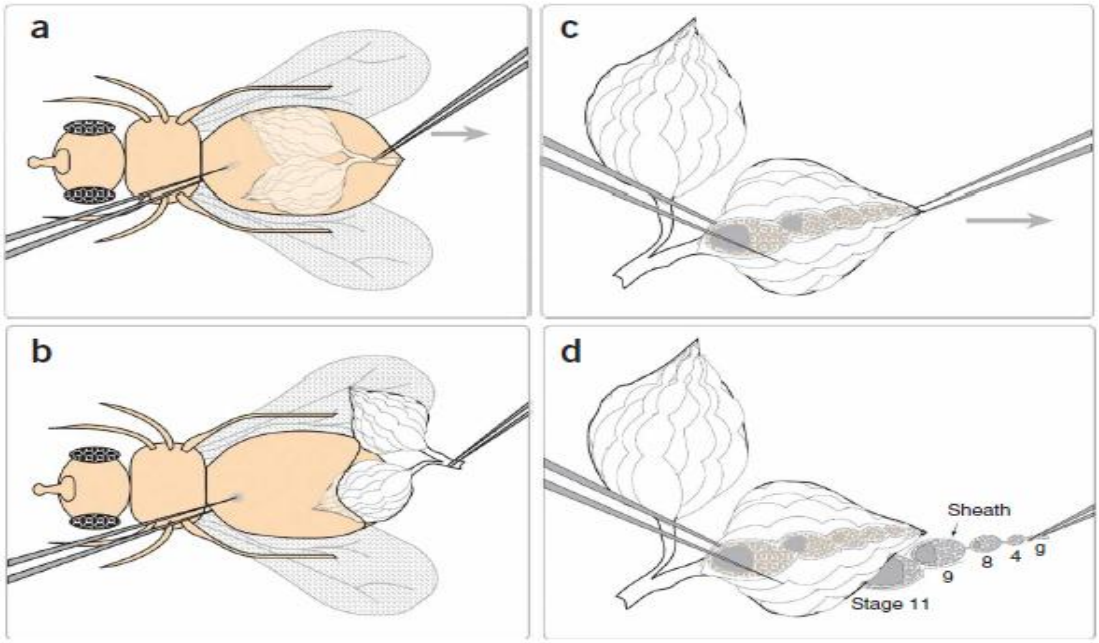

Figure 2.1. Removing the ovaries and individual ovarioles. Image taken from Prasad *et al* 2007 illustrating the initial stages of egg chamber dissection. In **(A, B)** a pair of forceps were used to hold the anesthetised fly and remove the abdomen. **(C)** Forceps were used to hold the individual ovary in place whilst the string of egg chambers were gently pulled and removed. **(D)** Illustrates the position of the egg chambers at various developmental stages in relation to removal from the ovary.

To remove the individual ovarioles the two ovaries had to be separated by shearing them with forceps. One of the forceps were then used to hold the ovary at the posterior end, with the more mature egg chambers. Again, care was taken not to damage the egg chambers in the middle as these often were of the appropriate stage to be imaged (Stages late 8 to early 9). To extract individual ovarioles, single strings of egg chambers were simply pulled then let go, releasing the string of egg chambers into the medium, without touching the egg chamber at the correct stage (in the middle) with forceps. Contact with the forceps can damage the egg chamber and prevent border cells from migrating. Some protocols (Tekotte

et al., 2007) suggested tungsten needles can be used to extract single ovarioles, or to tease apart the anterior end of the ovaries before extracting the ovarioles. Needles were tested for this purposed, but found to offer less control than forceps. In addition to this the process was quicker and more efficient using the same tools throughout. This helped minimise the time the egg chambers were left before imaging.

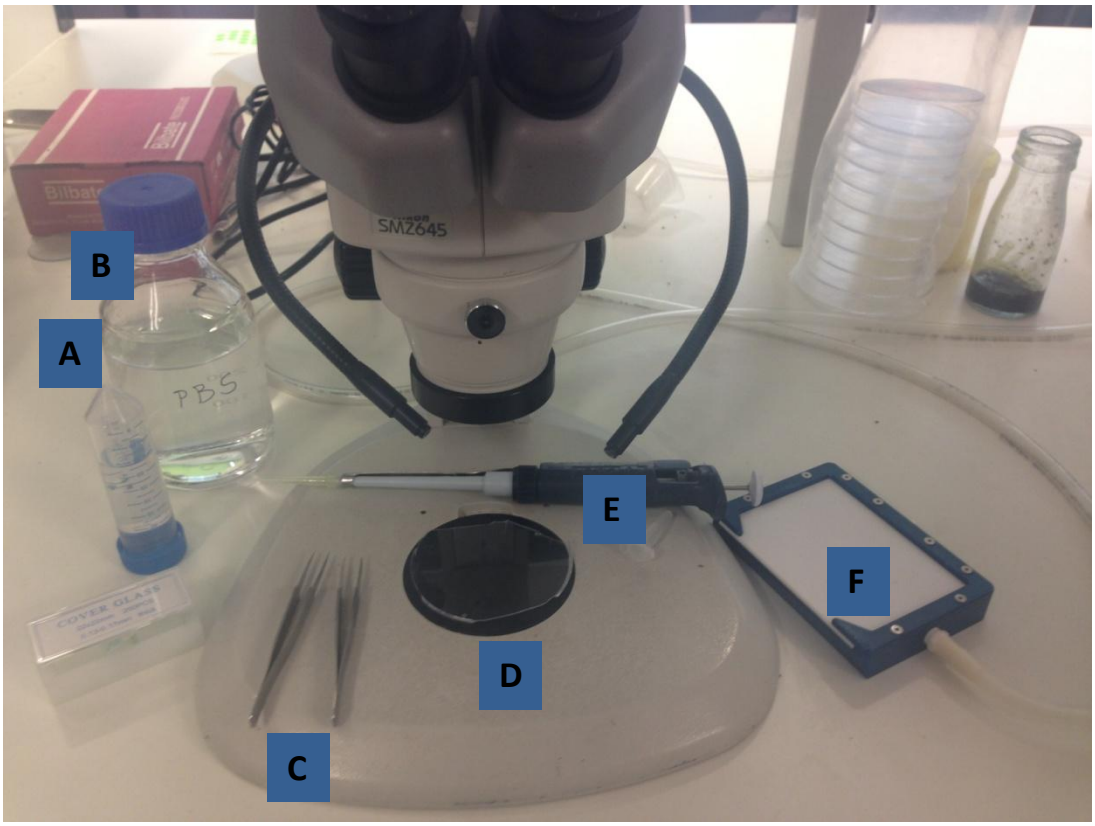

Figure 2.2. Picture showing some of the equipment used for egg chamber dissection. (A) Shows dissecting solutions such as PBS and the live imaging media, **(B)** Cover-slips used to make a platform in the Lumoux dish and cover the egg chambers. **(C)** Sharp forceps for pulling the ovarioles from the ovary. **(D)** Modified petri dish with sides removed, **(E)** P200 pipette with tip that has been cut. **(F)** CO_2 pad to anesthetize the fly.

2.3.4. *Drosophila* Genotypes Used for Live Imaging

Genotypes used to determine the role pico/SCAR plays in border cell migration (Chapter 5):

c306-GAL4/+; UAS-LifeAct-GFP/+

c306-GAL4/+; UAS-LifeAct-GFP/UAS-pico RNAi (line 9); UAS-pico RNAi (line 4)/+

c306-GAL4/+; UAS-LifeAct-GFP/+; UAS-pico/+

c306-GAL4/+; UAS-LifeAct-GFP/UAS-SCAR RNAi (VDRC 21908)

c306-GAL4/+; UAS-LifeAct-GFP/+; UAS-Pvr^{DN}/+

c306-GAL4/+; UAS-LifeAct-GFP/UAS-SCAR RNAi (VDRC 21908); UAS-pico/+

Genotypes used to test reporter expression/behaviour in border cell migration (Chapter 3):

slbo-GAL4, UAS-GFP, his2A-RFP/+

slbo-GAL4, UAS-mCD8-GFP/+

c306-GAL4; UAS-mCD8-GFP/+

slbo-GAL4, UAS-$dsRed^{NLS}$/+

slbo-GAL4, UAS-mCD8-GFP, UAS-$dsRed^{NLS}$/+

slbo-GAL4, UAS-LifeactGFP/+

slbo-GAL4, UAS-LifeactGFP/+; UAS-LifeactGFP/+

c306-GAL4; UAS-LifeactGFP/+; UAS-LifeactGFP/+

slbo-GAL4, UAS-GFP/+

slbo-GAL4, UAS-Lifeact-mTFP/+

2.4. Live Imaging Analysis

2.4.1. Rate/Duration

Duration was calculated based on the total number of frames per movie, multiplied by the time interval. Frames were counted once the border cell cluster had detached from the epithelium and until they had reached the nurse cell-oocyte boundary. In special cases where the cluster failed to detach, counting began 10 frames from the start. Counting was ended once anterior-posterior migration had stopped. Rate was calculated based on the distance from the most anterior tip of the epithelium to the nurse-cell oocyte boundary. To keep distances constant and compensate for egg chamber growth, measurements were taken in the last imaging frame, once the cluster had reached the oocyte boundary, this was considered as "As the Crow Flies" (ACF). The simple formula Speed = Distance/ Time was then used.

2.4.2. Tumbling Index

The tumbling index was shown as the percentage of movies and frames per genotype that show early tumbling. This was calculated using the number of movies per genotype that or the average percentage of frames per time lapse that showed early tumbling. Early tumbling is defined as a rounded cluster lacking protrusions in any direction for two or more consecutive frames, in the first half of migration. Clusters were considered to be tumbling with or without productive forward movement.

2.4.3. Manual Tracking Plugin

To track the border cell cluster in XY maximum intensity projected images of the GFP channel needed to be used, this was done using the Zeiss Laser Scanning Microscopy (LSM)

Image browser. Following this, ImageJ was used with a plugin named Manual Tracking (Fabrice Cordelieres, Institut Curie, Orsay (France). Once the plugin was opened a toolbar was displayed as shown in Figure 2.3 which controlled the plugin and enabled calibration values to be inputted.

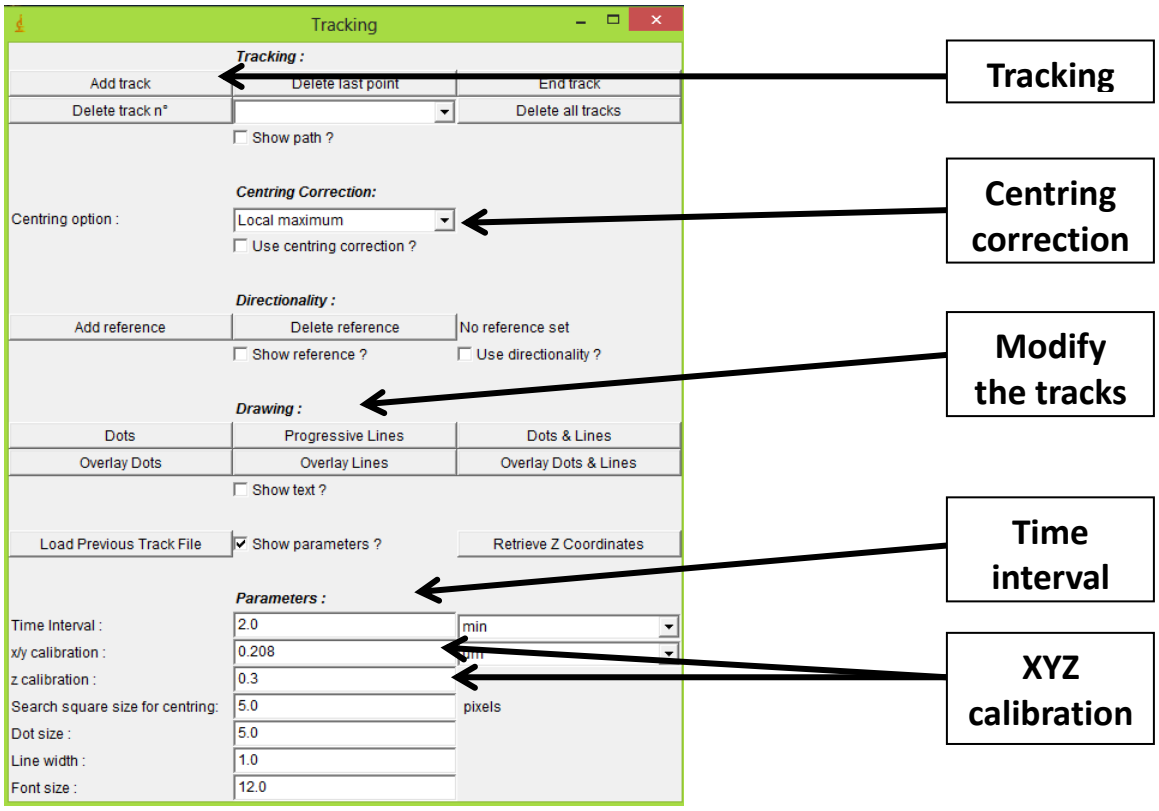

Figure 2.3. Shows the toolbar for the Manual Tracking plugin for ImageJ.

Important functions are labelled which ensure the tracking is accurate. Time interval - the time between consecutive frames, XY calibration- the number of pixels in 1 µm, Z calibration - depth of each section, Square size - determines the centre of a shape based on 5 pixels, Dot size - the size of the tracked point, Line width - width of the progressive line, Font size - Size of font in track annotation.

It was important that the XY calibration values were set and the interval rates for the movie being analysed, this was found under the "Parameters" heading. This ensured the distance

that the cluster moved was accurately measured and the velocity calculated using the correct time scale. If tracking in the Z plane was needed, Z values were also calibrated, however, it was discovered that tracking in Z was not an option with this plugin with images acquired using Zen 2010. In the toolbar there was also an option to modify the display of the tracks once they had been mapped onto the time series using the 'Drawing' options. These options included plotting the track using dots at each time point, progressive lines showing the pathway or a combination of the two. Progressive dots and lines were used when tracking. These could be shown individually in a channel of their own or overlaid over the original images. When tracking the pixel intensity readings were utilised for the correct placement of the track points. Track point placement can be based on minimum, barycentre or maximum intensity projections in the 'Centring Correction' heading. It was found that maximum intensity projections were most useful and enabled the process to be visualised more easily. Centring correction makes slight adjustments to the position of the track point for the area of the cluster based on the number of pixels specified in the toolbar. Using this function had both positives and negatives. On the plus side it ensured the track point was placed roughly in the same location of the cluster in each time frame, as projecting the image creates a local area of increased intensity. The main negative aspect was due to the constant changing shape of the cluster. In some time frames the cluster took on a ringed appearance as the border cells surround the non-fluorescent polar cells (when using *slbo-GAL4*). Under these circumstances, the non-fluorescent centre of the cluster was not used, as in other frames, as the tracking point. Tracking was started by selecting the "Add Track" function in the heading "Tracking". In the image window tracks were added by a single left click of the mouse, to move to the next frame the slider at the bottom of the image window was moved across. To finish tracking the "End Track" function was pressed. During tracking

an output table was present with each of the measurements for each specific point, this was saved as an Excel file before closing down each image. Velocity per time point was used to determine the average migration velocity in a single track (egg chamber).

2.4.4. MTrackJ ImageJ Plugin

Mtrack J is a plugin for ImageJ (Meijering et al., 2012). The toolbar appeared to be more user friendly than the manual tracking plugin but had hidden functions, within each of the options, this can be seen in Figure 2.4. This was due to most of the calibration settings that needed to be manually entered previously, being automatically recognised from the imaging file metadata. This should remove any errors in the data due to calibration issues. The only value that needed to be manually inputted into image J was the time interval, which allowed the correct velocities and measurements to be calculated. This was done using the commands Image>Properties, then using the time interval box. To track the migration of the cluster in XY, as previously described, maximum intensity projections were used. To add a track the "Add" function was selected in the toolbar and the first point placed using the left click of the mouse on the image window. The time series then automatically moved to the next frame. To finish the tracking process the mouse was double clicked on the final point/image window. The track in previous frames can be customized to be hidden or to be shown during the tracking process. It was found that hiding the previous tracks enabled placing the future points more easily as part of the cluster was not obscured by the track overlay. Track points could be easily customized with colour, size and shape and there are no constraints on the number of tracks that can be overlaid on an image file. These options were present under the "Colour" and "Options" tracks. To track, both the correct Z and time stack needed to be in the image viewer to include any movement in Z in the analysis. Once

the tracking was complete the "Measure" function was used which opened an output table, with the various measurements taken from the tracked image. This included pixel intensities, time units, XYZ coordinates, the distance and velocities between two consecutive points (all discussed in Chapter 4). To determine the velocity of the migrating cluster the average velocity per frame was used.

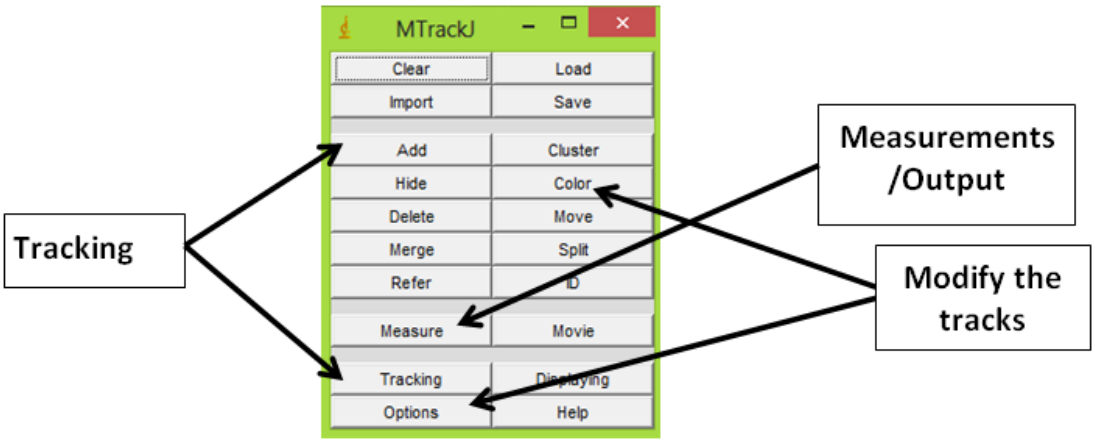

Figure 2.4. Shows the toolbar for the MTrackJ plugin for ImageJ.

The important functions are labelled by the black arrows. Clear, Delete, Hide, Move - all relate to modifying a single tracked point. Load, Save and Import - enable saved tracking files to be overlaid onto new image files. Color, Displaying, and Options - enable the tracks to be modified on the imaging window. Movie - converts the imaging window/time series with the track overlaid over into a movie.

2.4.5. Semi-automated Macro for ImageJ

The automated macro was obtained from Pernille Rorth (NUS, Singapore) as published (Poukkula et al., 2011). The plugin/macro came in two files: Common_Toolbar.class - this was placed in the plugins/tools folder of ImageJ, and StartupMacros.txt - placed in the 'macro' folder. Following this the macro toolbar, see Figure 2.5, automatically opened once ImageJ had been started up.

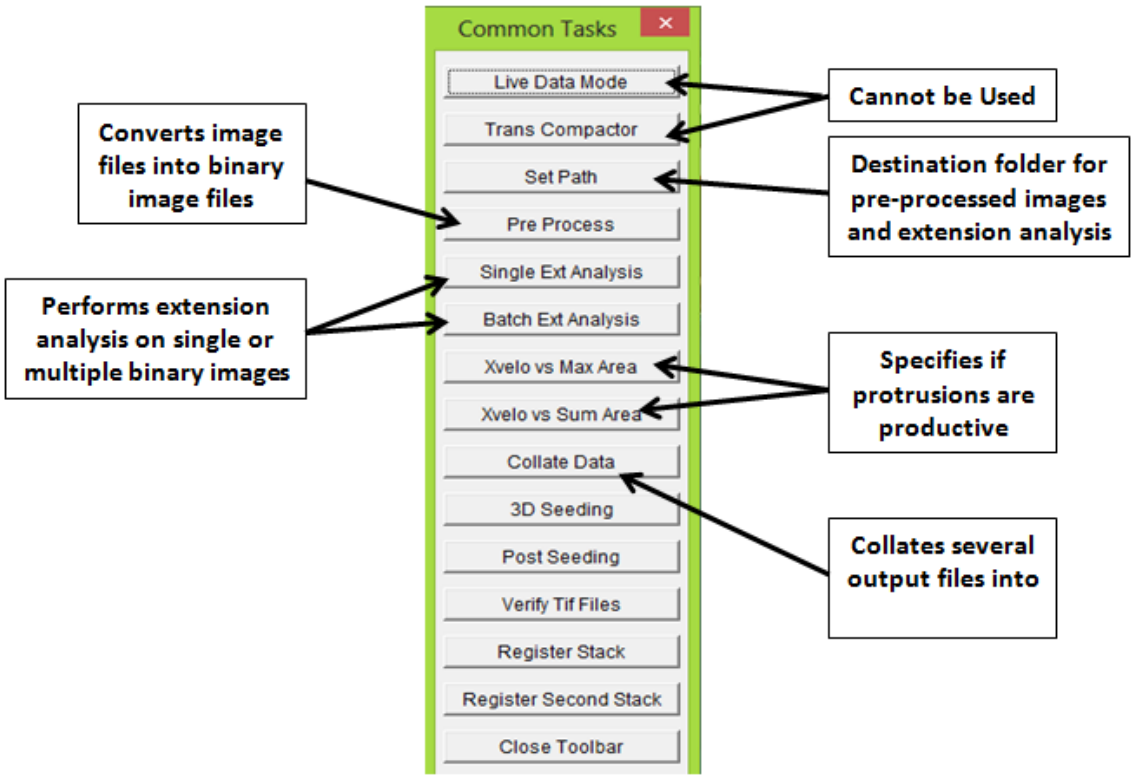

Figure 2.5. Shows the toolbar for the semi automated macro.

The individual macros used from top to bottom. The first two "Live Data Mode" and "Trans Compactor" cannot be used as they were custom built for a specific microscope in the Rorth lab. "Set Path" determined the destination folders from the outputs of pre-processing and Extension analysis, Single/Batch Extension analysis started the analysis of the pre-processed binary movies, depending on which was selected. Xvelo vs MaxArea/SumArea utilises the extension and tracking data to determine if the protrusions result in productive movement. Collate Data, collates all the single extension analysis files into one. The Final four, "Post Seeding", Verify Tif Files" Register Stack/Second Stack" cannot be used.

The order the macros were used ran downwards, vertically starting at 'Live Data Mode'. The first two macros, however, could not be used as they were written specifically for another microscope, essentially these perform some of the preparation needed before the imaging files can be inputted, such as image rotation and image projection. This was easily done manually. The next section will consist of the steps taken to get the macro output.

Additional channels such as transmitted light or reporter channels were removed using the Leica LSM image browser software, as the macro runs using the GFP projection only. It was determined that during all stages of the image preparation the files should be individually saved so if there were any issues backtracking would be easy. All files/genotype were saved in the same location as .Tif time stacks and named 'Something'_pro.tif enabling the macro to recognise them. Time frames after the first half of migration were cropped, if present, in addition to the very first few frames of migration before detachment had occurred.

Set path

Two destination folders, for pre-processed binary images and the final output needed to be defined, this was done before any image files were opened and needed to be refreshed each time ImageJ was opened, to prevent files being saved in the wrong location. It was found that setting different destination folders for each genotype was key to remaining organised, and was useful later on as the macro was constantly using and saving files, as the macro was being run. When running the macro you were prompted to define destination folders. The Pre-processed movies essentially were simpler, smaller files containing the information the macro needed to identify the cluster and analyse the protrusions.
A second prompt was to set a destination folder for the extension analysis files, this was the place the majority of the output from the analysis was stored.

Pre-process

Once a time series was opened in ImageJ the pre-process macro was started. The first prompt enabled the user to define the scale, which was used to determine the size of the cluster. This was important, as the centre of the circle is used to determine the centre and distance to the protrusion edge. As default the macro was set to 0.315 µm, this is based

upon the size of 1 pixel using the original settings, defined by the macro creator. This was changed to 0.208 for the settings used for the movies being analysed. The next step allowed the different stages of migration to be inputted, so that the outputs for the various sections were calculated and saved separately. In this case only the first half of migration was used (15 frames) immediately after detachment, so the second half of migration values were left as 0.

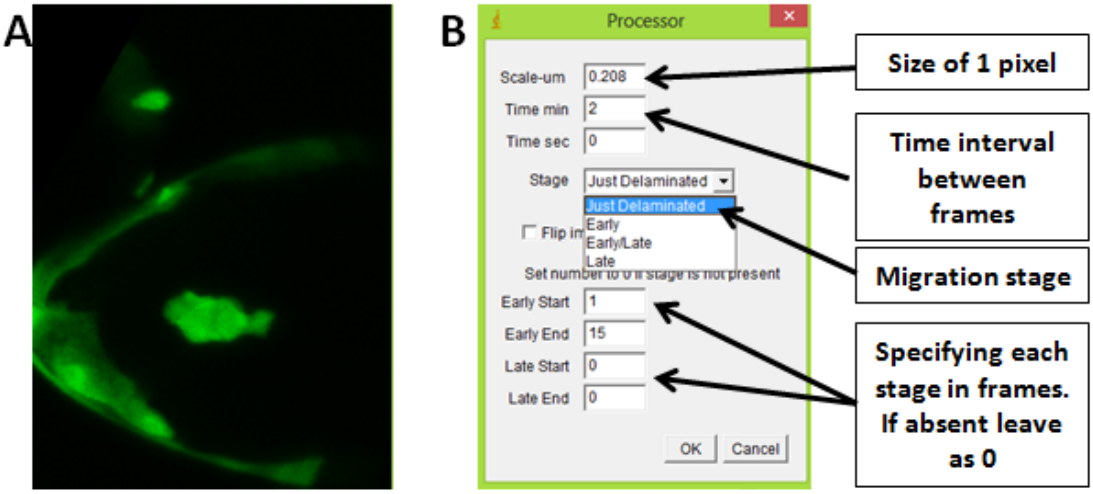

Figure 2.6. Shows the initial steps of the pre-processing stages of the semi automated macro. (A) Shows a GFP projected image of a border cell cluster used in the initial stages (*C306>Lifeact-GFP*). **(B)** Shows the first prompt of the pre processing stage. Key elements are identified with the black arrows.

Following this the macro showed the projected image, with all time points in the movie. A box needed to be drawn around the cluster ensuring the cluster did not touch the edges in any time point. It was found when doing this it was best to begin drawing the box slightly before the cluster and to end just past the oocyte-nurse cell boundary. Once it was drawn it was checked by running through all the time points, before the next step was moved on to. The next step of the pre processing thresholded the GFP cluster, this was important as it

determined which parts were going to be visible when the extension analysis macro was run.

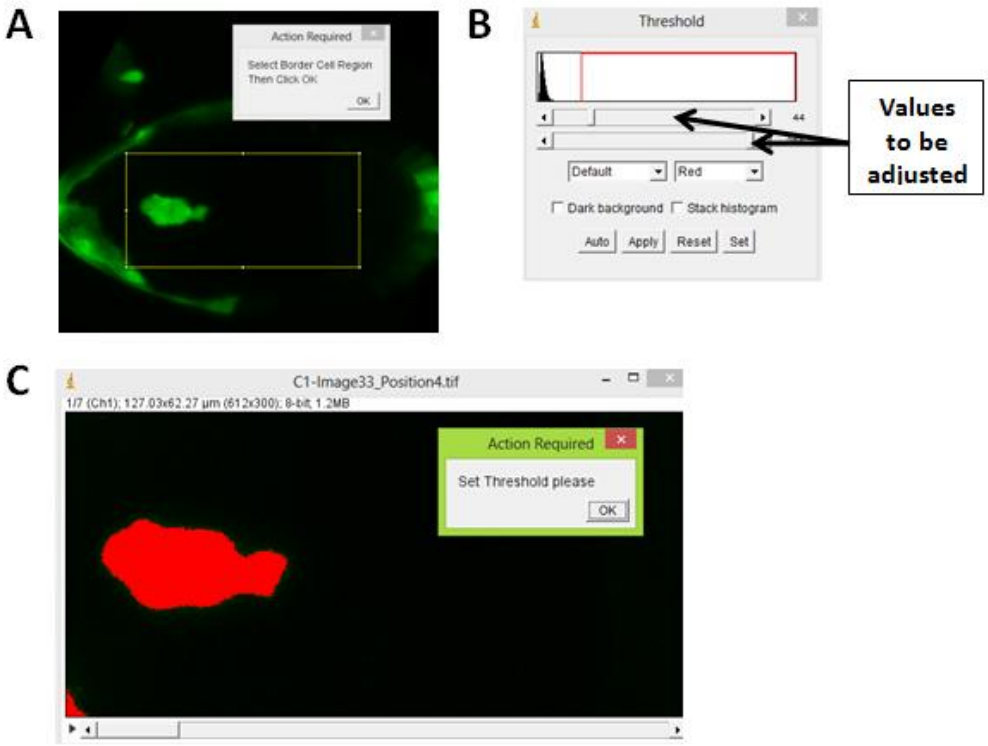

Figure 2.7. Shows the final steps of the pre-processing macro. (A) Shows a GFP projected image of the border cell cluster movie. The border cell region is defined by the yellow rectangle, this area is taken past where the cluster finishes its migration to ensure it does not touch the outline. **(B)** Thres-holding toolbar, the black arrows indicate the values that need to be adjusted. **(C)** Shows the border cell cluster in red and the background black. The red area indicates the parts of the movie that will be included in the binary image.

This was done firstly by sliding the bottom bar fully to the right (255) (See Figure 2.7) making the entire selected area red. The red area indicates a positive signal once the movies have been generated into binary images. The top bar, therefore, needed to be adjusted until only the cluster and the protrusions were positive (red). This is where extremely faint protrusions may be missed, however it was important that there was only one positive element (the

cluster) in the frame. Once complete the pre processed movie was saved in the destination folder specified previously ready for the extension analysis.

Extension Analysis

The extension analysis requires the pre processed binary movies generated by the pre processing steps. However, it was found that in most cases the binary movie could not be initially used and further formatting had to be performed. This was due to parts of the epithelium or other parts of the egg chamber, being included in the original selected area and subsequently converted into a binary signal. In addition to this, some clusters contained gaps between the cluster body and protrusion, where the extension was too thin or faint to detect due to the thresholding step. Any gaps were filled in by hand using the ImageJ draw tool, it was vital that the ultimate shape of the cluster or protrusions were not altered as this would influence the results obtained. Other positive (black) areas in the movie needed to be erased also, it was crucial for the accurate running of the macro that there was only one object (the cluster) in each of the frames. This can be easily done using the fill function in ImageJ (Details shown in Chapter 4.4.1).

A new folder was generated containing the modified binary movies, to prevent confusion when running the extension analysis. Storing all pre-processed movies in the same folder also enabled the batch extension analysis to be run if needed.

Following the extension analysis the image files were automatically shut down and the results saved in the specified destination folder.

Output

Once all analysis was finished it was important to check that the macro had run smoothly and the image had been properly segmented into the cell body and protrusion. This was done using the output file 'name_mass.tif' opened in ImageJ, Figure 2.8.

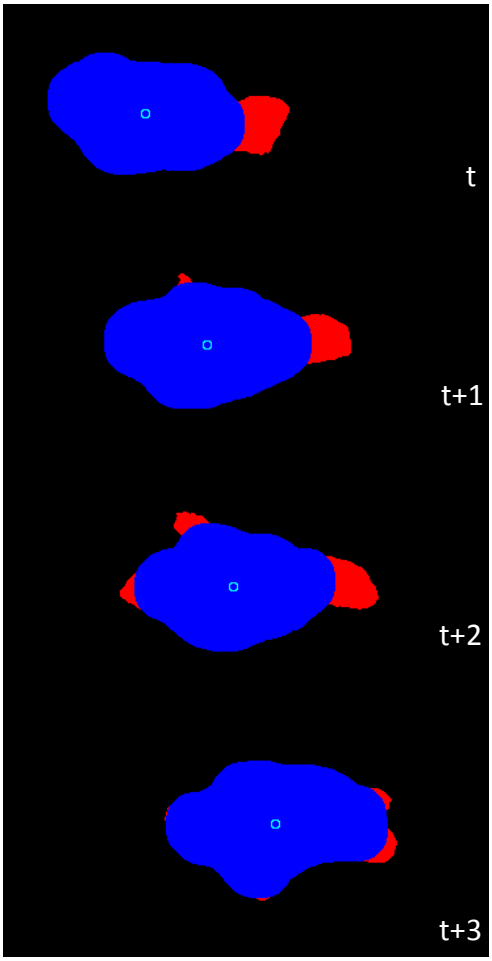

Figure 2.8. Shows the output file 'name _mass.tif' at four different time points. The cluster is travelling from left to right. The cell body is labelled in blue and the protrusions in red. The small circle indicates the centre of the cluster.

Essentially Figure 2.8 shows the entire time-lapse, in each frame the cluster is segmented into cell body (blue) and extension (red), the centre point of the cluster is mapped with a small circle. This part can show if the macro has failed. If the macro has determined that the

whole cluster is an extension (red) or if it decided there are no extensions (blue) the file would need to examined for errors. In some respects a completely blue cluster was not an issue as there may not have been any protrusions in that particular frame, however a completely red cluster indicated that something had gone wrong. In this case it was usually discovered that the macro cannot define the cell body correctly, due to another object in the analysis field.

Saved in the destination folder was a large number of files in .tif, .txt and .xls format displaying all the data extracted from the images, the text files (.txt) were not important as they only contained information that was already present in the excel files.

The .tif files showed the segmentation that had been carried out in a visual format, these are shown in Chapter 4.4.2. The 'mass' file showed the extensions in red, the cluster in blue and the centre of mass for each time frame, the 'Allcent' file was similar but showed the cluster in a stationary format. The path of the cluster in a tracked line format could also be displayed using the 'path' tif.

Visual information about the extensions was found in the 'extension' and 'marked' files. These files showed the extensions with and without the cell body, annotating the number of protrusions present in each frame. An additional file also showed the length that was measured for each extension to the centre of the cluster, similar to the method that was used in Chapter 4.4.3 to manually calculate the protrusion length.

The 'basic' file gave statistics about the whole cluster including speed, cluster shape, duration etc. This was important when initially looking at differences between genotypes, to see if there was an impairment for example.

The rest of the outputs gave information with regards to the extensions. 'Consol' file gave

valuable information, such as the speed of the cluster, extension area and length at each of the separate sections, front, back and sides. It also described the persistence and angle of each of the individual extensions. The output also contained information on a frame-by-frame basis including the direction of the extensions at each time point. These were represented as absolute and binary numbers for each direction in each frame, allowing direct frame-by-frame analysis to be carried out if necessary. Additional spreadsheets were also given with more detailed data about the maximum length and area of individual protrusions.

Collating Data

A macro was also written to easily collate all of the data files together. This was especially useful when more than one image file was being used to represent one egg chamber movement. It allowed the results files for all movie parts and genotypes, to be collated into one excel spreadsheet. This highlighted the importance of keeping the imaging and results files organised into individual folders, as the macro took all the excel files in a selected folder and combined the data into one. This macro was found to be extremely useful and saved a lot of time.

2.5. Generating UAS-Lifeact-mTFP

The *Drosophila* Gateway System enables an easy flexible introduction of different fluorescence tags with a gene of selection. This involves making an entry vector that is used to shuttle an open reading frame (ORF) into an expression vector simply, by swapping the ORF with a gene found in a destination vector through a site-specific recombination reaction. The Drosophila Gateway Vector Collection is a collection of 68 gateway-based destination vectors specifically designed for use in *Drosophila* cultured cells or flies to incorporate

epitope-tagged proteins. Invitrogens gateway recombination cassette enables an ORF to be recombined into any of the vectors, See figure 2.9.

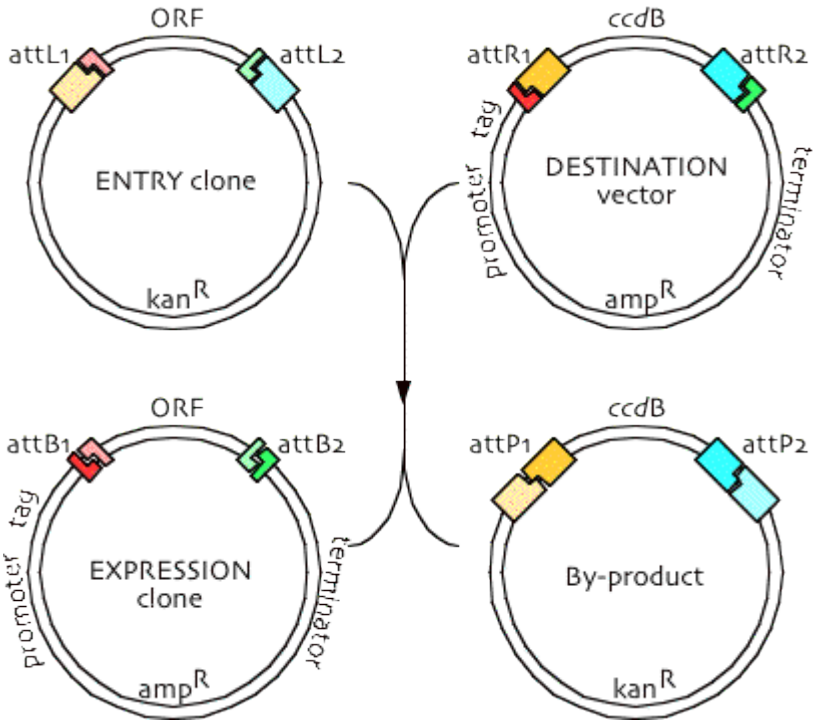

Figure 2.9. Schematic diagram showing the various vectors generated when using the *Drosophila* Gateway System. An entry clone is generated containing the ORF of interest. This is recombined with a destination vector containing the tag, from the *Drosophila* Genome Resource Centre, generating an Expression clone with the specified tag and the ORF.

An entry clone pDONR, was generated by another individual in the lab using the Invitrogen pENTR Directional TOPO Cloning kit containing Lifeact, which was flanked by two recombination sites attL1 and attL2 which are used in a recombination reaction with the Destination vector using its attR1 and attR2 sites.

2.5.1. Generating A UAS-mTFP Destination Vector

The problem was that the gateway collection does not contain a destination vector containing mTFP, only cyan fluorescent protein (eCFP). To incorporate mTFP into a destination vector an existing vector had to be modified by replacing the current fluorescent

protein sequence with that of mTFP. Primers were generated (Described later) to amplify the mTFP sequence. A construct containing mTFP was amplified using Polymerase Chain Reaction (Details later), the finished reaction was subject to electrophoresis and the mTFP DNA sequence extracted using gel purification (See Later). Restriction enzyme maps were generated for mTFP and pTVW (DGRC1091), a fly transformation vector containing an N-terminal Venus tag under the control of UAS, using NEBCutter (http://tools.neb.com/NEBcutter2/). Enzyme pairs were selected (See Restriction Enzyme section below) which enabled Venus encoding DNA to be extracted from the vector and produced complementary sticky ends in both sequences. The restriction digests were seperated by electrophoresis and the DNA sequences at the correct size, from pTVW and mTFP, were extracted from the gel. Both sequences were ligated together using T4 ligase, using a 3:1 ratio of mTFP to vector. Following ligation the sequence was transformed into One Shot ccdB Survival 2T1^{R} Competent cells (Invitrogen) and incubated overnight on LB Agar plates containing 100 µg/mL ampicillin, 30 µg/mL chloramphenicol. The next day 5 colonies were selected, scratched on a new agar plate and colony PCR performed. Part of the reaction was used, to check the size of the band, the rest was purified using chloroform extraction (See later). Restriction maps were generated for the resulting pUAS-mTFPvector containing N-terminal mTFP tag and two diagnostic restriction digests performed on a small fraction of the DNA, using different enzyme pairs. The restriction digest was subject to electrophoresis and bands at the correct size observed. Cultures were mini-prepped using Qiagen mini-prep kit, and pUAS-mTFP was sent for sequencing analysis using the pTVW-1091 primer pair. Using the correct sequence an Invitrogen LR Clonase II reaction (Invitrogen) was performed using the Lifeact entry vector (pDONR) and the mTFP modified destination vector, DNA was transformed into One Shot ccdb Survival 2 T1^{R} Competent cells

(Invitrogen). The expression vector was sent to be sequenced to confirm no changes in sequence had occurred during the clonase reaction. Correct cultures were midi-prepped and both cell cultures (50 % glycerol) and DNA stored at -80°.

Primer Design

The oligonucleotides were designed using Primer 3 and synthesized by Eurofins MWG|operon. The lyophilised primers were diluted in Tris-EDTA (TE) buffer, pH 8.0 making 100µM stocks and stored at -80°C. Working stocks of 10uM were made with double distilled water and stored at -20°C.

Primer Name	Forward Sequence (5' – 3')	Tm °C	Reverse Sequence (5' – 3')	Tm °C
N- Teal	AAGGTACCCTGCAGTGAATT CGGAGCTCCGCCACCATGGT GAGCAAGGGCGAGGAG	>75	TACCGGTTGCTTGTACAGCTC GTCCATGCCGTC	73.2
pTVW-1091	CAAGCGCAGCTGAACAAGCT AAAC	62.7	GAAACTGCCGGAAATCGTCG TGG	64.2
M13	GTAAAACGACGGCCAG	45.9	CAGGAAACAGCTATGAC	44.6

Table 2.1. Shows a table of primers generated and used to generate N-mTFP destination vector.

Forward and reverse sequences are given with the melting temperature.

Restriction Enzyme Digestion

The buffer required is specific to each enzyme, see table 2.2 below for specific details; re buffer type, DNA concentration and restriction enzyme used. DNA was incubated for 3 hours at 37°C, followed by 65°C for 10 minutes stops the reaction. The product was then

separated on a gel by electrophoresis and the size of the cleaved bands compared with the predicted sizes.

Sequence	Buffer Used	Enzyme 1	Enzyme 2	Fragment Sizes
1091 Destination Vector and mTFP Sequence (Sticky ends)	NEBuffer 1.1	Kpn1	Age1	10796bp and 777bp
mTFP Destination Vector (Diagnostic 1)	NEBuffer 1.1	Kpn1	Age1	749bp and 10796bp
mTFP Destination Vector (Diagnostic 2)	NEBuffer EcoRI	Eco R1	Eco R1	1192bp and 10354bp

Table 2.2. Shows a table of restriction enzymes, buffers used and size of fragments expected. Restriction enzymes were used to generate the sticky ends in the mTFP sequence and to excise the Venus sequence from the 1091 Destination Vector. They were also used as a diagnostic tool to determine mTFP insertion at the correct place and right orientation.

Buffer Contents:

1X NEBuffer EcoRI:
100 mM Tris-HCl
50 mM NaCl
10 mM $MgCl_2$
0.025% Triton® X-100
pH 7.5 @ 25°C

1X NEBuffer 1.1:
10 mM Bis-Tris-Propane-HCl
10 mM $MgCl_2$
100 µg/mL BSA
pH 7 @ 25°C

Polymerase Chain Reaction (PCR)

DNA fragments were amplified using *Taq* PCR Core Kit (Qiagen) or Platinum pfx (Invitrogen).

PCR reaction mix was set up as follows:

Components	
DNA Template	0.75 µL
Primers 1 & 2 (10mmol)	1 µL (each)
dNTPs (12.5mM each)	0.6 µL
Distilled Water	up to 20 µL
10x reaction buffer	2 µL
DNA Polymerase (Taq) (2.5 U/µL)	0.2 µL

Modified for the Platinum pfx kit (excludes Taq)

$MgSO_4$	0.4 µL
Pfx	0.25 µL
Final volume	20 µL

The Cycling times were as followed for each reaction:

Amplifying mTFP (Primer pair N-Teal): Invitrogen Platinum *pfx* Kit

Initial denature	94°C - 2.5 mins
	92°C – 30 secs
	60°C – 30 secs
	68°C – 1 min
Final Extension	68°C – 10 min

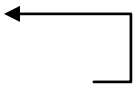

30 cycles

Colony PCR (Primer pair pTVW-1091): Taq Core PCR Kit

Initial denature	94°C - 2.5 mins
	92°C – 30 secs
	60°C – 30 secs
	72°C – 1 min
Final Extension	72°C – 10 min

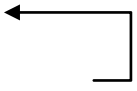

30 cycles

PCR products were used immediately, ran on a gel or stored at -20°C for later use.

Gel Electrophoresis

Agarose gels (1.2 %) were prepared by heating high gelling temperature agarose (Bioline) in 1×TAE buffer (0.04 M Tris-acetate, 1 mM EDTA) with Ethidium bromide (0.2-0.5 µg/mL). Samples were diluted with 2 µl 1× loading buffer (30 % v/v glycerol, 0.25 % bromophenol blue) and loaded into the gel. Samples subject to electrophoresis in 1 x TAE buffer at 100 V for 45 minutes, using Jencons Ltd gel electrophoresis equipment. Five µL of SmartLadder (Eurogentec) DNA ladder was used as the molecular weight marker. DNA fragments were visualised using an ultraviolet light source (UVi-tech) and documented with a video camera system (UVi-tech) and P90 thermal printer.

DNA Purification – Gel Extraction Using Qiaquick Gel Extraction Columns

Extraction of DNA from low gelling temperature (LGT) agarose was performed using Qiaquick gel extraction spin columns (Qiagen) according to the manufacturer's instructions. Gel slices containing the DNA band were cut from the gel, placed in a micro centrifuge tube and heated to 55°C for 10 minutes with chaotropic salts, melting the agarose. The solution was added to the Qiaquick columns and the DNA absorbed to the silica-gel membranes. Contaminants were removed by several washes, and the DNA eluted with TE. The samples were quantified using NanoDrop Spectrophotometer.

DNA Purification – Chloroform Extraction

Water was added to the finished PCR mix, to a total volume of 50 µL. 100 µL chloroform (BDH AnalaR) was added and mixed by shaking. The reaction was placed in a centrifuge at room temperature for 3 minutes at 14000rpm. The aqueous phase was removed and 5 µL sodium acetate (BDH) and 1 µL glycogen (Boehringer Mannheim) was added to it and mixed in a clean tube. Two volumes of ice cold 100 % ethanol was added and it was incubated on

ice for 30 minutes, allowing precipitation to occur. DNA was collected by centrifugation at 12000 rpm for 5 minutes. The supernatant was carefully removed and 500 µL of 70% (v/v) ethanol added to remove the electrolytes, mixture was incubated at room temperature for 5minutes. Following this the supernatant was carefully removed again and the DNA left to air dry. DNA was re-suspended in 10 µL double distilled water. The samples were quantified using NanoDrop Spectrophotometer.

DNA Ligation

The DNA ligation reaction was carried out with a vector/teal excess (40 ng/10 ng). Samples were incubated together with T4 Ligase and T4 Buffer overnight at room temperature to enable the ligation to occur (Approximately 16°C). The following day samples were incubated at 65°C for 30 minutes to stop the ligation reaction.

Transformation Into Competent Cells

Gateway® LR reactions were performed to shuttle the Lifeact ORF from the pDONR entry vector into the modified destination vectors pTVW mTFP (DGRC). 50-150 ng of the entry clone containing the gene of interest was mixed with 150 ng of the destination vector and TE buffer pH 8.0, to give a final volume of 8 µL. The LR clonase II enzyme mix (Invitrogen) was thawed on ice for 2 minutes, vortexed briefly, then 2 µL of the enzyme mix was added to the reaction mix. Reactions were incubated at 25°C for 1.5 hours. Following incubation, 1 µL of Proteinase K (Invitrogen) solution was added to the reaction mix and incubated at 37ºC for 10 minutes to stop the reaction. Five µL of the reaction mix was then transformed into One Shot® Top10 Chemically Competent Cells (Invitrogen). The transformed cells were plated onto ampicillin-LB agar plates and incubated at 37°C overnight.

For each transformation one vial of One Shot ccdB Survival 2 $T1^R$ competent cells (Invitrogen) were used, slowly thawed on ice and 1-5 µl of the DNA (10 pg to 100 ng) added and mixed gently. The cells were incubated on ice for 30 minutes before being heat shocked at 42°C for exactly 30 seconds. Following heat shock, the cells were placed on ice for two minutes and 250 µl of pre-warmed S.O.C Medium (Invitrogen) added to each vial. The vial(s) were then shaken horizontally at 225 rpm for 1 hour at 37°C in a shaking incubator before each transformation reaction was spread on pre-warmed selective plates. The plates were inverted and incubated overnight at 37°C. The following day colonies were picked and analysed by restriction digestion and sequencing.

Qiagen Mini/Midi Preps

QIAprep spin columns bind and purify DNA using simple bind-wash-elute procedure according to manufactures instructions (Qiagen). The overnight cell culture media was re-suspended, lysed and neutralised using solutions provided in the Qiaprep kit by centrifugation. The clear lysate was placed into one of the Qiaprep spin columns and through several centrifugation steps was firstly bound to the silica membrane, impurities washed away and then eluted in 30µl elution buffer (10 mM Tris·Cl, pH 8.5) as per instructions.

Sequencing

Plasmids were sent off to GATC Biotech in concentrations of 30-100 ng/µL dissolved in 30 µL volumes of water and PCR products at a concentration of 10-50 ng/µL. In addition primers were sent (30 µL at 10mM) for each of the samples to be sequenced. Sequence output files were analysed using DNA Star.

2.6. Testing mTFP Expression

2.6.1. Expression in S2 Cells

To test the UAS-mTFP construct to ensure the Teal can be expressed *Drosophila* S2R+ cells were used. For transient transfection S2R+ cells were plated at 3.5 x 105 in 4 mL growth media (approximately 60% confluency) in 6 well dishes. The cells were then transfected with Cellfectin (Invitrogen) as per manufacturer's instructions. Briefly, 1 µg plasmid DNA and 1 µg GAL4 construct was added with 15 µL Cellfectin to a total volume of 200 µL and incubated for 30 minutes at room temperature. The Cellfectin–DNA complexes were mixed with 800 µL complete Schneider's Medium (Containing 10% (v/v) FCS, 50 Units Penicillin and 50 µg Streptomycin) to aid faster diffusion and directly added to the cells. Cells were incubated for 24 hours at 25°C following transfection. The following day 1 mL of the DNA-Cellfectin mix was removed and replaced with 3 mL complete Schneider's Media. GAL4 expression was induced 18-22 hours before imaging using 1 mM $CuSO_4$ in media and left at 25°C until imaging.

2.6.2. Generating UAS-mTFP Flies

DNA (30-50 µg Qiagen purified) was sent to Genetic Services (www.Geneticservices.com) for site directed injection of the MTFP-Lifeact Construct. In brief, Genetic Services purified the DNA prior to injection, injected 30-100 embryos and reared them to adulthood. The G_0 injected adults were crossed to w1118 adults then transformant flies collected to generate independent lines.

2.6.3. Expression in Third Instar Larvae

Virgin female *engrailed-GAL4* (Guillen et al., 1995) flies were crossed to *UAS-mTFP* males. Flies were left to lay for 24 hours before being moved on to new vials, five days later wandering third instar larvae were imaged using a Leica ZF10 stereo dissecting microscope. The same settings were used to enable comparison across the different lines.

3. Development of Tools and Techniques for Live Cell Imaging *in vivo*

3.1. Introduction

Border cell migration is a part of normal cellular development of the *Drosophila* egg chamber. A group of 6-8 follicle cells become specialised, detach from their surrounding epithelia and form a cluster of cells, which then migrates from the anterior to the posterior end of the egg chamber (at stage 9) until it reaches the oocyte-nurse cell boundary (at stage 10) (Montell, 2003).

One key property of border cell migration is that it can be analysed in a quantitative manner to assess the effect of different genes on migration, using the retracting anterior follicle cells as a guide to normal border cell position (bcp). The retracting anterior follicle cells migrate towards the oocyte at a rate similar to the border cell cluster, with the cluster positioned a similar distance away from them throughout (Figure 3.1).

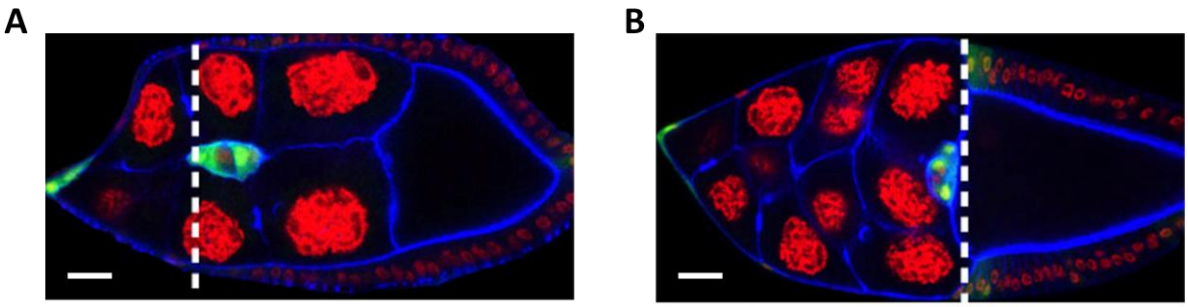

Figure 3.1. Border cell position in wild type egg chambers. (A) Shows a late stage 9 egg chamber from a slbo-GAL4, UAS-GFP His2A-RFP female. White line indicates the most anterior follicle cell position. Measurements of distance migrated were taken from the centre of the cluster to the line. **(B)** Shows a stage 10a egg chamber from a slbo-GAL4, UAS-GFP His2A-RFP female. White line indicates the most anterior follicle cell position at the oocyte-nurse cell boundary; migration at stage 10a was expressed as a percentage of the distance from this point to the anterior tip of the egg chamber. **(A-B)** Histone2A is in red, F-actin staining is shown in blue. White solid line represents 15 µm.

The exact position of the cluster in relation to the retracting follicle cells can differ depending on the border cell specific driver and the fluorescent reporter used, which will be discussed in more detail later in this chapter.

To further understand border cell migration and the mechanisms involved it has been important to develop a technique to culture and image live egg chambers using time-lapse microscopy (Figure 3.2.). Live imaging of border cell migration has the potential to provide greater insights into the behaviour and molecular dynamics of the cluster as it progresses towards the oocyte. Analysing border cell migration by live imaging is superior to using fixed samples, as these only show a brief snap-shot of the entire process, so key information can be lost.

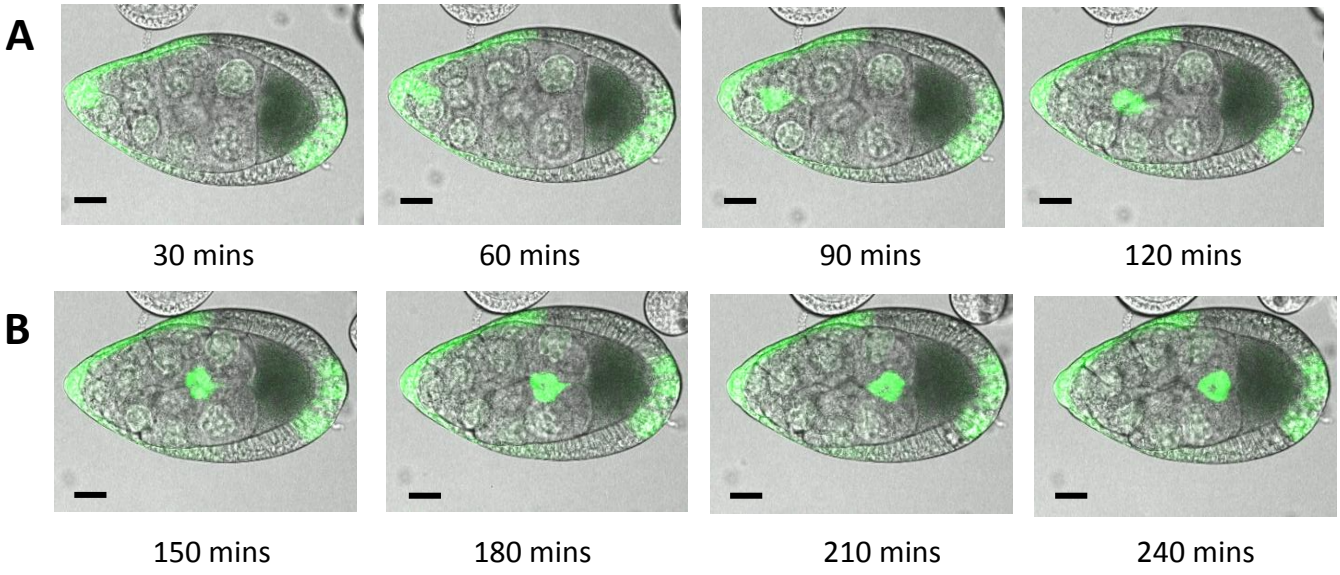

Figure 3.2. Shows the complete border cell migration in *slbo GAL4, UAS GFP* egg chambers, images acquired by live imaging. Frames 30 minutes apart were selected to demonstrate**, (A)** The first half of migration, characterised by an elongated, polarised cluster, and **(B)** The second half of migration, characterised by a more rounded appearance. Black solid line represents 20 µm.

Regulating and optimising the conditions needed for border cell migration is crucial to enable border cell migration to be imaged; a large amount of time was spent in this thesis trying to develop the right conditions and to optimise dissection procedures. As described in the Methods (Section 2.3), border cell imaging and dissection is a very sensitive procedure.

3.1.1. Aims

The main aim of this chapter is to outline the steps taken to develop protocols to successfully culture and image live egg chambers during border cell migration. Particular attention will be given to problems that were encountered and stages of the protocol deemed as critical to ensure the normal movement of the cluster during imaging. The protocol that was developed in this thesis will be discussed and compared with existing protocols, as well as the measures taken to try and prolong the time during which egg chambers could be imaged before signs of deterioration were observed.

3.2. Medium Optimisation

The composition of the culture medium for live imaging of egg chambers must be finely tuned if it is to sustain egg chamber development over the entire duration of border cell migration (up to 3-5hours). There are few laboratories who have successfully cultured live egg chambers and each have their own adaptations of an original protocol published in 2007 (Prasad et al., 2007).

Below is a summary table of the different medium components used by the various institutions.

Source of media composition	This thesis	Prasad *et al*	Prasad & Montell	Bianco *et al*, Poukkula *et al*, Lucas *et al*	Tekotte *et al*
Main Component	Schneider's Insect Media	Schneider's Insect Media	Schneider's Insect Media	Schneider's Insect Media	Halocarbon Oil
Insulin	1 µg/mL	200 µg/mL	200 µg/mL	5 µg/mL	NA
Serum	15 % FBS	15 % FBS	10 % FBS	2.5 % FCS	NA
Antibiotic	1 µg/ml Pen/Strep	0.6x Pen/Strep	0.6x Pen/Strep	NA	NA
pH	6.95-7.10	6.95-7.00	6.86-6.90	NA	NA
Additional Reagents	NA	NA	NA	2 µg Trehalose 5µM Methoprene 1 µg/mL 20HE 50 ng/mL Adenosine deamidase	NA

Table 3.1 Comparing the different media compositions. The composition of the media used in this thesis is a modified version of that reported by (Prasad et al., 2007). The media generated by (Bianco et al., 2007) has more reagents than the others with (Tekotte et al., 2007) imaging media consisting only of halocarbon oil. NA = No Addition

The Montell research group published two papers in 2007 (Prasad et al., 2007; Prasad and Montell, 2007) both with slightly different formulations of the medium; these in turn are noticeably different to the medium used by the Rorth group (Bianco et al., 2007), which contains additional reagents, trehalose (non-reducing sugar found in insects and animals), methoprene (Juvenile hormone), 20HE (ecdysteroid hormone) and adenosine deamidase (metabolic enzyme). The medium utilised in this thesis was based on the original Montell group formulation (Prasad et al., 2007), but with specific modifications that were made through several optimisation stages, as described below.

3.2.1. Schneider's Insect Medium

Schneider's insect medium is a mixture of amino acids, electrolytes and sugars and is the main constituent of all of the medium protocols. This was important when dissecting and imaging the tissues, as it mimicked the chemical properties of the insect bodily fluid, allowing the egg chamber to develop, as it naturally would. Keeping the medium as fresh as possible reduced the chance of failed migration, as it prevents deterioration of critical elements within the medium. Through trial and error, the shelf life of the Schneider's medium was established; complete medium was only ever made fresh on the day of use.

3.2.2. Serum - Fetal Bovine Serum/Fetal Calf Serum

Serum was needed to supplement the Schneider's media to promote growth and development of the egg chamber. Both Fetal Bovine serum (FBS) and Fetal calf serum (FCS) have been documented as being used for the live culturing of egg chambers. The live cell imaging experiments performed in this thesis were performed using FBS, however FCS was used at the same concentration and no problems were apparent. Very little batch-to-batch variation was observed using FBS, but batches were still kept constant where possible. In mammalian cell culture investigators commonly test a few batches, then bulk re-order the ones that worked best. It was found that a slightly older batch bought into the lab enabled a higher success rate in preliminary testing experiments. In these experiments egg chambers were dissected and border cells left to migrate in droplets of medium on coverslips, the approximate border cell position was noted at 0 and 4 hours post dissection and the percentage of egg chambers showing migration noted. FBS was used in a relatively high concentration (15 % (v/v)) compared to some of the published protocol (e.g. 2.5 %). This higher concentration was based on the recipe of (Prasad et al., 2007). One potential

drawback of using higher concentrations of serum in the media is the promotion of bacterial growth in the media whilst imaging, which was observed (data not shown) when leaving serum-containing media in the microscope room, when compared to incomplete medium. However, this was not observed to be a huge problem when imaging over 4-5 hours using media that had been made fresh the day of the experiment. Fresh FBS aliquots were made and frozen, due to the fact that live cell imaging can be a very sensitive procedure and minor differences such as those found in different batches of serum, or media, may result in changes in results, failed or abnormal migration.

3.2.3. Insulin

The Bianco *et al* (Bianco et al., 2007) and Poukkula *et al* (Poukkula et al., 2011) protocol has the lowest Insulin concentration of all the protocols (apart from in this thesis). This may be due to the fact that when quantifying border cell migration, data extraction begins after the cluster has fully detached from the epithelium, therefore, egg chambers may have been dissected with border cell clusters already detached. Imaging this initial detachment phase can be useful however, even if it is not critical for the experiment, because it establishes an approximate age of that particular egg chamber. It was found that depending on the genotype, the border cell cluster position may differ and be slightly ahead or behind the retracting follicle cells in 'Wild type', making the detection of impaired migration more difficult. Therefore, by imaging the detachment stage, based on experience and published border cell migration durations, approximations can be made to estimate where the cluster should be at a specific time. Two forms of insulin were used on a trial basis during media optimisation: a ready-made solution (Sigma I0516), and a powdered form (Sigma I6634). Initially the ready-made solution was used for convenience. However, it soon became

apparent that the aged insulin solution reduced the success rate of complete migration. This was evident as border cell clusters did not detach from the surrounding epithelium in early stage 9 egg chambers, although they would often continue migrating if detachment had already occurred. It was apparent that the insulin solution was not fit for purpose, especially if the solution had aged 5 to 6 months. To overcome this, the powdered form was trialled and a liquid solution made on a weekly basis and stored at 4 degrees. Trial and error showed a stock solution of dilute hydrochloric acid (HCL) (pH 5) was sufficient to reconstitute the Insulin powder and to allow Insulin addition to the media, without drastically altering the pH of the entire media. A low concentration of insulin (1 µg/mL, compared to 5-200 µg/mL) was used as it was found to be sufficient for migration; higher concentrations were also trialled during the optimisation steps, using concentrations similar to that used in Bianco *et al*, Prasad *et al,* however, it was found the larger concentrations were not needed. The presence of insulin in the complete medium is important especially, if the first part of migration is crucial for data analysis, in particular the initial detachment phase.

3.2.4. Media pH

pH plays a role in the success of border cell migration, although in this thesis it was found that higher pH values than those previously reported (Prasad et al., 2007) were optimal. A pH 6.86 - 6.90 was recommended, but values of 6.95-7.00 worked more robustly. A slightly higher pH of 7.10 still enabled border cell migration. However, to remain consistent throughout, the pH was adjusted to 7.00 when making the medium.

3.2.5. Additional Reagents

Other laboratories have a more complex media composition and have the addition of

trehalose, methoprene, 20HE and adenosine deamidase (Bianco *et al* 2007). These are all additional elements, such as sugars and hormones, that aid in the development of the egg chamber and help mimic the natural chemical environment of the egg chamber.

Even though these may aid the border cell migration process, initial positive results during experiments performed here obviated the need for these supplements to be added.

An additional protocol reported for culturing egg chambers utilised halocarbon oil as the mounting media (Tekotte et al., 2007). One of the main benefits of this protocol is the high refractive index of halocarbon oil, which is similar to glycerol so enables better imaging quality (Davis and Parton, 2006; Parton et al., 2010). The negative aspect of this protocol is the lack of time the egg chambers can be imaged for (2-4 hours), so the entire border cell process cannot be imaged.

3.3 Dissection

It was important to use sharp forceps and to dissect quickly and carefully when preparing egg chambers for live imaging, as the egg chambers continued to develop during dissection and any damage caused migration to fail.

3.3.1. Quality Control

Ensuring the egg chambers were not damaged during the dissection process was difficult because tissue damage is not always easy to recognise. Damage was only noticeable once egg chambers had been mounted and were ready to be imaged. Therefore any doubts or inclinations that an egg chamber had been touched or damaged resulted in its disposal. Culturing of damaged egg chambers impeded the development of healthy egg chambers,

presumably because crucial nutrition from the media became exhausted or because of release of toxic signalling molecules from the damaged samples. Another measure that had to be taken when dissecting, was the removal of larger, more mature egg chambers from the ovarioles. This served two purposes: first it prevented the uptake of nutrients in an egg chamber that suited no purpose in the experiment; and, secondly it prevented the egg chamber of interest being pushed from the field of view during imaging by the growth of a more mature one. To remove the mature egg chamber, a shearing method was used similar to that when separating the two ovaries. Care was taken to position the forceps towards the mature egg chamber and a saw and scrape method was applied, in a direction away from the chamber of interest. If the plastic base was damaged during this process this was found to cause issues once the string of egg chambers needed to be transferred to the imaging dish. The interconnecting tissue from the egg chamber of interest and the mature chamber occasionally became caught on the abrasive surface during shearing. Transfer using a pipette tip resulted in the removal of the medium alone; pulling on the egg chambers to release them stretched the egg chamber and caused damage. It was found that the germanium could be released by further scratching the surface and the egg chamber rescued, but as mentioned above if damage was suspected it was better to continue dissection using a different egg chamber. A critical part of the dissection process was avoiding touching and damaging the egg chambers. Damaged egg chambers appeared to develop normally, but frequently displayed failed or arrested border cell migration. It was therefore, important that damaged chambers were not confused with egg chambers that were unable to migrate due to genetic manipulations, intended to investigate gene function. In some cases where migration had already started and egg chambers were

damaged, migration continued, but the surrounding nurse cells and tissues collapsed and started to deteriorate (see Figure 3.3); these egg chambers were not used for analysis.

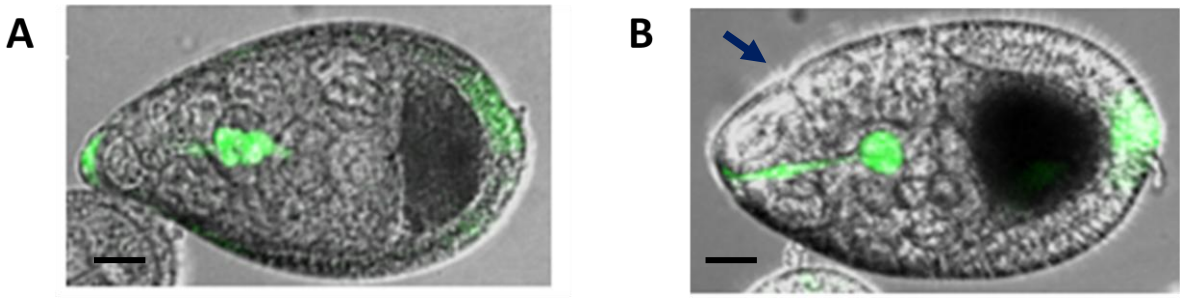

Figure 3.3. Shows representative *slbo GAL4, UAS-GFP* stage 9 egg chambers, that are normal and damaged. (A) Shows a normal looking egg chamber about halfway through migration, note the small oocyte at the posterior end, egg chamber is slightly elongated with smooth edges, retracting follicle cells are in line with the border cell cluster. **(B)** Shows a damaged egg chamber, in this example the cluster is not fully detached from the epithelium at the anterior end. Note migration is continuing despite the egg chamber deteriorating around it, the oocyte is larger and the nurse cell-oocyte boundary less clear. Blue arrows indicate a more rounded egg chamber shape lacking smooth outside edges. Solid black line indicates 15 µm scale bar.

3.4. Mounting

Mounting the egg chambers was a critical part of the entire process and could have easily resulted in perfectly good egg chambers going to waste, because they could not be imaged. Three key aspects to be considered were identified in the course of these studies and will be discussed in the sections below: imaging dish selection, egg chamber transfer and dish preparation/finalisation.

3.4.1 Lumoux Dish

The majority of live imaging experiments performed in this thesis utilised Greiner 50 mm Lumoux dishes (Sigma Z376744/Sarstedt 94.6077.410) to image the egg chambers. These dishes are specially designed with a gas permeable base to allow O_2/CO_2 transfer, which is important when culturing live cells.

The egg chambers were mounted in a droplet of fresh medium between two pieces of broken 22mm^2 coverslip, which acted as a platform for an additional cover slip to sit on. This served several purposes: it generated space between the cover slip and membrane base, which prevented the tissue from being crushed and or becoming growth restricted; it enabled adequate gas exchange to sustain development; and, finally it provided a deep well to pool sufficient medium to maintain the tissues for longer.

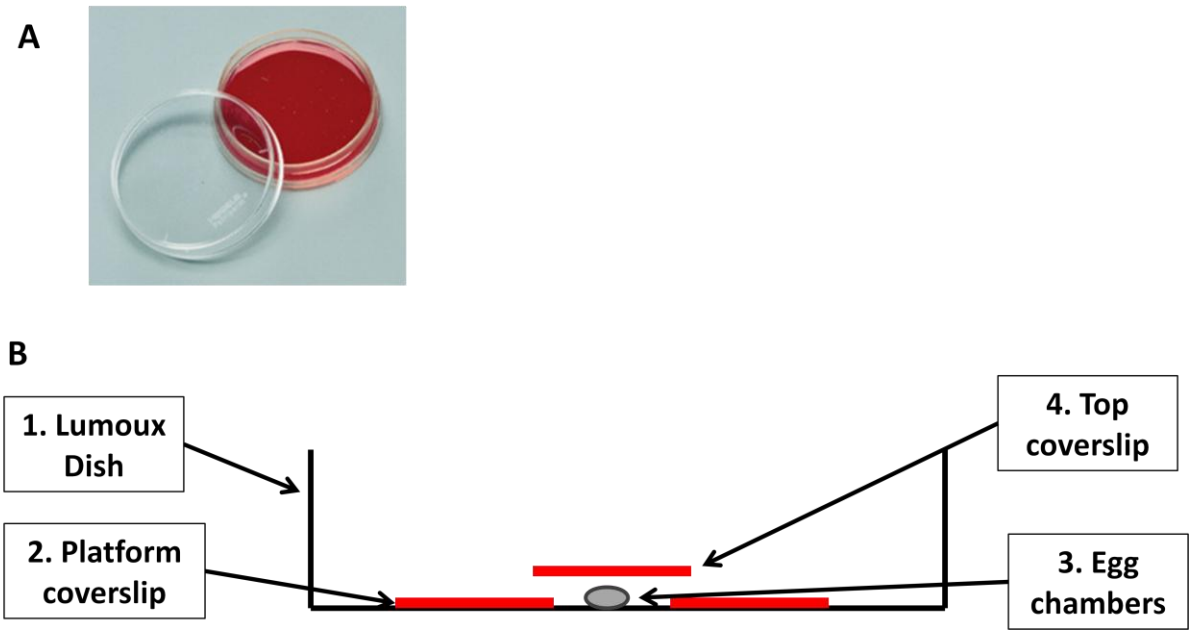

Figure 3.4. Shows the Lumoux dish used for live imaging and a schematic of the mounting protocol. **(A)** Shows the lumoux dish (with coloured medium), image taken from the Sarstedt online catalogue. **(B)** Shows the various aspects of the lumoux dish when imaging live egg chambers. The platform cover slips seen in label #2 are used to prevent the top cover slip (#4) from squashing the egg chamber (#3) positioned in between the two. The area surrounding the platform cover slip is covered in halocarbon oil (not shown).

I encountered very few problems with the standard mounting protocol for these dishes. One of the critical parts of mounting border cells could be applied to any dish being used, as all egg chambers need to be transferred from the media to the imaging dish.

Transferring the egg chambers to the dish was a potential step in damaging the egg chamber and thus preventing border cell migration. To overcome this, the end of the pipette tip was cut to widen the entrance when aspirating the egg chamber; a larger volume of medium than needed for each egg chamber was also taken and placed to form a large droplet. When using this method it was important to take away some of the excess medium once the egg chamber had been transferred. Excess medium caused issues when adding further egg chambers to the droplet, as it could cause the droplet to spread and cover the platform coverslip. In addition, although the gas permeable base is hydrophilic and provides a good surface for the egg chambers to adhere to, excess medium was found to cause the egg chambers to move during imaging. This is most probably due to changes in air temperature around the imaging dish (despite using a temperature controlled platform) and increased temperature generated during the imaging process. Conversely, however, too little medium impeded full migration, possibly due to consumption of nutrients within the medium. Halocarbon oil, which was applied around the platform and top coverslip, at the air/media boundary, allowed free diffusion of oxygen, has low viscosity and is used predominantly to reduce evaporation of the imaging media, and preventing hypoxia. Excess halocarbon oil resulted in the egg chambers moving around, and too little caused the egg chambers to drift due to movement during capillary action to fill empty spaces.
On the whole, the Lumoux dish was found to be excellent in enabling border cell migration to be imaged successfully. However, it was found there were issues when using these dishes

to image multiple positions (egg chambers) during one experiment using an immersion objective, where the objective needed to be in contact with the pliable membrane. This was a problem for two reasons: pressure from the objective moved the delicate, permeable membrane resulting in egg chambers being pushed out of the field of view and also it covered the gas permeable membrane affecting gas exchange. Immersion objectives offer better optical qualities enabling more detailed images to be taken of the border cell process. One way around this problem might be to use an imaging dish with a solid base. However, Prasad et al (Prasad et al., 2007) suggested that imaging on glass bottom dishes is not possible, since the egg chambers fail to migrate due to lack of gas diffusion to the egg chambers. To investigate this issue, different solid base dishes (Figure 3.5) were adapted and trialled to culture egg chambers for live imaging.

Figure 3.5. Solid base imaging dishes. (A) Iwaki dish (Iwaki 3931-035), these are small circular polystyrene dishes (35mm) that contain a small well (12mm) with a glass bottomed base. **(B)** Greiner CellView cell culture dish (Greiner 62786) with a glass bottomed base (35mm). **(C)** CellView cell culture dish. Red squares indicate positioning of broken pieces of cover glass used to make a platform for a cover slip to sit on, to allow gas exchange from the top/sides. Images taken from online catalogues from retailers.

3.4.2 Iwaki Dish

Initially it was decided to test Iwaki dishes (Iwaki 3931-035), which are circular polystyrene dishes (35 mm) that contain a small well (12 mm) within the surrounding plastic with a glass bottomed base. The glass is specialised for fluorescent imaging of live and dead cells at higher magnification and resolution. The egg chamber transfer procedure was similar to that used with Lumoux dishes, where excess medium was aspirated and then taken away, leaving behind a round droplet of media containing the egg chambers. The small size of the well meant that no coverslip was needed over the medium. Results from this were positive and border cells migrated successfully, once they had already started. One negative to using these dishes however was a slight amount of egg chamber movement at the beginning of the imaging process. This was most likely caused by changes in temperature experienced by the samples during egg chamber dissection and mounting, and when placed on the temperature controlled platform. To overcome this, samples were left for 10-15 minutes on the microscope platform prior to imaging to let them acclimatise. Following this, drift and movement were only rarely observed and evaporation seemed to be minimal. One reason for this may be due to the smaller surface area of the well and the increased volume of medium that could be used for imaging, compared to the thin flat surface using the Lumoux dish. Gas exchange did not appear to be a limiting factor despite the presence of a solid base. Unfortunately due to problems with availability from the supplier, it was impossible to obtain more of these dishes in a timely fashion for further experiments.

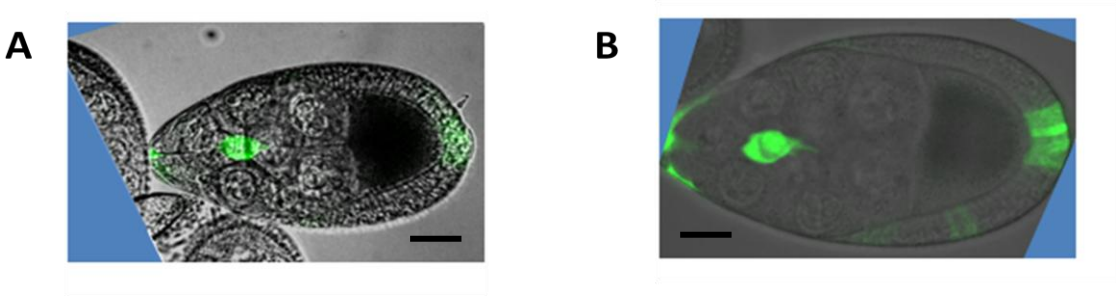

Figure 3.6. Representative images showing the difference between imaging using the Lumoux and Iwaki dishes. Both egg chambers are *slbo GAL4, UAS-mCD8-GFP* at late stage 9 and are a representative size for the field of view. **(A)** Egg chamber imaged using the Lumoux dish, imaged with a 20x Fluar 0.75 NA air objective, 1.5 zoom. Black solid line represents 30 µm scale bar. **(B)** Egg chamber imaged using the Iwaki dish, imaged with a 40x Fluar 1.3 oil objective, 1.0x zoom. Note the egg chamber is larger in the field of view and has increased detail. Extensions from the cluster can be clearly seen. White arrow points to extensions in both images. Images have been rotated only for accurate comparison, and the background filled blue for clarification. Black solid line represents 15 µm scale bar.

3.4.3 Greiner Dish

Due to lack of availability of Iwaki dishes, another circular dish, the Greiner CellView cell culture dish (627861) was trialled. The Greiner dishes are 35 mm disposable plastic dishes with a highly transparent borosilicate glass bottom, embedded into the plastic. The main difference between these and the Iwaki dishes is the size of the well in the bottom of the dish, the Greiner having a larger diameter. The first problem that was found using these dishes was that the egg chambers did not appear to adhere to the base and imaging without a coverslip resulted in extensive movement out of the field of view. In the first instance, the bottom of the wells were covered with Poly-L-Lysine (Sigma, P4707), as described in Bianco et al 2007, in which an 8 well chambered cover glass was coated for a similar purpose. However, despite using an adhesive cover on the base, the egg chambers still moved during imaging, especially if multiple positions were being imaged. This was most likely due to

small movements being exaggerated by having a larger amount of medium in the well. However, viewing the egg chambers several hours later showed that migration had occurred. Placing a cover slip over the well to prevent the movement of media within the well resulted in failed migration, presumably due to lack of gas exchange, so this was not a viable option.

In attempts to overcome this issue, broken pieces of 22 mm cover slips were used to build a platform around the well (See Figure 3.5) and the cover slip placed on top. This resembled the platform technique used in the Lumoux dishes and was designed to allow gas exchange through the gaps at the side. Different heights of the platform were used to determine the best compromise between potential gas exchange, and sample movement. Unfortunately, once the height was sufficient to enable border cell migration, problems with drift and movement reappeared.

3.4.4. LabTek Chambered Glass Slide

Finally, in another attempt to image border cells using a solid based dish, the LabTek chambered 8 well cover glass slide (154534) was used as detailed in Bianco *et al* 2007 (Bianco et al., 2007). These cover slides are borosilicate coated and later covered with Poly-L-Lysine as described in the Methods. The main issue with these dishes was also in relation to egg chamber movement, and not the success of border cell migration. This was due to difficulties modulating the amount of imaging medium to place into each of the chambers. Similar to the Lumoux dish, the presence of too much medium caused egg chamber movement and too little caused migration to fail, presumably due to evaporation and exhaustion of nutrients. One advantage of successfully imaging border cell migration in these dishes was the ability to image multiple genotypes in one time lapse experiment, as

the different genotypes can be placed in different chamber compartments. Unfortunately, it was impossible to successfully image complete migration in this dish, due to egg chamber movement, although with further optimisation this might be possible.

3.5. Imaging

Time lapse images were taken on a Zeiss 710 inverted confocal microscope. During imaging the microscope was set to take several images at different Z positions in the same XY field, and then again at different XY locations. Time series were then set up so that multiple images could be taken at each position at a time frame specified, then repeated until the time scale had expired. The Zeiss 710 is an automated system, which allows experiments to be left running. Therefore, making minor adjustments, for example changing the focus or compensating for drift, was not easily possible. If necessary, scans were stopped and restarted after adjusting the Z position. If this was the case, detachment of the border cell cluster, the first half and the last part of migration were segregated into separate imaging files. Small adjustments were needed especially in the Z directions and especially if the Z stack programmed was not very large. There are pros and cons to setting up a large Z stack. The first advantage is that it acquired a large amount of information, small drifts in Z focus were not a problem and the border cell cluster was always in focus, in any one optical slice. A disadvantage was that taking the Z stack was very time consuming and laser intensity was observed to damage the egg chamber over time and cause it to deteriorate quicker. Larger Z stacks meant that fewer positions on the stage could be imaged, especially when short time lapse intervals were required. The majority of the protocols for live imaging that have been reported take into consideration the need for multi-positional imaging. In instances where smaller time intervals are used (Poukkula et al., 2011) such as 1-1.5 minutes, fewer samples

are imaged, but are imaged at a higher magnification (63x). Due to the issues encountered with the glass bottomed dishes as discussed above, live imaging in this thesis was largely performed with the Lumoux dish using a 20x air objective.

	Myself	**Prasad *et al* (Nature)**	**Prasad & Montell**	**Bianco *et al* , Poukkula *et al*, Lucas *et al***	**Tekotte *et al***
Microscope	Zeiss LSM confocal	Zeiss Axioscope widefield	Zeiss Axioplan2 widefield	Zeiss LSM 510 Meta confocal Leica SP5 inverted confocal Zeiss LSM 780 confocal	Widefield Olympus inverted IX70 microscope
Imaging Time	4-5 hours	4-6 hours	4-6 hours	2-3 hours	<4hours
Time Interval	2-5 mins	2 mins	2 mins	1-2 mins	Not stated

Table 3.2. Comparing the different imaging set-ups used by different studies. Imaging time is defined as the amount of time a sample could be image before deterioration was observed; Time interval is the time between each frame.

3.6. Reporters for Border cell Detection

Fluorescently labelled molecules are routinely used to image cellular dynamics and/or monitor changes in the properties of subcellular structures or macromolecular complexes. The choice of reporter for border cell live imaging is an important aspect of the experimental design. It was critical that the reporter was expressed in the appropriate cell

type and that a suitable label(s) was utilised, especially when examining multiple parameters simultaneously. An important aspect of this thesis has been to generate and test different combinations of fluorescently-labelled proteins to assess their suitability for imaging border cell migration. Reporters were judged according to a number of criteria including: their signal-to-noise ratio, generation time, suitability for multi-channel imaging, and cytotoxicity.

3.6.1. Expression Pattern

To image border cell migration, reporter expression needed to be targeted to the population of motile cells that form the border cell cluster. This was done using the GAL4-UAS bipartite system in which a border cell specific driver linked to the activator GAL4 can drive UAS transgene or reporter expression (See Introduction, Section 1.3). Two GAL4 drivers, which have been extensively reported in the literature, were used to image border cell migration in this study: *slbo-GAL4* and *c306-GAL4*. *slbo* is a homologue of the C/EBP family of basic region-leucine zipper transcription factor (Montell et al., 1992) and is expressed in the follicle cells of the border cell cluster and the retracting centripetal cells, but not the polar cells. It has been shown to play a critical role in border cell migration, with *slbo* mutants unable to migrate or generate protrusions (Rorth et al., 2000). *slbo* expression is switched on early in the migration process when the follicle cells are becoming specialised to form the border cell cluster through the JAK/STAT signalling pathway. *c306-GAL4* is an enhancer trap line (Brand and Perrimon, 1993) with the *P* element (GawB) inserted downstream of an endogenous enhancer. *c306-GAL4* expression is switched on earlier than *slbo-GAL4*, and has a similar expression pattern to *slbo*, except expression is also observed in the non-migratory polar cells (Manseau et al., 1997; Montell et al., 1992). This results in

the border cell cluster resembling more of a ball of cells when imaged with a fluorescent protein, as the centre of the cluster (the polar cells) are also fluorescent. Using *c306-GAL4* has proved to be beneficial when needing to track the centre of the border cell cluster in a manual or automated way, as often maximum intensity projections were used and the centre of the cluster was calculated this way. However, having the centre of the cluster absent of fluorescence (as with *slbo-GAL4*) was found to make the manual tracking process easier when the cluster orientation was known, as the centre could be clearly identified.

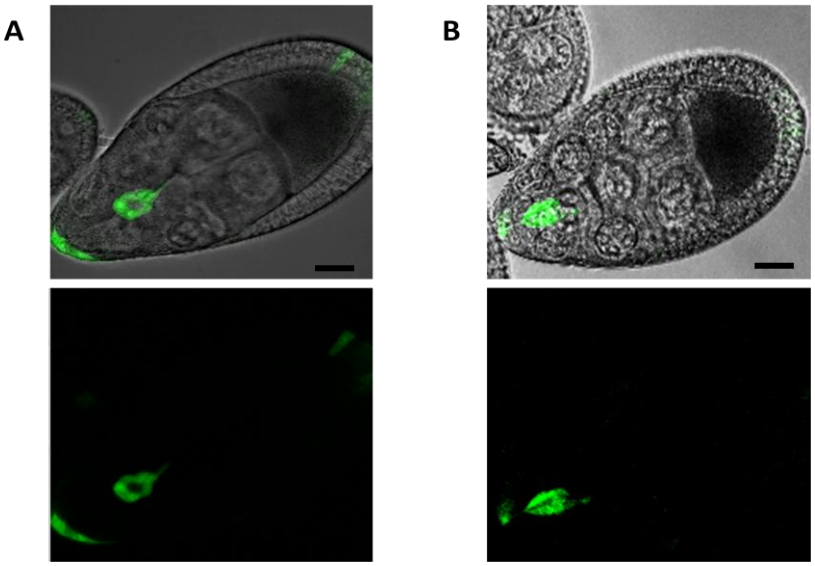

Figure 3.7. Shows the differing expression pattern of c306-GAL4 and slbo-GAL4 using *UAS-mCD8-GFP*. (A) Shows expression in *slbo-GAL4*, note the centre of the cluster (the polar cells) is absent of fluorescence. **(B)** Expression in *c306-GAL4*, note the entire cluster has GFP expression. Black solid line represents 15 µm scale bar.

3.6.2. Choice of Reporter

Enhanced Green Fluorescent Protein (eGFP) has emerged as an excellent fluorescent reporter, as it emits a strong signal when excited at 488nm. eGFP is derived from site directed mutagenesis of wild type GFP, from the anthozoan *Aequoria victoria* (jellyfish).

Mutagenesis of the GFP coding sequence has resulted in brighter, more stable variants of GFP with well-defined absorption profiles (Day and Davidson, 2009).

A range of fluorescently-tagged proteins were utilised in this thesis to visualise structures of interest and track cellular movements using time-lapse imaging.

Table 3.3 below lists fluorescent proteins used in this thesis, together with their excitation and emission wavelength, quantum yield and their relative brightness compared to eGFP.

Fluorescent Protein (acronym)	**Colour**	**Excitation (nm)**	**Emission (nm)**	**Quantum Yield**	**Relative Brightness (% of EGFP)**	**Quaternary Structure**
EGFP	Green	488	507	0.60	100	Monomer
EYFP	Yellow	514	527	0.61	151	Monomer
ECFP	Cyan	439	476	0.40	39	Monomer
mTFP	Blue	462	492	0.85	162	Monomer
dsRed	Red	558	583	0.79	176	Tetramer
mRFP1	Red	584	607	0.25	37	Monomer

Table. 3.3, showing the different fluorescent proteins that can were used to image border cell migration. The colour and structure are given in addition to the excitation and emission wavelengths, quantum yield and relative brightness as a percentage of EGFP.

The Zeiss 710 confocal microscope was equipped with five laser lines; 458 nm, 488 nm, 514 nm, 561 nm and 633 nm which influenced which flurophores/fluorescent proteins could be used.

Excitation and emission wavelength: It was important when selecting a flurophore that the microscope was equipped to visualise it. Specific fluorophores required specific laser excitation wavelengths. It was also critical that in systems where one or more fluorophores were present that there was no overlap in the excitation spectra. Overlap in the emission spectra can be an issue when trying to image two distinct populations of proteins and taking measurements of co-localisation. This overlap can be overcome if the two fluorophores are excited at different times with different wavelengths and their emissions collected separately. Where overlap was possible it was found it was always wiser to image separately using different imaging tracks and to narrow the detection of the emission spectra for each.

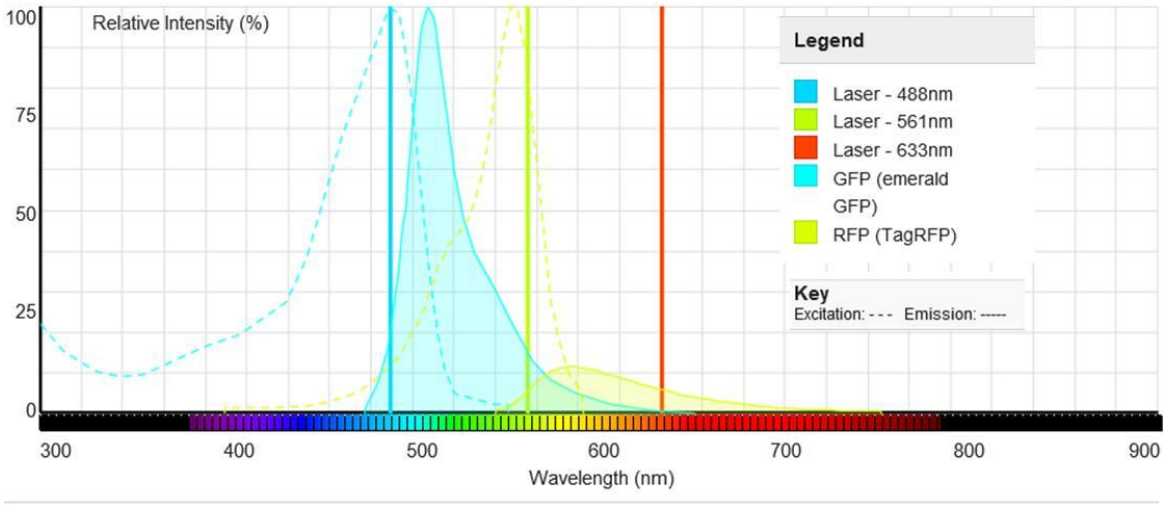

Figure 3.8 A graph generated in SpectralViewer (LifeTechnologies) showing key laser lines used on the Zeiss 710, and excitation/emission wavelengths of an example reporter combination used in this thesis. Laser lines are indicated by a solid vertical line in the corresponding colour, 488nm (blue), 561nm (yellow) and 633nm (red). Excitation peaks for each reporter (GFP and RFP) are indicated by a dashed line, emission peaks are displayed using a smaller dashed line (see key). The RFP emission peak is normalized by the GFP peak values.

Quantum yield: Microscope settings can only compensate slightly for dim fluorescence, the

intensity was, therefore, important when selecting reporters to use. If a structure is fine in detail and the fluorophore is dim, either due to its quantum yield or because the level of expression is low, detecting the light emitted is likely to be a problem. This was especially a problem for live imaging, since higher laser intensities (10-15 %) were observed to lead to photo-toxicity and bleaching. *UAS-eGFP* driven with either *slbo-GAL4* or *c306-GAL4* was found to be suitable for looking at the entire border cell cluster behaviour during migration, because the signal was bright. When the eGFP signal was thresholded it provided a simple indication of the centre of mass of the cluster (see Chapter 4, Section 4.4.1). This position could then be used, either by an automated software to detect high pixel intensity (see Chapter 4, Section 4.4) , or could be used by eye to track the movement of the cluster (see Chapter 4, Section 4.3.1 and 4.3.2). Although ubiquitous sub-cellular distribution was found to generate good signal to noise levels, targeting the reporter to different sub-cellular structures provided additional information about the dynamic behaviour of individual cells of the cluster. Targeting eGFP to the cell boundary of the border cells using CD8, a trans-membrane glycoprotein, enabled individual cells to be distinguished and the membrane protrusions to be more readily identified.

3.6.3. Generating mTFP-tagged reporter for F-actin

Although some sub-cellular structures, such as the plasma membrane were easily labelled with eGFP-tagged reporters, other structures can be more difficult to detect. We were interested in labelling actin-based protrusions, as these are the driving force for cellular locomotion and some of the proteins under investigation are known to regulate actin dynamics (see Introduction, Section 1.1). Filamentous actin can be detected with eGFP fused

to Lifeact. Lifeact (Lifeact-GFP) is a 17-amino acid peptide, which is a C-terminal eGFP fusion of the first 17 amino acids of a longer actin binding protein (Abp) Abp140-GFP. This peptide has been shown to stain F-actin structures in eukaryotic cells and tissues and does not interfere with actin dynamics (Riedl et al., 2008). Although this reporter was satisfactory for most purposes, we wondered whether it could be improved upon by utilising other fluorescent proteins with a higher quantum yield and better signal-to-noise ratio. Monomeric Teal fluorescent protein (mTFP) is a monomeric cyan fluorescent protein, often described as Teal, due to its position in the spectrum in between cyan and green fluorescent proteins. mTFP was identified as part of a synthetic gene library with MA484 variants of CFP all with a brightness greater than the wild type variant (Ai et al., 2006). mTFP has increased brightness [162 % of eGFP; (Day and Davidson, 2009)] and photo-stability relative to eGFP and a slightly different excitation/emission spectra (eGFP - 488/507 nm, mTFP - 462/492 nm) (Ai et al., 2006; Day et al., 2008). To generate fly strains in which F-actin was labelled with this improved fluorescent protein, a UAS-Lifeact-mTFP construct was made in three steps: 1) the Venus open reading frame in pTVW (Vector 1091 from DGRC) was replaced with mTFP; 2) the Lifeact reading frame was chemically synthesised and cloned into pENTR; 3) the Lifeact sequence in (2) was shuttled into the vector from (1) by Gateway cloning.

Validation of the destination vector (step 1): Having made pUAST-mTFP by PCR subcloning (see Methods 2.6), the functionality of the resulting Gateway destination vector was tested in S2R+ cells (Semi-adherent *Drosophila* cells) prior to further manipulations of the vector and injection into flies. Following transient transfection, expression of the mTFP was verified by fluorescence microscopy and spectral scanning, which was carried out to confirm the mTFP wavelength. The emission spectra of fluorophores can be broad and can result in

bleed-through to other imaging channels. Spectral imaging unravels the mixture of emission signals using linear unmixing formulas, from a fluorescent sample, resolving the signals into individual spectra. Scans of several fluorescent S2 cells showed that the peak emission of the cloned mTFP was approximately 495 nm (Figure 3.9), in line with the published literature (Ai et al., 2006; Day et al., 2008; Day and Davidson, 2009).

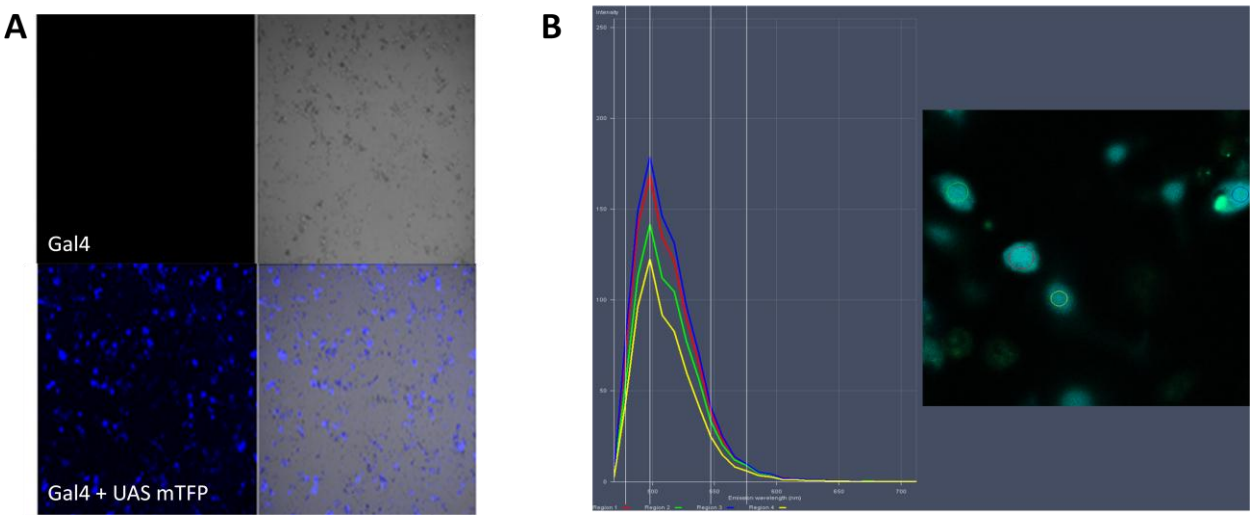

Figure 3.9. Shows S2R+ cells expressing (A) Metallothionein GAL4 driver (DGRC1042) and Metallothionein GAL4 driver (DGRC1042) & pUAST-mTFP. **(A) & (B)** demonstrates mTFP positive S2 cells . **(B)** Shows spectral scanning graph showing the peak emission wavelengths of four mTFP expressing S2R+ cells. Peak emissions for the cells were all the same, approximately 495nm, which is consistent with the literature. Image to the right indicates the regions of interest selected for the spectral scans.

Once the mTFP expression had been validated, the Lifeact open reading frame was shuttled into the destination vector, creating an expression clone containing N-terminally tagged Lifeact (mTFP-Lifeact). Transgenic flies carrying this construct were generated by *P* element mediated transformation. Chromosomal insertion sites of each of the transgenics were mapped and stable stocks of each line were generated for further analysis. Each line was

tested under the control of *engrailed-Gal4*, which is expressed in a segmented pattern down the length of the larvae (Guillen et al., 1995). Stage L3 larvae were then imaged using a sterodissecting fluorescence microscope to reveal relative expression level. Lines 3 and 6 were shown to have the high expression level. Preliminary analysis of border cells expressing mTFP-Lifeact under the control of *slbo-GAL4* in fixed samples revealed no toxic effects or impairment of migration, as stage 9 and stage 10 egg chambers showed clusters at an expected position. However, the brightness was an issue, 2% 458nm laser power (required for live imaging) resulted in dim fluorescence. This was unlike what was observed in L3 larvae, as the border cell cluster was only just visible.

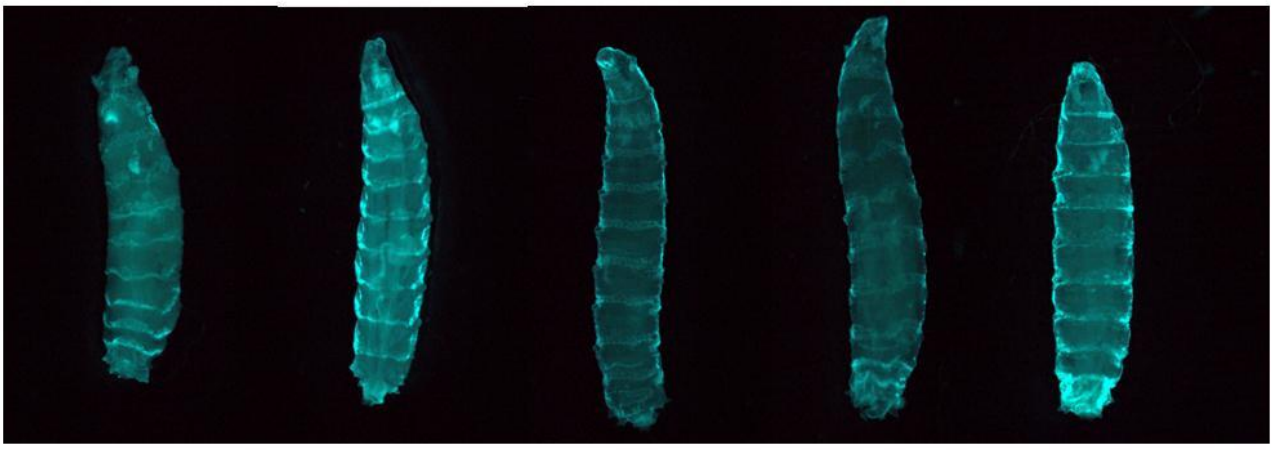

Figure 3.10. Shows expression levels of mTFP in L3 larvae. Image shows the various mTFP-Lifeact lines generated (Labelled Line 2-6). Expression is driven by *engrailed-GAL4*. All images were taken using the same settings, using larvae at the same developmental age.

3.6.4. Generation Time

When using reporters for live imaging it was important that they were fully functional and at their brightest during imaging. Nuclear dsRed ($DsRed^{NLS}$) brightly labels individual nuclei

within the border cell cluster, when expressed specifically in border cells and has the potential to be used to visualise the behaviour of individual nuclei within the cluster. This makes it possible to map the migration pathways of individual cells, to determine if any differences in migration are due to individual cell movements. However, some issues were discovered when using this fluorescent protein for live imaging, as documented elsewhere (Baird et al., 2000). In particular, the maturation of dsRed is slow and during its maturation emission occurs in the green spectra due to the formation of an intermediate chromophore. It is due to these problems that steps have been taken to produce a second generation of dsRed (dsRed-Express2 and dsRed-Max) (Strack et al., 2008) and other fluorescent proteins with optimal qualities for live imaging. However, due to the reported success of $DsRed^{NLS}$ in border cells and the potential to be combined with other reporters, I decided to test its ability to function as a marker during live cell imaging. Unfortunately, it was found there are indeed issues with the functionality of this reporter in this system, with the border cell specific drivers tested. $DsRed^{NLS}$ could be detected in border cells in stage 9 egg chambers that had been fixed and imaged at high laser intensity. However, during live imaging the signal was faint early on and only became robustly detectable by later stages, as shown in Figure 3.11. In addition to this, when comparing the mean border cell position of *UAS-$dsRed^{NLS}$* and another GFP reporter (*UAS-eGFP, His2A-RFP*), $dsRed^{NLS}$ egg chambers showed severely impaired migration (-70.1µm away from the retracting follicle cells, compared to -30.0µm).

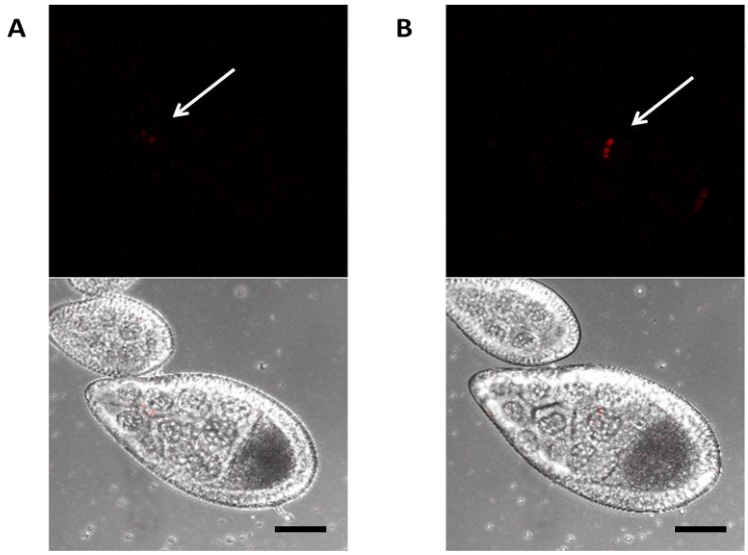

Figure 3.11. Shows expression levels of *slbo GAL4,UAS-dsRed*^{NLS} at two time points during border cell migration. (A) Representative early stage 9 egg chamber, individual nuclei are labelled. Note faint and incomplete expression. **(B)** Representative late stage 9 egg chamber, individual nuclei are brighter and can be seen more easily. White arrows indicate the border cell cluster. Frames show maximum intensity projections, the whole cluster cannot be seen due to its orientation. Solid black line represents 30 µm scale bar.

3.6.5. Non-UAS Reporters

In addition to UAS reporters, I trialled a range of reporters that were not under GAL4 control, such as Histone 2A-RFP (His2A-RFP). This consists of Red fluorescent protein fused to Histone 2A, one of the five main histone proteins, under control of its own promoter, resulting in nuclear expression throughout the whole fly. For instance, combination of the following genetic elements *slbo-GAL4*, *UAS-GFP*, *His2A-RFP* enabled the entire cluster to be labelled with GFP and the nuclei of the border cells, plus surrounding follicle cells and nurse cells to be labelled with RFP. When designing this combination it seemed like an ideal marker for live imaging, as previous imaging did not have any boundary markings, making it

difficult to distinguish where border cell migration was supposed to start and end. In addition to using a marker to highlight the different cell positions it was thought that it would make maximum intensity projections easier to visualise, as transmitted light images appear out of focus when combining Z stacks.

However, one of the problems encountered when using this genotype for live imaging was visualising the GFP cluster, when the signal from the RFP was higher surrounding it. Using the maximum intensity projected image, fluorescence surrounding the nurse cells completely obstructed the view of the cluster, rendering the Z stack ineffective in enabling more information to be obtained.

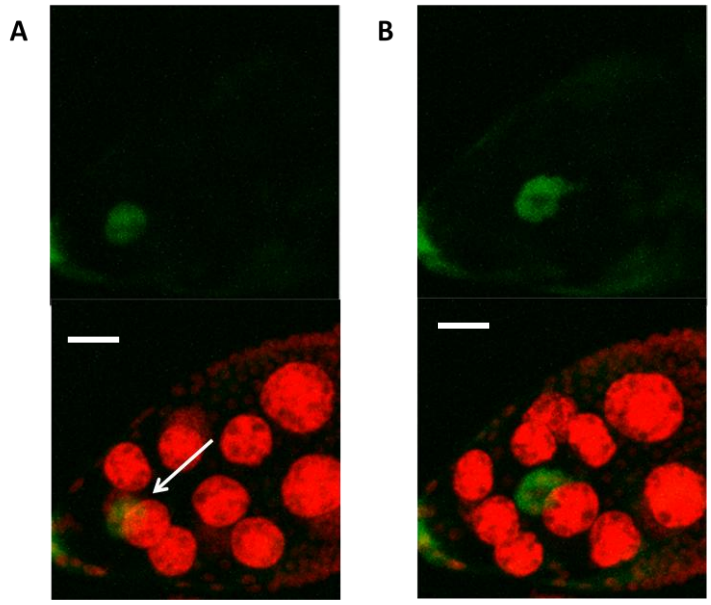

Figure 3.12. Shows maximum intensity projections of *slbo GAL4,UAS-GFP, His2A-RFP* at two time points during live imaging. (A) Border cell cluster cannot be clearly seen due to masking from the surrounding nurse cells, indicated by the white arrow. **(B)** Border cell cluster is mostly in view, however the RFP expression in the nurse cell nuclei prevents a clear view. Solid white line represents 15 µm scale bar.

Other research groups have addressed this problem by labelling cell membranes with FM4-64, a dye that is permeable and not toxic to living cells . FM4-64 is a lypophillic steryl compound used as a dye to study plasma membrane and vesicular structures, as it becomes inserted into the outer leaflet of the surface membrane. It is mostly used in live imaging of border cells to visualise the entire egg chamber in the fluorescence channels. It can also used as a diagnostic for egg chamber deterioration and damage during dissection. I tested FM4-64 for live imaging of egg chambers, but did not find it useful because it increased the time before imaging could start (FM4-64 requires a period of 10-15 minutes to fully penetrate the cells).

3.6.6. Scanning Time

When imaging border cell migration using live imaging, an appropriate time between frames is critical in efficient acquisition of accurate information. If the interval is too long crucial information may be missed. For example, the formation and retraction of a single protrusion has been shown to take less than 2 minutes in some cases (Prasad and Montell, 2007); if the interval is longer than this then some protrusions may not be accounted for. When tracking the speed of migration long time intervals were found to be a problem, as will be discussed in a later chapter, as small movements in the XY position may be missed and the speed calculated roughly on an 'as the crow flies' basis, as opposed to distance the cluster may have actually moved. In contrast, smaller time intervals were not always necessary and accelerated the deterioration of the egg chamber due to photo-toxicity. Therefore, routinely imaging multiple fluorescence channels and having excess Z stacks was found to be counterproductive. In addition to this, image quality and, ultimately, scanning time became important and compromises needed to be taken. Keeping the image resolution higher

(1024x1024), but reducing the average number of line scans was found to produce good image quality. To further reduce the scan time per image the microscope was set to scan in multi-directional mode as opposed to one. This was especially important when more than one egg chamber was being imaged in one experiment, as the scan time needed to be factored into the interval between frames. In essence if the time interval is two minutes, all image generation for all positions needed to be completed within this two minute interval. 6-8 egg chambers each with approximately 9-12 Z stacks could be imaged on the Zeiss 710 with 5 minute intervals. However, this number was reduced to 4 egg chambers when imaging with two minute intervals between scans.

3.6.7. Signal Strength

The strength of the reporter signal was found to be important when imaging live border cell migration. It was observed that reporters that emitted good signals in fixed egg chamber samples could not always be used for live imaging. One of the main reasons for this was due to the low laser intensity used for live imaging to prevent damage to the egg chamber. Generally when imaging fixed samples the laser intensity could be high, approximately 5-8 %, and samples could be imaged several times without bleaching effects being noticed. However, when imaging live samples laser intensity needed to be reduced to less than 2 %. One part of border cell migration where signal strength was an issue was in the imaging of protrusions from the cluster. Larger protrusions especially in the first half of migration were easily visualised, with several reporters. However, smaller thinner and less stable protrusions in the second half of migration were rarely seen. This was especially true when imaging Lifeact-eGFP.

3.6.8. Effect of Reporter

Various genotypes were imaged using time-lapse microscopy to identify fluorescently tagged proteins that could be used in live imaging to generate information about the process. An important issue to consider is the protein's ability to impact on the 'normal' border cell migration process. As discussed above, signal strength and laser intensity was found to be problematic when imaging living cells. To overcome this, one solution is to use more than one transgenic copy of a fluorescent protein. However, there is always a danger that the expression system can become titrated when more than one UAS element is being expressed. When either one or two copies of Lifeact-eGFP, one on the second chromosome and one on the third, were expressed in border cells using *slbo-GAL4* the fluorescence was not bright enough and could not be improved sufficiently by altering imaging settings. When Lifeact-eGFP was combined with *c306-GAL4*, the resulting fluorescence was adequate for live imaging. However, using two copies of Lifeact-eGFP severely delayed migration with most egg chambers displaying only approximately 25% migration by stage 10a. As there were no obvious signs of infertility amongst the adult flies, presumably the border cell cluster eventually reached the nurse cell-oocyte boundary in the majority of cases, although this has not been explicitly examined. This demonstrates that the reporter strain can adversely affect border cell migration and there are differences in the way that different reporter strains behave, in a GAL4-dependent manner.

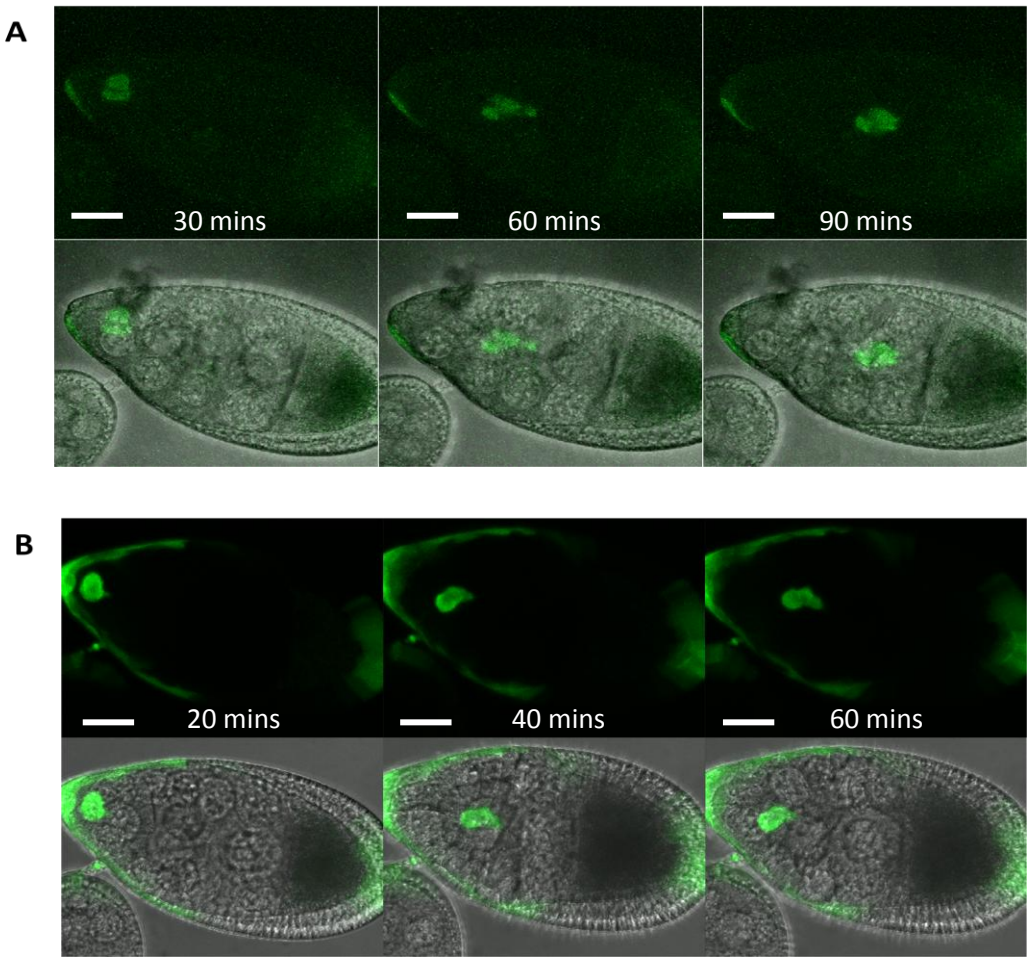

Figure 3.13. Shows maximum intensity projections of egg chambers expressing *one copy of UAS-LifeactGFP* driven by *slbo GAL4* and *c306 GAL4* (A) *slbo GAL4* egg chambers during live imaging, gain values had to be increased to clearly image the cluster, fine details are not seen. **(B)** *c306 GAL4, UAS-Lifeact GFP* egg chambers during live imaging. The cluster and protrusion details can be clearly seen. The solid white line represents 20 µm scale bar.

3.7. Discussion

Developing techniques to live culture *Drosophila* egg chambers is important in the advancement in the understanding of invasive cell migration. Utilising live cell imaging in addition to fixed samples has enabled a fuller description of the effect of genes on migration to be obtained. Both qualitative and quantitative data can be extracted from time-lapse movies of border cell migration. Here it was found that the amount of data that can be

extracted is dependent on the how the imaging is performed and the fluorophores used. Medium composition, although not seemingly important for data extraction, was found to affect how much information can be obtained from a single egg chamber. Having imaging medium that can support long time-lapse imaging without deterioration enabled data from the first and second halves of migration to be extracted and compared if desired. Adding additional reagents such as the hormone Insulin is important in supporting processes such as border cell detachment. The detachment process can vary in difficulty and time and is variable within genotypes; having suitable medium was found to influence detachment behaviour. The type of serum and imaging time did not appear to be changed by small differences in serum concentration or the use of FBS as compared to FCS. However, serum addition to the medium was important in supporting the development and behaviour of the border cell cluster; indeed, it is known that serum starved cells behave differently *in vitro* than those kept in medium. Optimisation of the medium showed that the pH of the medium is not as stringent as first described in Prasad *et al* 2007, as a slight increase/decrease still enabled migration. Dissection was also shown to be an important step in ensuring border cell migration is successful. Care and attention was given ensuring the procedure held minimum risk to egg chamber damage; rapid dissection was necessary however, as selection of the appropriate developmental stage was important. Dissection that took too long risked disturbing/damaging the egg chambers preventing migration; also time spent dissecting could result in key parts of the migration process being missed, if early stage 9 egg chambers were dissected. One way the dissection protocol could be improved would be to dissect using a sterodissecting fluorescence microscope. This way egg chambers at the right stage of development could be selected or eliminated before mounting, as unsuitable egg chambers use up valuable resources from the imaging media. Another way to dissect the

egg chambers was reported in (Tekotte et al., 2007), where dissection and mounting are carried out in a single step. It is highlighted in this article that using this single step method egg chambers are more easily mounted and easier to image as they are attached to the coverslip and do not have issues with focus as seen in aqueous mounting methods. In this method, ovaries are extracted as detailed in other protocols, then placed on a cover glass in a droplet of halocarbon oil. After pressing the posterior part of the ovary to the cover glass, a tungsten needle is then used to part individual ovarioles. These ovarioles are then wrapped around the needle with the germaria and younger egg chambers and pulled out in one stroke attaching them to the glass. This is not a protocol that I have used, however, with the imaging issues with solid bottom dishes attempting it might prove beneficial.

The use of glass bottomed dishes has the potential to greatly enhance the quality of time-lapse images of border cell migration. Using glass bottomed dishes for border cell migration enables immersion objectives to be used to generate high quality and high resolution images without interfering with the egg chamber development, or causing drift. This was successfully performed using Iwaki dishes, most likely because only a small volume of medium was required to fill the well and because no cover slip was needed to secure the egg chambers in place, enabling gas exchange. Continuing with the project would see more time spent developing the mounting protocol using the LabTek chambered cover glass as used by the Rorth group. When imaging border cell migration several aspects needed to be considered especially timing and photo-damage. Imaging live cell migration would yield more information if timing constraints were not an issue. The benefits of imaging more egg chambers consecutively were outweighed by the negatives, namely images would be of lower quality, number of channels would be reduced and Z stacks would be at a minimum.

Getting the balance right between individual scan time, number of Z stacks and number of reporter channels had to be carefully considered. Increasing image resolution and number of reporter channels increased the individual scan time per frame. If several frames in the form of Z stacks needed to be taken per egg chamber, and the number of egg chambers imaged was large, this increased the interval time between consecutive frames. With longer time intervals, valuable information such as stage distinctive behaviour, protrusion extension/retraction may be missed which may be vital in understanding the function of a gene in migration. Imaging several fluorescent channels purely for aesthetic reasons was found to reduce valuable scanning time and risk adversely affecting normal migration. This was observed when using multiple fluorescence live imaging using *slbo-GAL4, UAS-GFP, H2α-RFP*; extra time was needed to image the RFP channel, but no extra information was gained. On the contrary, this particular reporter combination resulted in parts of the border cell image being masked by the large nurse cells, resulting in less information being obtained. Ensuring that the fluorescence reporter/driver combinations are fit for purpose is vital when using the border cell model. Certain driver/reporter combinations were found to result in defective migration. Therefore, the behaviour of different reporter strains for live imaging need to be explored before experimental data can be gathered. Finally, the correct reporter for data extraction needs to be used, for example, if information about protrusion dynamics is needed, then a reporter that specifically labels actin structures is more suitable. Steps are needed to be taken to ensure fluorescence is bright and can be clearly seen, without causing photo-bleaching or damage to the egg chamber. Through modifying various protocols and trialling different reporter, driver, and medium combinations, it was possible to successfully culture egg chambers and image border cell migration over the entire course of egg chamber development.

4. Quantification of Border Cell Migration

4.1 Introduction

Border cell migration can be monitored both in fixed samples and by time-lapse imaging. The latter has the advantage that information is obtained about the whole process of migration, from detachment from the epithelium through to migration to the oocyte boundary. Furthermore, live imaging of fluorescently-labelled molecules can provide information about cellular dynamics, as well as the activation state of relevant intracellular signalling pathways (Janssens et al., 2010; Prasad et al., 2007; Prasad and Montell, 2007; Silver et al., 2005; Wang et al., 2010). In this chapter, different fluorescently-tagged reporter strains have been imaged by time-lapse imaging of dissected egg chambers and analysed in different ways, to determine which tools can accurately and easily be used to dissect mechanisms of border cell migration. Following imaging, information needs to be extracted from the resulting time-lapse images with regards to the behaviour of the border cell cluster. This can be done in a qualitative and quantitative manner. It is quite easy to infer the behaviour of the cluster by eye and, using simple measurements determine the time it took for migration to be completed. However, more sophisticated quantitative analysis is challenging, because of the complexity of the *in vivo* model and the richness of the resulting data. For comparisons to be made across a range of genotypes, quantitative data need to be obtained using consistent and robust methodology. Furthermore, due to the natural heterogeneity of the border cell migration process, experimental repeats need to be carried out and averages used to support any conclusions.

4.1.1 Aims

The aim of this chapter is to look at the different ways that live imaging data can be analysed to generate information about border cell migration. There are several different ways that live imaging data can be analysed both qualitatively and quantitatively. Data can be extracted based on individual or whole cluster cell movements, in addition to this protrusion dynamics can be measured, or adhesion properties monitored. The possibilities of data extraction are dependent on the properties of fluorescent proteins and the tools used to analyse the generated movies. Understanding the differences between the various methods of data extraction and how the outputs compare is important and beneficial, to ensure the accurate interpretation of new data.

4.2 Global Behaviour

Before focussing on specific aspects of the migration process, such as actin-based protrusions, cell adhesion and guidance signalling, it was important to understand the basic properties and behaviours of the border cell cluster. Understanding the behaviour of wild type egg chambers is key to identifying defects in mutant egg chambers.

4.2.1 Qualitative Data

Qualitative data can be extracted from time-lapse movies of border cell migration simply by observing the behaviour of the cluster in each of its designated phases, as described below.

Detachment

At the beginning of migration the border cell cluster detaches from its surrounding epithelium. This detachment usually proceeds with the formation of a single long

filamentous forward facing protrusion, starting at around stage 9 of egg chamber development (Fulga and Rorth, 2002; Prasad and Montell, 2007). This process was imaged well in egg chambers dissected at the correct stage, approximately 10-20 minutes before the onset of detachment, using *slbo-GAL4, UAS-eGFP* and *c306-GAL4, UAS-Lifeact-GFP*. Onset of detachment in these genotypes was marked by the cluster tumbling on the spot and an apparent increase in fluorescence. Detachment may fail to occur if migration is impaired or if the egg chamber deteriorates due to cellular damage caused by dissection. Several genes have been identified as being essential to border cell initiation and detachment such as the transcriptional activator *slbo*, where mutant border cells fail to migrate (Montell et al., 1992; Rorth et al., 2000). Ectopic Notch expression, on which border cell formation is dependent, can rescue the migration defects seen in DN-Kuz (Dominant negative Kuzbanian) egg chambers (Prasad and Montell, 2007; Wang et al., 2007). Kuz encodes a metalloproteinase, that activates Notch and cleaves other substrates (Wang et al., 2007). Loss of the serine/threonine kinase homologue, PAR-1, responsible for apical-basal polarity, results in disrupted detachment of the cluster (Majumder et al., 2012; McDonald et al., 2008). Noticing signs of deterioration can be very difficult with the absence of cellular markers such as FM4-64, as discussed in Chapter 3, Section 3.6.5. If detachment does not occur, usually there is an absence of the large transient protrusions needed to sense the environment and promote forwards movement towards the oocyte (Fulga and Rorth, 2002; Janssens et al., 2010).

First Half of Migration

Migration of the border cells between the germline nurse cells can be divided into early and late stages. The first part of migration has been characterised in the literature by a quicker

migration rate and the cluster was observed to be more polarised in the first half and more rounded in the second half. In the second half of migration the cluster also moved in a slightly different way, tumbling and shuffling towards the oocyte. Due to the characteristic direct movement during the first half, differences and problems with migration can be easily spotted. Delays in migration have been identified and related to numerous genes involved in all aspects of the border cell process such E-cadherin mediated cell adhesion (Niewiadomska et al., 1999; Oda et al., 1997), guidance sensing (Bianco et al., 2007; Duchek and Rorth, 2001; Janssens et al., 2010; McDonald et al., 2006; McDonald et al., 2003) and actin dynamics (Chen et al., 2001; Fulga and Rorth, 2002; Gates et al., 2009; Geisbrecht and Montell, 2002; Rorth, 2011, 2012; Verkhusha et al., 1999).

Some of the genotypes tested in this thesis, have shown a high frequency of premature tumbling behaviour in the first half of migration (see Chapter 5, Section 3.2), which is characteristic of defective early guidance signalling.

Second Half of Migration

Defects in the second half of migration may be more difficult to notice, as the cluster is more rounded and the cluster moves in a tumbling and shuffling motion. Unlike the first half of migration the cluster did not appear to be polarised and had no definitive front, back and side. On closer inspection, and in accordance to the literature (Bianco et al., 2007; Poukkula et al., 2011), the cluster was observed to tumble and shuffle, with individual nuclei constantly changing position within the cluster. The second half of migration has been reported to be slower than the first and the cluster lacking long protrusions. Examples of the characteristic shape of the cluster in both stages can be seen in Figure 4.1 below. The protrusions are less noticeable due to their small size and varied direction.

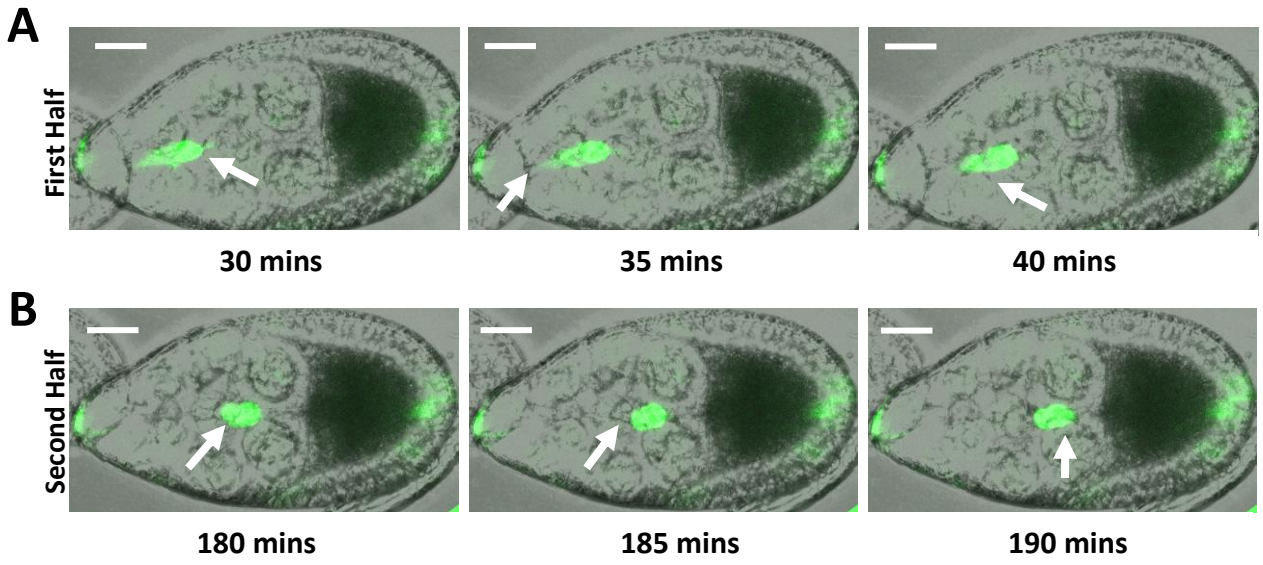

Figure 4.1. Shows the characterised stages of Border cell migration in *slbo GAL4, UAS mCD8-GFP* egg chambers. Images shown are maximum intensity projections of approximately 8-10 optical sections. White arrows indicate protrusions or rounded shape. **(A)** The first half of migration, characterised by an elongated, polarised cluster. **(B)** The second half of migration, characterised by a more rounded appearance. The solid white line indicates 15 µm scale bar.

Defects in border cell migration were noticed during live imaging experiments, resulting in a failure of the border cells to reach the oocyte by stage 10a. Stage 10a of development is characterised by the presence of the border cell cluster at the oocyte-nurse cell boundary and the retraction of overlying follicle cells to surround the oocyte (Montell, 2003). However, as discussed in Chapter 3, Section 3.6, fluorescent reporters can make the border cell migrate differently, usually resulting in slower migration rate than seen in wild type egg chambers. Whilst this issue did not affect the ability to track border cell migration in real-time, it highlighted the importance of using suitable controls and of obtaining quantitative data that can be used to make appropriate comparisons across different genotypes.

4.2.2 Quantitative Data

Basic quantitative data, such as border cell migration duration, rate and time, was extracted from live imaging time-lapse movies using ImageJ, a public domain, Java-based image

processing program developed at the National Institutes of Health. Some phenotypes displayed abnormal qualitative behaviour, such as early tumbling in the first half of migration, which were characterised as a percentage of the number of movies or average number of frames per movie (see Chapter 5, Section 5.3.2.).

Duration

The duration of border cell migration was determined by simply counting the number of time-lapse frames it took for the cluster to reach the oocyte, multiplying by the time interval between frames. It was important that the start point and end point were the same in all egg chambers. It was found that the most accurate way to do this was to set guidelines where border cell migration starts and ends. In this thesis, the start point was defined by the point at which the cluster had detached from the epithelium, checking all optical sections through a Z stack of time-lapse images. The end point was defined as the point at which the edge of the cluster had made contact with the oocyte-nurse cell boundary. However, it is important to note that not all egg chambers started and ended in the same way, either as a result of the variations in genotype or simply due to their heterogeneous nature. For instance, during the initial polarised phase of migration some border cell clusters remained attached to the epithelium, causing the cluster to form an elongated shape towards the oocyte. In this case, a decision was made to either exclude the egg chamber from analysis, as no clear start point could be defined, or include the egg chamber and risk a skew in the migration averages. These decisions were guided by examination of other egg chambers of the same genotype to determine what was the normal behaviour for that genotype. If using a genotype already published the findings were compared to the literature. If the egg chamber in question was included in the analysis, a pseudo-start point was designated, which represented the start point in all movies, to ensure all egg chambers were treated

similarly. Figure 4.2 below shows an example of an egg chamber where the cluster has started to migrate but failed to fully detach. Where only a single egg chamber was affected, these data were removed from the analysis to avoid error.

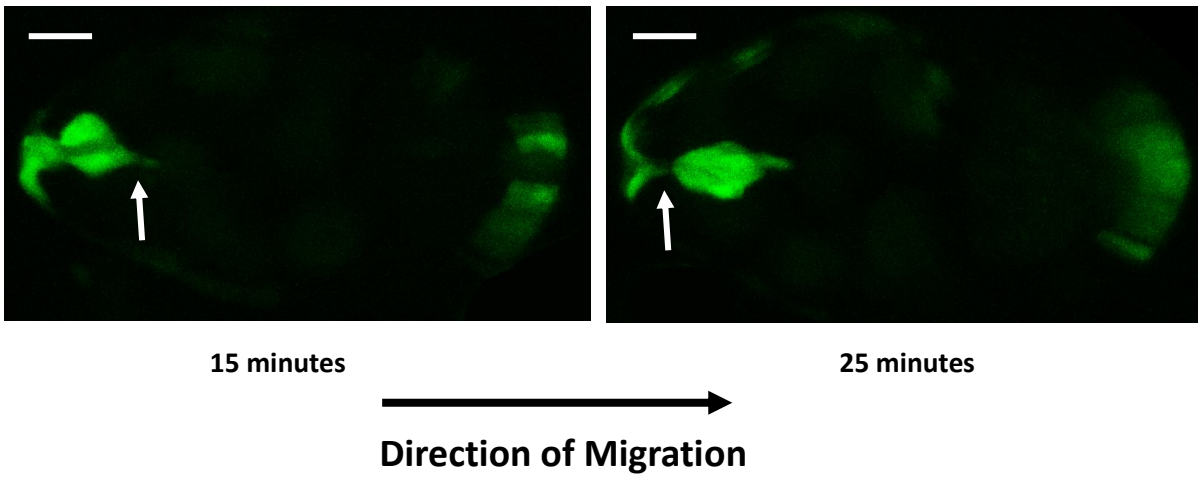

Figure 4.2. Shows *slbo GAL4, UAS mCD8-GFP* egg chambers where there is a delay in the full detachment of the Border cell cluster from the surrounding epithelia. Images are GFP maximum intensity projections of 8-10 Z stacks, taken from the time-lapse imaging of a single egg chamber. White arrows indicate the clusters connection to the epithelium. The pseudo-start point would be positioned at 15 minutes, as seen in the first image, irrespective that it is still attached to the epithelium. This enables a quantitative start point to be categorised. Solid white line indicates 15 µm scale bar.

On occasions where the end point of migration was not clear, usually due to the slow tumbling nature of the second half of migration, steps were taken to carefully define an end point. Dorsal migration of the cluster occurs at the end of anterior posterior migration, once the cluster has reached the oocyte (see Introduction 1.5.3.). Frames were not counted once forward migration had stopped and dorsal migration started. Having strict guidelines to adhere to when analysing qualitative elements ensured the data extracted was consistent and accurate throughout.

In addition to determining the duration of complete migration it was useful to compare the duration of the first half and the second half of migration. To do this, a midway point through migration needed to be determined. Unfortunately, although there are molecular changes in border cells that reflect the changes in behaviour of the border cell cluster during the migration process, no markers exist to easily discriminate between early and late phases. In the second half of migration there is a gradual transition from PVR to EGFR guidance signalling, which is thought to be responsible for the characteristic change in behaviour of the border cells during the second half of migration, as described above. Using a dominant negative version of the receptor responsible for first half of migration brings about second half behaviour prematurely (Poukkula et al., 2011). Due to the natural heterogeneity of border cell migration, this transition, which is in part determined by the concentration gradient of the ligands (PDGF and EGF) along the egg chamber, does not occur at the same distance throughout migration and can be dependent on the genotype. Using the cluster behaviour to guide when the first half ends and the second half begins was not an option, as the migration behaviour may be affected by the mutants under investigation. Since egg chambers are generally similar in size irrespective of their border cell genotype, it is reasonable to assume that the distance the cluster needs to travel from start to end point is the same. The length from start to finish consequently is a constant that can be used to determine a specific distance travelled during migration. Using projected images of the egg chamber, the distance from start (the edge of the anterior epithelium) to finish (nurse cell/oocyte boundary) along a straight line was measured (XY measurement), see Figure. 4.3.

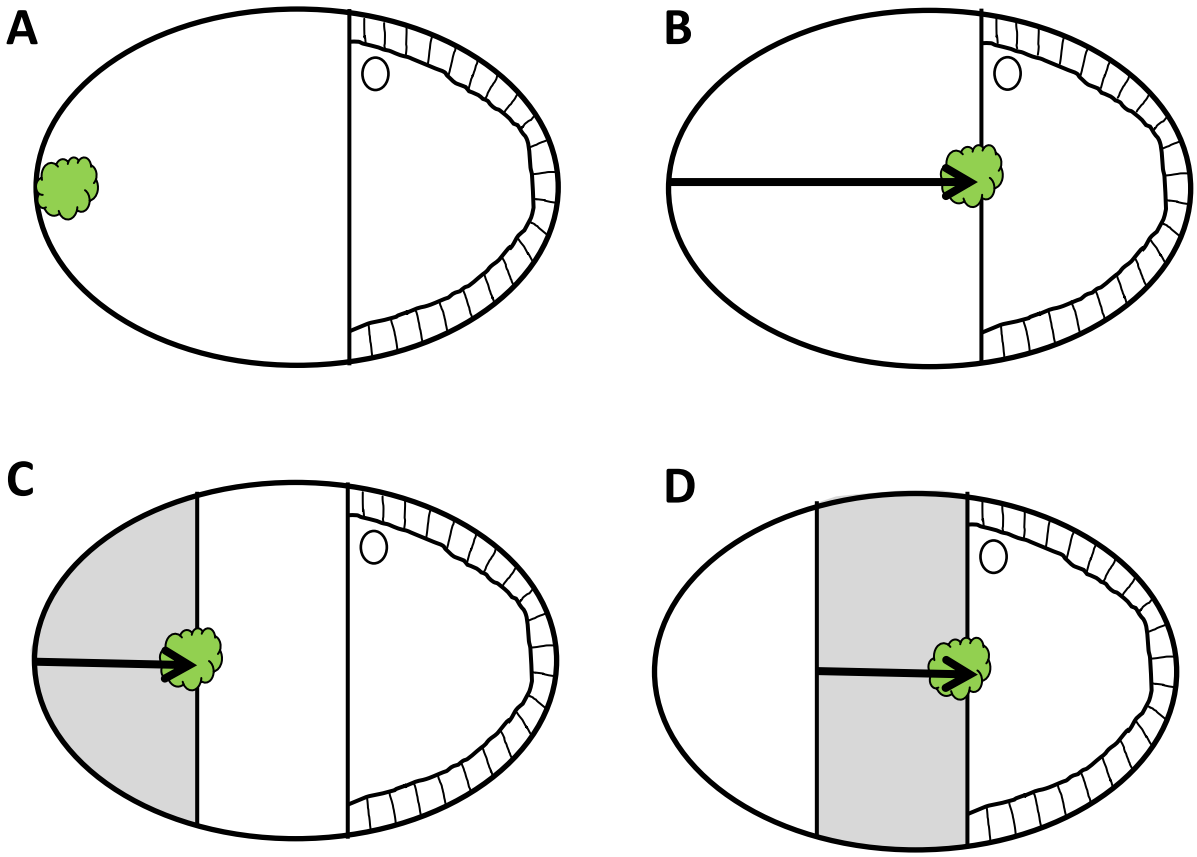

Figure 4.3. Shows schematic diagrams of egg chambers to highlight the XY measurements to determine different stages of migration, start and finish. Border cell cluster labelled in green. **(A)** Egg chamber with cluster still attached to the epithelium (Early stage 9) where the measurement starts. **(B)** Egg chamber with cluster at the end point (Stage 10a) where the measurement from the epithelium ends. **(C)** Egg chamber defining the first half of migration, with the area highlighted in grey. **(D)** Egg chamber defining the second half of migration, with the area highlighted in grey.

The projected image was found to give a good representation of the entire cluster and enabled a centre point to be determined. Using this approach, the midway point was determined and the first and second parts identified. The duration of each of the respective parts were calculated when the centre of the cluster reached that point.

Rate

The rate of migration was calculated based on basic measurements taken from the time-lapse movies. These rates were either calculated over the complete migration process or specifically in one half. Migration rate was calculated by dividing the distance the cluster had travelled by the time it had taken, averaged over a number of individual movies. Migration rate differences may indicate problems during migration contributing to abnormal migration behaviour e.g. the second half of migration may take less time than the first as the cluster is migrating at a quicker rate. However, measuring rates of migration 'as the crow flies' (ACF) underestimates the actual distance travelled. By monitoring a central point of the cluster over time it was clear that clusters did not migrate in a straight line.

4.3 Extracting Data Manually

For the reasons explained above, it is important that the accurate distance for border cell migration rate is measured. Border cell clusters that do not take a direct route to the end point may take longer to get there, but due to the increased migration distance, the rate may still be quicker than a cluster with the same duration, but travelling a shorter distance. Several methods were trialled in this thesis to manually track the path the border cell cluster takes through the egg chamber, using single channel and multichannel images.

4.3.1 Manual Tracking Image J Plugin

The manual tracking plugin for Image J enables the user to quantify the movement of objects from one frame to the next. This can be in two dimensions (2D) or in three dimensions (3D) by using time-lapse imaging with multiple Z stacks to track the migration of objects. The plugin works by providing the user with an additional toolbar in Image J (See

Methods 2.4.3). Custom values for the time-lapse were inputted so that the output from the tracking was accurate, using the correct unit of measurements.

XY (2D)Tracking

The tracking process was very simple once the calibration and modification steps were complete and the projected image file opened. This involved using single eGFP maximum projections of the time lapse movie, calibrating ImageJ so that pixel measurements represented actual sizes (µm), and time calculated using the actual time between frames. Using the 'Tracking' heading “add track” was selected and the mouse button pressed on the image file in the first time frame where tracking needed to begin. The next frame was then selected and the process repeated. Once all the frames had been tracked the process was ended by the 'end track' button. During the tracking procedure an output table automatically appeared with the calibrated measurements from the tracked time points. This table contained the XYZ coordinates of each tracked point along with the velocity and distance between each consecutive point. Additional information such as pixel intensity was also given. Figure 4.4 shows an example of the output. The first tracked point always had a distance and velocity measurement of -1, because there was no previous time point to calculate a value from. One of the negatives of using this plugin compared to others available is the lack of information given in the output. This will be explained in more detail in the next section (4.3.2).

A

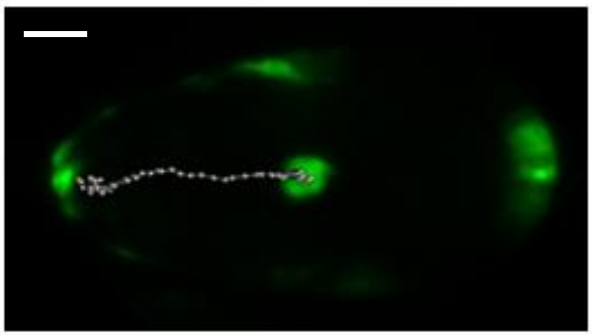

B

Results

File Edit Font Results

	Track n°	Slice n°	X	Y	Distance	Velocity	Pixel Value
1	1	1	355	151	-1	-1	149
2	1	3	352	149	0.465	0.093	127
3	1	5	347	147	0.695	0.139	137
4	1	7	343	151	0.730	0.146	111
5	1	9	344	151	0.129	0.026	140
6	1	11	343	151	0.129	0.026	178
7	1	13	339	151	0.516	0.103	182
8	1	15	339	152	0.129	0.026	188
9	1	17	342	154	0.465	0.093	127
10	1	19	348	156	0.816	0.163	115
11	1	21	346	158	0.365	0.073	186
12	1	23	345	162	0.532	0.106	231
13	1	25	346	159	0.408	0.082	117
14	1	27	347	161	0.288	0.058	85
15	1	29	343	156	0.826	0.165	91
16	1	31	341	155	0.288	0.058	81
17	1	33	343	154	0.288	0.058	115
18	1	35	342	158	0.532	0.106	85
19	1	37	344	162	0.577	0.115	122

Figure 4.4. Shows the output from the Manual Tracking plugin. (A) Dots and lines overlaying the GFP projected image of border cell migration. The cluster is moving from left to right. **(B)** Table output from tracking the cluster migration from (A). Note the first line indicates distance and velocity values of -1. Solid white line indicates 15 µm scale bar.

XY Results

The data resulting from this plugin to manually track border cell migration in a wild type egg chamber (*slbo>mCD8-GFP*) were impossible to validate. The tracking output as shown in Figure 4.4 calculated an average velocity of 0.32µm/min using the average tracked distance and migration rate per frame (n=5 movies). This value was checked using the formula Speed = Distance/Time using the average tracked migration distance, 69.2 µm and duration of 94.4 minutes, which equates to 0.73 µm/minute. Calculations were checked multiple times with the same result, which did not correspond to the plugin output. The difference between the two values is likely to be due to calibration issues with the tracking plugin. Correct values

were given later using different Image J plugins which automatically used the XYZ calibrations from the imaging file metadata, to determine the correct distances travelled (see Section 4.3.2). Since the results of the Manual Tracking plugin could not be verified alternative methods of tracking the cluster were sought.

Distance (µm)	Duration (mins)	Tracked Rate (µm/min)	Calculated Rate (µm/min)
69.2	94.4	0.32	0.73

Table 4.1. Table showing the average migration distance, duration, tracked rate and calculated rate (In XY) for a wild type egg chamber, genotype *slbo GAL4, UAS mCD8-GFP*.

XYZ (3D Tracking)

The plugin has a semi-automated function to track in three dimensions. This works by aligning the stacks from the projected image and generating a three dimensional matrix, onto which the XYZ coordinates from the tracked points can be placed, once the Z coordinates have been retrieved. This required the original image file to be in a less compressed format than that generated by Zen 2010. Using older Zeiss LSM software, multiple stacks for single time points were saved as individual files and needed to be concatenated into one. At this point the files for each stack were individually named with a common label to recognise the stack order. The plugin utilises the individual files to form the three dimensional matrix by linking the common label and generating a multi-stack image. As the time-lapse movies were already generated using Zeiss 710 software, three dimensional tracking was not possible using this plugin.

4.3.2. MTrackJ Image J Plugin

MTrackJ is another Image J plugin designed to track moving objects manually and to generate quantitative data from time lapse images. On first impressions, the MtrackJ plugin appeared to perform the same tasks as the Manual Tracking plugin but with a different style toolbar (See methods 2.4.4). However, the plugin is superior in the elements that can be modified, how it is calibrated and the detail given in the output. MtrackJ allowed more than one time-lapse movie to be analysed at any one time and supported all image formats used, including hyper-stacks and the compressed files from the Zeiss 710 microscope, enabling XYZ tracking.

XY (2D) Tracking

To start tracking, the "Add" function was selected and the position on the imaging file clicked with the mouse. As previous the centre of the cluster, the area with the highest intensity in the projected image, was used to track the whole cluster. Unlike the manual tracking plugin, once a particular frame had been marked the next frame was automatically moved to. Time stepping was also possible using this plugin, which makes it possible to track every n frame only, if desired. This automated movement prevented double points being placed on one time frame accidently and also decreased the time that it took to track the migration path. It was found whilst tracking that it was easier to see the cluster and to judge the cluster centre by hiding the previous tracks (Described in Methods 2.4.4).

A

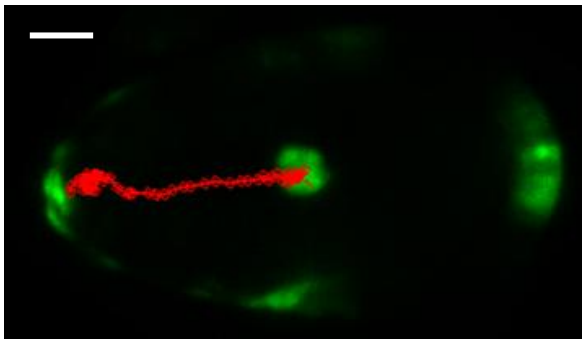

B

Results

File Edit Font Results

	Nr	TID	PID	x [µm]	y [µm]	z [µm]	t [sec]	c [idx]	I [val]	Len [µm]	D2S [µm]	D2R [µm]	D2P [µm]	v [µm/sec]
1	1	1	1	196.968	84.831	84.711	0	1	47	0	0	NA	NA	NA
2	2	1	2	195.876	86.288	84.711	300	1	14	1.820	1.820	NA	1.820	0.006
3	3	1	3	195.876	86.288	84.711	600	1	71	1.820	1.820	NA	0	0
4	4	1	4	196.604	86.652	84.711	900	1	52	2.634	1.856	NA	0.814	0.003
5	5	1	5	194.056	89.564	84.711	1200	1	14	6.505	5.558	NA	3.870	0.013
6	6	1	6	192.964	93.205	84.711	1500	1	62	10.306	9.282	NA	3.801	0.013
7	7	1	7	190.779	97.574	84.711	1800	1	101	15.191	14.166	NA	4.885	0.016
8	8	1	8	186.046	99.394	84.711	2100	1	45	20.262	18.204	NA	5.071	0.017
9	9	1	9	180.221	102.671	84.711	2400	1	119	26.945	24.470	NA	6.684	0.022
10	10	1	10	177.672	107.040	84.711	2700	1	77	32.003	29.421	NA	5.058	0.017
11	11	1	11	167.478	112.501	74.122	3000	1	177	47.684	41.803	NA	15.680	0.052
12	12	1	12	163.109	113.230	74.122	3300	1	153	52.113	45.443	NA	4.429	0.015
13	13	1	13	158.740	117.234	74.122	3600	1	165	58.040	51.220	NA	5.927	0.020
14	14	1	14	152.914	118.327	74.122	3900	1	156	63.967	56.346	NA	5.927	0.020
15	15	1	15	150.366	119.419	74.122	4200	1	49	66.739	58.994	NA	2.773	0.009
16	16	1	16	146.361	121.239	74.122	4500	1	85	71.139	63.236	NA	4.399	0.015
17	17	1	17	142.356	123.060	74.122	4800	1	110	75.538	67.499	NA	4.399	0.015
18	18	1	18	139.079	124.880	74.122	5100	1	87	79.286	71.184	NA	3.748	0.012
19	19	1	19	135.439	125.244	74.122	5400	1	141	82.945	74.372	NA	3.659	0.012
20	20	1	20	132.890	125.244	74.122	5700	1	140	85.494	76.494	NA	2.549	0.008

Figure 4.5. Shows the output from the MTrackJ plugin. (A) Circles and lines overlaying the GFP projected image of border cell migration. The cluster is moving from left to right. **(B)** Table output from tracking the cluster migration from (A). Note the first line indicates distance and velocity values of 0 and the increased number of outputs compared to the Manual Tracking. Output labels are as follows: Nr - identifies the frame number, TID - the track number, PID - frame a specific track, X(µm)/ Y(µm)/ Z(µm) - XYZ position based on the entire image window, t(sec) - time in seconds, c(idx) - channel identification, I(val) - intensity level, Len(µm) - total migration distance, D2S(µm) - distance from start (ACF), D2R(µm) - distance from a reference point, D2P(µm) - distance between two consecutive frames, V(µm/sec) - sped at the current point (calculated from the last point). Solid white line indicates 15 µm scale bar.

Results (XY)

border cell clusters from 5 wild type egg chambers (*slbo>mCD8-GFP*) were imaged and tracked for the whole migration process. Time points were cropped accordingly to the guidelines as described previously, projected images generated and rates calculated for the first half, second half and complete migration. The results show that the border cell cluster travelled at 0.61 µm/minute over the full migration path, based on an average velocity from one frame to the next. For the first and second half of migration the average values were similar at 0.61 µm/min and 0.64 µm/min respectively. These results are within the expected migration speeds previously published using this genotype (Prasad et al., 2007; Prasad and Montell, 2007) with an average migration speed of 0.59 µm/min in the first half (variation 0.32-1.04 µm/min) and 0.4 µm/min in the second half (variation 0.22-0.64 µm/min). However, unlike Prasad *et al* (Prasad et al., 2007), the first half of migration was not quicker than the second, in this set of movies.

To confirm this, the D2S (As The Crow Flies, ACF) output from the plugin, which provides the distance the cluster has migrated from the start point to the end point was analysed. Upon separation of the D2S outputs into first half and second half of migration, it was found that the average first half migration speed was 0.53 µm/min and the second half 0.61 µm/min, again indicating that the first half of migration was slower than the second. These migration rates are smaller but this is not significant (Student's T-Test, $P>0.05$), calculated using the entire migration distance when compared to the actual distance travelled. Using ACF distances, does not take into account the actual distance that the cluster has travelled, however the results suggest that the cluster does not significantly deviate from the direct migration path to the oocyte. The ACF values are more comparable to the values given in

Prasad *et al* (Prasad et al., 2007) as essentially they were calculated in the same way, using the duration and migration distance from start to finish.

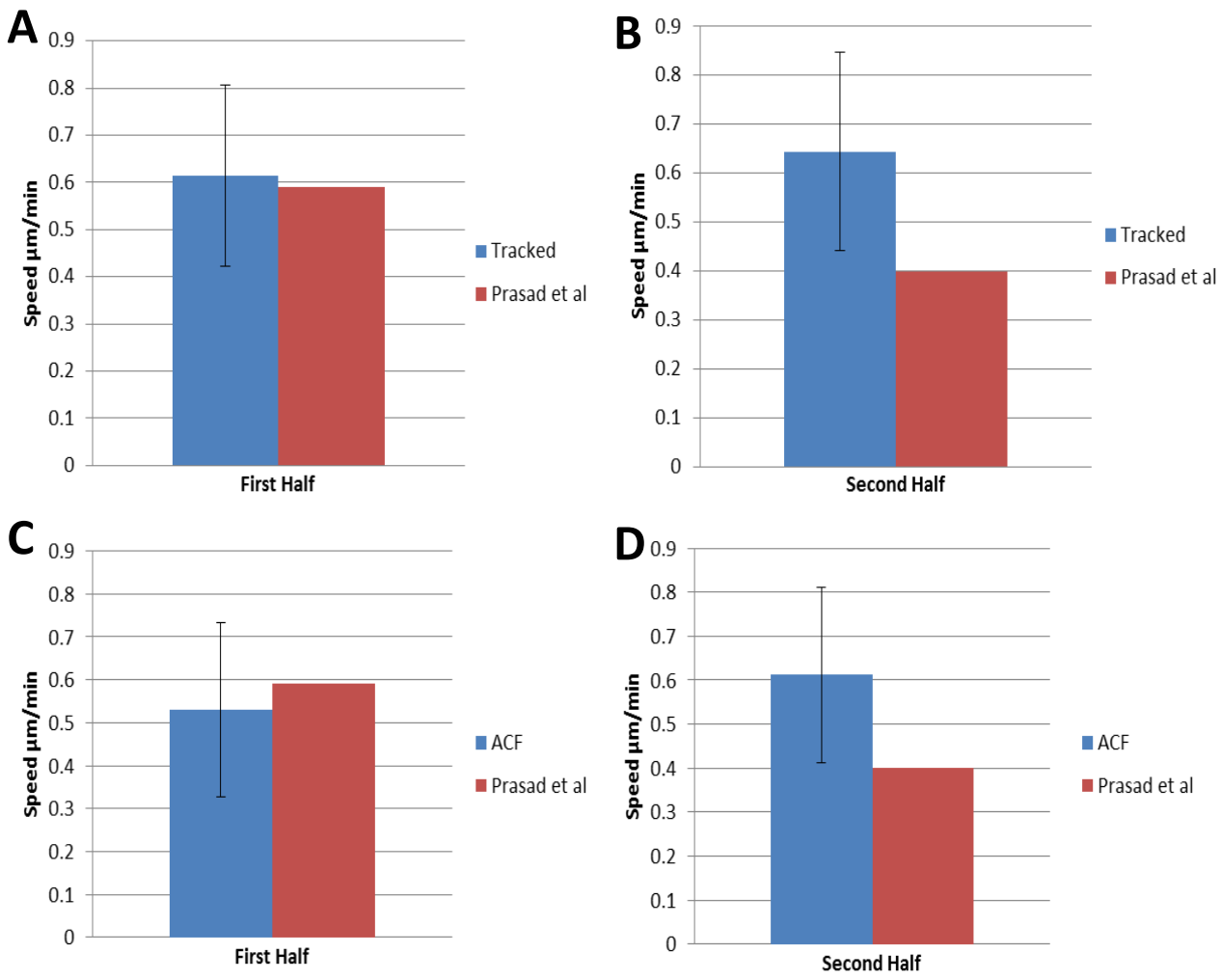

Figure 4.6. Shows graphs comparing the speeds of first half and second half of migration calculated in different ways. (A) & (B) compare the MtrackJ tracked results using the actual migration length, with the values published in Prasad *et al*. **(A)** Shows the first half of migration and **(B)** the second half of migration. The first half tracked values are similar to the published values, however the second half calculates the migration speed much higher. **(C) & (D)** compare the ACF tracked results with the values published in Prasad *et al*. **(C)** Shows the first half of migration and **(D)** the second half of migration. The first half tracked values are slightly slower but similar to the published values, however the second half migration speeds were much higher. Using both methods the first half of migration rate is slower than the second, unlike the results from Prasad *et al*. The same genotype *slbo GAL4, UAS mCD8-GFP* was used for all. Error bars represent the standard deviation.

Results (XYZ)

The clusters were also tracked in XYZ to determine if any differences in migration speeds could be due to movement of the cluster centre in the Z plane (See Figure 4.7). The average migration speeds were calculated as 0.76 µm/min and 0.75 µm/min for the first and second half of migration, respectively. Over the full migration path, the average migration speed per frame was 0.73 µm/min. These are higher than the original migration speeds calculated for XY (First = 0.61 µm/min, Second = 0.64 µm/min, Full = 0.61 µm/min). Single cell tracking has indicated that there is minimal movement of the border cell cluster in Z (Prasad et al., 2007), suggesting these increased values are possibly due to drift of the mounted egg chamber in Z. Slight movements of the egg chamber in Z can result in large distance measurements being recorded, compared to the normal migration distances measured each frame. These large distances cause the velocity calculations to be higher than they actually are, as the cluster has theoretically travelled a larger distance in a small amount of time. As the migration speeds are calculated using the averaged velocities from one point to the next, Z drift can cause large skews in the data and increase the average migration velocity.

It is apparent that tracking migration speed of the entire cluster is fraught with errors, difficulties and complications that cannot be easily avoided.

Explaining the migration process using the cluster as a whole may not give a detailed description of the mechanisms causing the behaviour of the cluster. Insight may be gained from looking at the behaviour of the individual cells within the cluster.

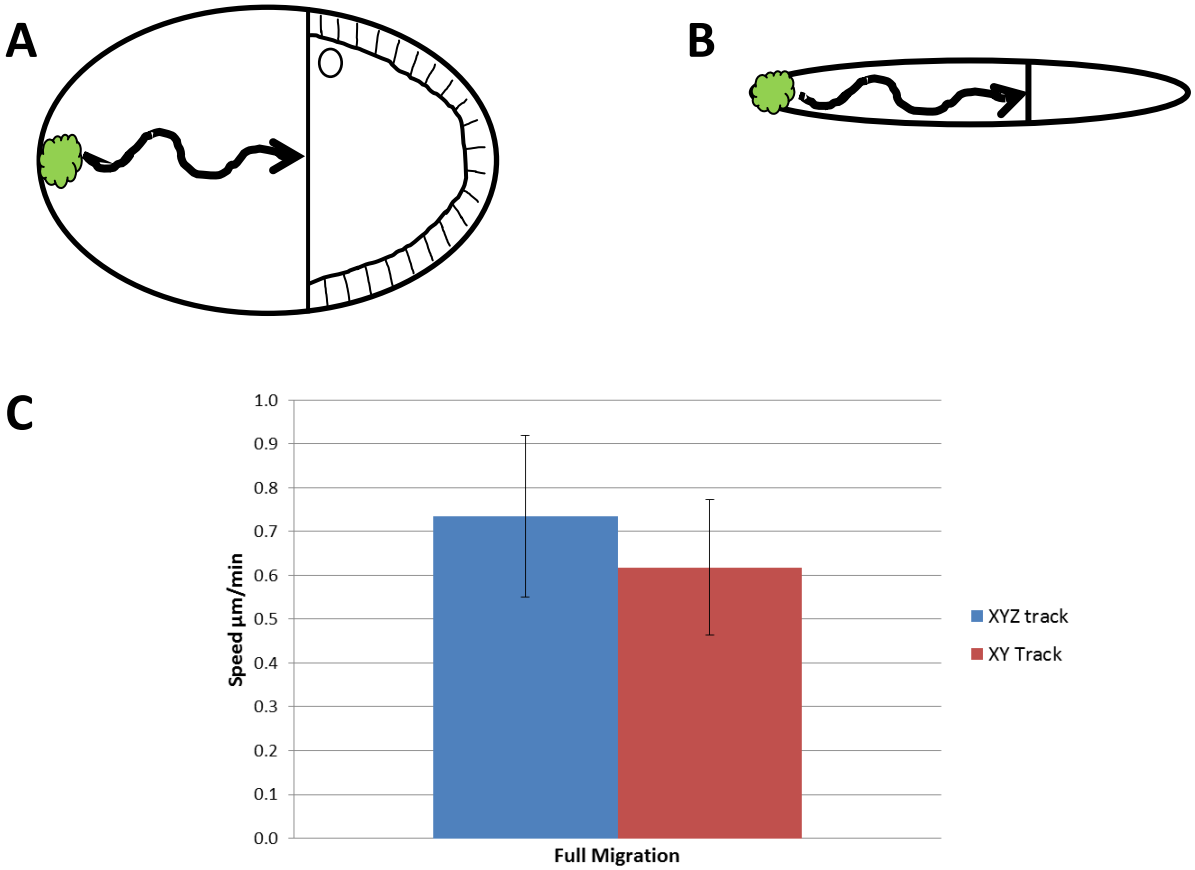

Figure 4.7. Shows a description of the tracked cluster movement in XYZ. (A) Shows a schematic representation of the migration path of the cluster in XY. **(B)** Shows a schematic representation in a cross section of an egg chamber, of the hypothesized XYZ migration of the cluster. **(C)** A graph comparing the migration speed of the tracked cluster in XY compared to XYZ. Note the XYZ migration speed is higher. Error bars represent the standard deviation.

Tracking Individual Cells

As described previously, there are different reporters that enable the border cell migration to be visualised in different ways. Utilising a nuclear marker such as dsRed^{NLS} it is possible to track the movement of individual nuclei within the cluster and to look at how movement of a single cell relates to the movement of the entire cluster. It has been previously described that a single cell at the front of the border cell cluster predominantly leads the way during the early phase of migration. Although the lead cell might initially direct the cluster from one end of the egg chamber to the other it does not remain at the front for the entire

duration (Prasad et al., 2007). *slbo>dsRed*^{NLS} egg chambers were imaged, enabling single cells within the cluster to be tracked. The front (leading) cell and back (trailing) cell of a *slbo>dsRed*^{NLS} border cell cluster was tracked, in one time lapse movie using maximum intensity projection images.

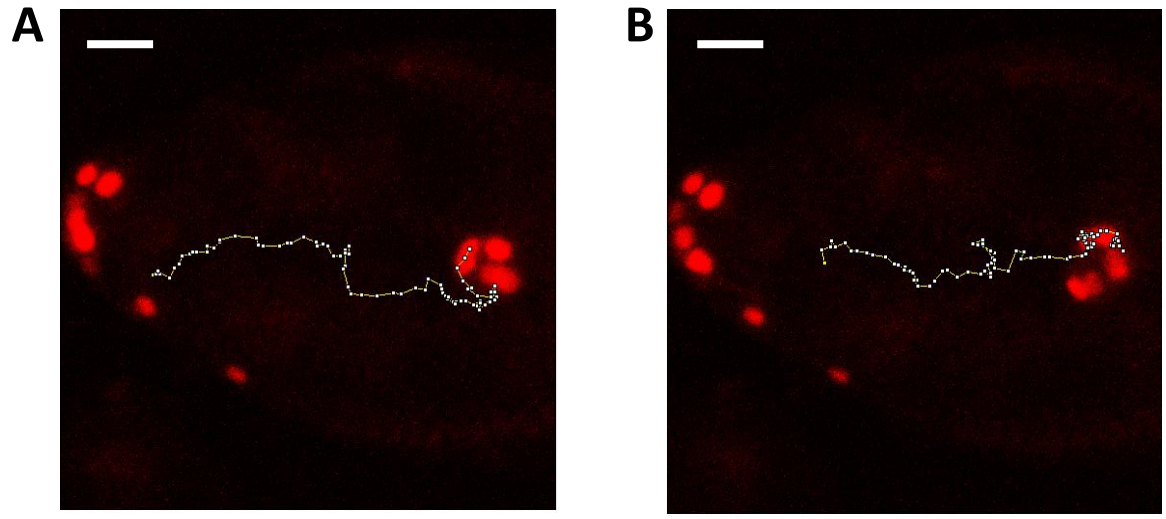

Figure 4.8. Shows egg chambers expressing *slbo Gal4, UAS DsRed*^{NLS} specifically in the Border cells. Figures have a 2D MtrackJ trace using over the projected image. **(A)** Shows the pathway taken by the leading border cell of the cluster. **(B)** Shows the pathway taken by the border cell at the rear of the cluster. Solid white line represents 20 µm scale bar.

When tracking the individual cells there were several issues that were not originally foreseen. Despite taking a large number of images in the Z plane there were still issues associated with the egg chambers drifting from focus, although not a major issue when using projected images. It did, however, prevent analysis in the XYZ plane which would have been the most beneficial; it was thought imaging single cell movements may yield more information about movement Z than when tracking the entire cluster, as it was anticipated that there would be more movement in this direction due to the smaller size of the

individual cells. Tracking using the maximum intensity projection for DsRed^{NLS}-labelled cells also presented some problems. As the cluster is a three-dimensional shape that is flattened for the projection, nuclei that are situated on top of one another in the Z plane were essentially lost from view for that track. Therefore, in some frames it was impossible to locate the position of the nuclei that were being tracked. This same issue was apparent when the cluster was tumbling or in its more rounded form, as the individual cells were closer together. Unlike tracking using the whole cluster, the time interval of 2 minutes was too long in some situations, for example, when the cluster was tumbling. It became impossible to determine which cell was originally being tracked from one frame to the next, due to the close proximity of the cells within the cluster and also the random movement. Without constant imaging it was found that there is no guarantee that the same nuclei will be tracked in one frame to the next. When there was a clear front and trailing cell as seen in the initial stages of migration, tracking using this reporter was possible and could potentially provide lots of information if the cell position had changed during migration.

4.3.3 Extracting Protrusion Data

Actin protrusions play a key role in border cell migration (Fulga and Rorth, 2002; Montell, 2003). The formation of actin rich protrusions, predominantly at the leading edge, along with adhesion molecules are responsible for the generation of traction to pull the cluster along (Montell, 2003). Understanding the distribution of protrusions during migration of wild type border cell clusters compared with mutant border cells has the potential to provide insight into the role different genes play in modulating the actin cytoskeleton during cell migration. Altered migration rate or failed migration may be a result of poor protrusion formation, persistence or directionality, or neither. Confirming or eliminating protrusion

dynamics as being involved in impaired migration can be important when trying to pin-point the role genes play in migration. To analyse the protrusions in a single cluster, important guidelines and rules needed to be implemented to ensure continuity between samples, to keep judgement calls to a minimum and to remove the possibility of bias.

Machacek *et al.* developed a system to track complex cell boundary protrusion and retraction by following the path length of a virtual edge marker moving continuously perpendicular to a cell boundary. Using this, protrusion and retraction rates were accumulated in space-time charts revealing different morphodynamic states that described the phenotypical profile of epithelial cell protrusions (Machacek and Danuser, 2006).

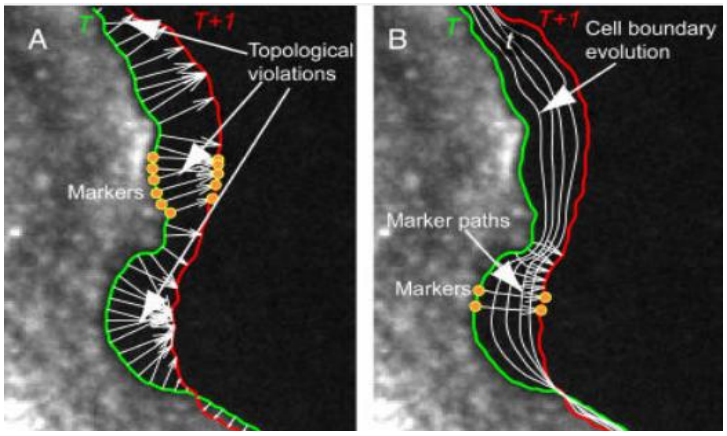

Figure 4.9. Image taken from Machacek *et al.*, showing cell boundaries tracked with virtual edge markers. (A) Shows the markers following normal direction where markers can cross paths (topological violations). **(B)** Shows continuous normal propagation of the cell boundary avoiding topological violations.

In the 42nd annual Asilomar Conference of Signals, Systems and Computers in 2008, Shann-Ching Chen *et al.* presented a paper titled 'Quantitative Analysis of Border Cell Migration' in which they describe a novel way to quantify border cell migration. Shann-Ching Chen *et al* use the system Machacek *et al.* developed to track cluster boundary displacement through the different frames. This displacement was then mapped into a kymograph revealing the

spatiotemporal coordination of the different protrusion/retraction events. Following this, the boundary sectors were grouped into three parts: front, back and side and associated with a movement label. This was all used to model the degree of coordination between the front and the back of the cluster using a finite state machine.

Prasad and Montell (Prasad and Montell, 2007) developed a way of quantifying the protrusions by developing a directionality index of the cluster activity (Figure 4.10). This involved measuring the length, direction and duration of every protrusion greater than 18 μm from the centre of the cluster. Protrusion direction was determined based upon a 180° angle measured with respect to the direction of migration. In the directionality profile, each protrusion was represented as an arrow at its respective direction/angle. In addition to demonstrating protrusion direction, the directionality profile indicated maximum protrusion length by the length of the arrow shown, and duration (persistence) by the width of the arrow shown. For illustrative purposes the forward (positive) protrusions were coloured in greens and the negative protrusions in reds.

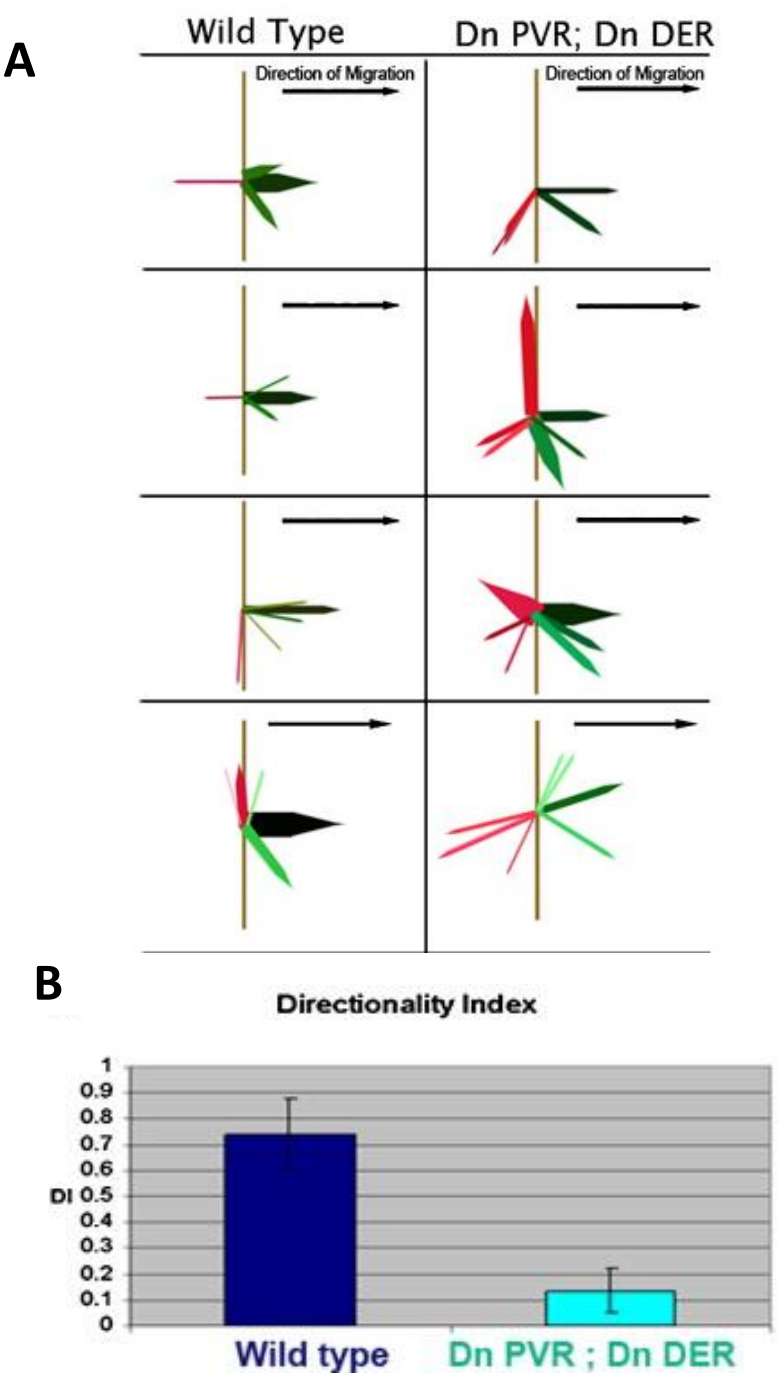

Figure 4.10. Figure taken from (Prasad and Montell, 2007) Showing the results of manual protrusion analysis of Wild type and co expression of DN PVR, DN EGFR. (A) Shows the representation of the protrusions with the arrows representing their direction, persistence and length. Forward (positive) protrusions are labelled in green and backwards (negative) protrusions labelled in red. Note the vertical line representing the 180° angle with which the protrusions were segregated. **(B)** Shows the graphical representation of a directionality index generated by the protrusion results. A directionality index of 0 indicates the number of positive and negative protrusions are equal.

A directionality index was also calculated corresponding to the number of forwards vs. reverse protrusions. A directionality index of 0 meant that there were equal number of forwards and reverse protrusions. Although this method was informative and demonstrated the importance of polarised forward protrusions in successful migration, it did not take into account the effect that protrusions at the side may have on migration. It can be interpreted by the tumbling behaviour of the cluster during certain parts of migration, that it is not as simple as positive protrusions result in forward movement and negative protrusions in reverse or no migration. The wandering behaviour of the cluster during its migration path would suggest that protrusions at the side may act as an inhibitor of polarised movement or distraction from a straight path to the ooycte-nurse cell boundary. This disoriented movement could be crucial to determining the cause of border cell impairment, increased duration or reduced migration rate. Therefore, segregating the cluster into four parts, a front, back and two sides based on protrusion angle would overcome this issue. This was done later by the Rorth group, who subsequently published an automated macro for ImageJ that could recognise the direction, length and persistence of protrusions (Poukkula et al., 2011). This macro will be discussed in more detail later.

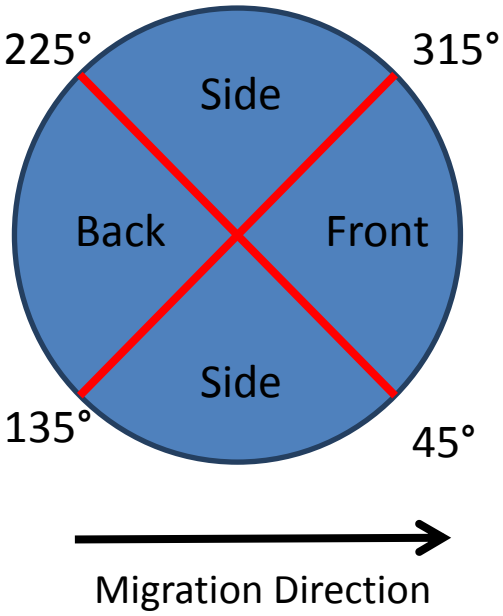

Figure 4.11. Shows a schematic representation of a cluster segregated into four sections based upon the angles specified in Poukkula *et al*. Angles between 315-45° are labelled as front protrusions, 135-225° as back, and 45-135° & 225-315° as side. The angles are calculated based on the migration of the cluster from left to right.

Using a manual method, similar to that used by Prasad *et al.*, but using sectioning guidelines established by Poukkula *et al.*, an attempt was made to map the protrusions of border cell clusters over-expressing dominant-negative PVR (PVR-DN). This genotype was selected as PVR-DN border cells display a clear variation in protrusion directions from wild type as documented elsewhere (Poukkula et al., 2011). The aim was to construct a directionality profile of protrusions eventually in different genotypes, trying to link direction, length and possibly area and persistence to the BC migration phenotype. The mapping was more difficult than first anticipated and a number of key issues were highlighted during the process.

Identifying Protrusions

Identifying what is, and is not a protrusion was the first difficulty that had to be overcome. Protrusions are essentially extensions of the cell body of the entire cluster. The cluster shape is constantly changing with protrusions being generated and retracted; membrane ruffles are also present at the cell edge. Membrane ruffles are densely packed arrays of actin filaments crossed links to specific actin binding proteins such as filamin and erzin that are present at the cell edge due to failed or retracting lamellipodia (Krause et al., 2004; Small et al., 2002). To distinguish between membrane ruffles and protrusions it was important to identify the main cell body of the cluster. The easiest way to do this was by using a circle of approximately the same diameter of the cluster in a rounded shape. This was positioned over the cluster in all frames being analysed. The parts that were covered by the circle were excluded as protrusions and fell under the category of 'cell body'. In addition to this, using a circle of a set diameter for all clusters ensured consistency between frames and genotypes. The schematic in Figure 4.12 shows how the overlapping circle enabled protrusion identification.

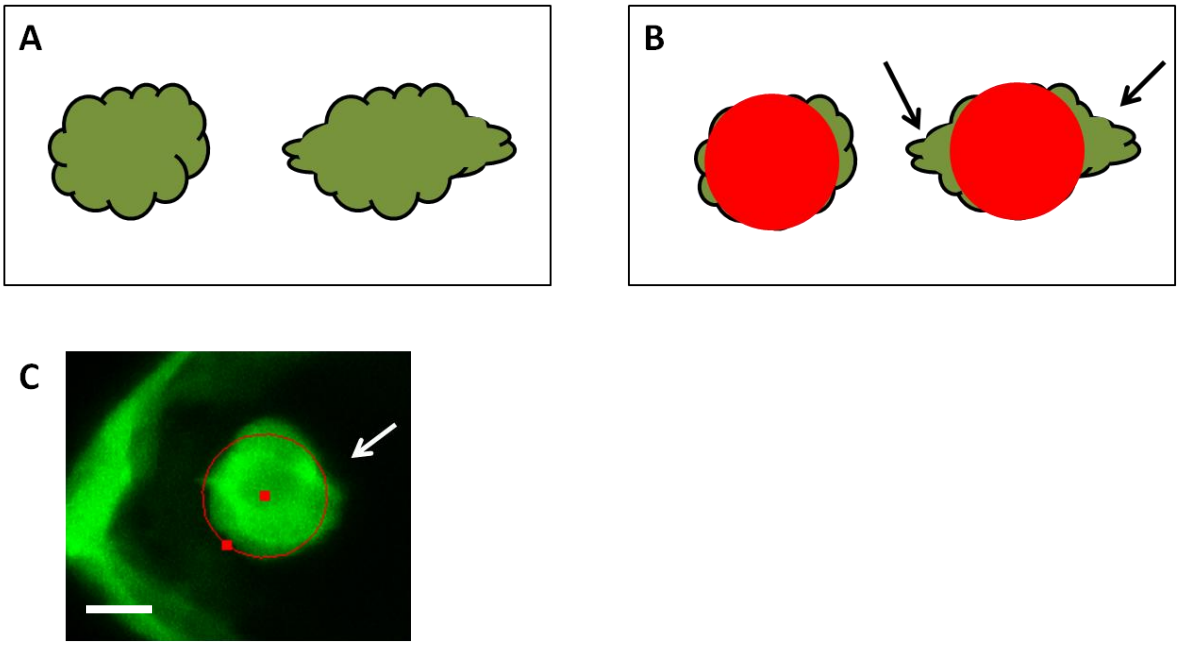

Figure 4.12. Shows how protrusions can be identified and differentiated from the cell body.

(A) Shows a schematic representation of a rounded and polarised cluster. **(B)** A schematic representation of the overlaying circle over a rounded and polarised cluster. The black arrows indicate the protrusions. **(C)** Shows a border cell cluster with the cell body area circled, however the cell body in this example mostly masks the small spike at the rear of the cluster, highlighting a possible problem in this method. The white arrow indicates a forward protrusion. Thick white line represents a 15 µm scale bar.

One issue with this technique however, was that it did not differentiate between a membrane ruffle and a protrusion. In addition, clusters that were elongated, such as those in a polarised migration phase, did not enable the cell body to be encapsulated by a circle. This resulted in part of the cell body being incorrectly classified as a protrusion. To prevent this, additional guidelines were set in place to limit errors in protrusion identification. Similarly to Poukkula *et al.*, (Poukkula et al., 2011) upper and lower size limitations were imposed on protrusions preventing them from having length less than 3 µm, and width more than 9.45 µm, the approximate width of a border cell single nuclei. This prevented part of the cell body being classified as a protrusion. For the majority of time-lapse frames

analysed this was not an issue, most of the cluster extensions were visibly larger than the guidelines. Where it did occur, measurements were taken to determine where the cell body ended and protrusion began, and protrusion measurements taken from that point. This practice became more difficult and the analysis increasingly complex once multiple protrusions from a single source were being analysed; this will be discussed in more detail later (see Section 'New versus Persistent protrusions' below). To differentiate between membrane ruffles and protrusions, minimum values were also characterised preventing membrane ruffles being counted.

Protrusion Length

Protrusions were identified as having a length of more than 3 µm and a width of less than 9.45µm. A standard way of measuring protrusions was determined by measuring from the centre point of the cluster cell body (identified by the centre point of the circle labelling the cell body) to the edge of the protrusion. The diameter of the circle was then subtracted from the total length to give an absolute value of protrusion length. Relative values could also be used by keeping the measurements including the cell body diameter, however it was important that the measurements remained constant to enable the data to be comparable. It was important to measure to the centre of the cluster as it removed judgemental errors with regards to the angle of the protrusion and the point that it intercepted the cell body. This can have an impact on the protrusion length as a smaller angle may result in a shorter distance being measured from the protrusion tip to the edge of the cell body.

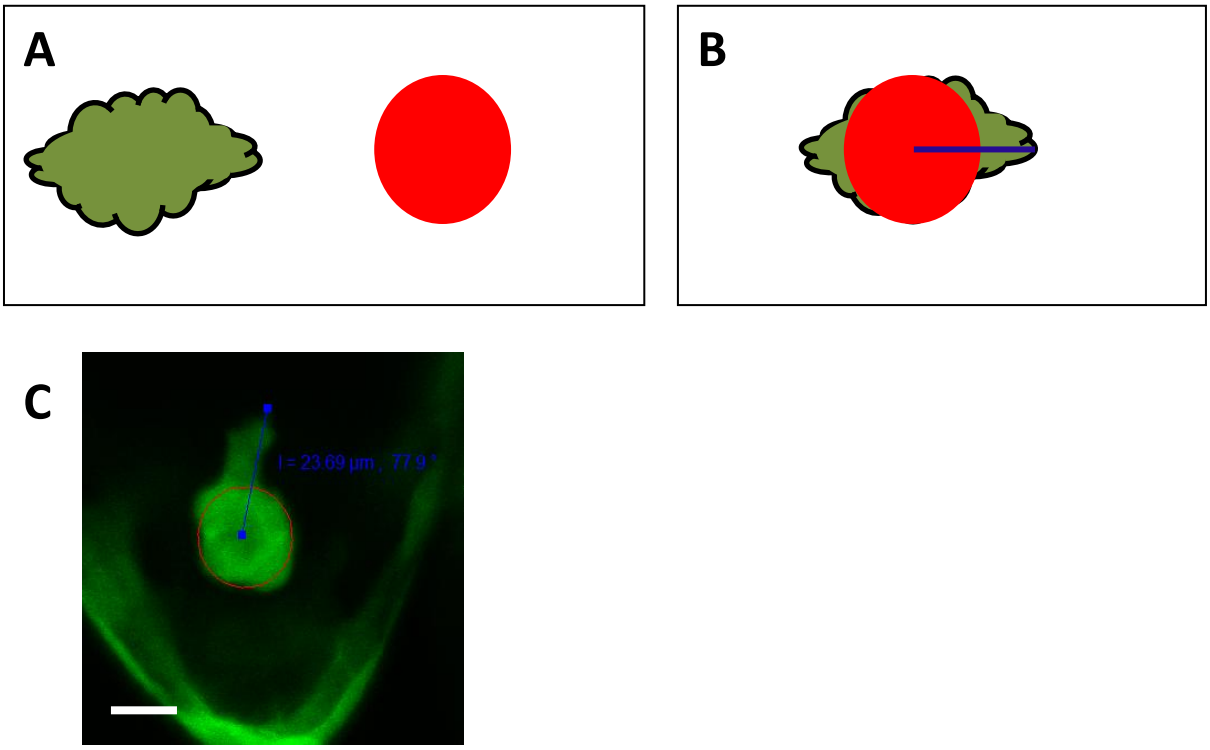

Figure 4.13. Shows how protrusion length can be measured. (A) Shows a schematic representation of a polarised cluster and the circle overlay. **(B)** A schematic representation of the overlaying circle over a polarised cluster, the length is measured from the centre of the circle to the edge of the protrusion (blue line). **(C)** Shows a border cell cluster with the cell body area circled (red) and the protrusion measurement (blue) from the circle centre. Note length and angle measurements are given. Thick whit e bar indicates 15 µm scale bar.

Protrusion Area

As an additional measurement, the area of the protrusion was determined in a basic way, utilising the length measurements and taking a single measurement of the intercepting cell body perimeter. Most outlines of protrusions form an isosceles triangle when drawing a line from the tip to the cell body using the outer edges as both lengths will be the same. Measuring the base of the triangle (where the two points meet the cell body) and separating the triangle into two right angled triangles, it was possible to calculate the area using the simple formula 1/2bh (b= base, h= height) for one of the triangles and doubling. In

the cases where the protrusions were irregular and did not from an isosceles triangle the separate right angled triangle areas were calculated and then simply added together.

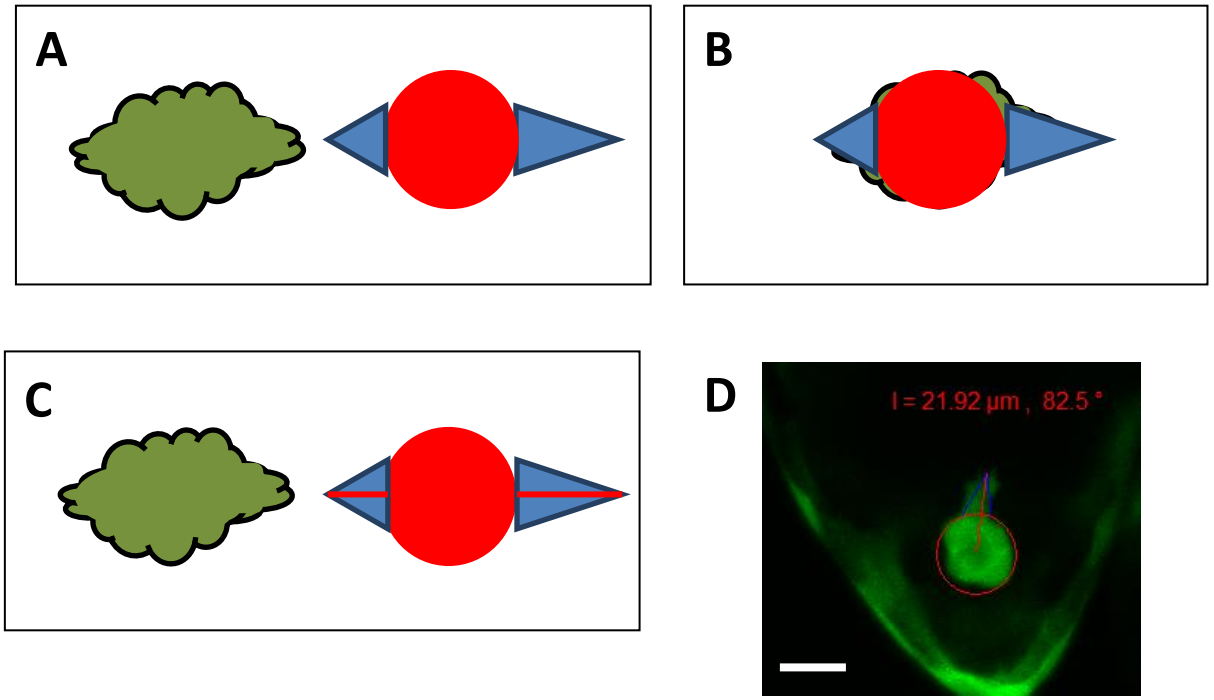

Figure 4.14. Shows how protrusion area can be measured. (A) Shows a schematic representation of a polarised cluster with the circle and triangle overlay. **(B)** A schematic representation of the overlaying circle and triangles over a polarised cluster. **(C)** A schematic polarised cluster with the cell body area circled (red), the area guidelines (blue triangle) and the triangle height measurement (red) from the circle edge. **(D)** Shows a border cell cluster with the triangle area marked in blue and the triangle height in red. Note length and measurements are calculated based upon the distance to the centre of the cluster, the circle radius needs to be subtracted. Thick white line indicates 15 µm scale bar.

Protrusion Angle

As briefly described above, the protrusion angle was measured in different ways, depending on the start and end point selected. Protrusion angles can also be expressed differently depending on the method and software used to analyse them. Prasad *et al.* (Prasad and

Montell, 2007) expressed the protrusion measurement relative to 180° and labelled them as positive or negative protrusions depending on the direction they protruded from. Poukkula *et al* (Poukkula et al., 2011) used specific angles splitting the cluster into four segments and measuring the angles relative to 360°. The angle that is measured was used to categorise the protrusion, as shown in Figure 4.15, into its respective direction, front back or side. The benefits of choosing to categorise the angles in this way avoids accidental errors or mistaken identification, as there are no positive or negatives to consider. If all egg chambers are positioned in the same way, with migration occurring left to right, all angles between the set points of 0° - 45° are front protrusions. When measuring angles from the time-lapse movies it was decided that the Zeiss Laser Scanning Microscope (LSM) Image Browser would be sufficient. This software enabled the length to be measured using a straight line tool and the angle of the line was automatically given. The main issue with this software was that the angle was only available relative to 90°, and that the clusters needed to be analysed with migration moving vertically, as opposed to horizontally. Despite having to measure the angles in a disadvantageous way, the method was implemented as the software was otherwise user friendly and well described.

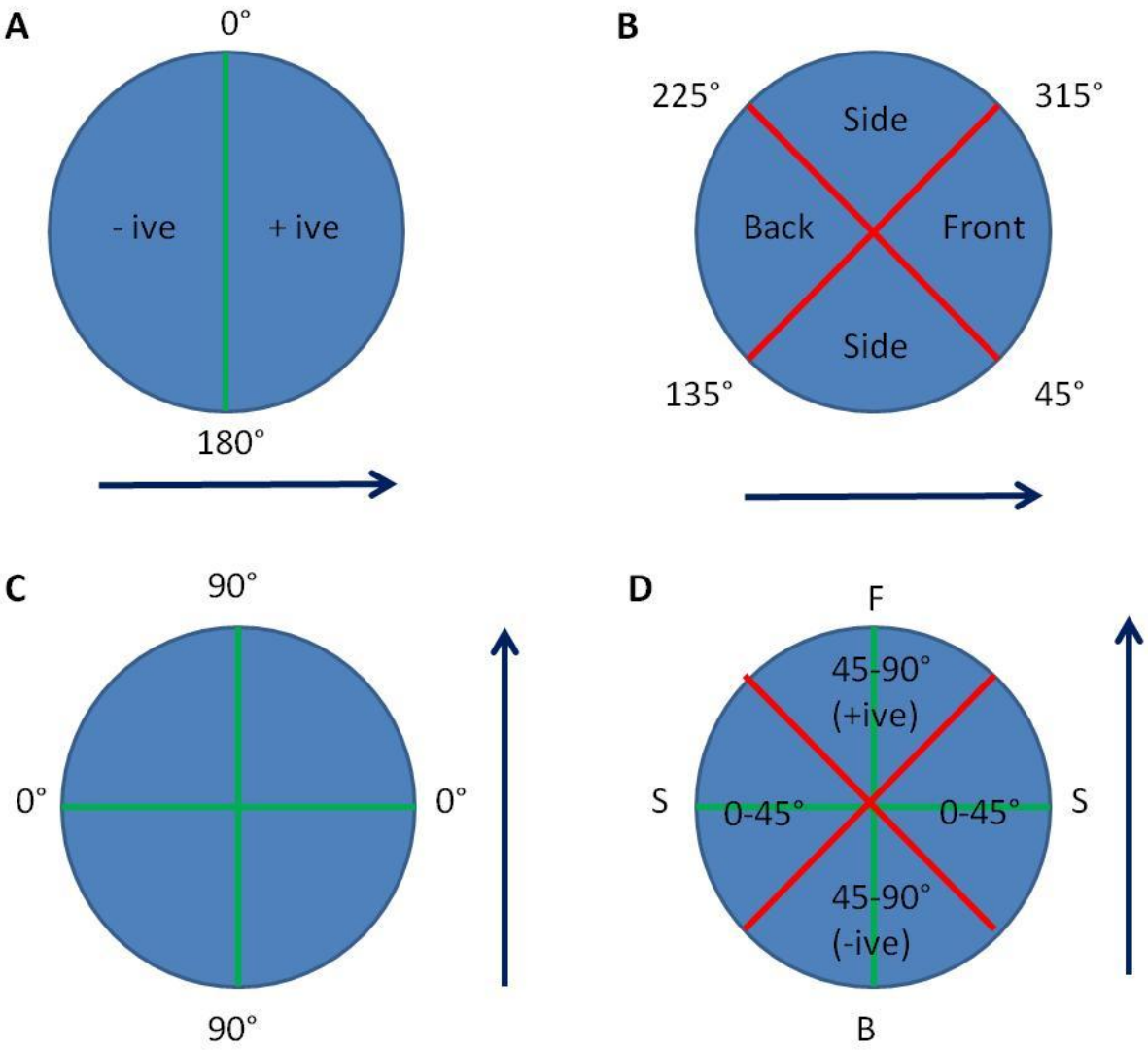

Figure 4.15. Shows schematic representations of the cluster segregation by angle. (A) The cluster is segregated into two parts front and back based upon positive and negative protrusion direction based upon 180° (Prasad and Montell, 2007). **(B)** The cluster is segregated into four parts front, back and sides based upon protrusion direction around 360° (Poukkula et al., 2011) In **(A) & (B)** angles are calculated based upon migration of the cluster from left to right. **(C)** Shows the angle representation used to measure protrusions using my own manual technique using 90°. **(D)** Shows the cluster segregation used to determine front back and side protrusions based on 90° angles. In **(C) & (D)** angles are calculated based upon migration of the cluster from bottom to top. Large blue arrows represent migration direction.

As shown in Figure 4.15, angles were based upon 90° and given a positive or negative value in relation to the direction of migration. This was easy to determine using this software as the horizontal marker was always 0°, so anything above this line was always considered positive and anything below negative. As the front, back and side, segmentation did not fall directly into 90° categories and angle values for each protrusion direction had to be selected. As shown in Figure 4.15, any protrusion angle measured between 45° and 90°, that was positive, was considered to be a front protrusion (or back if negative direction). Any angles 0° - 45° were considered to be side. Working with the two sets of angles instead of four, in some respect made the process easier, despite having to consider protrusion direction. Using 360° as reported previously however, would enable the different side (left and right) protrusions to be identified and would enable a more detailed understanding of the protrusion dynamics.

New versus Persistent Protrusions

It was important when looking at protrusions to identify if the protrusions were newly formed or existing from a previous frame(s). The danger of counting every protrusion as "new" results in the overestimation of the quantity and may prevent genes responsible for protrusion persistence from being identified, or overlooked. As frames were captured with 2 minute intervals, in some cases protrusions could have come and gone or could have been present throughout. To overcome this issue, careful consideration was given to how the protrusions were ordered, including how to identify if protrusions were persistent in consecutive frames. It was important to consider the possibility that in some frames there would be more than one active protrusion at different angles, and these protrusions may or may not be present in the proceeding frames. Another issue that was highlighted, once the analysis had been started, was that in some cases single protrusions had developed into two

protrusions in the next frame (Figure 4.16). In situations like this guidelines were put in place to differentiate between the new protrusion and the existing protrusion.

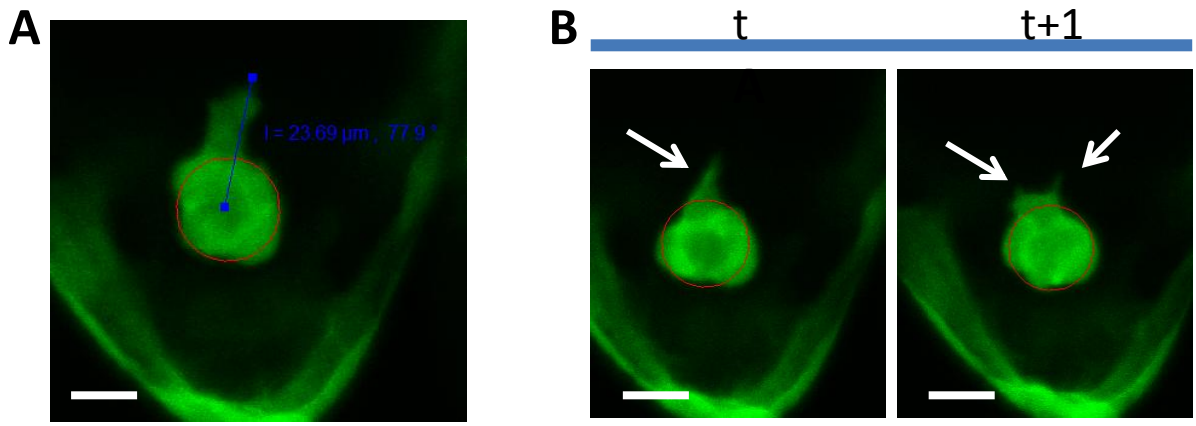

Figure 4.16. Shows Border cell clusters labelled with GFP during the manual measuring process. **(A)** Shows the cell body circled in red and the protrusion length measured in blue. **(B)** Shows the same border cells in two consecutive frames. In the second frame the single protrusion has further developed into two. Thick white line represents 15 µm scale bar.

For the purposes of this analysis, a persistent protrusion was therefore defined as one that was present in more than one consecutive frame. In addition to this, a protrusion was not considered to be persistent if the angle of the protrusion between the first and last frames had a difference of more than 5°. Persistent protrusions were also seen to follow a pattern of increasing length (expansion) and decreasing length (retraction). Protrusions that did not follow this pattern, or followed this pattern and then increased again were labelled as two protrusions, despite having the original protrusion angle value. This was probably due to the newer protrusion expanding as the older persistent protrusion had fully retracted, and could be explained by the forward movement of the cluster during this time. To easily record the confusing behaviour of the protrusions an Excel spreadsheet was generated with the different columns labelled to coincide with the frame number of the time series. Protrusion

length measurements and angle in each frame were logged under each frame title and any multiple protrusions present in that particular frame listed in the rows underneath. Single frame protrusions and persistent protrusions were identified on the spreadsheet by a thick outline of the cells with the corresponding measurements. An example of this for one of the time lapse movies can be seen in Figure 4.17.

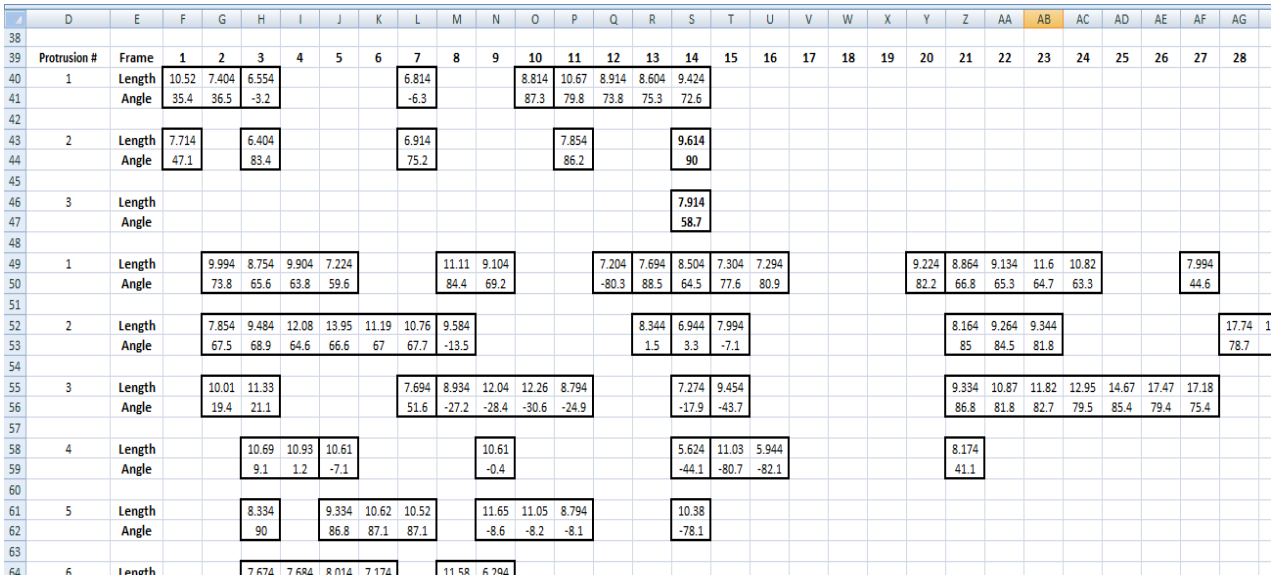

Protrusion #	Frame	1	2	3	4	5	6	7	8	9	10	11	12	13	14	15	16	17	18	19	20	21	22	23	24	25	26	27	28
1	Length	10.52	7.404	6.554				6.814			8.814	10.67	8.914	8.604	9.424														
	Angle	35.4	36.5	-3.2				-6.3			87.3	79.8	73.8	75.3	72.6														
2	Length	7.714		6.404				6.914				7.854			9.614														
	Angle	47.1		83.4				75.2				86.2			90														
3	Length														7.914														
	Angle														58.7														
1	Length		9.994	8.754	9.904	7.224			11.11	9.104			7.204	7.694	8.504	7.304	7.294				9.224	8.864	9.134	11.6	10.82			7.994	
	Angle		73.8	65.6	63.8	59.6			84.4	69.2			-80.3	88.5	64.5	77.6	80.9				82.2	66.8	65.3	64.7	63.3			44.6	
2	Length		7.854	9.484	12.08	13.95	11.19	10.76	9.584					8.344	6.944	7.994						8.164	9.264	9.344					17.74	1
	Angle		67.5	68.9	64.6	66.6	67	67.7	-13.5					1.5	3.3	-7.1						85	84.5	81.8					78.7	
3	Length		10.01	11.33				7.694	8.934	12.04	12.26	8.794			7.274	9.454						9.334	10.87	11.82	12.95	14.67	17.47	17.18	
	Angle		19.4	21.1				51.6	-27.2	-28.4	-30.6	-24.9			-17.9	-43.7						86.8	81.8	82.7	79.5	85.4	79.4	75.4	
4	Length			10.69	10.93	10.61				10.61					5.624	11.03	5.944					8.174							
	Angle			9.1	1.2	-7.1				-0.4					-44.1	-80.7	-82.1					41.1							
5	Length			8.334		9.334	10.62	10.52		11.65	11.05	8.794			10.38														
	Angle			90		86.8	87.1	87.1		-8.6	-8.2	-8.1			-78.1														
6	Length			7.674	7.684	8.014	7.174		11.58	6.294																			

Figure 4.17. Shows a spreadsheet displaying results from manually recording the protrusions during the first half of migration. Single protrusion values are identified by a thick border. Protrusion length and angles measurements are recorded in the column respective to the frame number.

Results

The total number of protrusions measured using the manual technique overestimated the number of protrusions relative to the number measured using a custom semi-automated macro of Poukkula *et al*. (see Section 4.3.4 below). This could be due to several reasons. A circle defining the cell body may have been too small, resulting in more of the cluster being identified as a protrusion when measured manually. In addition to this, membrane ruffles may have been counted as protrusions, whereas these may have been discounted by the

macro. Some protrusions may have been incorrectly labelled as short lasting, single framed and not persistent, due to the small angle guideline of 5° being used. One issue that was not considered during the manual analysis was the presence of protrusions in a single frame that are indeed not active protrusions but the remains of the cluster, a trailing edge, as a result of its movement. Using the manual analysis technique all parts of the cluster that were not part of the main cell body in that particular frame, were classified and measured as a protrusion. This could have caused an overestimation of the protrusion number. The average directionality of the protrusions was also observed to be different, with the manual analysis classifying more protrusions as side-orientated as a percentage of the total, and less at the back compared with the macro output.

The number of extensions per frame was also compared across the methods: these were calculated manually by dividing the total number of extensions per direction to the total number of frames. When comparing the manual results to the published results from DN-PVR in Poukkula *et al.* (Poukkula et al., 2011) the number of extensions per frame followed the same pattern, with more extensions at the front, followed by the sides, then the back. However, when comparing the macro results (see Section 4.4) to the published data, there were more protrusions at the back than the side (see Figure 4.18).

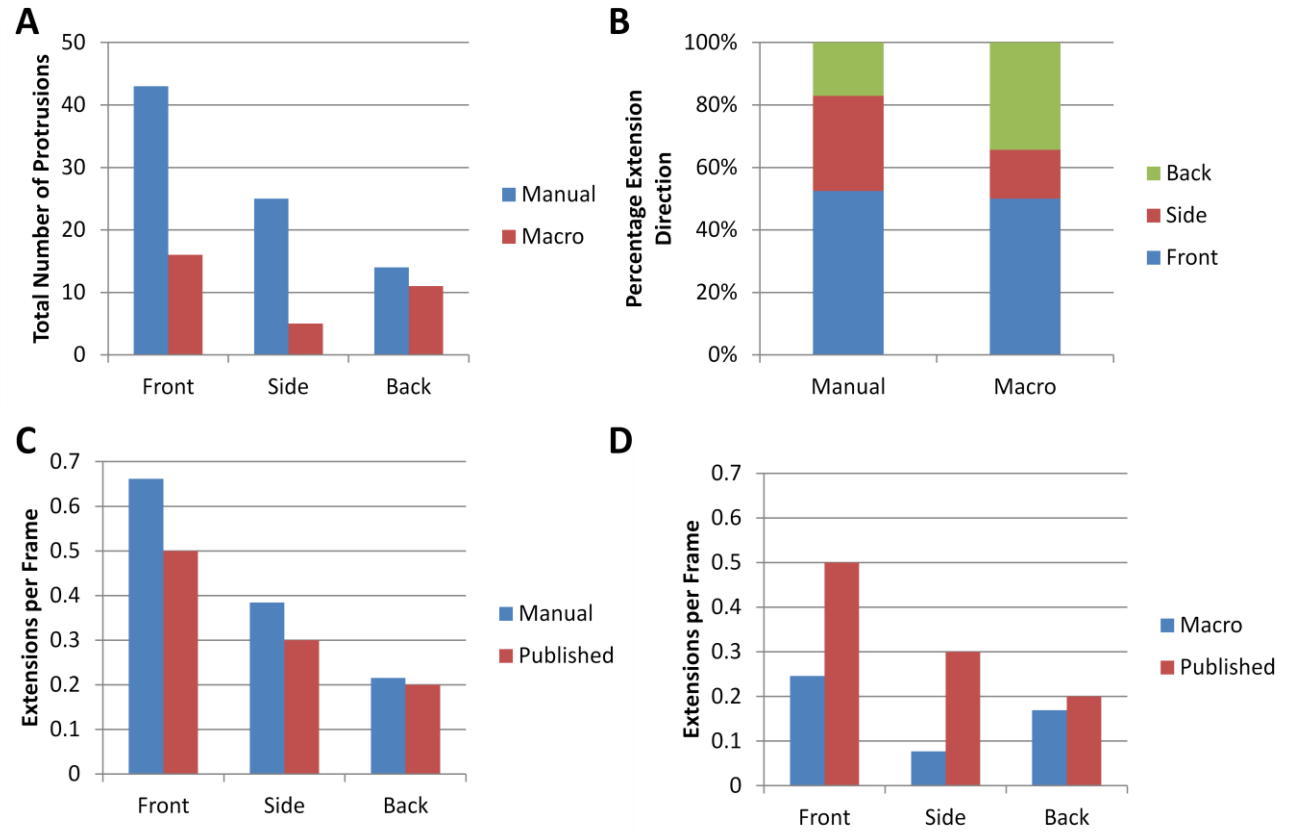

Figure 4.18. Shows the results from manually recording the protrusions during the first half of migration. (A) A graph comparing the total number of protrusions measured using the manual technique compared to values obtained using a semi automatic macro using the same image file. In all directions number of protrusions were overestimated with respect to (Poukkula et al., 2011). **(B)** Shows the same values represented as a percentage of the total number of protrusions in their respective directions. **(C)** A graph comparing the number of extensions per frame measured using the manual technique compared to the published data. **(D)** A graph comparing the number of extensions per frame measured using the automated macro compared to the published data.

In summary, there are inherent weaknesses in manual analysis as, despite having robust guidelines when measuring the protrusions, errors and incorrect judgements can be made. One issue relates to the characteristic shape of the cluster during the polarised first stages of migration. The extension and rapid forward movement of the cluster results in parts of the cluster forming a trailing end, which can be incorrectly labelled as a protrusion instead

of the retracting cell body. Using the automated macro described below, which tracks cluster movement in addition to protrusion dynamics, takes this into consideration.

4.4 Semi-Automated Data Extraction

Using an automated plugin to accurately track the border cell cluster and protrusion dynamics can make quantifying time-lapse movies more time effective, accurate and ensures consistency between different egg chambers and genotypes. Poukkula *et al.* (Poukkula et al., 2011) developed a macro to specifically analyse border cell migration behaviour and protrusion dynamics. Poukkula *et al.* further characterised border cell migration phenotypes following disruption of receptor tyrosine kinase guidance signalling, by linking cluster behaviour to effects on actin-based protrusions. In essence the macro segregates the cluster into front, back and side segments and records and measures the protrusions for each of the sections. In addition to logging the protrusion behaviour, the macro automatically tracks the movement of the cluster in XY, enabling information such as migration speed and directed movement to be calculated.

The macro has been designed to be user friendly and straightforward when simple adjustments need to be made for individual egg chambers.

4.4.1. Using the Macro

The macro used the maximum intensity projected images from the time lapse movies that had been generated, similarly to those used for the manual tracking and MTrackJ plugins. It was important when looking at protrusion dynamics to use a fluorescent reporter that accurately labelled the protrusions. For the protrusion analysis Lifeact-eGFP was used, which labels F-actin, driven by the border cell specific driver *c306-GAL4*, as described in

Chapter 3, Section 3.6.3. Although the macro had the ability to separate full migration into first and second halves, analysis of the first half of migration only was used. In order for the macro to work accurately, the cluster had to be fully detached, and not be in contact with the surrounding epithelium. The projected cropped image had to be rotated so that it was orientated with the cluster migrating from left to right. This was important as the macro assumes that the cluster is migrating in this direction and assigns the front, back and side directions based on this.

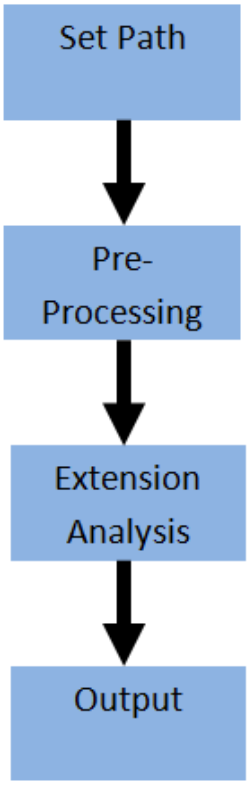

Figure 4.19 Flow diagram showing some of the key steps in the automated macro. Set paths describes the file preparation needed to determine where outputs from the pre-processing steps and final results are stored. Pre-processing steps essentially convert the image files into smaller binary images following thresholding steps. These files need to be modified to ensure the cluster is the only object in the field of view. Extension analysis uses the generated binary images to generate protrusion and cluster data.

Set Path

This part of the macro was in preparation for the pre-processing and extension analysis steps. It was found that setting different destination folders for each genotype was key to remaining organised, and was useful later on. This is because the macro was constantly using and saving additional files, in different specified locations during the running of the macro. When running the macro there were prompts to define a destination folder primarily for the pre-processed movies (See Methods 2.4.5).

Pre-processing

The pre-processing stage converted the large projected movies into smaller binary movies containing the information the macro needed to identify the cluster and analyse the protrusions. Turning the movies into binary form essentially simplified the cluster, removing the need for the macro to consider cluster signal intensities, as everything was categorised as either having a signal or having none at all. This stage consisted of defining the cluster migration region, and thresholding the eGFP-labelled cluster, ensuring the cluster and protrusions could be identified.

When selecting the eGFP reporter it was important that the protrusions could be easily seen (see Chapter 3.6.2). Despite a thres-holding step, extremely faint protrusions may have been missed, as the signal from the whole cluster was defined from the background signal. This may have resulted in key protrusion data being lost.

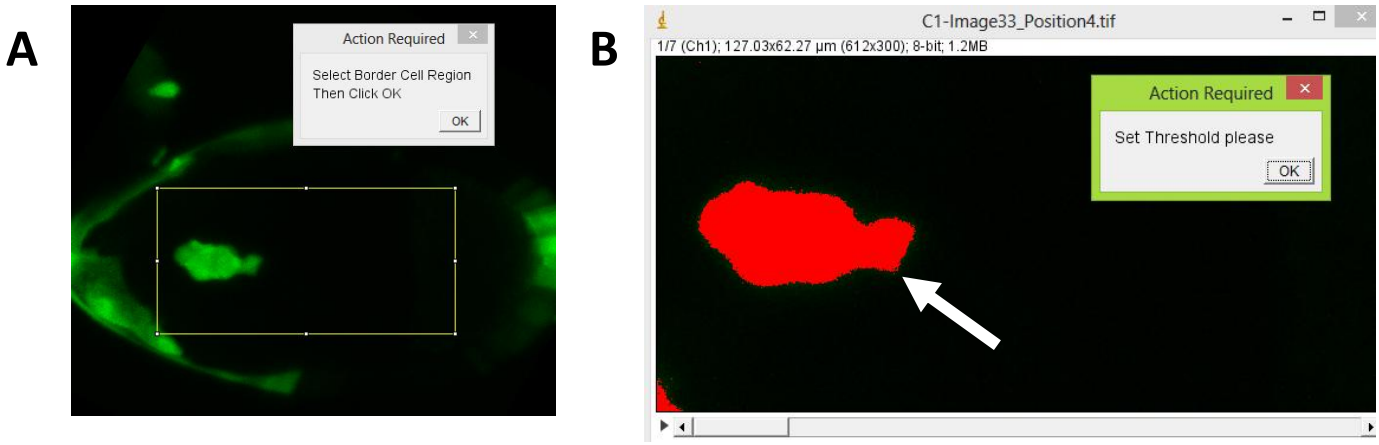

Figure 4.20. Shows the final steps of the pre-processing macro. (A) Shows a projected image of the Border cell cluster movie. The border cell region (labelled with eGFP) is defined by the yellow rectangle, this area is taken past where the cluster finishes its migration to ensure it does not touch the outline. Touching the outline results in part of the migration process being missed **(B)** Shows the border cell cluster from the defined region from image **(A)** in red and the background black. The red area indicated by the white arrow displays the parts of the movie that will be included in the binary image.

Extension Analysis

The extension analysis required the pre-processed binary movies generated by the pre-processing steps. However, it was found that in most cases the binary movie could not be initially used and further formatting had to be performed. This was due to parts of the epithelium or other parts of the egg chamber being included in the original selected area, and subsequently converted into a binary signal. It was crucial for the accurate running of the macro that there was only one object (the cluster) in each of the frames.

In addition to this, some clusters contained gaps between the cluster body and protrusion, where the extension was too thin or faint to detect due to the thresholding step. Any gaps needed to be filled in by hand using the ImageJ draw tool; it was vital that the ultimate

shape of the cluster or protrusions were not altered as this would have influenced the results obtained.

Figure 4.21. Shows the binary image files of the Border cell cluster generated by the pre-processing steps. **(A)** Shows the same frame before and after part of the epithelium has been masked, indicated by the red arrows. **(B)** Shows the same frame before and after part of the protrusion has been filled in, indicated by the red arrows. Note only one object can be present in each frame for the macro to function correctly.

4.4.2. Output

Saved in the destination folder was a large number of files in .tif, .txt and .xls format displaying all the data extracted from the images.

The .tif files showed the segmentation that had been carried out in a visual format; a representative of these is shown in Figure 4.22 below.

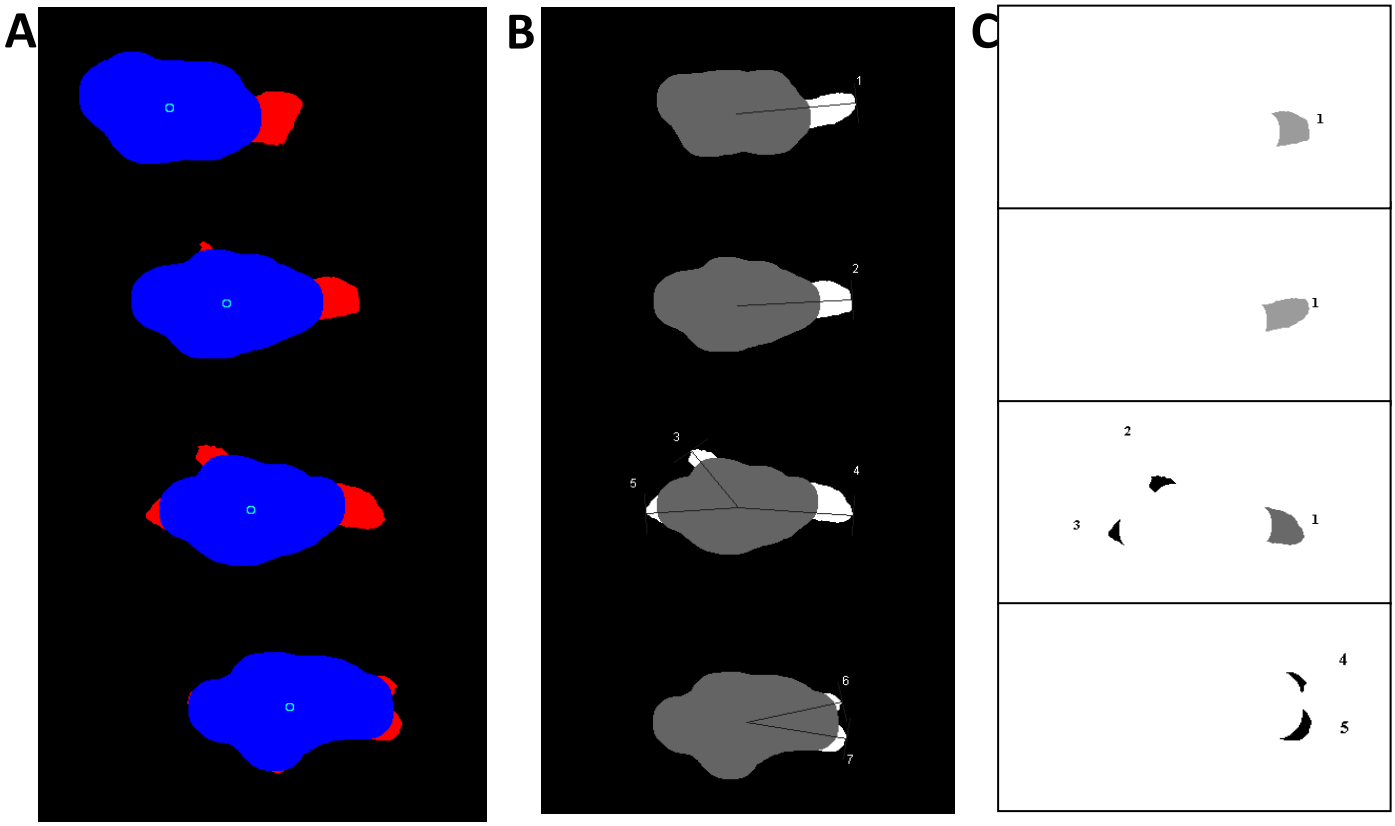

Figure 4.22. Shows representative visual output of the extension analysis at four consecutive time points (2mins apart). Here, the cluster is travelling from left to right. **(A)** The cell body is labelled in blue and the protrusions in red; the .tif file was used to determine if the image segmentation has taken place correctly. The small circle indicates the centre of the cluster and is used to calculate migration distance. **(B)** Shows each of the protrusions measured in each time frame. Each protrusion was measured from the centre of the cluster. All protrusions were counted, resulting in data on the actual number of protrusions; it did not distinguish new from old protrusions. **(C)** Shows the number of protrusions counted as single protrusions. The cell body was not present, only the protrusions. These were counted and identified as persistent or new and labelled singularly or in multiple frames.

The excel files in the output contained most of the useful information about the cluster migration and the protrusions. Each of the files was separated based on specific information about the cluster, for example data such speed, cluster shape, duration etc. This was important when initially looking at differences between genotypes, to see if there was an

impairment.

Other outputs gave information with regards to the extensions such as the speed of the cluster, extension area and length, at each of the separate sections, front, back and sides. It also described the persistence, angle of each of the individual extensions. The output also contained information on a frame-by-frame basis, including the direction of the extensions at each time point. These were represented as absolute and binary numbers for each direction in each frame, allowing direct frame-by-frame analysis to be carried out if necessary. Additional spreadsheets were also given with more detailed data about the maximum length and area of individual protrusions.

Using all the data combined enabled a clear accurate picture of the migration process, which could be used to compare the behaviour in different genotypes.

Additional Macro Uses

In addition to extension analysis, information about the effects of the protrusions on the migration process could also be generated using the X-velocity and Max/Sum macros. This used the pre-processed movies generated to determine what effect the extension size, area and persistence etc. related to the cluster velocity in the X axis. It was found to give a more informative view on the role protrusions play in the migration process, especially if no differences were seen in protrusion number or direction. It used the velocities that the centre of mass travelled, to determine if any protrusions were productive in forwards movement. The macro essentially reuses data generated by the extension analysis and displays it in a different way.

Another operation of the macro was to collate all of the data files together. This was especially useful when more than one image file was being used to represent movement

within a single egg chamber, e.g., when adjustments were made in the focus during imaging. It allowed the results files for all movie parts and genotypes to be collated into one excel spreadsheet, making analysis easier.

Results

This results section is going to focus on the tracking aspects of the macro, and not the protrusion analysis, which has been briefly described earlier and will be discussed in more detail in Chapter 5, Section 5.3.

border cell clusters from wild type egg chambers (*c306 GAL4, UAS Lifeact-GFP*) were imaged and tracked for the first half of migration. The results from the automated macro show that the border cell cluster travelled on average 1.42 µm/minute, based on the average velocity from one frame to the next, using XY values only. These values are much higher than seen previously in XY (Section 4.3.2) with *slbo GAL4, UAS mCD8-GFP* in the first half of migration (0.61µm/min). As all imaging techniques were the same, the differences in speeds are either a result of the genotype or the tracking method used. To determine the cause of the discrepancy, *c306 GAL4, UAS Lifeact-GFP* border cell clusters were tracked in XY and XYZ using the MTrackJ plugin to compare the migration rates using the same genotype. In XY, the tracked migration rate was very similar to the macro at 1.39 µm/minute. The rate in XYZ was higher (1.68 µm/minute), again most likely because of drift in the Z direction. Therefore the differences seen in migration rate can be attributed to the genotype of the reporter strains and not due to discrepancies in the tracking methods.

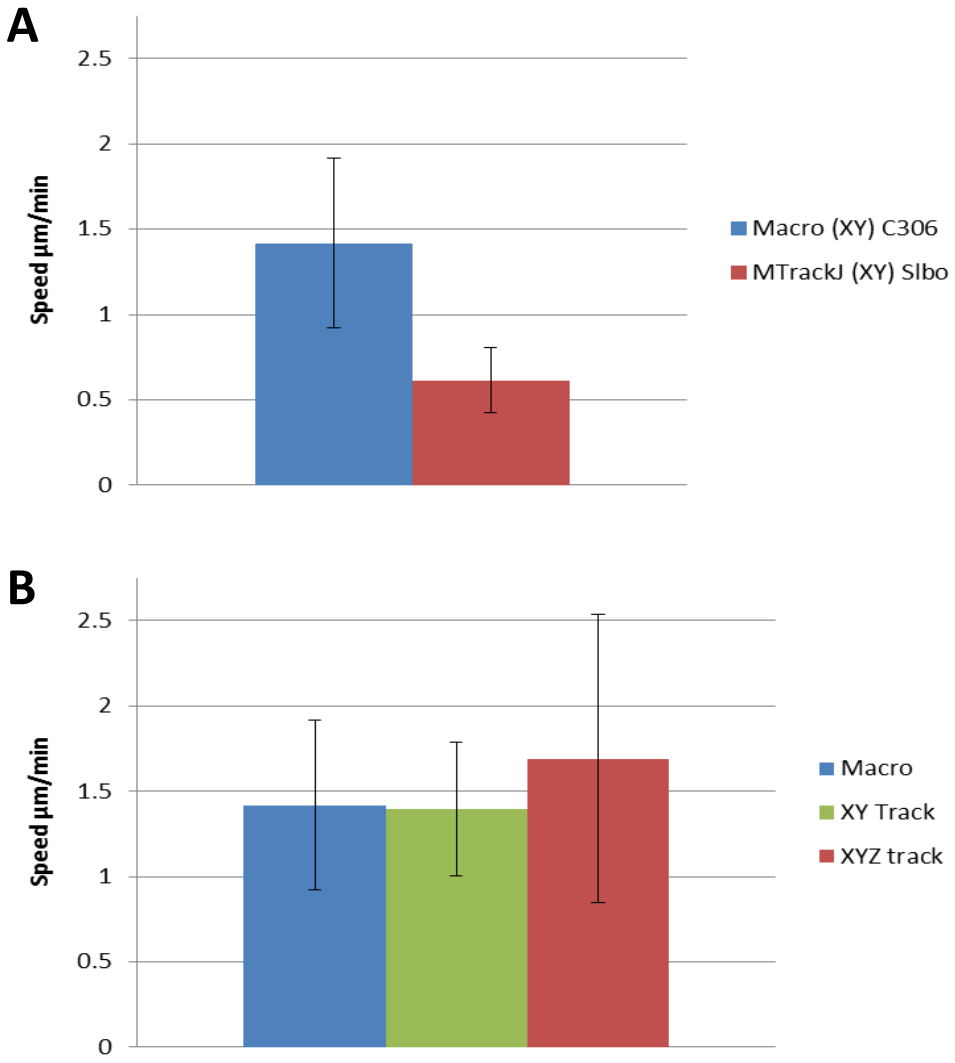

Figure 4.23. Shows graphs comparing the migration speed calculated by the automated macro and MtrackJ. (A) Shows the migration speed during the first half of migration in two different genotypes, analysed by two different methods, automated and MtrackJ.

Genotypes are as follows*: c306 GAL4, UAS-LifeactGFP*, an actin based reporter under the control of c306 which enables expression in the follicle and polar cells. *slbo GAL4, UAS-mCD8-GFP* a membrane based reporter under the control of Slbo expressing in the follicle cells but not the polar cells. **(B)** Shows the migration speeds of the same genotype (*c306 GAL4, UAS-LifeactGFP*) using three different methods. Error bars represent the standard deviation of the mean.

4.5. Discussion

Using live imaging techniques to dissect the behaviour of border cell migration enables a better understanding of invasive cell migration. It is important, however, that the information generated through time-lapse imaging is analysed correctly and is consistent across multiple egg chambers. Extracting basic quantitative data, such as duration or migration rate (speed), can only provide limited insights, and in some respects can lead to false conclusions about cluster behaviour. Although the direct migration distance in all egg chambers can be considered constant, not all border cells migrate the same distance, as tracking results show. Increased migration distance could therefore alter the duration of border cell migration. Accurate measurements of migration rate depend on reliable measurements of the migration distance, and although most egg chambers did not significantly deviate from a direct route to the oocyte, small differences can result in the over or underestimates of migration rate. Behaviour such as premature early tumbling can also influence migration duration and rate, as this delay can cause the duration to be increased and the migration rate to be decreased, when globally calculated. The more accurate way to determine migration rate and to understand differences in border cell migration was found to be through tracking the movement of the cluster. This was done manually using MTrackJ and in a semi-automated way using a custom macro. Both methods had their strengths and weaknesses: manual MTrackJ tracking was slower and was open to user error, as the tracks were being manually plotted; the automated macro could not make any exceptions or adjustments if there were problems in single frames and lack of polar cell staining impaired the ability of the macro to identify the centre of the cluster. The automated macro did however enable all egg chambers to be consistently analysed using the same strict guidelines and was very quick to use once images had been appropriately

processed. Reassuringly, both MTrackJ (XY tracking) and the automated macro returned similar values for distance migrated and rate of migration. Of the two methods, MTrackJ was much more convenient to use for simple measurement of this type due to the extensive amount of image preparation needed for the automated macro. Tracking in XYZ suggested that the border cell cluster does not significantly move in the Z plane during the course of migration, as suggested previously in the literature. However tracking XYZ migration in egg chambers was more difficult than first thought due to the large amount of Z drift. Despite trying different imaging methods, as described in Chapter 3, this remains a problem. Stopping and starting the time series to accommodate for large changes in drift may result in information being missed and still did not enable XYZ tracking to be performed, as there was no way that the exact position of the cluster could be calibrated between time series. Having a large number of Z frames was found to overcome small changes in Z drift, however this caused problems in itself. Extra Z images taken per time frame increased the time interval between consecutive images for each egg chamber. If protrusion data was important, information would have been lost as extensions may have extended and retracted within that time. Therefore, the number of egg chambers imaged per experiment needed to be reduced, to overcome this. Another solution would be to utilise the advantages of another type of microscopy such as Light sheet fluorescence microscopy (LSFM). LSFM produces 3D images by imaging samples within tissues, by illuminating a specific Z section of the sample, through focussing the laser from the side. This enables higher resolution and faster images to be acquired. Having higher resolution images will enable more information to be gathered about the migration process, such as adhesion properties of the cluster during migration. It can also enable us to generate models of how clusters of cells move in response to local chemotactic gradients. This will reveal under what

circumstances collective migration of a cluster is favoured over polarized movement (in which one cell is dominant), and what mechanisms are employed to maintain this mode of migration.

5. The Requirement for Pico and SCAR in Border Cell Migration

5.1. Introduction

Drosophila border cell migration is a genetically tractable *in vivo* system in which to study the regulation of migratory genes. Whilst much is known about the mechanisms that enable single cells to migrate *in vitro*, less is known about how cells migrate collectively, especially *in vivo*. The border cell migration system is a good way to explore the behaviour of collective migration as it enables the mechanisms that are responsible for different parts of the process to be dissected. This is due to the now larger understanding of how normal, wild type border cells migrate and the ability to visualise the process in real time. In addition to this there are an ever expanding number of genes being linked to the process (see Introduction 1.3).

The driving force for migration in this system, as in many others, is the formation of actin-based protrusions. However, the identity of the regulatory proteins that coordinate remodelling of the actin cytoskeleton during border cell migration has not been fully determined.

The actin regulatory proteins SCAR/WAVE and Arp2/3 have been found to be recruited to lamellipodium by phospholipds and active Rac (Campellone and Welch, 2010; Insall and Machesky, 2009), to promote lamellipodial extension and to regulate migration of mammalian cells in culture (Suraneni et al., 2012). Recent evidence indicates that the SCAR/WAVE complex also interacts with members of the MIG-10/RIAM/Lamellipodin (MRL) proteins (Law, 2013; McShea et al., 2013; Xu and Quinn, 2012). MRL proteins link activated RAS-GTPases with the actin regulator proteins Ena/VASP to induce chances in actin

dynamics, cell motility and the cytoskeleton (Krause et al., 2004; Lafuente et al., 2004). In mammalian cells, Lamellipodin (Lpd) has been shown to control protrusions, dorsal ruffling of fibroblasts, axon elongation and branching of hippocampal neurons (Krause et al., 2004; Michael et al., 2010). However, the role of these proteins in epithelial cell migration had not been determined.

pico, the only member of the MRL family of proteins in *Drosophila*, has been shown to be required for tissue and organismal growth. Modulation of *pico* levels results in altered cell division, growth and changes in G: F actin ratios, which in turn affects activation of the Serum Response Factor (SRF) (Lyulcheva et al., 2008). Preliminary data had also suggested a role for *pico* in border cell migration via its effects on the actin cytoskeleton (E. Taylor Thesis). However, these experiments had been performed using RNAi lines that have since been shown to have off-target effects (Jonchere and Bennett, 2013).

5.1.1. Aims

The aims of this chapter were, therefore, to develop a better understanding of the role that SCAR and Pico play in border cell migration by analysing fixed samples and by utilising the tools and techniques for live cell imaging described in Chapters 3 and 4.

5.2. Quantitative Analysis of Border Cell Migration in Fixed Tissues

In the first instance, fixed samples of egg chambers were analysed to assess the effect of different genetic backgrounds on border cell migration. When analysing fixed samples, the retracting anterior follicle cells (also known as centripetal cells) were used to assess normal border cell position (bcp) as described in Chapter 3, Section 3.1. The retracting anterior

follicle cells migrate towards the oocyte during stage 9 of development at a rate similar to the border cell cluster. During posterior migration the border cell cluster is positioned a similar distance away from the migrating follicle cells throughout. Despite there being a large amount of variation in border cell migration rate and position observed in live imaging (Prasad et al., 2007; Prasad and Montell, 2007), as a general rule the border cell position is located slightly behind the most anterior retracting follicle cell. The exact position of the cluster however can differ depending on the border cell specific driver and the fluorescent reporter used, as discussed in Chapters 3 and 4.

Using this predictive distance as a constant, the distance from the most anterior follicle cell to the border cell cluster was measured to define the border cell position (bcp). For the benefit of my analysis, stage 9 egg chambers were identified by the follicle cells having begun their migration to cover the oocyte. Early stage 9 egg chambers where the follicle cells had just left the anterior tip were not used to quantify bcp, as the bcp is typically slightly behind the retracting cells. This reflects the fact that there is a slight delay in the follicle cell retraction process and the initial detachment of the border cell cluster. Stage 10a was defined as the stage by which the follicle cells have reached the oocyte boundary and have formed a columnar epithelium. It is apparent when looking at very late stage 9 egg chambers and very early stage 10a when this stage is; at the transition between the two stages, the retracting follicle cells are at the boundary, but have not yet formed a columnar epithelium. At stage 10a the follicle cells have 'bunched up' almost at the boundary, ready to migrate inwards to fully surround the oocyte. Once this inward migration has begun, egg chambers are no longer classed as stage 10a (See Chapter 3, 3.1 for definitions of Stage 9 and Stage 10).

5.2.1. Pico levels need to be tightly controlled during border cell migration

The bipartite GAL4-UAS system (see Introduction 1.3) was utilised in transgenic flies carrying an inverted repeat construct (*pico*^{IR}), capable of expressing intron-spliced hairpin dsRNA for a sequence common to *pico*. *UAS-pico*^{IR49} (described as pico RNAi^{49}) was used to knock down the levels of *pico* and was shown to have no off-target effects using dsCheck (http://dscheck.rnai.jp/), indicating its specificity to *pico* transcripts (Jonchere and Bennett, 2013). dsCheck searches for on and off-target sequence homologies exhibited by short inhibitory fragments produced from long dsRNA fragments typically used to induce RNAi. *slbo-GAL4 was used* to continuously drive *UAS-pico*^{IR49} and *UAS-GFP* expression specifically in the migratory cells of the border cell cluster, but not the central (non-migratory) polar cells. Ovaries were dissected from 3 day old fattened adult females of *slbo-GAL4, UAS-picoRNAi*^{49} (*slbo>picoRNAi*^{49}) containing *UAS-GFP, His2A-RFP* and *slbo>GFP, His2A-RFP*. Egg chambers at stage 9 and 10a were selected and imaged, and the bcp and percentage migration for the respective stages measured and calculated (n=50 egg chambers/genotype/stage). Knocking down the levels of *pico* significantly impaired border call migration at stage 9 with *slbo>picoRNAi*^{49} egg chambers having a mean bcp of -21.8 µm compared to *slbo>GFP* +4.9 µm (One-way ANOVA, Dunett's, $P<0.001$; n=50). The distribution of the bcp distances followed a similar pattern to wild type (WT) with a larger number of bcp being ahead of the anterior follicle cells, however there were a larger number of bcp measured from -50 µm to -30 µm and <-50 µm (see Figure 5.1). Stage 10a egg chamber bcp was measured as a percentage of the total migration distance and categorised into four groups representing the percentage of migration: 0-25 %, 25-50 %, 50-75 % and 75-100 %. At stage 10a border cell migration in *slbo>picoRNAi*^{49} fully resembled wild type as 100 % of the egg chambers had migrated 75-100 % of the way (WT = 99 %).

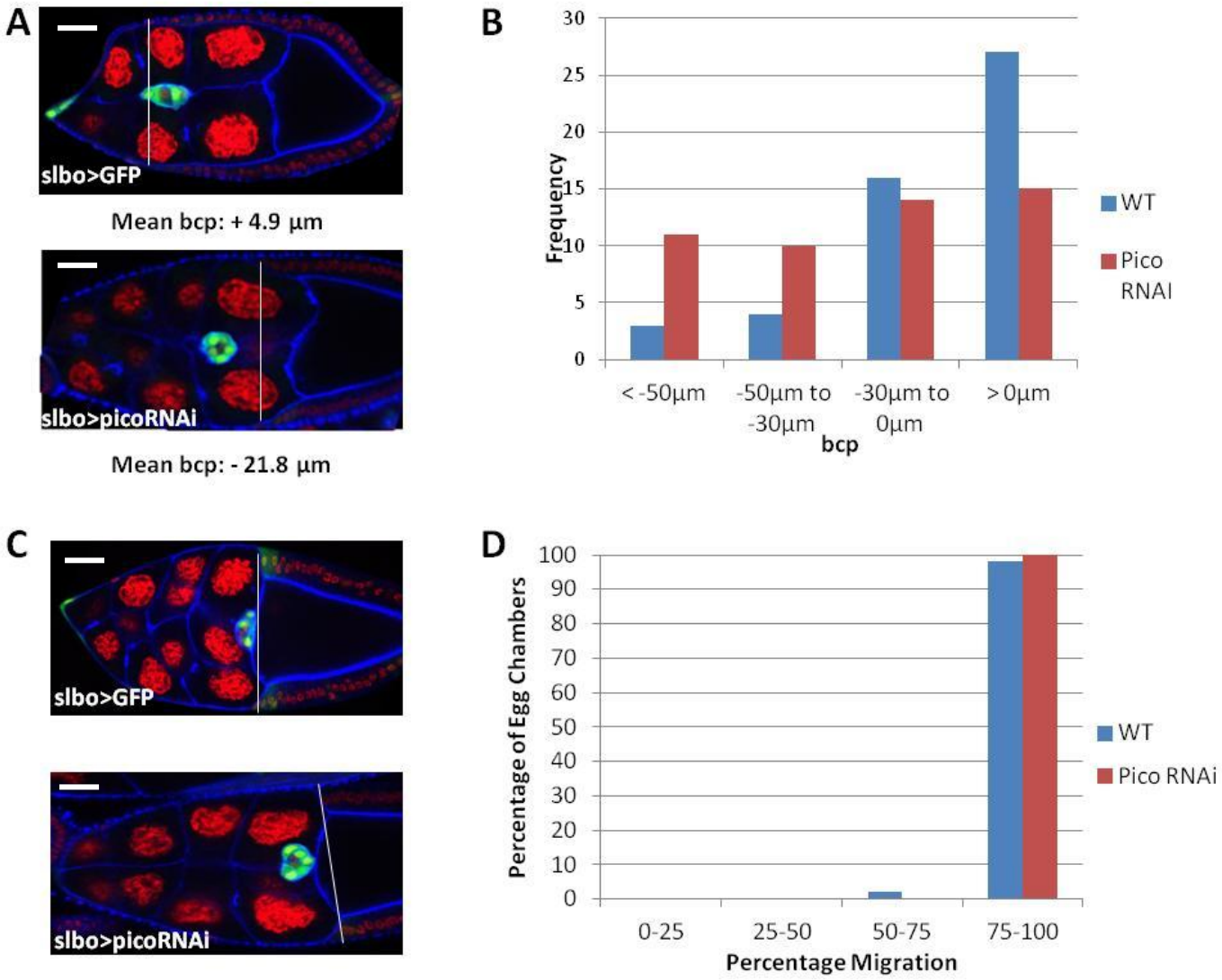

Figure 5.1. Reducing levels of *pico* delays border cell migration progress.

(A) Representative images of late stage 9 egg chambers; border cell labelled with GFP, nuclei labelled with RFP and F-actin shown in blue. Solid white lines across the egg chamber indicate position of the most anterior overlying follicle cells. Thick solid white line indicates 15 µm scale bar. The mean bcp of *slbo>GFP* (WT) and *slbo>picoRNAi* [49] are indicated. **(B)** Distribution profile of bcp comparing WT and *picoRNAi*[49]. **(C)** Representative stage 10b egg chambers labelled as in (A), showing representative position of border cells in relation to the oocyte/nurse cell boundary. **(D)** Graph comparing the percentage migration of wild type and *slbo>picoRNAi*[49] egg chambers at stage 10b.

This indicated that between mid stage 9 and stage 10a, the border cell cluster had someway caught up with the anterior follicle cells, resulting in a normal migration finish. This may suggest that *pico* function is more important in controlling the first part of migration and compensatory mechanisms in the second half of migration can make up for this.

The effects of over-expressing *pico* were also examined, to determine if increased levels of the protein increased the migration rate, resulting in the border cell cluster reaching the ooycte early. However over-expression of *pico* (*UAS-pico*) significantly impaired migration at stage 9; the mean bcp of *slbo>pico* cells was -45.2µm compared to +4.9 µm for controls (One-way ANOVA, Dunett's, $P<0.001$; $n=50$). At stage 10a border cell migration was still abrogated, with only 26 % of egg chambers having migrated 75-100 % of the way. Together, these data indicate that *pico* levels need to be tightly controlled in the border cell cluster in order for normal migration to occur.

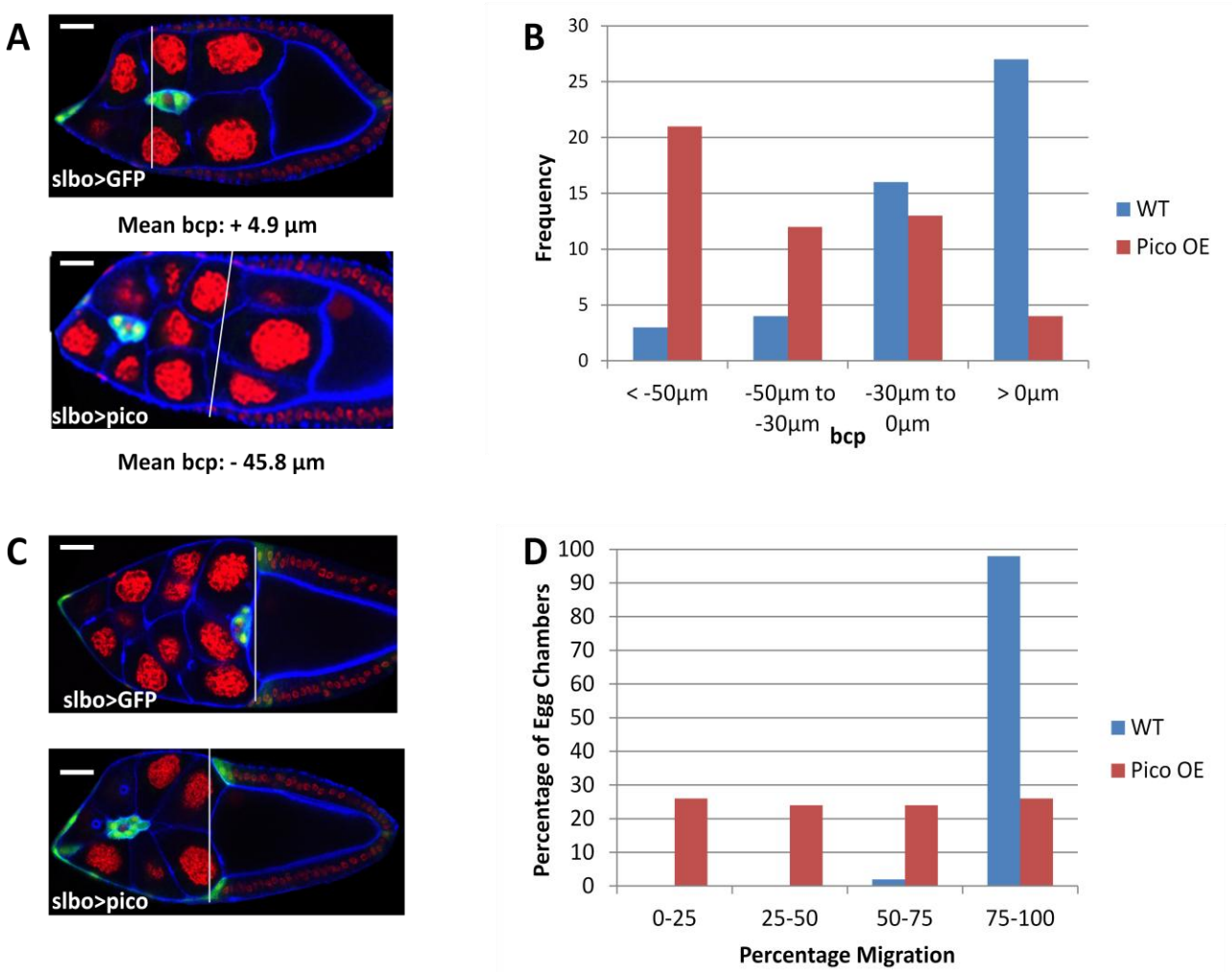

Figure 5.2. Over expressing *pico* severely impairs border cell migration.

(A) Representative images of late stage 9 egg chambers; border cell labelled with GFP, nuclei labelled with RFP and F-actin shown in blue. Solid white lines across the egg chamber indicate position of the most anterior overlying follicle cells. Thick white line indicates 15 µm scale bar. The mean bcp of *slbo>GFP* (WT) and *slbo>pico* are indicated. **(B)** Distribution profile of bcp comparing WT and *UAS-pico*. **(C)** Representative stage 10b egg chambers labelled as in (A), showing representative position of border cells in relation to the oocyte/nurse cell boundary. **(D)** Graph comparing the percentage migration of wild type and *slbo>pico* egg chambers at stage 10b.

5.2.2. Human MRL protein Lpd can cooperate with pico in Border cell Migration

The MRL proteins share common structural characteristics, such as the presence of a consecutive RA (Ras-association) PH domain and proline rich regions (Holt and Daly, 2005). Human homologues of *Drosophila* pico have been found to share a functional role in the regulation of actin polymerisation, altering the cellular ratio between monomeric (G) and filamentous (F) actin. To test whether ectopic human Lpd behaved like ectopic *pico* in the border cell model, *UAS-human Lpd* was put under the control of *slbo-GAL4*. Surprisingly unlike *UAS-pico*, *Lpd* over-expression had no significant effect on border cell migration (mean bcp +3.1 µm, compared to the wild type +4.9 µm; One-way ANOVA, Tukeys, $P>0.05$). This was most likely because of lower levels of *Lpd* expression relative to ectopic *Pico*. To test whether *Lpd* over-expression complemented *pico* knockdown, *Lpd* was ectopically expressed with or without *picoRNAi*^{49}. There was a significant difference between the bcp in *UAS-lpd* (+3.1 µm) and pico*RNAi*^{49} (-21.8 µm) with migration being impaired following *pico* knockdown (One-way ANOVA, Tukeys, $P<0.01$). When both pico*RNAi*^{49} and Lpd were expressed together, the migration was restored (average bcp -2.9 µm, compared to -21.8 µm in pico*RNAi*^{49} egg chambers). These results indicate functional conservation between human and fly homologues, as ectopically expressed human Lpd can partially suppress the effects of knocking down *pico* on border cell migration. In addition to this, the cross-species rescue further validates the specificity of RNAi-mediated *pico* knockdown.

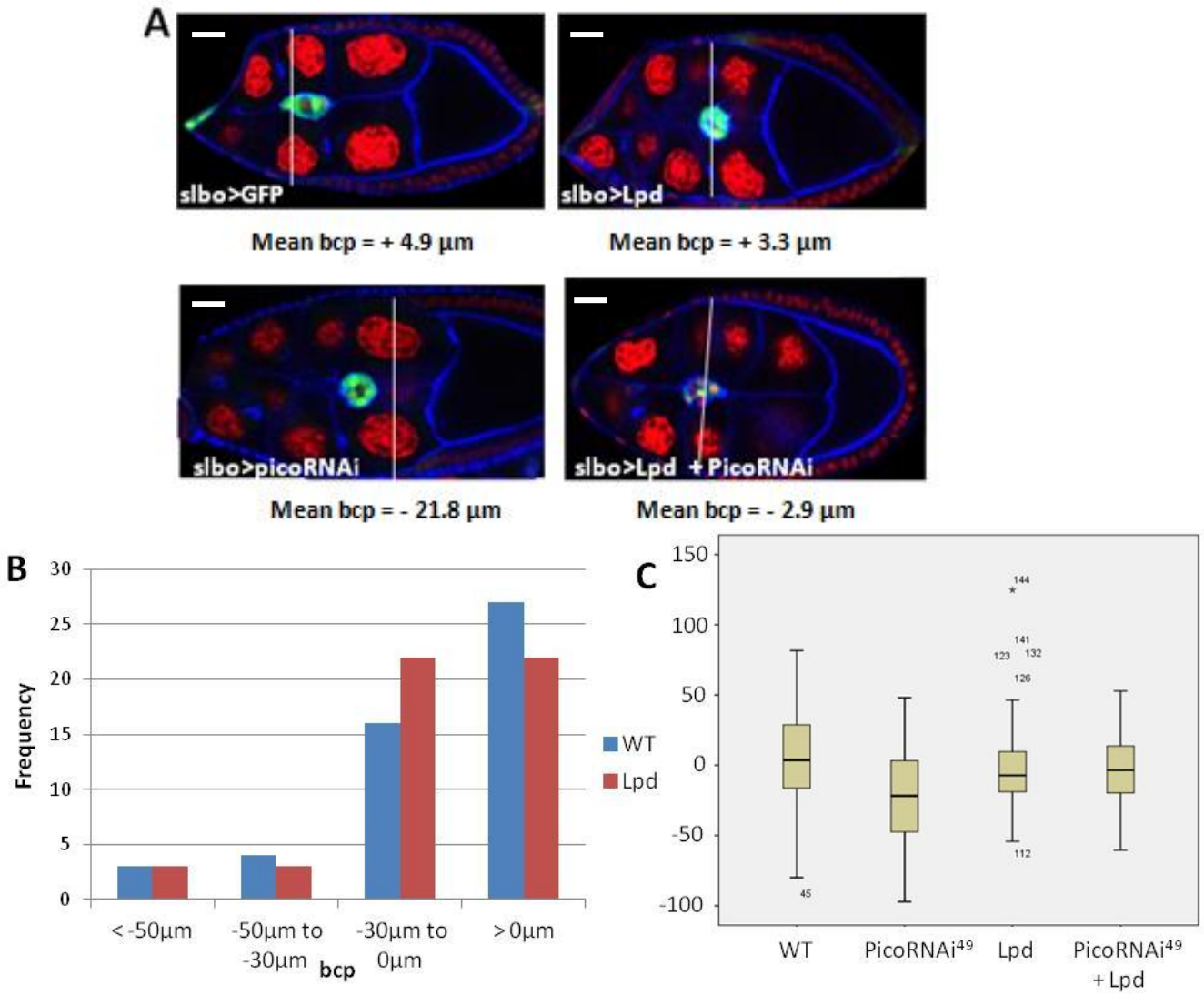

Figure 5.3. Over expressing *Lpd* does not affect border cell migration.

(A) Representative images of late stage 9 egg chambers; border cell labelled with GFP, nuclei labelled with RFP and F-actin shown in blue. Solid white lines across egg chambers indicate position of the most anterior overlying follicle cells. Thick white line indicates 15 µm scale bar. The mean bcp of *slbo>GFP* (WT), *slbo>lpd, slbo>picoRNAi*^{49} and *slbo>lpd+ picoRNAi*^{49} are indicated. **(B)** Distribution profile of bcp comparing WT and *UAS-lpd*. **(C)**Box and whisker plot showing the mean border cell positions and distribution of bcp's in of *slbo>GFP* (WT), *slbo>lpd, slbo>picoRNAi*^{49} and *slbo>lpd+ picoRNAi*^{49}

5.2.3. Scar Plays A Role In Border Cell Migration

A key aspect of border cell migration is the ability of the cluster to detach from the epithelium and acquire motile properties, rearranging the actin cytoskeleton to form a polarised cell body, capable of migrating through the nurse cells to the oocyte in a directed manner. Changes in actin dynamics play an important role in the migration process, specifically the first half of migration when the cluster is elongated with large extensions (Bianco et al., 2007; Fulga and Rorth, 2002; Poukkula et al., 2011). It is clear that different actin regulatory, nucleating and polymerising proteins work in a cell-specific way to promote or inhibit migration.

Actin polymerisation at the leading edge of cells is largely responsible for the ability of cells to migrate (Webb et al., 2005). It is tightly controlled by various actin binding proteins such as the Arp2/3 complex and Ena/VASP, which are recruited to the leading edge, through actin regulators such as Lpd and the SCAR/WAVE proteins. These control the speed and stability of actin protrusions, thereby affecting cell migration (Campellone and Welch, 2010). In collaboration with the Krause lab, it was found that Lpd and Pico bind SCAR. Given the importance of SCAR in cell migration in single cells (Suraneni et al., 2012), its role was assessed in border cells. Knocking-down the levels of SCAR by RNA interference resulted in a significantly reduced mean bcp of -36.1 µm compared to WT +4.9 µm (One-way ANOVA, Dunett's, $P<0.001$; $n=50$) in stage 9 egg chambers. However, similar to picoRNAi[49], at stage 10a border cell migration appeared to be normal in SCAR RNAi with 100 % of egg chambers showing migration of 75-100 %.

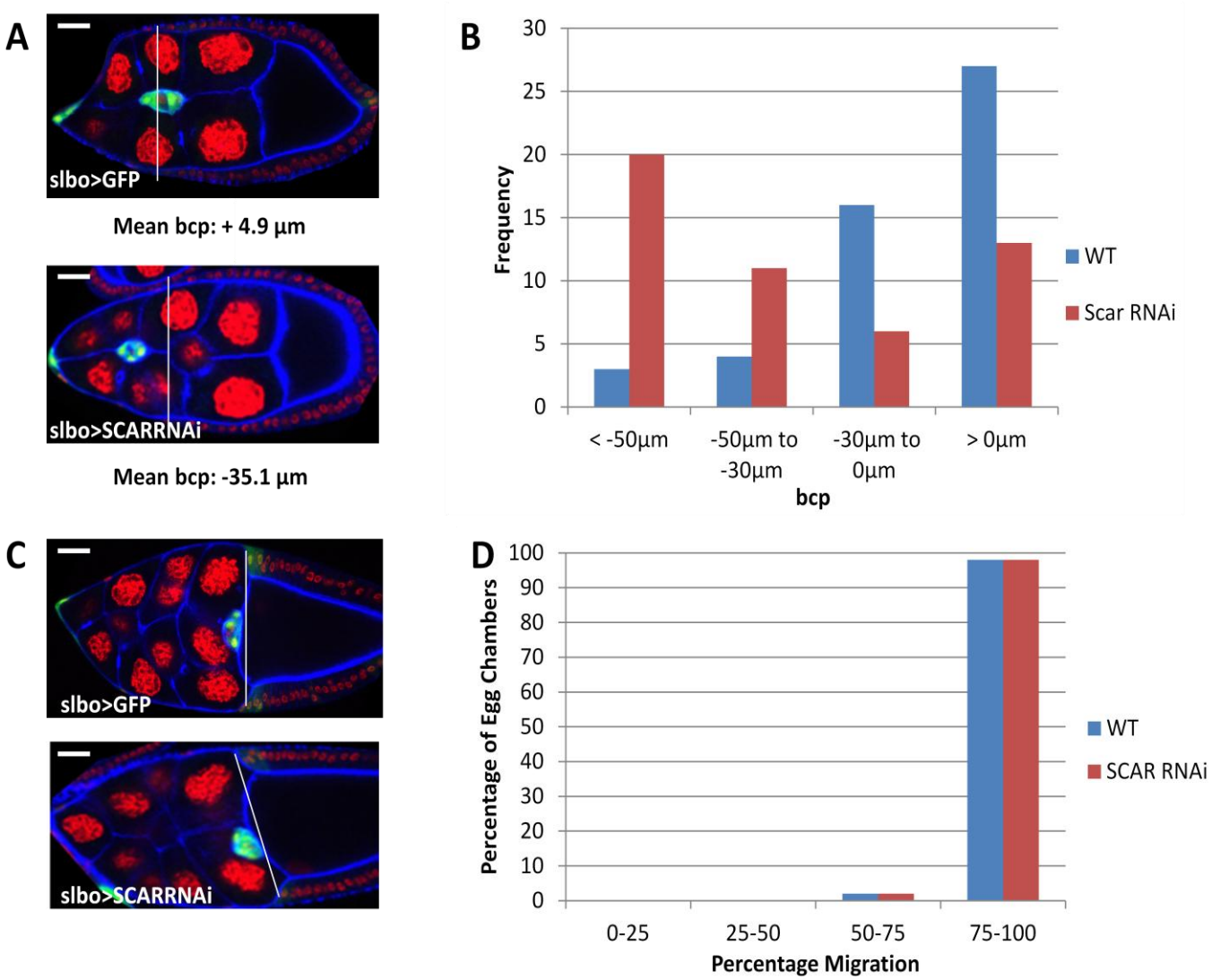

Figure 5.4. Knocking down levels of SCAR delays border cell migration at stage 9.

(A) Representative images of late stage 9 egg chambers; border cell labelled with GFP, nuclei labelled with RFP and F-actin shown in blue. Solid white lines indicate position of the most anterior overlying follicle cells. The mean bcp of *slbo>GFP* (WT) and *slbo>SCARRNAi* are indicated. **(B)** Distribution profile of bcp comparing WT and *SCARRNAi*. **(C)** Representative stage 10b egg chambers labelled as in (A), showing representative position of border cells in relation to the oocyte/nurse cell boundary. **(D)** Graph comparing the percentage migration of wild type and *slbo>SCARRNAi* egg chambers at stage 10b.

5.2.4. Pico and Scar Interact and Regulate Border Cell Migration

The next step was to see if *SCAR* and *pico* genetically interact during border cell migration to determine if *pico* function in this process is mediated by the SCAR/WAVE complex. *slbo-GAL4, UAS-GFP, His2A-RFP; UAS-pico* flies were crossed *with UAS-SCAR RNAi* virgin females, resulting in adults containing the fluorescent reporters and both *UAS-pico* and *UAS-SCAR RNAi* transgenes under *slbo* control. Egg chambers at stage 10a were imaged and the percentage migration calculated based on the bcp and total migration distance. The effect of pico over-expression on border cell migration was ameliorated by SCAR RNAi, with 68% of egg chambers migrating 75-100% of the distance. This is compared to *pico* over-expression alone with only 26% migrating 75-100% of the way.

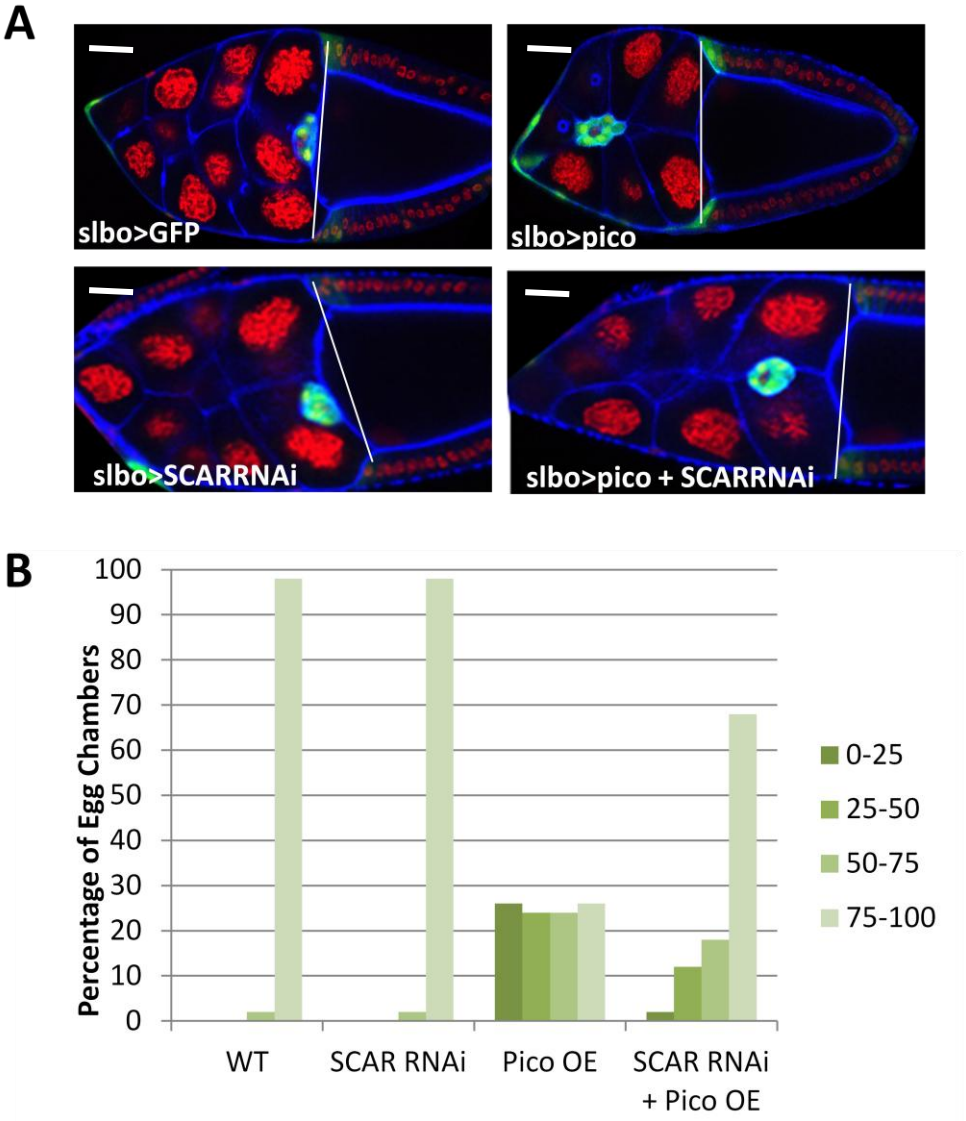

Figure 5.5. Both pico and SCAR/WAVE complex regulate border cell migration.

(A) Representative images of stage 10a egg chambers; border cell labelled with GFP, nuclei labelled with RFP and F-actin shown in blue. Solid white lines across egg chamber indicate position of the most anterior overlying follicle cells. Thick white line represents 15 µm scale bar. **(B)** Graph comparing the percentage migration of wild type, *slbo>SCARRNAi* , *slbo>pico* and both *slbo>pico+SCARRNAi* egg chambers at stage 10a.

5.3. Live Imaging of Border Cell Migration

There is a limit to the amount of information that can be gathered from the analysis of fixed images, as only one time point is displayed. Live imaging of border cell migration has revealed two phases of migration. The first half of migration has been characterised as having a fast migration rate and polarised cluster following detachment from the epithelium. By adapting the medium conditions, the initial phase of migration, the detachment, can be imaged (See Chapter 3, Section 3.2.3). During the second half of migration the cluster appears to shuffle towards the nurse cell-oocyte boundary, with the individual cells tumbling and changing position constantly in the cluster; the second half of migration has been reported to be slower than the first in some studies (Poukkula et al., 2011; Prasad et al., 2007; Prasad and Montell, 2007). To determine the underlying causes of the defects observed in border cells with abnormal levels of *pico*, the live imaging techniques and tools described in Chapters 3 and 4 were employed to obtain a more detailed description of the *pico* phenotype.

5.3.1. Over expression of Pico affects Border Cell Migration Rate

To further test the hypothesis that *pico* function is mediated by the SCAR/WAVE complex, the migration rate was quantified using live cell imaging of border cell migration. Using an automated ImageJ plugin to accurately track the border cell cluster and protrusion dynamics made quantifying the time lapse movies more time effective, accurate and ensured consistency between different egg chambers and genotypes, as described in Chapter 4, Section 4.4.

A macro for Image J was used developed within the Rorth lab (Poukkula et al., 2011) to

specifically analyse border cell migration behaviour and protrusion dynamics. Poukkula *et al.* further described a border cell migration phenotype for two receptor tyrosine kinase guidance cues by linking cluster behaviour and actin based protrusions, when a dominant negative form of the receptor was expressed. Multiple chemoattractants are responsible for the distinctive migratory behaviour of the border cell cluster. PVF1 (Platelet derived growth factor - PDGF) and vascular endothelial growth factor (VEGF) bind to two receptor tyrosine kinases present on follicle cells. When PVR and EGFR signalling is blocked border cell activity is disturbed, despite frequent protrusion activity (Duchek et al., 2001; Janssens et al., 2010; Prasad and Montell, 2007). The first half of migration has been shown to be mostly controlled by PVR activation, whereas the second half relies on EGFR. In egg chambers where PVR guidance was reduced, EGFR activation occurred earlier resulting in premature tumbling behaviour normally only seen in the second half of migration. Active PVR receptors have been found to be highly concentrated at the front of polarised cells, compared to sides and been shown to play a key role in the stabilisation of forward facing protrusions (Janssens et al., 2010; McDonald et al., 2006; Poukkula et al., 2011).

The custom macro was used to separate the cluster into front, back and side segments, and record and measure the protrusions for each of the sections. In addition to logging the protrusion behaviour, the macro automatically tracked the movement of the cluster in XY, enabling information such as migration speed and directed movement to be calculated. *c306-GAL4, UAS-Lifeact-eGFP* female flies were crossed to males of various genotypes, generating adult flies expressing the *UAS-Lifeact-eGFP* construct and one of the following UAS transgenes, Dominant negative (DN)-PVR, picoRNAi[49], Pico OE, SCAR RNAi, and both pico OE and SCAR RNAi together. *c306-GAL4* expressed UAS transgenes in both the

migratory border cells and the polar cells, as a result expression is switched on earlier than with *slbo-GAL4*, which expresses in the migratory follicle cells only. The first half of migration was imaged by live cell imaging with a two minute time interval. Lifeact-eGFP was used to generate these movies, as it specifically labels actin-based protrusions (Riedl et al., 2008). The average duration of the first half of migration was calculated for the various genotypes using half the total distance of migration (As the crow flies), measured from the anterior tip of the egg chamber to the nurse cell-oocyte boundary. Frames where the cluster was still partially attached to the epithelium were not counted.

The results indicate that there is a significant decrease in migration duration between wild type (*c306>Lifeact-eGFP*) (48.6 mins) and DN-PVR (134.8 mins) (One-way ANOVA, Tukeys, $P<0.001$). However, this is not surprising as PVR is well documented to play an important role in border cell migration. Border cells deficient in PVR signalling have been characterised to show premature tumbling behaviour and a delay in the initial phases of migration (Poukkula et al., 2011). Surprisingly there was no significant difference in migration duration when comparing wild type to picoRNAi^{49} (73.1 mins), picoOE (93.25 mins), SCAR RNAi (56 mins).

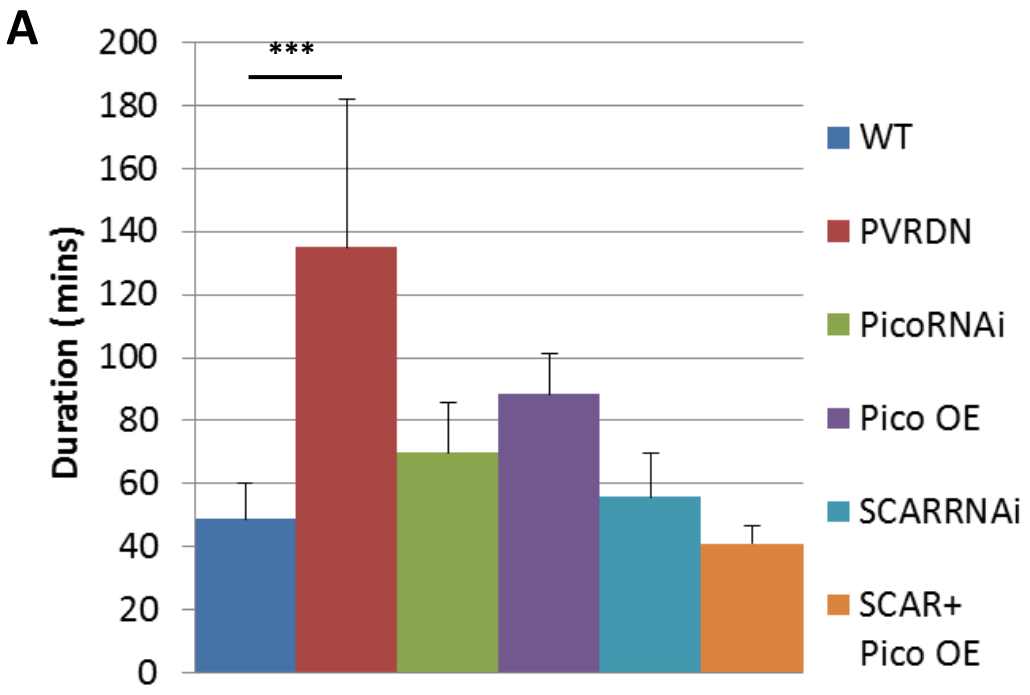

Figure 5.6. Border cell migration duration is not an indicator of defective migration.

(A) Graph showing duration in minutes of Wildtype, DN-PVR, PicoRNAi[49], PicoOE, SCAR RNAi and SCARRNAi + PicoOE, displayed in different colours. Error bars show the standard error of the mean. Significance bar represents a P value less than 0.001.

To further investigate the function of different UAS transgenes GFP projected images were analysed using the custom border cell macro. The migration rate per frame was calculated for each of the genotypes, including wild type. The macro calculated the average migration rate based upon the distance travelled by the centre of the cluster between each frame. The results show that *c306>GFP* had a migration rate of 1.4 µm/min. The previously documented DN-PVR had a migration rate of 0.88µm/min which was significantly lower than wild type (One-way ANOVA, Tukeys, $P<0.001$, $n=9$). This value differs from the published frame by frame rate of DN-PVR in early migration (Approximately 0.2 µm/min), however the wild type control also had a lower rate (Approximately 0.9 µm/min) (Poukkula et al., 2011). These differences can be explained by the difference in border cell specific driver and

reporters used (see Chapter 3 discussion). picoRNAi^{49} and picoOE also showed a significant decrease in migration rate, 1.2 µm/min and 1.1 µm/min, respectively relative to wild type, 1.4 µm/min (One-way ANOVA, Tukeys, $P<0.05$, n=12 and 12). There was no significant difference in the migration rate of SCAR RNAi, 1.4 µm/min (One-way ANOVA, Tukeys, $P>0.05$, n=8) which was surprising given that picoRNAi^{49} and SCAR RNAi displayed similar behaviour when fixed samples were analysed.

When both SCAR RNAi and pico OE were expressed together there was a slight increase in migration rate 1.8 µm/min, however this was not significant when compared to wild type (One-way ANOVA, Tukeys, $P>0.05$, n=7). When comparing pico OE + SCAR RNAi migration rates to the two transgenes individually, expressing both together showed a significant increase in migration rate, 1.79µm/min compared to picoOE (1.1 µm/min) and SCAR RNAi (1.4 µm/min) (One-way ANOVA, Tukeys, $P<0.001$). Expressing both together rescued the migration rate back to the wild type value, again suggesting that SCAR RNAI can suppress the negative effect of ectopic pico on border cell migration.

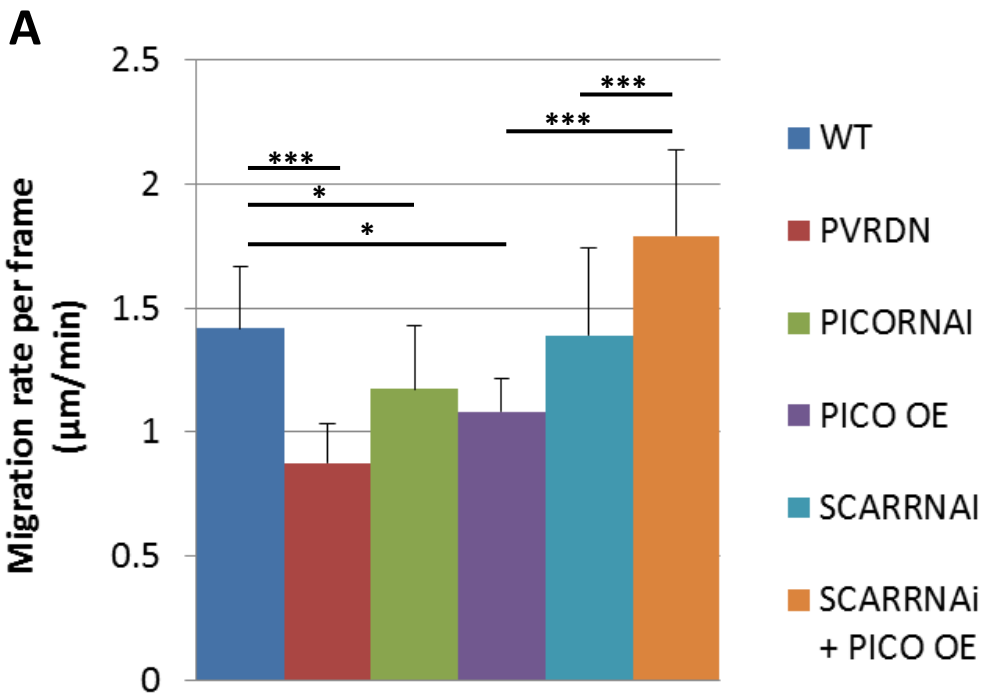

Figure 5.7. Border cell migration rate is negatively affected by pico levels.

(A) Graph showing migration rate per frame, in µm per minute, in Wildtype, DN-PVR, PicoRNAi[49], Pico OE, SCAR RNAi and SCAR RNAi + Pico OE, shown in different colours. Error bars show the standard error of the mean. Significant bar represents a P values, less than 0.001***, Less than 0.05*.

5.3.2. Premature Tumbling is a Sign of Defective Border Cell Migration

Basic qualitative data was also extracted from live imaging time-lapse movies to complement quantitative data. On inspection of the time-lapse movies it was apparent that premature tumbling was being observed in a large portion of the movies. All genotypes examined alongside wild type movies showed early tumbling in the first half of migration to some degree. The point at which the premature tumbling occurred and the number of frames, differed by genotype. Therefore a way of quantifying the tumbling was generated to enable a comparison of the movies generated. The same time lapse movies used to calculate the rate of migration were used to quantify the degree of early tumbling. Early tumbling was calculated firstly as the percentage of movies per genotype that showed

rounded clusters. Early tumbling was defined as the border cell cluster exhibiting changes in the position of individual cells within the cluster, for two or more consecutive frames in the first half of migration. The number of frames that showed early tumbling was also counted per genotype, using the same guidelines as above and represented as the average percentage of frames per time lapse movie.

Results indicated that premature tumbling occurred at a higher frequency of movies in some genotypes, 89 % of DN-Pvr, 67 % pico RNAi[49], 100 % pico OE, 75 % SCAR RNAI and both SCAR RNAi and pico OE 71 %, compared to 22 % in wild type. The increased tumbling seen in DN-PVR and pico OE movies may partly explain the increased duration seen in border cell migration. This does not explain the increased percentage of movies showing tumbling in egg chambers expressing SCAR RNAi + pico OE (71 % compared to 22 % in WT). It is apparent that expressing both together rescues the tumbling frequency seen in pico OE, to a certain degree (75 % compared to 100 % in pico OE), however the migration duration for this genotype is similar to wild type (40.9 mins compared with 48.7 mins). It would therefore be expected that the percentage of movies showing premature tumbling would also be similar.

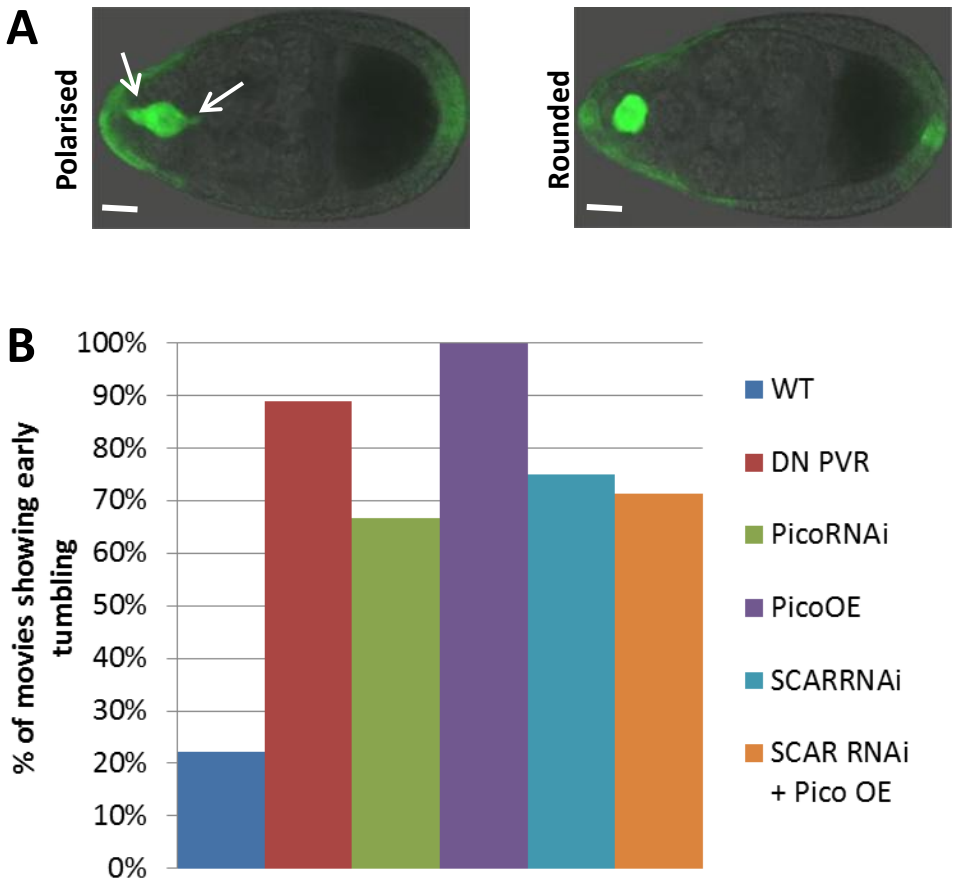

Figure 5.8. Border cells exhibiting early tumbling behaviour may indicate defects in migration.

(A) Images of *C306>Lifeact-GFP* egg chambers in a polarised and rounded state. Cluster extensions labelled with white arrows. Solid white line indicates 15 µm scale bar. **(B)** Graph showing percentage of movies showing early tumbling behaviour, in Wildtype, DN-PVR, PicoRNAi[49], Pico OE, SCAR RNAi and SCAR RNAi + Pico OE.

One reason for this discrepancy may be due to the way the tumbling behaviour has been quantified. Quantifying tumbling on a 'per movie' basis may under or overestimate the degree of premature tumbling in a genotype, as only two consecutive frames needed to exhibit tumbling behaviour for this classification. Analysing tumbling behaviour based on a 'per frame' method not only identifies how frequent early tumbling is observed, but demonstrates how long during the duration of its early stage of migration the cluster is tumbling. When characterised in this way, the results show that *c306>GFP* showed

premature tumbling in an average of 5 % of movie frames, compared to 45 % in DN-PVR which was significantly higher (One-way ANOVA, Tukeys, P<0.01). picoRNAi[49] and SCAR RNAi also showed an increase in premature tumbling, however this was not found to be significant (One-way ANOVA, Tukeys P>0.05). pico OE however showed a significant increase in tumbling behaviour with an average of 53 % of frames (One-way ANOVA, Tukeys P>0.001). When both SCAR RNAi and pico OE were expressed together there was a slight increase in tumbling 16 %, this was not significant when compared to wild type (One-way ANOVA, Tukeys, P>0.05) as expected. When comparing expression of both pico OE and SCAR RNAi together, compared to the two genes individually, expressing both showed a significant decrease in tumbling behaviour, 16% compared to 53% in pico OE (One-way ANOVA, Tukeys, P<0.05). Expressing both together returned the migration rate back to the wild type value, again suggesting that SCAR RNAI can suppress the premature tumbling phenotype observed in ectopic *pico* egg chambers.

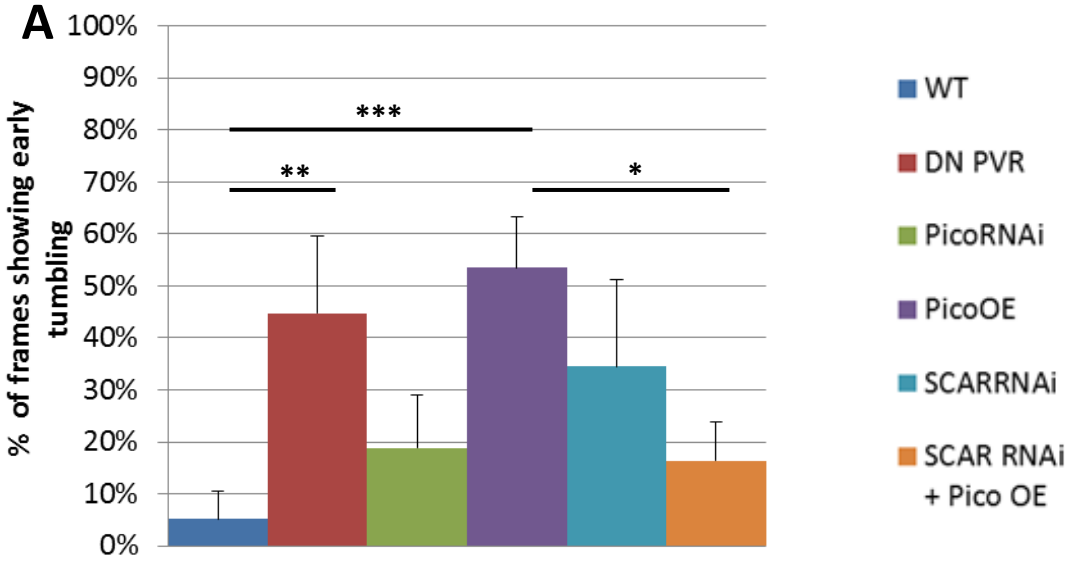

Figure 5.9. Border cells exhibit early tumbling behaviour when pico is over expressed.

(A) Graph showing percentage of frames showing premature tumbling in Wildtype, DN-PVR, PicoRNAi[49], Pico OE, SCAR RNAi and SCAR RNAi + Pico OE. Error bars show the standard error of the mean. Significant bar represents a P values, less than 0.001***, Less than 0.01** Less than 0.05*.

5.3.3. Protrusions/Extensions Regulate Border Cell Migration

Understanding the distribution of protrusions during migration of wild type and defective border cell clusters will provide insight into the role different genes play on cell migration. Linking differences in migration rates and border cell behaviour to protrusion dynamics could enable a significant insight into the biological functions of genes during migration. Migration defects in duration, rate, or failed migration may be a result of poor protrusion formation, persistence or directionality, or neither. Confirming or eliminating protrusion dynamics as being implicated in impaired migration can be important when trying to pin point the role genes play in migration. Protrusion dynamics, especially in genotypes showing premature tumbling may help explain the behaviour and other defects seen during migration.

The number of extensions per frame was calculated by the macro for each of the genotypes. DN-PVR showed a significant decrease in the average number of extensions per frame (0.40), compared to wild type, (1.07) (One-way ANOVA, Tukeys, $P<0.01$), which may explain the reduced migration rate observed. picoRNAi[49] and pico OE however did not show a significant decrease in the average number of extensions, 0.9 and 1.03 respectively, when compared to wild type (One-way ANOVA, Tukeys, $P>0.05$), despite migration rate and migration behaviour being defective in both genotypes, in particular pico OE. Surprisingly SCAR RNAi showed a significant decrease in the number of extensions (0.63) compared to wild type (One-way ANOVA, Tukeys, $P<0.05$) despite no significant difference in migration duration, rate, or tumbling behaviour. There was no significant difference in extension number compared to wild type or any of the individual transgenes when both pico OE and SCAR RNAi were expressed together, as expected (0.61 extensions/frame) (One-way ANOVA, Tukeys, $P>0.05$). To further dissect the protrusion behaviour of the cluster in the

various genotypes, the protrusion direction was measured for each genotype and represented as a percentage of the total number of extensions. What was immediately noticeable was the large proportion of back facing extensions compared to front in DN-PVR (66 %), pico OE (39 %) and SCAR RNAi (36 %) compared to wild type (14 %). It can therefore be hypothesised that the premature tumbling behaviour observed in these genotypes can be a result of miss- guided protrusions, preventing directed polarised migration.

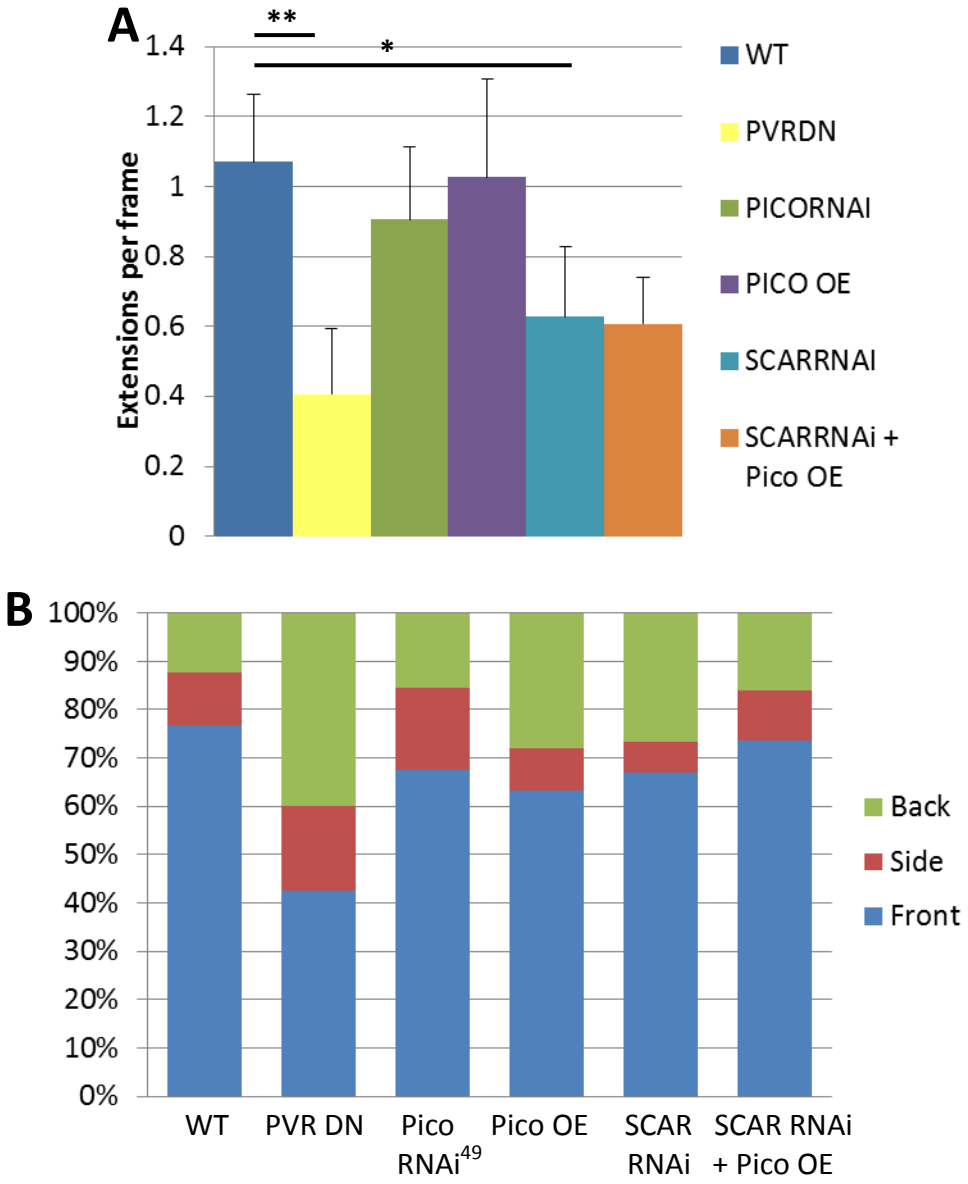

Figure 5.10. Border cell protrusions play a key role in whole cluster behaviour. (A) Graph showing average number of extensions per frame in Wildtype, DN-PVR, PicoRNAi[49], Pico OE, SCAR RNAi and SCAR RNAi + Pico OE. **(B)** Graph showing protrusion distribution by angle. Protrusions between 315° and 45° were considered to be front, 45-135° and 225-315° side and 135-225° back. Error bars show the standard error of the mean. Significant bar represents a P values, less than 0.001***, Less than 0.01** Less than 0.05*.

5.4. Discussion

The data presented in this chapter demonstrate how the border cell migration model can be used to dissect gene function at a basic and more advanced level. Using only fixed samples of *Drosophila* egg chambers can lead to partial or inaccurate conclusions being formed about the role certain genes play on migration. Investment into culturing and analysing border cell live imaging has expanded the amount and quality of data that can be extracted. With a combination of live imaging and fixed samples the effect the MRL protein, Pico has on border cell migration has been described, in addition to some of its interactions within the system. It has been shown that knocking down and increasing the levels of *pico* in the border cell system results in impairment of migration at stage 9, more severely in the latter. However when *pico* levels are reduced this impairment is not seen later on in development at stage 10a, suggesting that the border cell cluster somehow manages to catch up with the anterior follicle cells and finish at the correct time. Analysis of *slbo>mCD8-GFP* time-lapse imaging comparing the first and second half of migration, shows that although the average migration rate is quicker in the second half than the first, in DN-PVR, picoRNAi[49], and SCAR RNAi (contrary to wild type where the first half is quicker than the second) this increase is not significant. The analysis therefore reflects that one reason the border cells are observed to "catch up" with the retracting follicle cells at stage 10a, is due to the fact it is not a single defined time point, but instead a developmental window during which migration is normally completed. Over expressing *pico* has a more detrimental effect with egg chambers showing defective migration at stage 10a. Taking these points together it is obvious that Pico protein levels need to be tightly controlled, as too much and too little causes defects in migration. Live imaging analysis of the first half of migration indicated that although knocking-down *pico* levels can impair migration, it is not enough to severely affect migration. Duration,

protrusion behaviour and protrusion direction are not significantly altered, however knocking down *pico* levels has a negative effect on migration rate. This may be due to the *pico* phenotype resembling DN-PVR but weakly. This effect is different to when *pico* is over expressed, migration is severely affected by slower migration rates, defective premature tumbling in a large percentage of frames and a change in the distribution of protrusions from the front to the back. The large differences between ectopic *pico* expression and reducing the levels may be due to level of knockdown of the *pico* protein using RNAi.

Actin polymerisation at the leading edge of cells is the driving force for cell migration. Through collaborative work with another research group that are interested in the functional role of SCAR in relation to other actin binding proteins, the effect that the actin regulator SCAR has on border cell migration was tested. Knocking down the levels of SCAR by RNAi resulted in impaired migration at stage 9 and seemingly normal migration at stage 10a. This delay in migration resembled that seen in picoRNAi[49] in fixed samples, however, through live imaging it was observed that migration rate was not reduced in the first half of migration, as seen in picoRNAi[49]. Border cells with lower levels of SCAR had reduced protrusion frequency and a higher proportion of backwards-facing protrusions than wild type or picoRNAi[49], similar to that seen in *pico* over-expression egg chambers. This prompted experiments to see if there was in interaction between *SCAR* and *pico*. Indeed, knocking down levels of SCAR could partially rescue the migration defect seen when *pico* was over expressed, suggesting that both function together to effectively control border cell migration. Further experiments to confirm the role of SCAR/WAVE in *pico*-mediated control of migration would be to examine the effect of overexpressing a version of Pico that fails to bind SCAR. Lpd binds SCAR via the regulatory protein Abl-interactor (Abi) (Law et al,. 2013) and disrupting this interaction abrogates the effect of Lpd over-expression. For instance,

over-expression of Lpd in MDA-MB231 cells in a scratch wound healing assay increased cell migration, whereas a non-Abi binding mutant of Lpd fails to have this effect. A similar mutant of Pico might be expected to resemble the effect of co-overexpressing wild type Pico in a SCAR RNAi background.

Finally, the role of the human MRL protein Lpd was tested in border cells to determine if there was functional conservation between the homologues. Surprisingly, ectopic Lpd expression alone did not affect border cell migration but was able to partially rescue the defects seen in border cells following *pico* knockdown. This shows that there is a functional, in addition to the previously reported structural, conservation between the fly and human forms.

6. Thesis Summary

In this thesis a methodology to culture and image live egg chambers has been developed through adaptation and optimisation of published protocols. Critical steps, discussed in Chapter 3, include the importance of adequate media that is able to support egg chamber growth and development during stage 9, and steps that can be taken to ensure successful border cell migration following dissection and mounting. Gas exchange, which was found to be critical for successful border cell migration, was satisfactory in Lumoux, membrane–based dishes, but not the majority of glass-bottomed dishes tested here. Additional results in Chapter 3 showed that border cell migration can be adversely affected by the ectopic expression of fluorescent reporters; consequently data from experiments utilising different driver/reporter combinations cannot be compared against one another. Novel tools were generated, such as a Gateway UAS-mTFP vector, to gain more information about how different genes affect border cell migration. Importantly, the protocols and parameters to enable imaging of cultured egg chambers reported here, will be essential for future efforts to investigate the regulation of border cell migration.

In Chapter 4, various analytical approaches were developed to ensure data could be easily and accurately extracted from time-lapse movies, acquired by confocal microscopy. Various ImageJ plugins and a semi-automated macro were used to accurately extract quantitative data from images of the migrating cluster. It was discovered that although tracking using the Z plane is possible, this information does not contribute to the understanding of the cluster behaviour, as the significant migration steps occur in XY only. The suitability of manual tracking versus semi-automated tracking was compared, and it was concluded that unless protrusion details were important in dissecting cluster behaviour, the MtrackJ ImageJ plugin

was more suitable; although the macro provided more detailed information, it was far more time-consuming to use due to the large amount of manual image preparation required. Following trials of the analytical tools, a robust protocol was generated enabling the properties and behaviour of migrating border cells to be analysed. Future work towards accurately extracting information about the behaviour of the border cell cluster may be focussed on the different type of movements exhibited, at various parts of the migration process. For example at the moment border cell cluster movement is universally classified into three distinct phases of migration; i) first half, with fast polarised movement, ii) second half, with slow tumbling movement and iii) dorsal migration, movement towards the nuclei once the cluster has reached the oocyte. Examining the time-series movies has demonstrated that not all egg chambers adhere to this 'normal' behaviour, with the point at which the first and second half starts differing by egg chamber and genotype, and also switching between behaviours/phases several times during the migration. Generating a way to segregate these different behaviours and analyse the movement individually, will enable a more accurate description of the velocities of the migrating cluster, in relation to the phase of migration. Using this information the migration phase of the cluster can easily be determined by its velocity, and not through assumptions based on what is considered 'normal' in what is a highly varied process.

Finally the approaches developed in Chapters 3 and 4 were utilised to investigate the role of MRL and other actin regulatory proteins during border cell migration. Results from fixed samples and live imaging described in Chapter 5, showed that *pico* plays a role in border cell migration and is dependent on SCAR. This relationship is demonstrated through analysis of the cluster behaviour as well as dynamics of cellular protrusions, that are the driving force for migration. Data reported in Chapter 5 has contributed to a paper entitled “Lamellipodin

and the Scar/WAVE complex cooperate to promote cell migration *in vivo*" (Law et al., 2013). Following in-depth analysis of border cell migration and protrusion dynamics in the first half of migration, future work should focus on imaging the whole migration process using high resolution solid-based dishes. This would answer some key questions with regards to the ability of *pico* and *SCAR* loss-of-function cells to 'catch up' during the second half of migration, as well as provide better resolution of the protrusion dynamics. In this respect, the LabTek chambered coverglass slides are of interest because they have the ability to simultaneously image mutant and wild type egg chambers at the same time. These have been successfully used by other labs to culture and image border cell migration over the period of several hours. I believe one of the key contributing issues that I have been experiencing with sample drift, can be overcome by modulating the amount of media present in each chamber, as gas exchange is not a problem. Generating a media with a higher viscosity may also aid in preventing the egg chambers from moving once, the time series have started. However, the Iwaki dishes, which were successfully used in this thesis to image egg chambers, may offer a more immediate solution now that they have become available from several suppliers. Implementation of mTFP-Lifeact in border cells should also allow actin dynamics to be visualised more clearly, with less chance of photo-damage during the imaging process.

One of the main issues throughout the live imaging process has been the ability to acquire high resolution images, whilst avoiding photo-toxicity and preventing drift in all directions, specifically in Z. A solution to these issues could be to use a light sheet fluorescence microscope instead of a confocal. Light sheet fluorescence microscopy (LSFM) has the ability to image large, live 3D samples at sub cellular resolution, at a fraction of the time it would

take normally. The microscope generates thin optical sections by illuminating only the in focus plane, from the side of the sample, resulting in good sample depth penetration, high spatial resolution and minimal photo-bleaching. As the samples are contained in low concentration agarose cylinders, previous issues associated with drift are not likely to be a problem. However, until the imaging setup has been trialled for egg chambers, it is not known if it will be successful for imaging border cell migration. Ensuring the culture environment is suitable will be critical in the success of this technique, as too tight constraints on egg chamber growth may result in unsuccessful migration. LSFM will allow in depth resolution of border cell clusters in Z over time, and will overcome time restraints associated with multi channel imaging, due to fast acquisition times, and will allow precise tracking of clusters in 4 dimensions. This system may enable us to increase our understanding of how cells respond to local chemotactic gradients, and to define what circumstances collective migration of a cluster is favoured over a more polarised movement (where one cell is dominant), and what mechanisms are involved in this action. The role adhesion molecules play in the different phases of migration can be explored using photo-switchable fluorescent proteins, this would involve looking at the adhesion distribution and turnover at the leading edge of the cluster, whilst the cluster is migrating.

Further experiments, primarily in fixed samples could be carried out to try and fully understand the effect of expressing Lpd in border cells. Various individual Lpd lines can be tested and the protein expression levels quantified using western blots, this would support the assumption that expressing ectopic Lpd has a lesser effect than expressing ectopic pico due to expression levels.

In summary, this thesis describes the optimisation of a number of tools and approaches

that, when coupled with the genetic tractability inherent to the experimental model, can provide novel insights into the processes and mechanisms of invasive cell migration *in vivo*.

7. Acknowledgements

I would firstly like to thank my parents and grandparents for their constant support and always believing in me, whatever I do. I would also like to thank Martyn for his understanding and patience throughout my PhD. I am forever grateful to my supervisor Dr Daimark Bennett, for the opportunity to conduct these investigations and for his continued support throughout, including critically reading this thesis. In addition, I wish to thank Dr Marco Marcello for his microscopy advice and willingness to help when things went wrong.

I would also like to extend my gratitude to all the members of the Bennett lab, Eleanor Taylor, Louise Duncalf, Nick Jones, Nick Lansdale, Christopher Lofthouse, Mirel Lucaci, Vincent Jonchere and Nada Alqadri; for their advice and company throughout this experience. In particular I would like to thank Neville Cobbe and Anita Lucaci for being good mentors and true friends.

Finally I would like to thank God for his strength to continue when things are hard.

8. References

Ai, H.W., Henderson, J.N., Remington, S.J., and Campbell, R.E. (2006). Directed evolution of a monomeric, bright and photostable version of Clavularia cyan fluorescent protein: structural characterization and applications in fluorescence imaging. Biochem J *400*, 531-540.

Ananthakrishnan, R., and Ehrlicher, A. (2007). The forces behind cell movement. International Journal of Biological Sciences [Electronic Resource] *3*, 303-317.

Arbouzova, N.I., and Zeidler, M.P. (2006). JAK/STAT signalling in Drosophila: insights into conserved regulatory and cellular functions. Development *133*, 2605-2616.

Bacac, M., and Stamenkovic, I. (2008). Metastatic cancer cell. Annual Review Of Pathology *3*, 221-247.

Bai, J., Uehara, Y., and Montell, D.J. (2000). Regulation of invasive cell behavior by taiman, a Drosophila protein related to AIB1, a steroid receptor coactivator amplified in breast cancer. Cell *103*, 1047-1058.

Baird, G.S., Zacharias, D.A., and Tsien, R.Y. (2000). Biochemistry, mutagenesis, and oligomerization of DsRed, a red fluorescent protein from coral. Proc Natl Acad Sci U S A *97*, 11984-11989.

Bear, J.E., and Gertler, F.B. (2009). Ena/VASP: towards resolving a pointed controversy at the barbed end. Journal of cell science *122*, 1947-1953.

Bear, J.E., Loureiro, J.J., Libova, I., Fassler, R., Wehland, J., and Gertler, F.B. (2000). Negative regulation of fibroblast motility by Ena/VASP proteins. Cell *101*, 717-728.

Bear, J.E., Svitkina, T.M., Krause, M., Schafer, D.A., Loureiro, J.J., Strasser, G.A., Maly, I.V., Chaga, O.Y., Cooper, J.A., Borisy, G.G.*, et al.* (2002). Antagonism between Ena/VASP proteins and actin filament capping regulates fibroblast motility. Cell *109*, 509-521.

Bianco, A., Poukkula, M., Cliffe, A., Mathieu, J., Luque, C.M., Fulga, T.A., and Rorth, P. (2007). Two distinct modes of guidance signalling during collective migration of border cells. Nature *448*, 362-365.

Borghese, L., Fletcher, G., Mathieu, J., Atzberger, A., Eades, W.C., Cagan, R.L., and Rorth, P. (2006). Systematic analysis of the transcriptional switch inducing migration of border cells. Dev Cell *10*, 497-508.

Brand, A.H., and Perrimon, N. (1993). Targeted gene expression as a means of altering cell fates and generating dominant phenotypes. Development *118*, 401-415.

Buszczak, M., Freeman, M.R., Carlson, J.R., Bender, M., Cooley, L., and Segraves, W.A. (1999). Ecdysone response genes govern egg chamber development during mid-oogenesis in Drosophila. Development *126*, 4581-4589.

Campellone, K.G., and Welch, M.D. (2010). A nucleator arms race: cellular control of actin assembly. Nature reviews Molecular cell biology *11*, 237-251.

Carlier, M.F., and Pantaloni, D. (1997). Control of actin dynamics in cell motility. Journal of molecular biology *269*, 459-467.

Chen, J., Godt, D., Gunsalus, K., Kiss, I., Goldberg, M., and Laski, F.A. (2001). Cofilin/ADF is required for cell motility during Drosophila ovary development and oogenesis. Nature cell biology *3*, 204-209.
Cobreros-Reguera, L., Fernandez-Minan, A., Fernandez-Espartero, C.H., Lopez-Schier, H., Gonzalez-Reyes, A., and Martin-Bermudo, M.D. (2010). The Ste20 kinase misshapen is essential for the invasive behaviour of ovarian epithelial cells in Drosophila. EMBO reports *11*, 943-949.
Davis, I., and Parton, R.M. (2006). Time-lapse cinematography in living Drosophila tissues: preparation of material. CSH protocols *2006*.
Day, R.N., Booker, C.F., and Periasamy, A. (2008). Characterization of an improved donor fluorescent protein for Forster resonance energy transfer microscopy. J Biomed Opt *13*, 031203.
Day, R.N., and Davidson, M.W. (2009). The fluorescent protein palette: tools for cellular imaging. Chem Soc Rev *38*, 2887-2921.
Denef, N., and Schupbach, T. (2003). Patterning: JAK-STAT signalling in the Drosophila follicular epithelium. Current biology : CB *13*, R388-390.
Desai, R.A., Gopal, S.B., Chen, S., and Chen, C.S. (2013). Contact inhibition of locomotion probabilities drive solitary versus collective cell migration. Journal of the Royal Society, Interface / the Royal Society *10*, 20130717.
Dietzl, G., Chen, D., Schnorrer, F., Su, K.C., Barinova, Y., Fellner, M., Gasser, B., Kinsey, K., Oppel, S., Scheiblauer, S.*, et al.* (2007). A genome-wide transgenic RNAi library for conditional gene inactivation in Drosophila. Nature *448*, 151-156.
Duchek, P., and Rorth, P. (2001). Guidance of cell migration by EGF receptor signaling during Drosophila oogenesis. Science *291*, 131-133.
Duchek, P., Somogyi, K., Jekely, G., Beccari, S., and Rorth, P. (2001). Guidance of cell migration by the Drosophila PDGF/VEGF receptor. Cell *107*, 17-26.
Fulga, T.A., and Rorth, P. (2002). Invasive cell migration is initiated by guided growth of long cellular extensions. Nature cell biology *4*, 715-719.
Gates, J., Nowotarski, S.H., Yin, H., Mahaffey, J.P., Bridges, T., Herrera, C., Homem, C.C., Janody, F., Montell, D.J., and Peifer, M. (2009). Enabled and Capping protein play important roles in shaping cell behavior during Drosophila oogenesis. Developmental biology *333*, 90-107.
Geisbrecht, E.R., and Montell, D.J. (2002). Myosin VI is required for E-cadherin-mediated border cell migration. Nature cell biology *4*, 616-620.
Gertler, F., and Condeelis, J. (2011). Metastasis: tumor cells becoming MENAcing. Trends in cell biology *21*, 81-90.
Ghiglione, C., Devergne, O., Georgenthum, E., Carballes, F., Medioni, C., Cerezo, D., and Noselli, S. (2002). The Drosophila cytokine receptor Domeless controls border cell migration and epithelial polarization during oogenesis. Development *129*, 5437-5447.

Goode, S., Wei, J., and Kishore, S. (2005). Novel spatiotemporal patterns of epithelial tumor invasion in Drosophila discs large egg chambers. Developmental dynamics : an official publication of the American Association of Anatomists *232*, 855-864.
Guillen, I., Mullor, J.L., Capdevila, J., Sanchez-Herrero, E., Morata, G., and Guerrero, I. (1995). The function of engrailed and the specification of Drosophila wing pattern. Development *121*, 3447-3456.
Hanahan, D., and Weinberg, R.A. (2000). The hallmarks of cancer. Cell *100*, 57-70.
Holt, L.J., and Daly, R.J. (2005). Adapter protein connections: the MRL and Grb7 protein families. Growth Factors *23*, 193-201.
Hu, K., Ji, L., Applegate, K.T., Danuser, G., and Waterman-Storer, C.M. (2007). Differential transmission of actin motion within focal adhesions. Science *315*, 111-115.
Humphries, J.D., Byron, A., and Humphries, M.J. (2006). Integrin ligands at a glance. Journal of cell science *119*, 3901-3903.
Insall, R.H., and Machesky, L.M. (2009). Actin dynamics at the leading edge: from simple machinery to complex networks. Dev Cell *17*, 310-322.
Jang, A.C., Chang, Y.C., Bai, J., and Montell, D. (2009). Border-cell migration requires integration of spatial and temporal signals by the BTB protein Abrupt. Nature cell biology *11*, 569-579.
Janssens, K., Sung, H.H., and Rorth, P. (2010). Direct detection of guidance receptor activity during border cell migration. Proc Natl Acad Sci U S A *107*, 7323-7328.
Jonchere, V., and Bennett, D. (2013). Validating RNAi Phenotypes in Drosophila Using a Synthetic RNAi-Resistant Transgene. PloS one *8*, e70489.
Kaiser, D.A., Vinson, V.K., Murphy, D.B., and Pollard, T.D. (1999). Profilin is predominantly associated with monomeric actin in Acanthamoeba. Journal of cell science *112*, 3779-3790.
Klueg, K.M., Alvarado, D., Muskavitch, M.A., and Duffy, J.B. (2002). Creation of a GAL4/UAS-coupled inducible gene expression system for use in Drosophila cultured cell lines. Genesis *34*, 119-122.
Krause, M., Leslie, J.D., Stewart, M., Lafuente, E.M., Valderrama, F., Jagannathan, R., Strasser, G.A., Rubinson, D.A., Liu, H., Way, M., *et al.* (2004). Lamellipodin, an Ena/VASP ligand, is implicated in the regulation of lamellipodial dynamics.[see comment]. Developmental Cell *7*, 571-583.
Kuttenkeuler, D., and Boutros, M. (2004). Genome-wide RNAi as a route to gene function in Drosophila. Brief Funct Genomic Proteomic *3*, 168-176.
Lafuente, E.M., van Puijenbroek, A.A., Krause, M., Carman, C.V., Freeman, G.J., Berezovskaya, A., Constantine, E., Springer, T.A., Gertler, F.B., and Boussiotis, V.A. (2004). RIAM, an Ena/VASP and Profilin ligand, interacts with Rap1-GTP and mediates Rap1-induced adhesion.[see comment]. Developmental Cell *7*, 585-595.
Lauffenburger, D.A., and Horwitz, A.F. (1996). Cell migration: a physically integrated molecular process. Cell *84*, 359-369.

Law, A.L., Vehlow, A., Kotini, M., Dodgson, L., Soong, D., Theveneau, E., Bodo, C., Taylor, E., Navarro, C., Perera, U.*, et al.* (2013). Lamellipodin and the Scar/WAVE complex cooperate to promote cell migration in vivo. J Cell Biol *203*, 673-689.
Le Clainche, C., and Carlier, M.F. (2008). Regulation of actin assembly associated with protrusion and adhesion in cell migration. Physiol Rev *88*, 489-513.
Lyulcheva, E., Taylor, E., Michael, M., Vehlow, A., Tan, S., Fletcher, A., Krause, M., and Bennett, D. (2008). Drosophila pico and its mammalian ortholog lamellipodin activate serum response factor and promote cell proliferation. Developmental Cell *15*, 680-690.
Macdonald, A., Horwitz, A.R., and Lauffenburger, D.A. (2008). Kinetic model for lamellipodal actin-integrin 'clutch' dynamics. Cell adhesion & migration *2*, 95-105.
Machacek, M., and Danuser, G. (2006). Morphodynamic profiling of protrusion phenotypes. Biophys J *90*, 1439-1452.
Machesky, L.M., and Cooper, J.A. (1999). Cell motility. Bare bones of the cytoskeleton. Nature *401*, 542-543.
Machesky, L.M., and Insall, R.H. (1999). Signaling to actin dynamics. J Cell Biol *146*, 267-272.
Majumder, P., Aranjuez, G., Amick, J., and McDonald, J.A. (2012). Par-1 controls myosin-II activity through myosin phosphatase to regulate border cell migration. Current biology : CB *22*, 363-372.
Manseau, L., Baradaran, A., Brower, D., Budhu, A., Elefant, F., Phan, H., Philp, A.V., Yang, M., Glover, D., Kaiser, K.*, et al.* (1997). GAL4 enhancer traps expressed in the embryo, larval brain, imaginal discs, and ovary of Drosophila. Developmental dynamics : an official publication of the American Association of Anatomists *209*, 310-322.
Mattila, P.K., and Lappalainen, P. (2008). Filopodia: molecular architecture and cellular functions. Nature reviews Molecular cell biology *9*, 446-454.
McDonald, J.A., Khodyakova, A., Aranjuez, G., Dudley, C., and Montell, D.J. (2008). PAR-1 kinase regulates epithelial detachment and directional protrusion of migrating border cells. Current biology : CB *18*, 1659-1667.
McDonald, J.A., Pinheiro, E.M., Kadlec, L., Schupbach, T., and Montell, D.J. (2006). Multiple EGFR ligands participate in guiding migrating border cells. Developmental biology *296*, 94-103.
McDonald, J.A., Pinheiro, E.M., and Montell, D.J. (2003). PVF1, a PDGF/VEGF homolog, is sufficient to guide border cells and interacts genetically with Taiman. Development *130*, 3469-3478.
McShea, M.A., Schmidt, K.L., Dubuke, M.L., Baldiga, C.E., Sullender, M.E., Reis, A.L., Zhang, S., O'Toole, S.M., Jeffers, M.C., Warden, R.M.*, et al.* (2013). Abelson interactor-1 (ABI-1) interacts with MRL adaptor protein MIG-10 and is required in guided cell migrations and process outgrowth in C. elegans. Developmental biology *373*, 1-13.
Meijering, E., Dzyubachyk, O., and Smal, I. (2012). Methods for cell and particle tracking. Methods in enzymology *504*, 183-200.

Michael, M., Vehlow, A., Navarro, C., and Krause, M. (2010). c-Abl, Lamellipodin, and Ena/VASP proteins cooperate in dorsal ruffling of fibroblasts and axonal morphogenesis. Current biology : CB *20*, 783-791.
Miralles, F., Posern, G., Zaromytidou, A.I., and Treisman, R. (2003). Actin dynamics control SRF activity by regulation of its coactivator MAL. Cell *113*, 329-342.
Montell, D.J. (2003). Border-cell migration: the race is on. Nature reviews Molecular cell biology *4*, 13-24.
Montell, D.J., Rorth, P., and Spradling, A.C. (1992). slow border cells, a locus required for a developmentally regulated cell migration during oogenesis, encodes Drosophila C/EBP. Cell *71*, 51-62.
Naora, H., and Montell, D.J. (2005). Ovarian cancer metastasis: integrating insights from disparate model organisms. Nat Rev Cancer *5*, 355-366.
Neuman-Silberberg, F.S., and Schupbach, T. (1993). The Drosophila dorsoventral patterning gene gurken produces a dorsally localized RNA and encodes a TGF alpha-like protein. Cell *75*, 165-174.
Niewiadomska, P., Godt, D., and Tepass, U. (1999). DE-Cadherin is required for intercellular motility during Drosophila oogenesis. J Cell Biol *144*, 533-547.
Oda, H., Uemura, T., and Takeichi, M. (1997). Phenotypic analysis of null mutants for DE-cadherin and Armadillo in Drosophila ovaries reveals distinct aspects of their functions in cell adhesion and cytoskeletal organization. Genes to cells : devoted to molecular & cellular mechanisms *2*, 29-40.
Oliver, T.N., Berg, J.S., and Cheney, R.E. (1999). Tails of unconventional myosins. Cellular and molecular life sciences : CMLS *56*, 243-257.
Pantaloni, D., Le Clainche, C., and Carlier, M.F. (2001). Mechanism of actin-based motility. Science *292*, 1502-1506.
Parton, R.M., Valles, A.M., Dobbie, I.M., and Davis, I. (2010). Isolation of Drosophila egg chambers for imaging. Cold Spring Harbor protocols *2010*, pdb prot5402.
Poukkula, M., Cliffe, A., Changede, R., and Rorth, P. (2011). Cell behaviors regulated by guidance cues in collective migration of border cells. J Cell Biol *192*, 513-524.
Prasad, M., Jang, A.C., Starz-Gaiano, M., Melani, M., and Montell, D.J. (2007). A protocol for culturing Drosophila melanogaster stage 9 egg chambers for live imaging. Nat Protoc *2*, 2467-2473.
Prasad, M., and Montell, D.J. (2007). Cellular and molecular mechanisms of border cell migration analyzed using time-lapse live-cell imaging. Dev Cell *12*, 997-1005.
Riedl, J., Crevenna, A.H., Kessenbrock, K., Yu, J.H., Neukirchen, D., Bista, M., Bradke, F., Jenne, D., Holak, T.A., Werb, Z.*, et al.* (2008). Lifeact: a versatile marker to visualize F-actin. Nature methods *5*, 605-607.
Rorth, P. (2011). Whence directionality: guidance mechanisms in solitary and collective cell migration. Dev Cell *20*, 9-18.
Rorth, P. (2012). Fellow travellers: emergent properties of collective cell migration. EMBO reports *13*, 984-991.

Rorth, P., Szabo, K., and Texido, G. (2000). The level of C/EBP protein is critical for cell migration during Drosophila oogenesis and is tightly controlled by regulated degradation. Molecular cell *6*, 23-30.
Schober, M., Rebay, I., and Perrimon, N. (2005). Function of the ETS transcription factor Yan in border cell migration. Development *132*, 3493-3504.
Silver, D.L., Geisbrecht, E.R., and Montell, D.J. (2005). Requirement for JAK/STAT signaling throughout border cell migration in Drosophila. Development *132*, 3483-3492.
Silver, D.L., and Montell, D.J. (2001). Paracrine signaling through the JAK/STAT pathway activates invasive behavior of ovarian epithelial cells in Drosophila. Cell *107*, 831-841.
Small, J.V., Stradal, T., Vignal, E., and Rottner, K. (2002). The lamellipodium: where motility begins. Trends in cell biology *12*, 112-120.
Sokol, N.S., and Cooley, L. (2003). Drosophila filamin is required for follicle cell motility during oogenesis. Developmental biology *260*, 260-272.
Somogyi, K., and Rorth, P. (2004). Evidence for tension-based regulation of Drosophila MAL and SRF during invasive cell migration. Developmental Cell *7*, 85-93.
Starz-Gaiano, M., Melani, M., Wang, X., Meinhardt, H., and Montell, D.J. (2008). Feedback inhibition of Jak/STAT signaling by apontic is required to limit an invasive cell population. Dev Cell *14*, 726-738.
Stavoe, A.K., Nelson, J.C., Martinez-Velazquez, L.A., Klein, M., Samuel, A.D., and Colon-Ramos, D.A. (2012). Synaptic vesicle clustering requires a distinct MIG-10/Lamellipodin isoform and ABI-1 downstream from Netrin. Genes & development *26*, 2206-2221.
Strack, R.L., Strongin, D.E., Bhattacharyya, D., Tao, W., Berman, A., Broxmeyer, H.E., Keenan, **R.J., and Glick, B.S. (2008).** A noncytotoxic DsRed variant for whole-cell labeling. Nature methods *5*, 955-957.
Suraneni, P., Rubinstein, B., Unruh, J.R., Durnin, M., Hanein, D., and Li, R. (2012). The Arp2/3 complex is required for lamellipodia extension and directional fibroblast cell migration. J Cell Biol *197*, 239-251.
Svitkina, T.M., and Borisy, G.G. (1999). Arp2/3 complex and actin depolymerizing factor/cofilin in dendritic organization and treadmilling of actin filament array in lamellipodia. J Cell Biol *145*, 1009-1026.
Tanentzapf, G., Smith, C., McGlade, J., and Tepass, U. (2000). Apical, lateral, and basal polarization cues contribute to the development of the follicular epithelium during Drosophila oogenesis. J Cell Biol *151*, 891-904.
Tekotte, H., Tollervey, D., and Davis, I. (2007). Imaging the migrating border cell cluster in living Drosophila egg chambers. Developmental dynamics : an official publication of the American Association of Anatomists *236*, 2818-2824.
Theriot, J.A., and Mitchison, T.J. (1991). Actin microfilament dynamics in locomoting cells. Nature *352*, 126-131.
Van Haastert, P.J., and Devreotes, P.N. (2004). Chemotaxis: signalling the way forward. Nature reviews Molecular cell biology *5*, 626-634.

Verheyen, E.M., and Cooley, L. (1994). Profilin mutations disrupt multiple actin-dependent processes during Drosophila development. Development *120*, 717-728.
Verkhusha, V.V., Tsukita, S., and Oda, H. (1999). Actin dynamics in lamellipodia of migrating border cells in the Drosophila ovary revealed by a GFP-actin fusion protein. FEBS Lett *445*, 395-401.
Vicente-Manzanares, M., and Horwitz, A.R. (2011a). Adhesion dynamics at a glance. Journal of cell science *124*, 3923-3927.
Vicente-Manzanares, M., and Horwitz, A.R. (2011b). Cell migration: an overview. Methods Mol Biol *769*, 1-24.
Vicente-Manzanares, M., Webb, D.J., and Horwitz, A.R. (2005). Cell migration at a glance. Journal of cell science *118*, 4917-4919.
Wang, X., Adam, J.C., and Montell, D. (2007). Spatially localized Kuzbanian required for specific activation of Notch during border cell migration. Developmental biology *301*, 532-540.
Wang, X., Bo, J., Bridges, T., Dugan, K.D., Pan, T.C., Chodosh, L.A., and Montell, D.J. (2006). Analysis of cell migration using whole-genome expression profiling of migratory cells in the Drosophila ovary. Dev Cell *10*, 483-495.
Wang, X., He, L., Wu, Y.I., Hahn, K.M., and Montell, D.J. (2010). Light-mediated activation reveals a key role for Rac in collective guidance of cell movement in vivo. Nature cell biology *12*, 591-597.
Wang, Y.L. (1985). Exchange of actin subunits at the leading edge of living fibroblasts: possible role of treadmilling. Journal of Cell Biology *101*, 597-602.
Webb, D.J., Parsons, J.T., and Horwitz, A.F. (2002). Adhesion assembly, disassembly and turnover in migrating cells -- over and over and over again. Nature cell biology *4*, E97-100.
Webb, D.J., Zhang, H., and Horwitz, A.F. (2005). Cell migration: an overview. Methods Mol Biol *294*, 3-11.
Wiesner, S., Helfer, E., Didry, D., Ducouret, G., Lafuma, F., Carlier, M.F., and Pantaloni, D. (2003). A biomimetic motility assay provides insight into the mechanism of actin-based motility. J Cell Biol *160*, 387-398.
Wolf, K., and Friedl, P. (2006). Molecular mechanisms of cancer cell invasion and plasticity. The British journal of dermatology *154 Suppl 1*, 11-15.
Xu, Y., and Quinn, C.C. (2012). MIG-10 functions with ABI-1 to mediate the UNC-6 and SLT-1 axon guidance signaling pathways. PLoS genetics *8*, e1003054.
Xue, C., Wyckoff, J., Liang, F., Sidani, M., Violini, S., Tsai, K.L., Zhang, Z.Y., Sahai, E., Condeelis, J., and Segall, J.E. (2006). Epidermal growth factor receptor overexpression results in increased tumor cell motility in vivo coordinately with enhanced intravasation and metastasis. Cancer Res *66*, 192-197.
Yao, T.P., Forman, B.M., Jiang, Z., Cherbas, L., Chen, J.D., McKeown, M., Cherbas, P., and Evans, R.M. (1993). Functional ecdysone receptor is the product of EcR and Ultraspiracle genes. Nature *366*, 476-479.

Yarmola, E.G., and Bubb, M.R. (2006). Profilin: emerging concepts and lingering misconceptions. Trends in biochemical sciences *31*, 197-205.
Yilmaz, M., and Christofori, G. (2010). Mechanisms of motility in metastasizing cells. Molecular cancer research : MCR *8*, 629-642.
Yoshida, H., Cheng, W., Hung, J., Montell, D., Geisbrecht, E., Rosen, D., Liu, J., and Naora, H. (2004). Lessons from border cell migration in the Drosophila ovary: A role for myosin VI in dissemination of human ovarian cancer. Proc Natl Acad Sci U S A *101*, 8144-8149.
Yoshida, H., Liu, J., Samuel, S., Cheng, W., Rosen, D., and Naora, H. (2005). Steroid receptor coactivator-3, a homolog of Taiman that controls cell migration in the Drosophila ovary, regulates migration of human ovarian cancer cells. Mol Cell Endocrinol *245*, 77-85.
Zhang, L., Luo, J., Wan, P., Wu, J., Laski, F., and Chen, J. (2011). Regulation of cofilin phosphorylation and asymmetry in collective cell migration during morphogenesis. Development *138*, 455-464.

9. Appendix

The following contains information about the journal article in which data from this thesis contributed to.

Law, A.L., Vehlow, A., Kotini, M., Dodgson, L., Soong, D., Theveneau, E., Bodo, C., Taylor, E., Navarro, C., Perera, U.*, et al.* (2013). Lamellipodin and the Scar/WAVE complex cooperate to promote cell migration in vivo. J Cell Biol *203*, 673-689.

Data from this thesis contributed to figures 9 and 10 on pages 684 and 685 respectively.

Experiments on fixed samples were performed providing the data for Figure 9 B and C following initial experimental work by E. Taylor.

All *Drosophila* live imaging experiments and data analysis was performed by myself, generating the entire Figure 10.

D. Bennett conceived, designed and aided in the analysis of the data.

Published November 18, 2013

Lamellipodin and the Scar/WAVE complex cooperate to promote cell migration in vivo

Ah-Lai Law,[1] Anne Vehlow,[1] Maria Kotini,[3] Lauren Dodgson,[4] Daniel Soong,[2] Eric Theveneau,[3] Cristian Bodo,[1] Eleanor Taylor,[4] Christel Navarro,[1] Upamali Perera,[1] Magdalene Michael,[1] Graham A. Dunn,[1] Daimark Bennett,[4] Roberto Mayor,[3] and Matthias Krause[1]

[1]Randall Division of Cell and Molecular Biophysics, and [2]British Heart Foundation Centre of Excellence, James Black Centre, Cardiovascular Division, King's College London, London SE1 1UL, England, UK
[3]Department of Cell and Developmental Biology, University College London, London WC1 6BT, England, UK
[4]Institute of Integrative Biology, University of Liverpool, Liverpool L69 7ZB, England, UK

Cell migration is essential for development, but its deregulation causes metastasis. The Scar/WAVE complex is absolutely required for lamellipodia and is a key effector in cell migration, but its regulation in vivo is enigmatic. Lamellipodin (Lpd) controls lamellipodium formation through an unknown mechanism. Here, we report that Lpd directly binds active Rac, which regulates a direct interaction between Lpd and the Scar/WAVE complex via Abi. Consequently, Lpd controls lamellipodium size, cell migration speed, and persistence via Scar/WAVE in vitro. Moreover, Lpd knockout mice display defective pigmentation because fewer migrating neural crest-derived melanoblasts reach their target during development. Consistently, Lpd regulates mesenchymal neural crest cell migration cell autonomously in *Xenopus laevis* via the Scar/WAVE complex. Further, Lpd's *Drosophila melanogaster* orthologue Pico binds Scar, and both regulate collective epithelial border cell migration. Pico also controls directed cell protrusions of border cell clusters in a Scar-dependent manner. Taken together, Lpd is an essential, evolutionary conserved regulator of the Scar/WAVE complex during cell migration in vivo.

Introduction

Tightly controlled cell migration is essential for the development of multicellular organisms, and deregulation is a hallmark of diseases such as metastatic cancer (Hanahan and Weinberg, 2011). The force for cell migration is largely provided by actin polymerization at the leading edge of cells, the lamellipodium, and is controlled by actin-binding proteins including Ena/VASP and the Arp2/3 complex. These proteins are recruited to the leading edge by regulators such as Scar/WAVE for the Arp2/3 complex or Lpd for Ena/VASP proteins. The Scar/WAVE complex is composed of five proteins (Sra1/Pir121, Nap1, Scar/WAVE1-3, Abi1-3, and HSPC300) and is activated by Rac to interact with the Arp2/3 complex, thereby nucleating branched actin filament networks. In this way, both Scar/WAVE and Arp2/3 complexes regulate cell migration (Suetsugu et al., 2003; Yan et al., 2003; Insall and Machesky, 2009; Campellone and Welch, 2010; Michael et al., 2010; Suraneni et al., 2012; Wu et al., 2012). However, the regulation of the Scar/WAVE complex in migrating cells is not well understood.

Ena/VASP proteins localize to lamellipodia, tips of filopodia, and focal adhesions, and regulate lamellipodial dynamics and cell migration. Ena/VASP regulate actin filament length at the leading edge of cells by temporarily protecting actin filament ends from capping protein and recruiting polymerization-competent G-actin bound to profilin. Scar/WAVE–Arp2/3–mediated actin filament branching and Ena/VASP-regulated actin filament elongation together control speed and stability of lamellipodial protrusions, but it is not known how these mechanisms are coordinated (Bear et al., 2001, 2002; Krause et al., 2003; Pula and Krause, 2008).

A. Vehlow, M. Kotini, L. Dodgson, D. Soong, and E. Theveneau contributed equally to this paper.

D. Bennett and R. Mayor contributed equally to this paper.

Correspondence to Matthias Krause: Matthias.Krause@kcl.ac.uk

Abbreviations used in this paper: 4-OHT, 4-OH-tamoxifen; ANOVA, analysis of variance; DCT, dopachrome tautomerase; E, embryonic day; KO, knockout; MBP, maltose binding protein; MEF, mouse embryonic fibroblast; MO, morpholino; NC, neural crest; P, postnatal day; PH, pleckstrin homology; RA, Ras association; TR, time ratio; WT, wild type.

Supplemental Material can be found at:
http://jcb.rupress.org/content/suppl/2013/11/13/jcb.201304051.DC1.html

The Rockefeller University Press $30.00
J. Cell Biol. Vol. 203 No. 4 673–689
www.jcb.org/cgi/doi/10.1083/jcb.201304051

Published November 18, 2013

Lpd and its *Drosophila melanogaster* orthologue Pico interact with Ena/VASP proteins, and harbor a proline-rich region with putative SH3 domain binding sites, a Ras association (RA) domain, and a pleckstrin homology (PH) domain. Lpd localizes to lamellipodia, and both RA and PH domains cooperate in membrane targeting of Lpd upon growth factor stimulation of fibroblasts. Lpd recruits Ena/VASP proteins to lamellipodia and to dorsal ruffles of fibroblasts, thereby controlling lamellipodia protrusion dynamics, dorsal ruffling of fibroblasts, axon elongation, and branching of primary hippocampal neurons, but its role in mesenchymal and epithelial cell migration is unknown. Surprisingly, knockdown of Lpd decreased F-actin content, resulted in the absence of a dense lamellipodial F-actin meshwork, and impaired lamellipodium formation (Krause et al., 2004; Lyulcheva et al., 2008; Michael et al., 2010). These phenotypes were not observed with loss of Ena/VASP, which suggests that Lpd regulates other effectors of the actin cytoskeleton in addition to Ena/VASP. Interestingly, recent reports suggest that the Lpd orthologue in *Caenorhabditis elegans*, MIG-10, may directly or indirectly bind to Abi-1, and both genetically interact to regulate axon guidance, synaptic vesicle clustering, and excretory canal outgrowth in *C. elegans* (Stavoe et al., 2012; Xu and Quinn, 2012; McShea et al., 2013).

Here, we show that Lpd is in complex with Scar/WAVE, mediated by a direct binding of the Abi SH3 domain to three sites in Lpd. In addition, Lpd directly interacts with active Rac, which positively regulates the Lpd–Scar/WAVE interaction. Therefore, Lpd functions as a Rac effector and controls lamellipodia formation via the Scar/WAVE complex. Lpd knockout (KO) mouse embryonic fibroblasts (MEFs) are impaired in cell migration, whereas Lpd overexpression dramatically increased cell migration speed in a Scar/WAVE-dependent manner. Most Lpd KO mice die shortly after birth, and the few surviving mice are reduced in body weight and display missing pigmentation on their ventral side because fewer migrating neural crest (NC)–derived melanoblasts reach their target during development. In agreement, Lpd and the Scar/WAVE complex cooperate to regulate NC migration in vivo and in vitro in *Xenopus laevis*. This cooperation is evolutionary conserved in invertebrates because Lpd's orthologue Pico also binds the Scar/WAVE complex and regulates epithelial collective border cell migration in the fly ovary in a Scar/WAVE-dependent manner. Taken together, we have identified a novel pathway in which Lpd functions as an important evolutionary conserved regulator of the Scar/WAVE complex during cell migration in vivo.

Results

Lpd colocalizes and interacts with the Scar/WAVE complex

We previously reported that Lpd knockdown impairs lamellipodium formation (Krause et al., 2004). In contrast, loss of the Lpd-binding proteins Ena/VASP only altered lamellipodial dynamics (Bear et al., 2002; Krause et al., 2003). Therefore, we hypothesized that the Scar/WAVE complex, a key regulator of lamellipodia, may mediate Lpd's function in lamellipodium formation.

Coimmunoprecipitation with GFP-Lpd and Myc-tagged Scar/WAVE complex revealed that Lpd interacts with both Scar/WAVE1 (Fig. 1 A) and Scar/WAVE2 complexes (Fig. 1 B). Endogenous Lpd and Scar/WAVE1 also coimmunoprecipitated from lysates of primary cortical neurons (Fig. 1 C), which suggests that Lpd and Scar/WAVE indeed form a protein complex in cells.

The stability of the Scar/WAVE complex is tightly controlled, such that knocking down one protein of the core complex results in proteasomal degradation of the remaining proteins of the complex (Kunda et al., 2003). The expression of the Scar/WAVE complex was unaltered when Lpd protein levels were reduced using siRNA (Fig. 1 D), which suggests that Lpd is not part of the core complex but may associate with it to control its function.

Both Lpd and the Scar/WAVE complex have been reported to localize to lamellipodia (Hahne et al., 2001; Stradal et al., 2001; Krause et al., 2004). Consistently, immunofluorescence analysis revealed that Lpd colocalizes with Scar/WAVE1 (Figs. 1 E and S1), Abi1 (Figs. 1 F and S1), and Sra1 (Figs. 1 G and S1) at the very edge of lamellipodia in B16F1 mouse melanoma cells (Fig. 1, E–G) or CAD mouse neuronal cells (Fig. S1).

The interaction between Lpd and the Scar/WAVE complex is mediated by the Abi SH3 domain and three sites in Lpd

Abi harbors an SH3 domain, which could bind to putative SH3 binding sites in the C terminus of Lpd. To test this, we purified a GST-Abi1-SH3 domain fusion protein and pulled down Lpd from NIH3T3 cell lysates, revealing an interaction of the Abi SH3 domain with Lpd (Fig. 2 A). In Far-Western blot experiments with fragments of Lpd, we observed that only full-length Abi1 but not a truncated form without the SH3 domain (Abi1$^{\Delta SH3}$) directly interacted with two fragments (GST-Lpd-C4 and GST-Lpd-C6) and weakly with a third (GST-Lpd-C5; Fig. 2, B–D). A Far-Western experiment on a peptide array covering the C terminus of Lpd as 12-mer peptides that overlap each other by three amino acids revealed two strong class II SH3 domain–binding sites: one in each fragment Lpd-C4 and Lpd-C6, and one weak class II binding site in fragment Lpd-C5 (Fig. 2, E and F).

To test whether the SH3 domain of Abi mediates the interaction between Lpd and the Scar/WAVE complex, we attempted to coimmunoprecipitate GFP-Lpd and all Myc-tagged components of the Scar/WAVE complex, including either full-length Abi1 or Abi1$^{\Delta SH3}$. This analysis revealed that expression of Abi1$^{\Delta SH3}$ disrupts the interaction between Lpd and the Scar/WAVE complex (Fig. 3, A and B), which suggests that the SH3 domain of Abi is required for this interaction. To explore whether the three Abi SH3 domain binding sites are sufficient for the Lpd interaction with Abi, we mutated them in full-length Lpd (Lpd^{AbiMut}). Comparing coimmunoprecipitations between wild-type (WT) Lpd or Lpd^{AbiMut} and Abi1 revealed that Lpd^{AbiMut} is defective in Abi binding (Fig. 3, C and D). Because Lpd interacts with Ena/VASP proteins (Krause et al., 2004), we

Published November 18, 2013

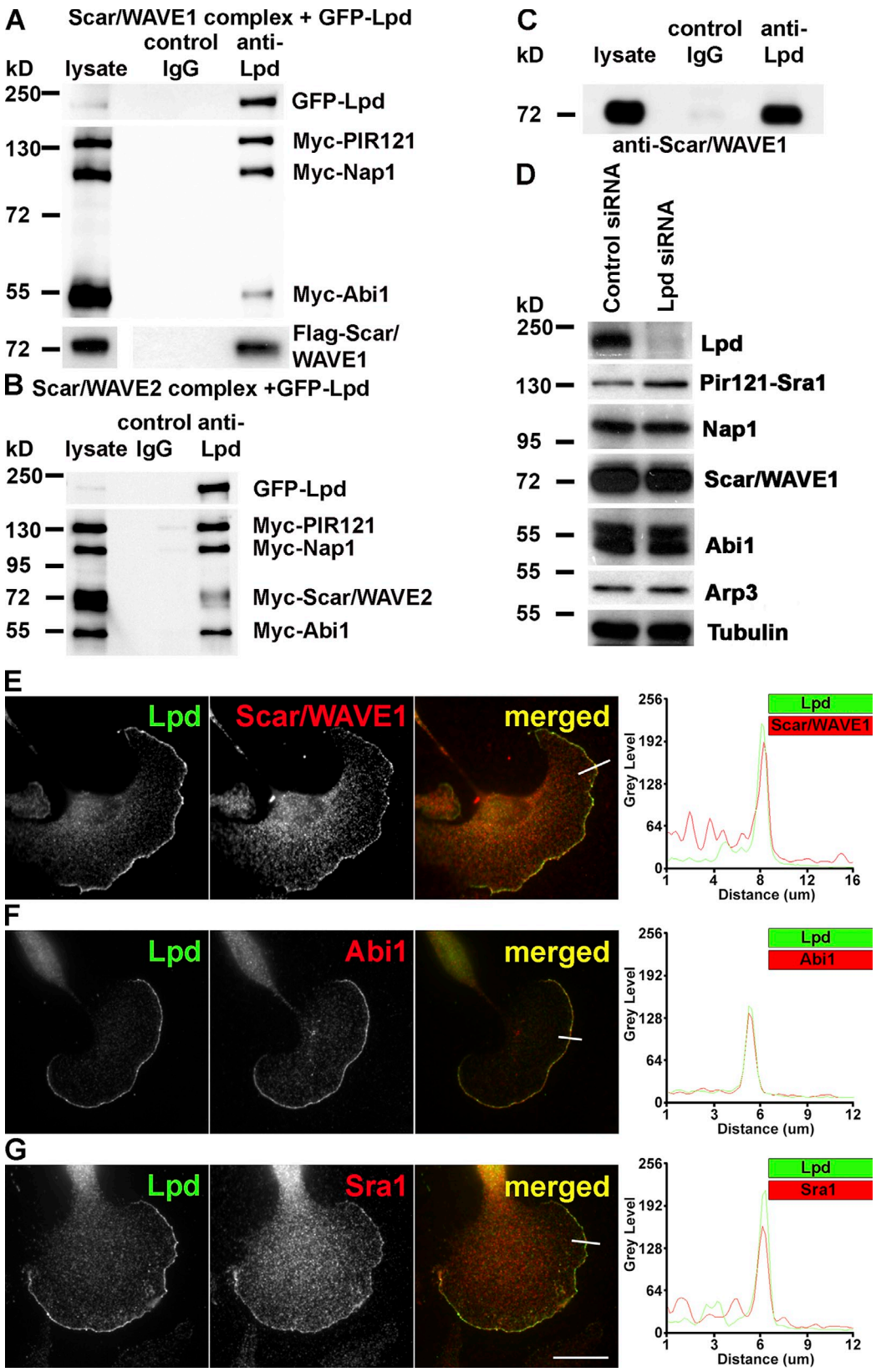

Figure 1. **Lamellipodin interacts with the Scar/WAVE complex.** (A and B) Coimmunoprecipitation using Lpd or IgG control antibodies from HEK293 cell lysates expressing GFP-Lpd and the tagged Scar/WAVE complex including FLAG-WAVE1 (A) and Myc-WAVE2 (B). Myc-HSPC300 is not shown. (C) Endogenous Scar/WAVE1 and Lpd coimmunoprecipitate from lysates of primary cortical neurons using Lpd antibodies but not with IgG control. (D) Knockdown of Lpd by siRNA in B16F1 cells does not reduce expression of the Scar/WAVE complex (HSPC300 not shown) or Arp3. Loading control: Tubulin. (E–G) Endogenous Lpd (green) colocalizes with Scar/WAVE1 (E), Abi1 (F), and Sra1 (G; red) at the very edge of lamellipodia in B16F1 mouse melanoma cells. Representative line scan from multiple experimental repeats across the leading edge (location indicated on merged images) shows colocalization of Lpd (green) and Scar/WAVE1 (E), Abi1 (F), and Sra1 (G; red). Bar, 25 µm. See also Fig. S1.

Published November 18, 2013

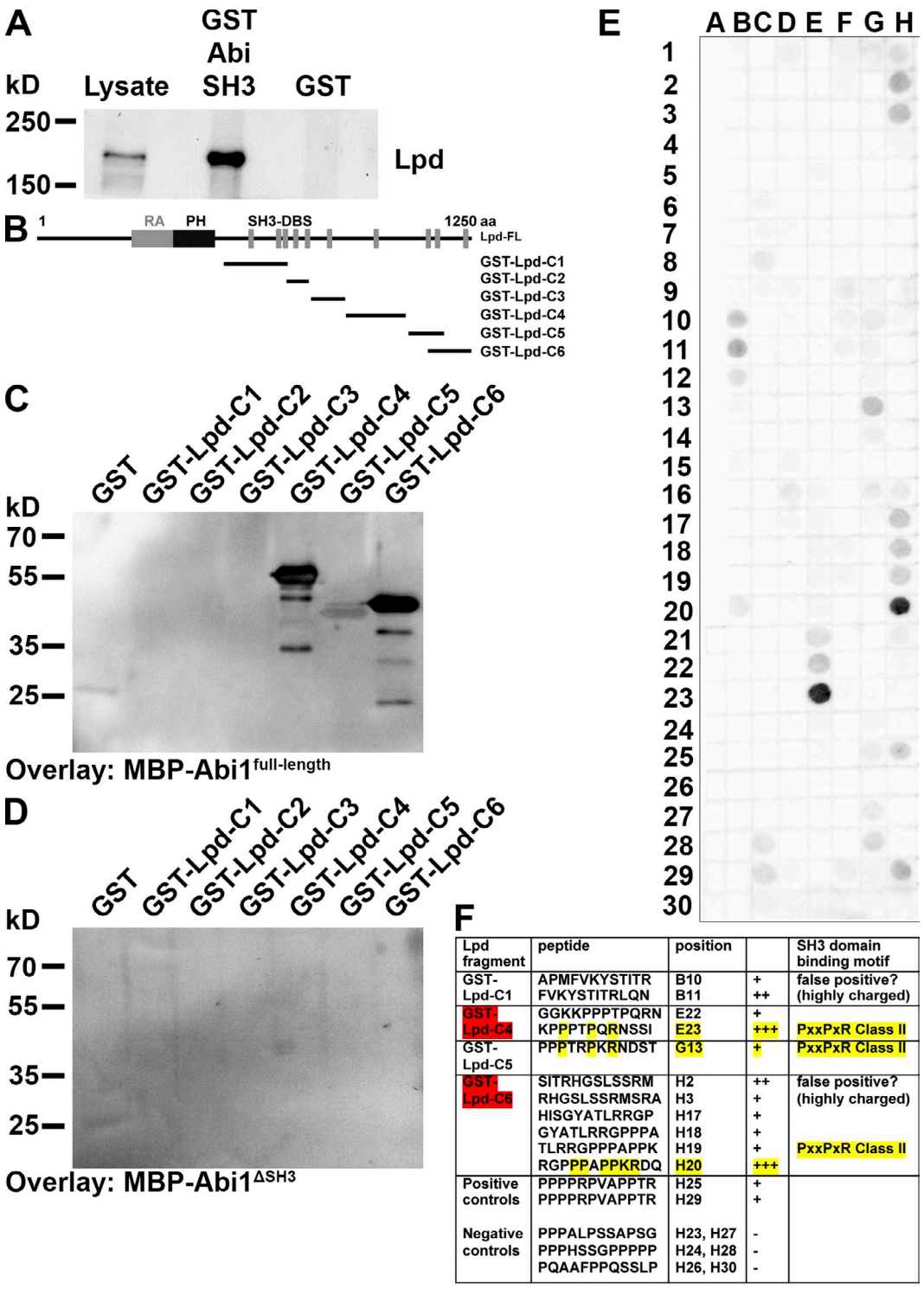

F

Lpd fragment	peptide	position		SH3 domain binding motif
GST-Lpd-C1	APMFVKYSTITR	B10	+	false positive?
	FVKYSTITRLQN	B11	++	(highly charged)
GST-Lpd-C4	GGKKPPPTPQRN	E22	+	
	KPPPTPQRNSSI	E23	+++	PxxPxR Class II
GST-Lpd-C5	PPPTRPKRNDST	G13	+	PxxPxR Class II
GST-Lpd-C6	SITRHGSLSSRM	H2	++	false positive?
	RHGSLSSRMSRA	H3	+	(highly charged)
	HISGYATLRRGP	H17	+	
	GYATLRRGPPPA	H18	+	
	TLRRGPPPAPPK	H19	+	PxxPxR Class II
	RGPPPAPPKRDQ	H20	+++	
Positive controls	PPPPRPVAPPTR	H25	+	
	PPPPRPVAPPTR	H29	+	
Negative controls	PPPALPSSAPSG	H23, H27	-	
	PPPHSSGPPPPP	H24, H28	-	
	PQAAFPPQSSLP	H26, H30	-	

Figure 2. **Lpd directly interacts with the SH3 domain of Abi.** (A) Pull-down of Lpd from NIH/3T3 cell lysate using the GST-Abi-SH3 domain or GST as control. (B–D) Far Western overlay on different GST-Lpd truncation mutants (B) or GST control using purified (C) MBP-Abi1$^{full\text{-}length}$ or (D) MBP-Abi1$^{\Delta SH3}$ was detected with anti-MBP antibodies. Three independent experiments were performed. (E) Far-Western overlay with MBP-Abi1$^{full\text{-}length}$ on a peptide array covering the C terminus of Lpd with 12-mer peptides overlapping each other by three amino acids was detected with anti-MBP antibodies. (F) Table shows Abi SH3 domain–binding motifs in the Lpd sequence. The two GST-Lpd fragments highlighted in red correspond to the most strongly interacting Lpd fragments in the Far-Western experiment in C. The amino acid residues highlighted in yellow correspond to the core residues required for class II SH3 domain binding.

also coimmunoprecipitated Lpd with GFP-Abi and GFP-VASP from HEK cell lysates (Fig. S2 A), which suggests that Lpd forms a complex with both Abi and Ena/VASP proteins.

Collectively, we have shown that the interaction between Lpd and Abi is direct and mediated by the SH3 domain of Abi and three binding sites in Lpd, and that this interaction is

Published November 18, 2013

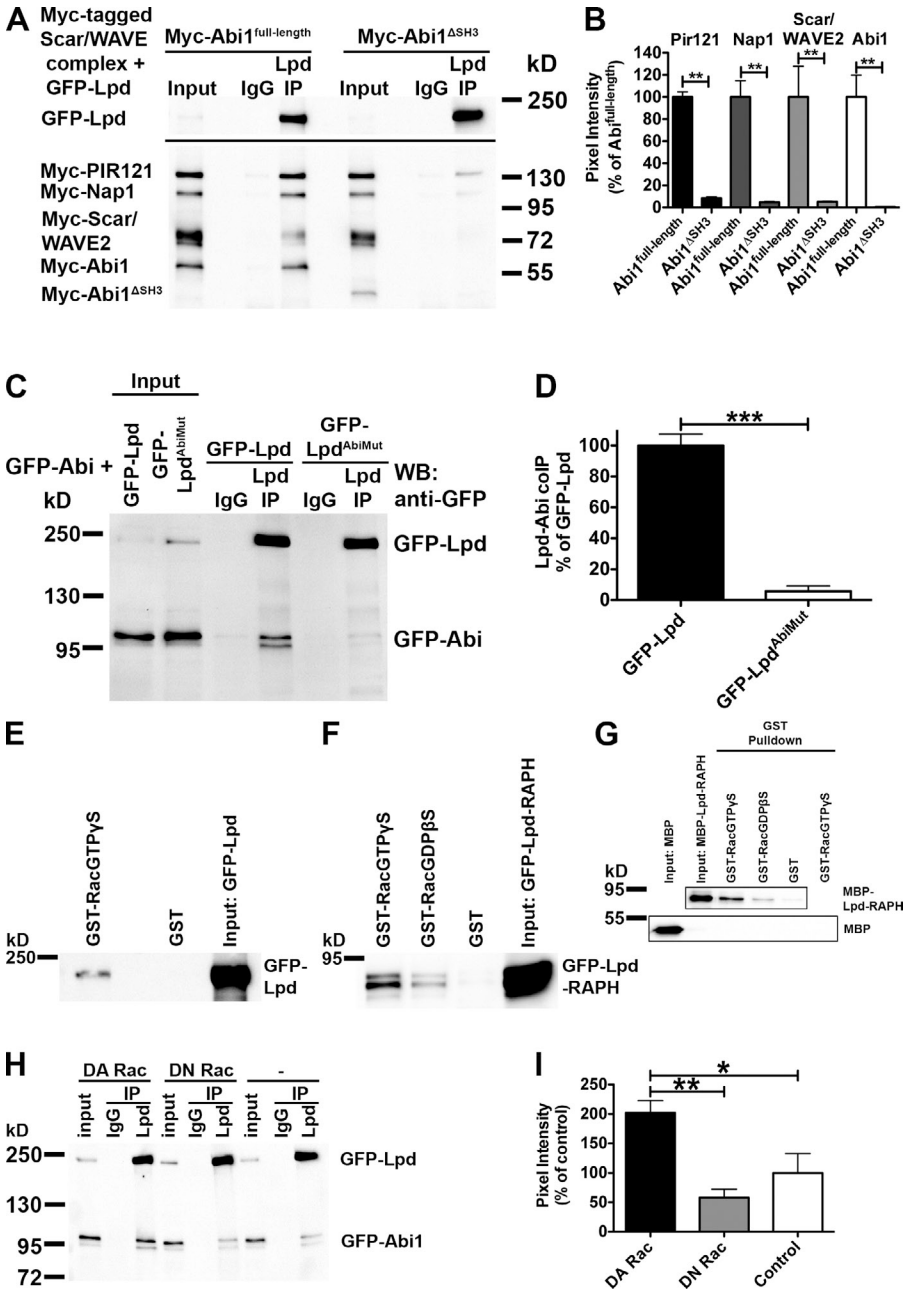

Figure 3. **The interaction between Lpd and the Scar/WAVE complex is mediated by the Abi SH3 domain and positively regulated by active Rac.** (A–D) The Abi SH3 domain and three Abi binding sites in Lpd mediate the interaction between Lpd and the Scar/WAVE complex. Immunoprecipitation using Lpd antibodies or IgG control from HEK293 cell lysates (A) expressing GFP-Lpd and all Myc-tagged components of the Scar/WAVE complex, including Myc-Abi1$^{full\text{-}length}$ (A, left), Myc-Abi1$^{\Delta SH3}$ (A, right), or GFP-Abi and GFP-Lpd (C, left) or GFP-Lpd^{AbiMut} (C, right), show coimmunoprecipitation between Lpd and all components of the Scar/WAVE complex only when the Abi SH3 domain is present (A; Myc-HSPC300 is not shown) or between Lpd and GFP-Abi only when the Abi binding sites are present (B). Western blot: anti-GFP. (B and D) Comparison of efficiency of coimmunoprecipitation of Lpd with all components of the Scar/WAVE complex (B) or GFP-Lpd or GFP-Lpd^{AbiMut} with Abi (D). Quantification of band intensity of chemiluminescence imaged with a charge-coupled device camera. (B) Coimmunoprecipitation is reduced by >90%. Error bars indicate mean ± SEM, $n = 3$. One-way analysis of variance (ANOVA) and Tukey's test were used; **, $P < 0.01$. (D) Coimmunoprecipitation is reduced by >94%. Error bars indicate mean ± SEM, $n = 3$. An unpaired t test was used; ***, $P < 0.001$. (E and F) Lpd and the RA-PH domains of Lpd are in complex with active Rac. Purified GTPγS- or GDPβS-loaded GST-Rac, or GST only as control, on Sepharose beads were incubated with lysates from HEK cells expressing GFP-Lpd (E) or GFP-Lpd-RAPH (F) and bound with GFP-Lpd or GFP-Lpd-RAPH. Samples were detected in a Western blot against GFP. (G) The RA-PH domains of Lpd directly interact with active Rac. Purified GTP-γS- or GDPβS-loaded GST-Rac or GST only as control Sepharose beads were incubated with MBP-Lpd-RAPH or MBP only as control, and direct interaction was detected in a Western blot against MBP. (H and I) The interaction between Lpd and Abi is positively regulated by active Rac. Immunoprecipitation using Lpd-specific antibodies or IgG control from HEK293 cell lysates expressing GFP-Abi, GFP-Lpd, and dominant-active Rac (DA Rac; H, left) or dominant-negative Rac (DN Rac; H, middle), or empty vector control (H, right) show increased coimmunoprecipitation between Lpd and GFP-Abi only when dominant-active Rac is coexpressed. Western blot: anti-GFP. (I) Comparison of efficiency of coimmunoprecipitation of Lpd with GFP-Abi from blots in H. Quantification of band intensity of chemiluminescence imaged with a charge-coupled device camera. Coimmunoprecipitation is increased by >100% compared with empty vector and 150% compared with DN-Rac. Error bars indicate mean ± SEM, $n = 3$. One-way ANOVA and Tukey's test were used. *, $P < 0.05$; **, $P < 0.01$.

sufficient and necessary for the interaction of Lpd with the Scar/WAVE complex.

Lpd directly interacts with active Rac, which positively regulates the interaction between Lpd and the Scar/WAVE complex

It has been shown that MIG-10 is in complex with Rac (Quinn et al., 2008). To explore whether Lpd is also in complex with Rac, we pulled down GFP-Lpd or the GFP-Lpd-RA-PH domains from HEK lysates with purified GST-Rac. This revealed that Lpd (Fig. 3 E) and the RA-PH domains of Lpd are in complex with active Rac (Fig. 3 F). To assess whether this interaction is direct we pulled down purified maltose binding protein (MBP)-tagged RA-PH domains of Lpd with GTPγS- or GDPβS-loaded purified GST-Rac protein and found that it preferentially directly interacts with active Rac (Fig. 3 G).

This prompted us to explore whether active Rac regulates the interaction between Lpd and the Scar/WAVE complex. We expressed GFP-Lpd and GFP-Abi with and without all Myc-tagged components of the Scar/WAVE complex in HEK cells and found that significantly more Abi coimmunoprecipitates with Lpd when dominant-active Rac (DA Rac) was coexpressed compared with coexpression of dominant-negative Rac (DN Rac) or when Rac was not coexpressed (Fig. 3, H and I;

Published November 18, 2013

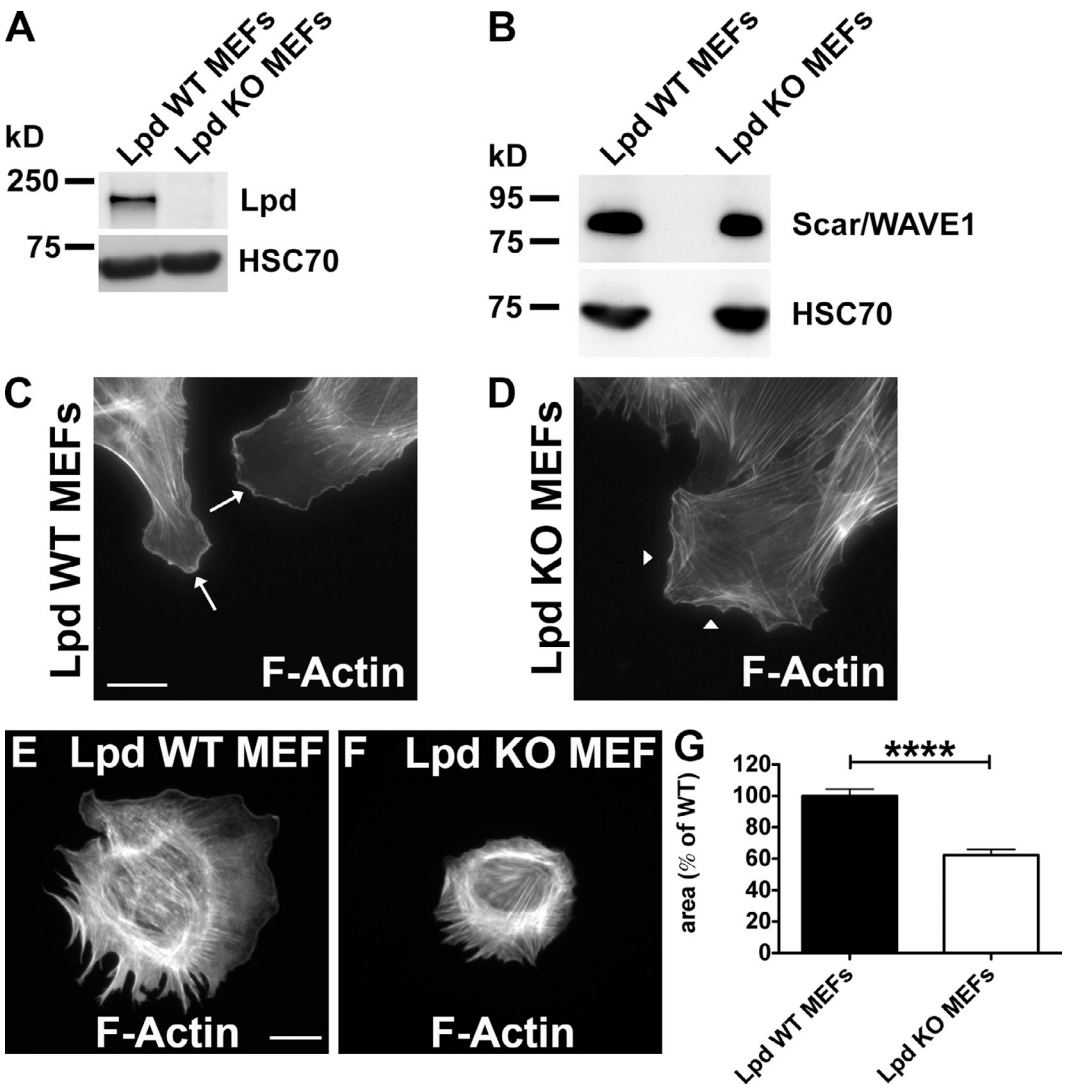

Figure 4. **Lpd regulates cell spreading.** (A and B) Western blot of cell lysates of Lpd WT and Lpd KO MEFs using anti-Lpd (A) or Scar/WAVE1 (B). Loading control: anti-HSC70. (C and D) F-actin staining (phalloidin) in Lpd WT (C) and Lpd KO MEFs (D). Arrows in C indicate the presence of lamellipodia in Lpd WT MEFs. Arrowheads in D indicate the absence of lamellipodia. (E and F) F-actin staining (phalloidin) determines the area of Lpd WT (E) and Lpd KO MEFs (F) after 60 min of spreading on fibronectin. (G) Quantification of the spreading area of MEFs from E and F. Values are mean ± SEM (error bars) of 131 (KO) or 155 (WT) cells. Unpaired, two-tailed *t* test: ****, $P \leq 0.0001$. Bars, 25 µm.

and Fig. S2, B and C). This suggests that Lpd functions as a novel Rac effector because the interaction between Lpd and the Scar/WAVE complex is positively regulated by active Rac.

Lpd regulates cell migration via Abi and the Scar/WAVE complex

The Scar/WAVE complex regulates lamellipodium formation by activating the Arp2/3 complex (Machesky and Insall, 1998; Miki et al., 1998), and both complexes regulate cell migration (Suetsugu et al., 2003; Yan et al., 2003; Suraneni et al., 2012; Wu et al., 2012). We identified Lpd as a protein that regulates lamellipodia formation (Krause et al., 2004), but its role in mesenchymal and epithelial cell migration had not been determined.

To explore the role of Lpd in mesenchymal cell migration, we generated conditional KO MEFs (Lpd WT MEFs) from Lpd KO mice (see Fig. 6) and transduced them with retroviruses conferring 4-OH-tamoxifen (4-OHT) inducible CreERT2 (Oskarsson et al., 2006). When treated with 4-OHT, these Lpd WT MEFs lose the *Lpd* gene and Lpd expression (Lpd KO MEFs; Fig. 4 A). Expression levels of Scar/WAVE1, RIAM, Mena, VASP, or EVL did not change in the Lpd KO MEFs compared with Lpd WT MEFs (Figs. 4 B and S2 D). Lpd KO MEFs were impaired in lamellipodium formation (Fig. 4, C and D), which is consistent with earlier observations that Lpd knockdown cells are devoid of lamellipodia (Krause et al., 2004).

Cells use lamellipodia for spreading on extracellular matrix and during cell migration. Lpd KO MEFs spread significantly more slowly (spread area reduced by 38% at 60 min) compared with Lpd WT MEFs (Fig. 4, E–G). We then analyzed random cell migration and found that migration speed and persistence were significantly reduced by 45% and 36%, respectively (Fig. 5, A and B). Likewise, directional migration into a scratch wound was impaired in the Lpd

Published November 18, 2013

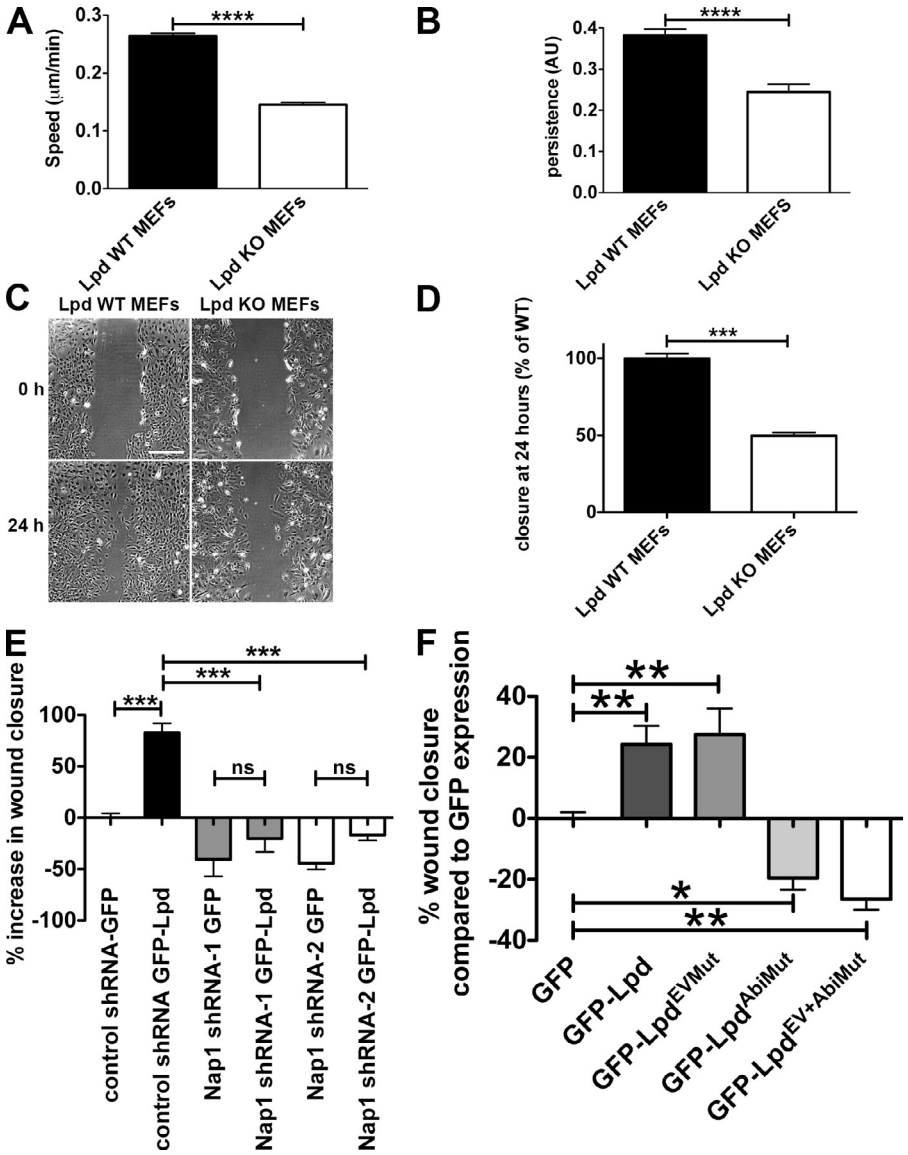

Figure 5. **Lpd regulates cell migration via Abi and the Scar/WAVE complex.** (A and B) Quantification of velocity (A) and persistence (B) of randomly migrating Lpd WT or KO MEFs. Mean population speed and persistence (dt = 2, TR = 4; see Materials and methods for calculation). Results are mean ± SEM (error bars), with three independent experiments. ****, $P \leq 0.0001$, unpaired *t* test. (C and D) A confluent layer of WT or KO Lpd MEFs was scratched, and the area of the scratch measured at 0 and 24 h. Bar, 500 µm. Area closure is shown as the percentage of WT cells. (D) Results are mean ± SEM, with four independent experiments. ***, $P \leq 0.001$, unpaired *t* test. See also Fig. S3 and Videos 1 and 2. (E and F) Lpd overexpression increases cell migration speed via Abi and Scar/WAVE. MDA-MB231 breast cancer cells, stably expressing Nap1-specific (Nap1 shRNA 1 or 2) or scrambled control shRNA were transiently transfected with GFP-Lpd or GFP as control (E) or GFP-Lpd, GFP-Lpd^{EVMut}, GFP-Lpd^{AbiMut}, GFP-Lpd$^{EV+AbiMut}$, or GFP as control (F). A confluent cell layer was scratched and the area of the scratch was measured at 0 and 24 h. Area closure is shown as percentage increase over GFP cells. Results are mean ± SEM (error bars), from three independent experiments. *, $P \leq 0.05$; **, $P \leq 0.01$; ***, $P \leq 0.001$; ns, not significant; one-way ANOVA was used. (E) Tukey's test. (F) Newman-Keuls method.

KO MEFs compared with the Lpd WT MEFs (reduced by 50%; Fig. 5, C and D). In agreement, we found that directional migration into a scratch wound was also highly reduced when Lpd expression was knocked down in the Rat2 fibroblast cell line (Fig. S3, A and B), which indicates that this defect is not cell line dependent. WT Rat2 fibroblasts migrated with a polarized lamellipodium, whereas Lpd knockdown cells migrated by extending filopodia (Video 2), which was also observed in the Lpd KO MEFs (Video 1), similar to Arp2/3 knockdown and KO cells (Suraneni et al., 2012; Wu et al., 2012). We also overexpressed Lpd in MDA-MB231 breast cancer cells and found that this dramatically increased migration in a scratch wound healing experiment (Fig. 5 E).

Because the Scar/WAVE complex regulates lamellipodia formation and cell migration through activation of the Arp2/3 complex (Machesky and Insall, 1998; Suetsugu et al., 2003; Yan et al., 2003), we hypothesized that Lpd may function upstream of the Scar/WAVE complex to control cell migration. To explore this, we stably knocked down Nap1, which leads to proteasomal degradation of the other members of the Scar/WAVE complex (Kunda et al., 2003). Overexpressing GFP-Lpd resulted in increased wound closure in nontargeting shRNA control but not in Nap1 knockdown cell lines (Fig. 5 E), which suggests that Lpd function in cell migration is mediated by the Scar/WAVE complex.

To further assess whether the direct interaction between Lpd and the Scar/WAVE complex is required for Lpd's role in cell migration, we overexpressed the Lpd mutant in all three Abi binding sites (GFP-Lpd^{AbiMut}), which significantly reduced wound closure compared with GFP expression in MDA-MB231 cells, whereas overexpression of GFP-Lpd increased cell migration (Fig. 5 F).

To explore Ena/VASP's contribution to Lpd's role in cell migration, we overexpressed an Lpd mutant in all seven Ena/VASP binding sites (GFP-Lpd^{EVMut}) and a GFP-Lpd mutant harboring mutations in both Ena/VASP and Abi binding sites (GFP-Lpd$^{EV+AbiMut}$). We observed that the GFP-Lpd^{EVMut} increased cell migration into the scratch wound to a similar extent

Published November 18, 2013

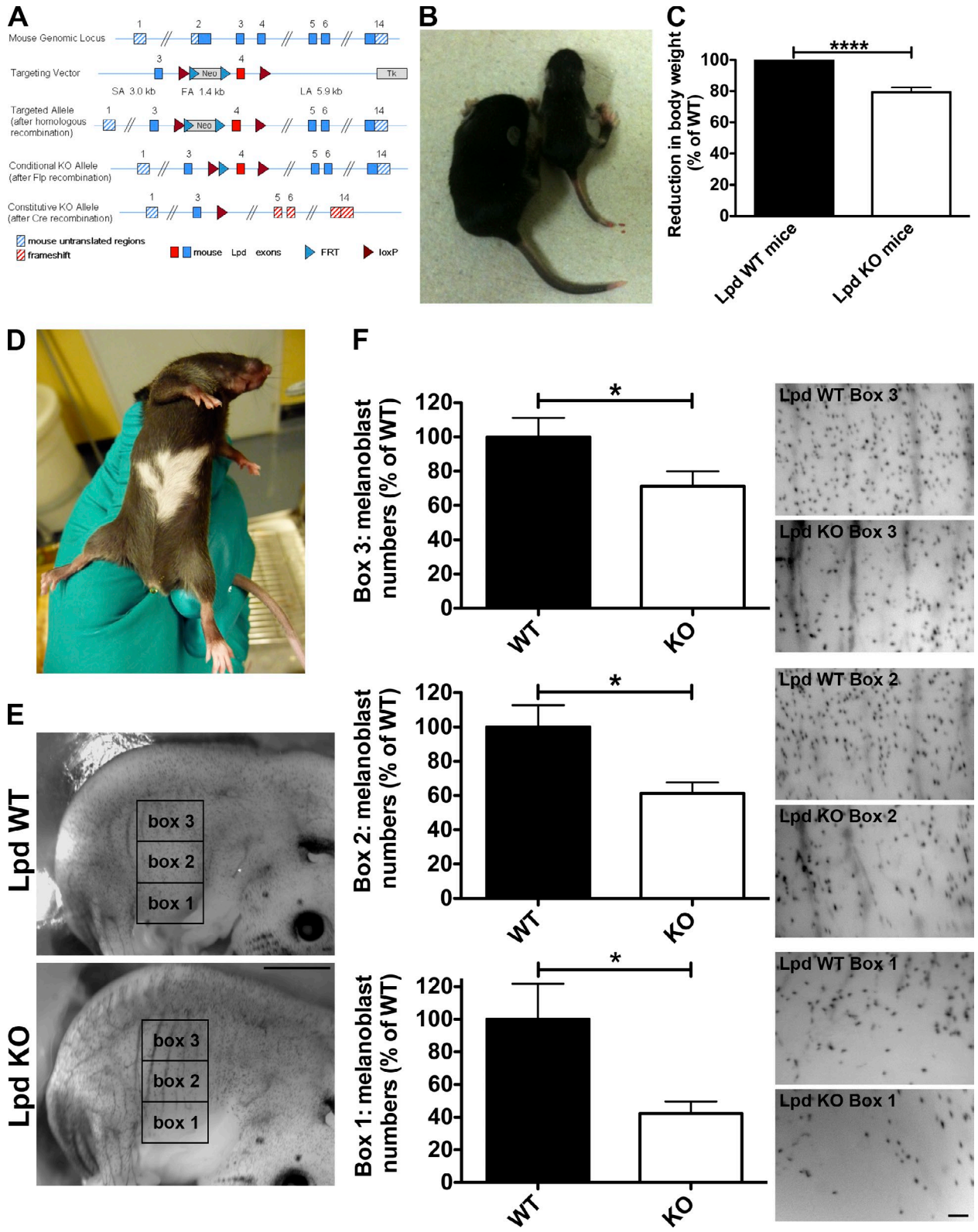

Figure 6. **Lpd functions to regulate melanoblast migration.** (A) Conditional Lpd KO mice were generated by flanking exon 4 with loxP sites. Cre-mediated recombination of the loxP sites results in the removal of exon 4, creating a frame shift between exon 3 and 5 and premature termination. (B and C) Conditional Lpd KO mice crossed with β-actin-Cre mice on a mixed genetic background produced mice with a reduced body size (−20.6 ± 3.0% SEM; ****, $P \leq 0.0001$, unpaired *t* test), which also display missing pigmentation on the ventral side (D). (E and F) To visualize melanoblasts, DCT-LacZ$^{tg/tg}$;β-actin-Cre$^{tg/+}$;Lpd$^{flox/flox}$ whole-mount embryos at E14.5 were stained for β-galactosidase expression in the melanoblasts. (E) Areas within three 1 mm × 1.5 mm boxes positioned at the middle of the trunk between the fore and hind limbs were quantified in WT and KO animals. Bar, 1.5 mm. (F) Lpd KO mice show a significant reduction in the number of melanoblasts in all three boxes. Bar, 150 µm. Melanoblast numbers were reduced by ∼60%, ∼40%, and ∼30% for boxes 1, 2, and 3, respectively (20 KO or WT embryos from three litters; unpaired *t* test; *, $P < 0.05$; error bars indicate SEM). See also Fig. S4.

Published November 18, 2013

as WT Lpd. In contrast, the double mutant GFP-Lpd$^{EV+AbiMut}$ decreased cell migration compared with GFP expression to a similar extent as the Lpd Abi binding mutant (GFP-Lpd^{AbiMut}; Fig. 5 F).

Collectively, this suggests that Lpd's function in cell migration is not mediated by Ena/VASP proteins but is predominantly facilitated by the Scar/WAVE complex.

Lpd KO mice have pigmentation defects

To explore the role of Lpd in cell migration in vivo, we generated conditional Lpd KO mice (Fig. 6 A). We crossed these mice to PGK-Cre (ubiquitous deletion) mice on a pure C57BL/6 genetic background to delete the *Lpd* gene in all cells. The PGK-Cre;Lpd$^{flox/flox}$ KO mice have a reduced body size, show no ingestion of milk, and tend to die shortly after birth. From crosses of PGK-Cre$^{tg/+}$;Lpd$^{flox/+}$ × PGK-Cre$^{+/+}$;Lpd$^{flox/flox}$ we obtained the expected Mendelian ratio directly after birth (postnatal day 0 [P0]), but at P10 (n = 208) only 10.6% of PGK-Cre$^{tg/+}$;Lpd$^{flox/flox}$ compared with the expected 25% survived. Many of these PGK-Cre $^{tg/+}$;Lpd$^{flox/flox}$ mice died before the age of 6 wk, and those that reached sexual maturity were infertile.

We also used β-actin-Cre (ubiquitous deletion) mice on a mixed genetic background to obtain more viable Lpd KO mice. Western blots of tissue lysates from homozygous β-actin-Cre$^{tg/+}$;Lpd$^{flox/flox}$ mice showed loss of Lpd protein expression as expected (Fig. S4 A). Some homozygous β-actin-Cre$^{tg/+}$;Lpd$^{flox/flox}$ mice died within 4 wk after birth (at P14 only 42% and at P28 only 33% of expected mutants survived). The surviving β-actin-Cre$^{tg/+}$;Lpd$^{flox/flox}$ mice had a reduced body weight (reduced by 20%; Fig. 6, B and C) but were viable, and some were fertile, most likely due to modifier genes differently expressed in the mixed genetic background. Interestingly, the few surviving PGK-Cre$^{tg/+}$;Lpd$^{flox/flox}$ mice and the β-actin-Cre$^{tg/+}$;Lpd$^{flox/flox}$ mice displayed missing pigmentation on their ventral side ("white belly spots"; Fig. 6 D), which suggests NC/melanoblast migration defects. We observed that Lpd is expressed in melanoblasts in agreement with a putative role for Lpd in this cell type (Fig. S4 B).

NC cells that are destined to become melanoblasts emigrate at embryonic day 9.5 (E9.5) from the neural tube after undergoing EMT. Dopachrome tautomerase (DCT) is a melanogenic enzyme required for hair and skin pigmentation. DCT is expressed from E10.5 and serves as a marker for the melanoblast lineage migrating dorsolaterally through the dermis around E11.5. At E13.5, these cells migrate from the dermis into the epidermis, where they distribute evenly at E14.5 (Wehrle-Haller et al., 2001; Lin and Fisher, 2007). To visualize melanoblasts, we used a transgenic mouse line (DCT-lacZ mice) that expresses lacZ from the DCT promoter and allows visualization of melanoblast distribution by β-galactosidase staining in whole mount embryos (Mackenzie et al., 1997). We generated DCT-lacZ$^{tg/tg}$;β-actin-Cre$^{tg/+}$;Lpd$^{flox/flox}$ embryos to compare the number and distribution of melanoblasts at E14.5 with that of WT (DCT-lacZ$^{tg/tg}$;β-actin-Cre$^{+/+}$;Lpd$^{flox/flox}$) littermates. We quantified the number of melanoblasts in the trunk region (three 1.5-mm × 1-mm boxes between fore and hind limb; Fig. 6 E) where ventral depigmentation had been observed (Fig. 6, D and E). We observed that Lpd KO embryos had significantly fewer melanoblasts in all three areas (reduced by: box 1, ∼60%; box 2, ∼40%; box 3, ∼30%) along the dorso-ventral path (Fig. 6 F), which suggests that Lpd functions to regulate NC/melanoblast development. However, this analysis does not allow us to distinguish between a problem in NC formation versus migration. To test this, we examined NC development in *Xenopus* embryos, a system in which NC migration can be directly assessed in vivo (Theveneau and Mayor, 2012).

Lpd and the Scar/WAVE complex cooperate to regulate NC migration in vivo

X. laevis embryos were injected with Lpd mRNA, antisense morpholinos (Lpd MO, Abi MO), and dominant-negative Lpd constructs (Lyulcheva et al., 2008) containing only the N terminus, including the RA-PH domain of Lpd (Lpd N1, Lpd N6), and NC migration was analyzed by examining expression of the NC marker gene *Twist* (Hopwood et al., 1989). Overexpression of Lpd did not affect NC migration. Strikingly, knockdown of Lpd or Abi expression and expression of Lpd dominant-negative constructs (Lpd N1, Lpd N6) impaired the migration of the NC streams (Fig. 7, A–D), which indicates that Lpd, Abi, and the Scar/WAVE complex regulate NC migration in vivo.

Coexpression of Lpd or Abi mRNA with the Lpd or Abi MOs rescued NC migration, which suggests that the effect of the Lpd and Abi MO is specific (Fig. 7, E and F). No effect on NC formation was observed under any treatment (Fig. S5), which indicates that Lpd and the Scar/WAVE complex specifically function in NC migration.

To test whether Lpd and Abi act within NC cells or in the surrounding tissue to control NC migration, we performed experiments in which we grafted NC tissue from Lpd or Abi MO–injected embryos into nontreated control hosts. Conversely, we grafted control NC tissue into embryos injected with Lpd or Abi MOs. We observed that Lpd- or Abi-deficient NC grafted into normal hosts exhibited migration defects in 60–80% of embryos, whereas when normal NC was grafted into Lpd or Abi deficient hosts, NC migration was normal (Fig. 7, G–I). This experiment indicates that Lpd and Abi function cell-autonomously to regulate NC migration.

Because Lpd functions in cell migration upstream of the Scar/WAVE complex (Fig. 5, E and F) and interacts with the Scar/WAVE complex via the SH3 domain of Abi (Fig. 2 and Fig. 3, A–D), we hypothesized that the Abi1$^{\Delta SH3}$ construct would block the interaction between Lpd and the Scar/WAVE complex and therefore might have a dominant-negative function. Notably, expression of Abi1$^{\Delta SH3}$ impaired NC migration (Fig. 7, A–D), which suggests that Lpd and the Scar/WAVE complex cooperate to regulate NC migration.

Lpd's function in regulating lamellipodia formation and cell migration is mediated by the Scar/WAVE complex

As previously described for other cell types (Krause et al., 2004), Lpd was localized to the very edge of lamellipodia in *Xenopus* NC cells (Fig. 8 A and Video 3). To further analyze the function of Lpd and the Scar/WAVE complex in lamellipodium

Published November 18, 2013

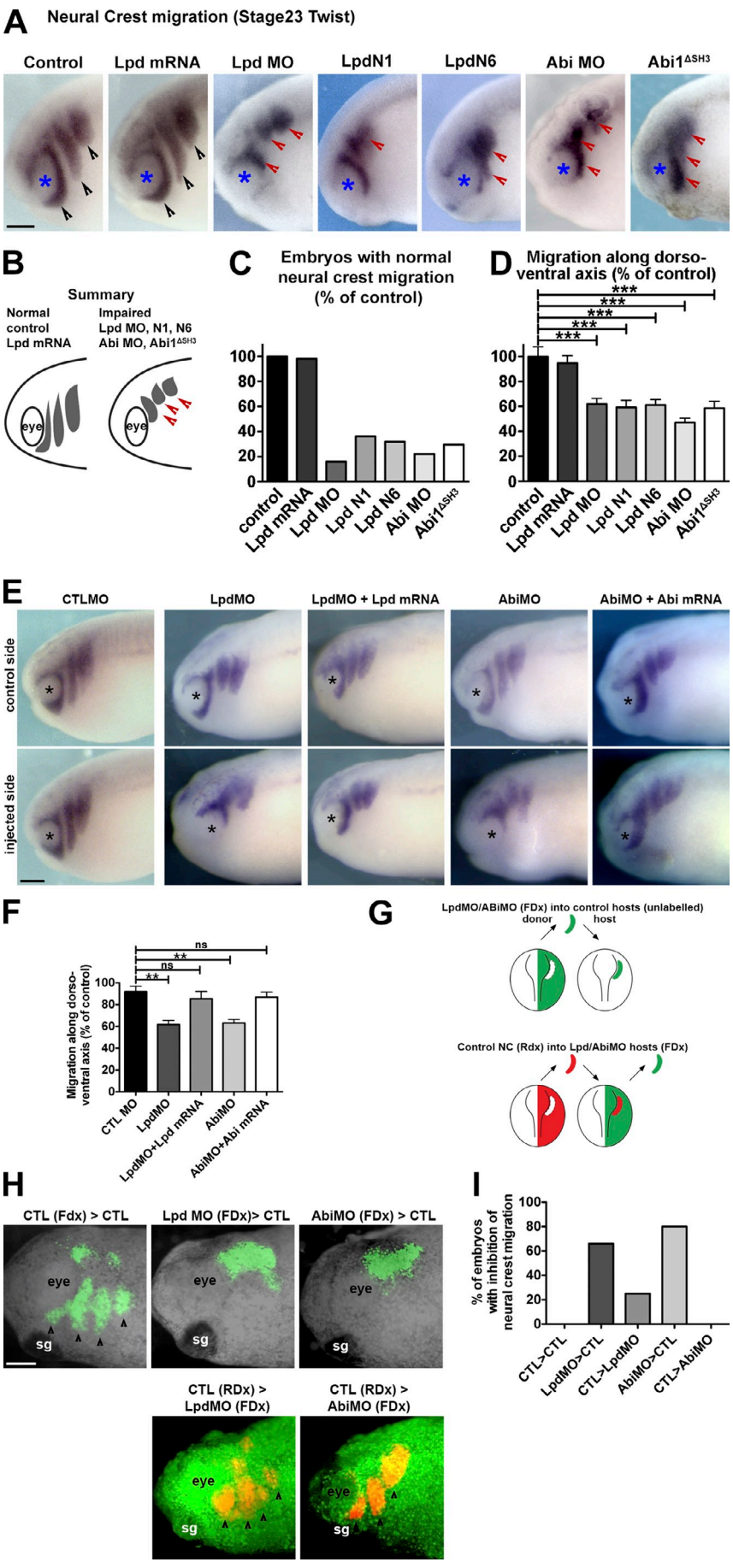

Figure 7. **Lpd regulates NC migration via Abi.** (A) In situ hybridization for *Twist* (Hopwood et al., 1989; migratory NC marker) in control embryos or embryos injected with Lpd mRNA, Lpd, or Abi MOs (Lpd MO or Abi MO) or the dominant-negatives Lpd N1, Lpd N6, and Abi1$^{\Delta SH3}$. Black arrowheads, normally migrating NC streams. Red arrowheads, streams with impaired migration. Blue asterisks, the eye. (B) Summary of phenotypes. Lpd overexpression has no effect on overall NC cell migration. Lpd MO, Abi MO, and the dominant-negatives Lpd N1, Lpd N6, and Abi1$^{\Delta SH3}$ all impair NC cell migration. (C) Percentages of embryos with normal migration along the dorso-ventral axis (n_{ctl} = 26, n_{LpdRNA} = 41, n_{LpdMO} = 37, n_{LpdN1} = 26, n_{LpdN6} = 49, n_{AbiMO} = 16, and $n_{Abi1\Delta SH3}$ = 24). (D) Mean distance of migration along the dorso-ventral axis as a percentage compared with control embryos (n_{ctl} = 12, n_{LpdRNA} = 14, n_{LpdMO} = 12, n_{LpdN1} = 14, n_{LpdN6} = 14, n_{AbiMO} = 12, $n_{Abi1\Delta SH3}$ = 12). One-way ANOVA and Dunnett's test were used. ***, P < 0.001. (E) In situ hybridization for *Twist* in Lpd or Abi (Lpd MO or Abi MO), Lpd mRNA and Lpd MO, or Abi mRNA and Abi MO or control MO injected embryos. (F) Mean distance of migration along the dorso-ventral axis compared with control MO embryos ($n_{ctl\ MO}$ = 13, n_{LpdMO} = 14, n_{LpdMO} = 26, $n_{LpdMO+LpdmRNA}$ = 20, n_{AbiMO} = 19, $n_{AbiMO+AbimRNA}$ = 26). One-way ANOVA and Dunnett's test were used. **, P < 0.01; ns, nonsignificant. (G–I) Lpd and Abi function cell-autonomously in NC migration. (G) Schematic diagram of graft experiment in H. (H) NC from MO-treated embryos or WT embryos was grafted into WT or MO-treated embryos, and NC migration was analyzed. (I) Quantification of NC migration phenotypes from H. Numbers (embryos with inhibition of NC migration/total): $n_{ctl>ctl}$ = 0/4 (0%), $n_{LpdMO>ctl}$ = 4/6 (66%), $n_{ctl>LpdMO}$ = ¼ (25%), $n_{AbiMO>ctl}$ = 4/5 (80%), $n_{ctl>AbiMO}$ = 0/5 (0%). Bars, 150 µm.

Published November 18, 2013

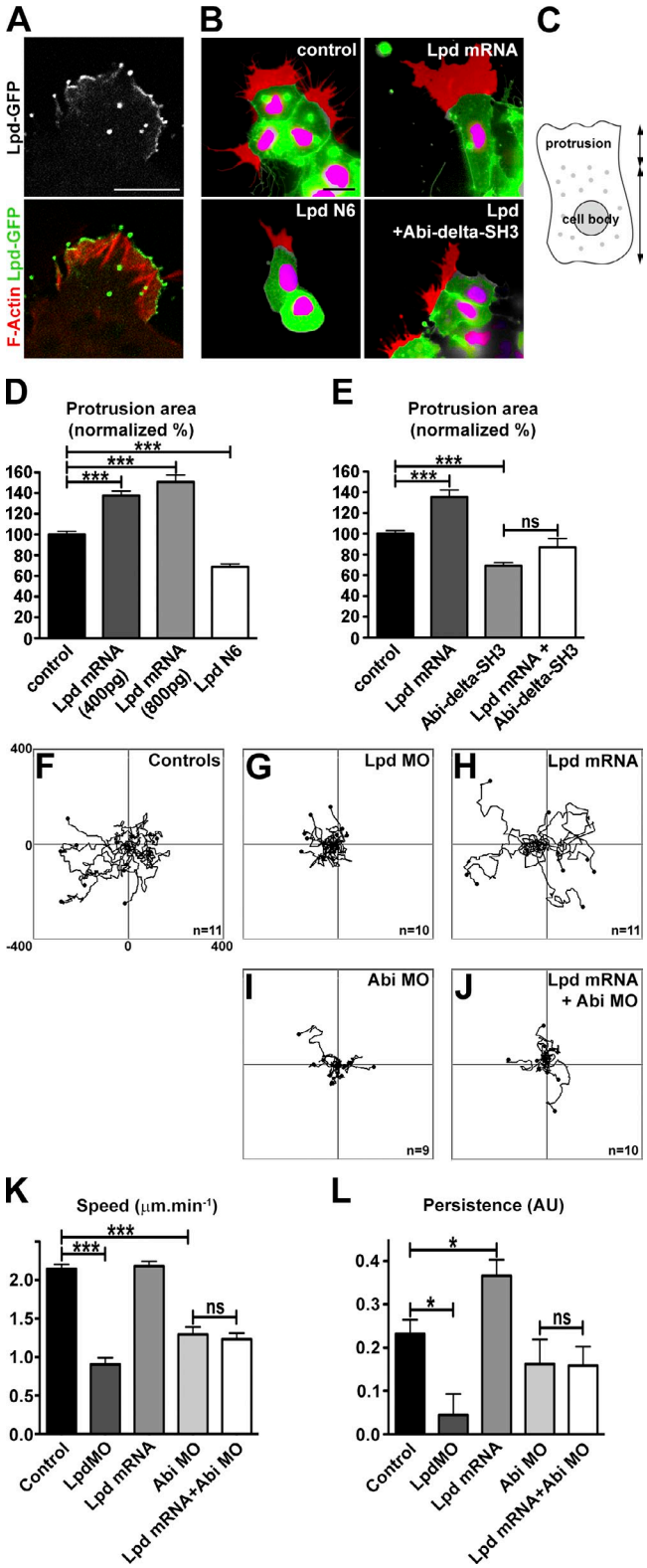

Figure 8. **Lpd regulates lamellipodia protrusion and cell migration via Abi in *Xenopus* NC cells.** (A) Localization of Lpd-GFP in *Xenopus* NC cells cultured on fibronectin. Actin filaments are stained with TRITC-Phalloidin. (B) Cells expressing nuclear mCherry (pseudocolored magenta by thresholding) and membrane GFP (pseudocolored green by thresholding) were used to analyse cell protrusions (pseudocolored red). Cell protrusions were defined as the area of protrusion that extends beyond the cell body. Cell protrusions are shown for control cells and cells injected with Lpd mRNA, Lpd N6 or co-injected with Lpd mRNA and Abi-Δ-SH3. Note that Lpd overexpression leads to enlarged protrusions. This effect is abolished by co-injection with Abi-Δ-SH3.. (C–E) Area of cell protrusions expressed as a proportion of normal protrusions (graph in D: n_{ctl} = 58, $n_{Lpd800pg}$ = 33, $n_{Abi1\Delta SH3}$ = 24, $n_{Lpd+Abi1\Delta SH3}$ = 17 [one-way ANOVA and Dunnett's test; ***, P < 0.001]; graph in E: n_{ctl} = 154, $n_{Lpd400pg}$ = 148, $n_{Lpd800pg}$ = 157, n_{LpdN6} = 121 [one-way ANOVA and Tukey's test; ***, P < 0.001]). (F–J) Tracks of NC cells cultured on fibronectin (a subset of the analyzed tracks are shown). (K and L) Velocity and persistence from tracks performed on all conditions (n_{ctl} = 543, n_{LpdMO} = 240, $n_{LpdmRNA}$ = 297, n_{AbiMO} = 180, $n_{Lpd+AbiMO}$ = 290). One-way ANOVA and Dunnett's test were used. *, P < 0.05; ***, P < 0.001. Error bars indicate SEM. See also Fig. S5 and Videos 3–6.

protrusion and cell migration, the behavior of *Xenopus* NC explants was analyzed in vitro using time-lapse video microscopy. Overexpression of Lpd or Lpd dominant-negative (Lpd N6) led to a significant increase or decrease in the size of the lamellipodia at the edge of explants, respectively (Fig. 8, B–E; and Video 4). Importantly, the increase in lamellipodia size induced by Lpd could be reversed by coexpression of dominant-negative Abi (Abi1$^{\Delta SH3}$; Fig. 8, B and E; and Video 4), which indicates that Lpd's function to regulate lamellipodia size is mediated by the Scar/WAVE complex.

Because Lpd and the Scar/WAVE complex regulate NC migration in vivo, we explored their cooperation in more detail using cells from dissociated explants. Lpd overexpression increased persistence, whereas knockdown reduced migration speeds and persistence of NC cells (Fig. 8, F–L; and Video 5). To test whether the Scar/WAVE complex is required for Lpd's function in migration of individual NC cells, we overexpressed Lpd and knocked down Abi with a MO. The increase in persistence upon Lpd overexpression was dependent on the presence of Abi (Fig. 8 L and Video 6), which suggests that in NC cells the Scar/WAVE complex functions downstream of Lpd during cell migration.

Collectively, these data suggest that in both mammalian cells and *Xenopus* NC cells, Lpd's function in regulating cell migration is mediated by the Scar/WAVE complex.

Lpd and the Scar/WAVE complex regulate epithelial collective cell migration in vivo

So far we have shown that Lpd controls cell migration in mesenchymal cells, such as fibroblasts, melanoblasts, and NC cells; however, epithelial cells are also migratory during collective cell migration. To examine whether Lpd's function to regulate the Scar/WAVE complex is a general feature of different modes of cell migration and to test whether it is evolutionarily conserved in invertebrates, we turned to a model for collective cell migration in the *Drosophila* ovary. In this system, a group of epithelial-derived somatic follicle cells are recruited into a migratory cluster of border cells that delaminates from the epithelium and migrates between neighboring nurse cells to the oocyte. First, we examined whether the fly orthologue of Lpd, Pico, forms a complex with Scar/WAVE. GST-Pico but not GST pulled down all five proteins of the tagged Scar/WAVE complex expressed in HEK293 cells (Fig. 9 A), indicating that this interaction is evolutionary conserved. To test the involvement of *pico* and *Scar* in border cell migration, we specifically

Published November 18, 2013

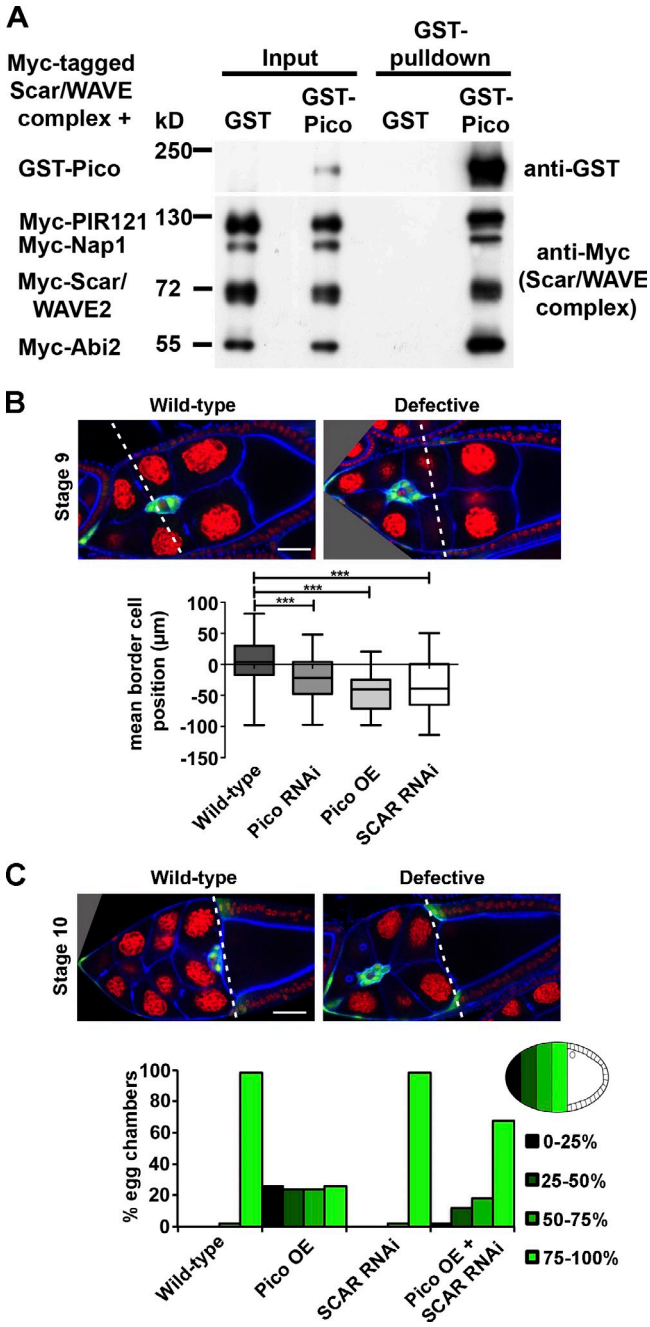

Figure 9. ***pico* regulates *Drosophila* border cell migration via *SCAR*.** (A) GST-Pico, the fly orthologue of Lpd, pulled down all Myc-tagged components of the Scar/WAVE complex. Myc-HSPC300 is not shown. (B) *pico* knockdown or overexpression, or *SCAR* RNAi under the control of *slbo-GAL4* abrogate migration at stage 9. (B, top) Representative images of WT and defective egg chambers. Green, GFP-labeled border cells; red, DNA; blue, F-actin. The box and whiskers plot shows mean border cell position: distance of the cluster relative to the most anterior position of the overlying follicle cells (broken lines). Top and bottom box: 75th and 25th quartile; whiskers indicate minimum and maximum. One-way ANOVA and Dunnett's test were used. ***, $P < 0.001$; $n = 50$. (C) *pico* overexpression abrogates migration at stage 10A, and this is ameliorated by *SCAR* RNAi. Histogram summarizes migration defects in the indicated genotypes. Migration was calculated as a percentage of the distance traveled to the oocyte/nurse cell boundary (broken lines in top panels). For each genotype, $n = 50$ egg chambers.

knocked down their expression in the border cell cluster by RNAi. Both *pico* and *Scar* RNAi resulted in reduced border cell migration at stage 9 (Fig. 9 B). *pico* overexpression also impaired border cell migration at stage 9 and 10 (Fig. 9, B and C), which suggests that Lpd/Pico and the Scar/WAVE complex regulate collective cell migration.

To explore whether *pico* function in this process is mediated by the Scar/WAVE complex, we tested if *pico* and *Scar* genetically interact. The effect of *pico* overexpression on border cell migration was ameliorated by *Scar* RNAi, which suggests that *pico* function is indeed mediated by the Scar/WAVE complex during collective cell migration (Fig. 9 C). To further test this, we quantified the migration speed by live-cell imaging and observed that both *pico* RNAi and *pico* overexpression reduced the rate of border cell cluster movement per frame in the first half of migration (Fig. 10 A). Consistent with our earlier observations, *Scar* RNAi rescued the migration defect induced by *pico* overexpression.

Border cell migration is characterized by polarized cell behavior in the first half of migration, followed by dynamic collective behavior, in which the cluster travels in shuffling and tumbling movements (Bianco et al., 2007). Unlike WT border cells, which normally show little or no tumbling in the first half of migration, we observed a high frequency of premature tumbling in *pico*-overexpressing clusters, which was dependent on *Scar* (Fig. 10 B), similar to what has been observed when overexpressing a dominant-negative PDGF receptor (PVR^{DN}) in border cells (Poukkula et al., 2011). To explore the underlying causes of migration defects further, we quantified the number and direction of actin-based cellular protrusions from the border cell clusters. Overexpression of PVR^{DN} resulted in a reduction in the total number of protrusions and a higher proportion of protrusions at the rear of the cluster when compared with WT, as reported previously (Poukkula et al., 2011). In many respects, the effect of *pico* and *Scar* RNAi on both the number and directionality of protrusions was similar to, but weaker than, PVR^{DN}. *pico* overexpression too showed similar effects to PVR^{DN}, with the notable exception that the absolute number of protrusions did not change, but many more rear facing protrusions appeared (Fig. 10, C and D). Importantly, *Scar* knockdown ameliorated the *pico* overexpression phenotype and restored the WT distribution of protrusions at the back of the cluster (Fig. 10 D), further demonstrating that *pico* function is mediated by the Scar/WAVE complex.

Discussion

Here we reveal that Lpd colocalizes with the Scar/WAVE complex at the very edge of lamellipodia and directly interacts with this complex by binding to the Abi-SH3 domain. Active Rac directly binds Lpd, thereby regulating the interaction between Lpd and the Scar/WAVE complex. We therefore postulate that Lpd acts as a platform to link active Rac and the Scar/WAVE complex at the leading edge of cells to regulate Scar/WAVE-Arp2/3 activity and thereby lamellipodium formation and cell migration.

Published November 18, 2013

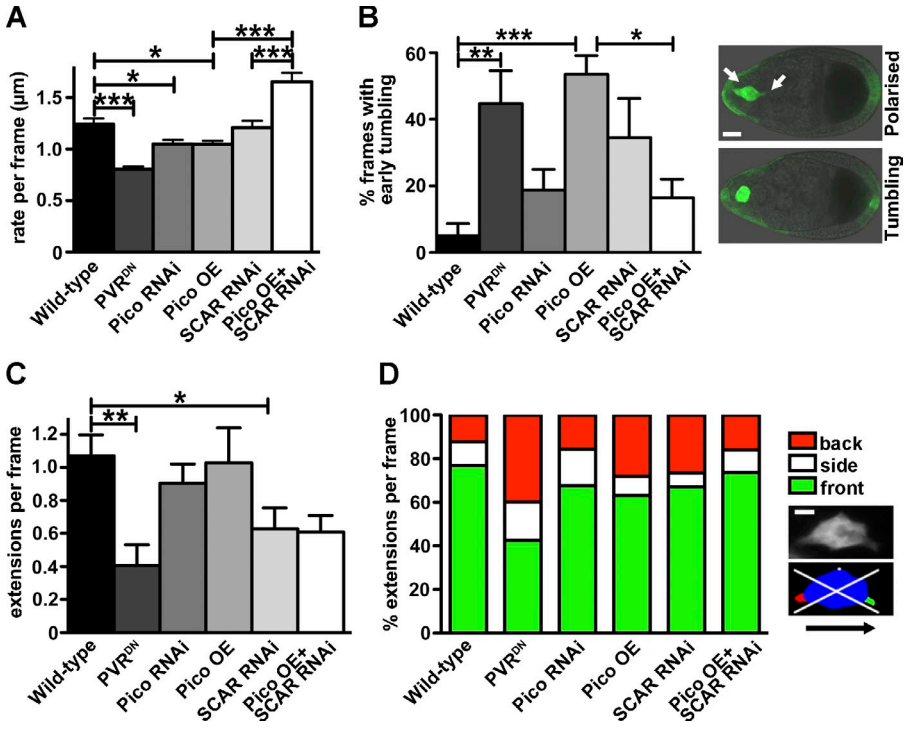

Figure 10. ***pico* regulates *Drosophila* border cell migration via *SCAR*.** (A–D) Analysis of time-lapse images of LifeAct-GFP–labeled border cells, using *c306-GAL4* to drive the indicated genotypes (graphs indicate mean ± SEM; WT, $n = 9$; PVR^{DN}, $n = 9$; pico RNAi, $n = 12$; pico OE, $n = 12$; SCAR RNAi, $n = 8$; SCAR RNAi, pico OE, $n = 7$). (A) Graph summarizing migration rate/frame calculated using a custom macro (Poukkula et al., 2011). (B) Graph showing percentage frames from the first half of migration with tumbling border cell clusters (see Materials and methods). (B, right) GFP-labeled clusters display a polarized or tumbling phenotype. Bar, 15 µm. (A and B) Tests used were one-way ANOVA ($P < 0.0001$) and Tukey's test. *, $P < 0.05$; **, $P < 0.01$; ***, $P < 0.001$. (C) Graph showing number of cellular extensions per frame, irrespective of their direction. One-way ANOVA and Dunnett's test were used. *, $P < 0.05$; **, $P < 0.01$. (D) Graph summarizing percentage extensions/frame at front, back, or sides of the cluster. (D, right) Image of a border cell cluster before and after image segmentation. The body of the cluster is shown in blue, cellular extensions at the front in green, the back in red, and the sides in white. White lines indicate quadrants, representing front, back, and sides for quantification. Bar, 5 µm.

Knockdown of Lpd expression (Krause et al., 2004) or KO of Lpd (Fig. 4) highly impaired lamellipodium formation, phenocopying the effect of Scar/WAVE complex knockdown on lamellipodium formation (Machesky and Insall, 1998; Innocenti et al., 2004; Steffen et al., 2004). Conversely, we observed that overexpression of Lpd increased lamellipodia size in *Xenopus* NC cells, and this was dependent on the interaction with Abi, linking it to the Scar/WAVE complex. Overexpression of Pico, the Lpd fly orthologue, aberrantly increased the number and frequency of cellular protrusions at the rear of border cell clusters in a Scar-dependent manner, which suggests that the regulation of Scar/WAVE by Lpd is evolutionary conserved. Collectively, these data suggest that Lpd functions to generate lamellipodia via the Scar/WAVE complex.

We found that Lpd or Pico knockdown or Lpd KO impaired cell migration in vitro and in vivo in *Drosophila*, *Xenopus*, and mice. Lpd KO or knockdown cells were unable to migrate via lamellipodia but instead migrated very slowly by extending filopodia. The same residual migration mode had been observed for Arp2/3 knockdown cells (Suraneni et al., 2012; Wu et al., 2012). Arp2/3 is activated by the Scar/WAVE complex to regulate cell migration (Insall and Machesky, 2009; Campellone and Welch, 2010). We also observed that both Lpd and Abi knockdown impaired NC migration in vivo. Consistently, we found that Lpd and Abi-Scar/WAVE are in the same pathway regulating cell migration. This is consistent with recent studies suggesting that the Lpd orthologue in *C. elegans*, *mig-10*, genetically interacts with *abi-1* to regulate axon guidance, synaptic vesicle clustering, and excretory canal outgrowth in *C. elegans* (Stavoe et al., 2012; Xu and Quinn, 2012; McShea et al., 2013). Collectively, our results suggest that Lpd functions in cell migration via the Scar/WAVE complex in mammalian cells, *Xenopus* NC cells, and *Drosophila* border cells.

Lpd not only interacts with the Scar/WAVE complex but also directly binds to Ena/VASP proteins (Krause et al., 2004; Michael et al., 2010). Ena/VASP proteins regulate actin filament length by temporarily preventing capping of barbed ends and by recruiting profilin-actin to the growing end of actin filaments (Bear et al., 2002; Krause et al., 2003). In contrast, the Scar/WAVE–Arp2/3 complexes increase branching of actin filaments. Lamellipodia with a highly branched actin network protrude more slowly but are more persistent, whereas lamellipodia with longer, less branched actin filaments protrude faster but are less stable and quickly turn into ruffles (Bear et al., 2002; Krause et al., 2003). We observed that Lpd overexpression increases cell migration in a Scar/WAVE- and not Ena/VASP-dependent manner (Fig. 5 F). This is consistent with a predominant function of Scar/WAVE downstream of Lpd to regulate a highly branched actin network supporting persistent lamellipodia protrusion and cell migration. Other actin-dependent cell protrusions such as axon extension or dorsal ruffles of fibroblasts require Lpd-Ena/VASP–mediated F-actin structures (Michael et al., 2010).

Collective cell migration describes a group of cells that moves together and affect each other (Rørth, 2012), and various types of collective cell migration exists during development and cancer invasion (Friedl and Gilmour, 2009; Friedl et al., 2012). *Xenopus* NC cells migrate as loose streams, whereas *Drosophila* border cells migrate as a cluster of cells with close cell–cell contacts (Rørth, 2012; Theveneau and Mayor, 2012). We found that Rac regulates Lpd and Scar/WAVE interaction and that both are required for *Xenopus* NC migration, which is consistent with our previous work in which Rac activity mediates this type of migration (Carmona-Fontaine et al., 2008; Matthews et al., 2008; Theveneau et al., 2010). Similarly, NC–derived melanoblast migration in the mouse depends on Rac–Scar/WAVE–Arp2/3 (Li et al., 2011), and we found that Lpd functions in this process as well.

Published November 18, 2013

Drosophila border cell clusters migrate through the fly egg chamber in two phases: an early part characterized by large and persistent front extensions, which are regulated predominantly by PVR (the fly PDGF receptor); and a late part characterized by dynamic collective "tumbling" behavior (Bianco et al., 2007; Poukkula et al., 2011). Surprisingly, Pico overexpression resulted in the appearance of a higher proportion of rear facing extensions, a phenotype previously observed with dominant-negative PVR (Prasad and Montell, 2007), causing premature tumbling of the border cell cluster. This suggests that Pico function is normally tightly controlled to stabilize specific extensions and functions also in guidance of collective cell migration. Because Lpd-Scar/WAVE control single cell migration as well as collective cell migration, this suggests that they function as general regulators of cell migration.

Collectively, we have identified a novel pathway in which Lpd functions as an essential, evolutionary conserved regulator of the Scar/WAVE complex during cell migration in vivo.

Materials and methods

Molecular biology, plasmids, and reagents

The following materials were used. GFP-Lpd (Krause et al., 2004). Lpd-N1 (aa 1–592) and Lpd-N6 (aa 242–592) was amplified from human Lpd (AY494951), cloned into KpnI-EcoRI of pENTR3C (Invitrogen), and transferred into pDEST-EGFP (which was generated by subcloning the destination cassette [Invitrogen] into pEGFP-N1 [Takara Bio Inc.]). Pico-L (Lyulcheva et al., 2008) in pDEST27 (Invitrogen). Sra1 (CYFIP1; HsCD00042136), PIR121 (CYFIP2; HsCD00045545), Nap1 (NCKAP1; HsCD00045562), Abi-2 (HsCD00042752), and HSPC300 (C3orf10; HsCD00045008) in pDONR221 (Harvard Institute of Proteomics). pDONR221-WAVE-2 (Deutsches Ressourcenzentrum für Genomforschung). hsAbi1d (BC024254; Geneservice) full-length and Abi1d-Δ-SH3 (aa 1–417) cloned into pENTR11 and transferred to pRK5-Myc-DEST, pV16-gateway (MBP). Abi1d SH3 (aa 410–472) in pGEX-6P1. pCDNA3-2×FLAG-hsScar/WAVE1 was a gift from J. Scott (University of Washington, Seattle, WA). Nap1-shRNA-1 (5′-GCTCACCATCCTCAAC-GAC-3′) and Nap1-shRNA-2 (5′-CCAGATTGCTGCAGCTTTG-3′) in pLL3.7 puro. *Xenopus laevis* Lpd (5′-TCTTCATCCGATAATTGCTCCATCT-3′) and Abi (5′-AACATCTGTAGCTCAGCCATCTTCC-3′) MOs (Gene Tools LLC).

Antibodies

The following antibodies were used: Lpd pab 3917 (Krause et al., 2004), RIAM 4613 (Lafuente et al., 2004), VASP pab 2010 (Bear et al., 2000; a gift from F. Gertler, Massachusetts Institute of Technology, Cambridge, MA), EVL mAb 84H1 (Lanier et al., 1999), Mena mAb A351F7D9 (Lebrand et al., 2004), Hsc70 mAb (Santa Cruz Biotechnology, Inc.), GST pab (GE Healthcare), Myc mAb 9E10, FLAG mAb M2 (Sigma-Aldrich), GFP mAb (Roche), Scar1 (BD), Sra1 mAb 30A4 (Synaptic Systems), Nap1 pab 5151 (peptide HAVYKQSVTSSA; Eurogentec), Abi mAb (Abcam), Arp3 mAb (BD), Tubulin, β-actin mAbs (Sigma-Aldrich), MBP mAb (New England Biolabs, Inc.), and glyceraldehyde 3-phosphate dehydrogenase (GAPDH) mAb (EMD Millipore). Secondary antibodies used were: HRP-goat anti–rabbit, goat anti–mouse, and rabbit anti–goat (Dako).

Cell culture

MEFs isolated from E13 embryos from conditional Lpd KO mice were immortalized using the 3T3 method (Todaro and Green, 1963) and transduced with retroviruses conferring 4-OHT inducible CreERT2 (Oskarsson et al., 2006; a gift from A. Trumpp, Deutsches Krebsforschungszentrum, Heidelberg, Germany). The melanoblast stem cell line melb-a was grown using conditions described in Sviderskaya et al. (1995; provided by E. Sviderskaya, Wellcome Trust Functional Genomics Cell Bank at St. George's, University of London, London, England, UK). B16F1, HEK293FT, NIH/3T3, MDA-MB231, or Lpd WT and KO MEFs were grown in DMEM (high glucose 4,500 mg/liter). CAD cells were grown in DMEM-Hepes/F12-Ham's (1:1), 10% FCS, or 12.5% FCS for MEFs, or 10% calf serum for NIH/3T3, L-Glutamine, and penicillin/streptomycin. Cells were maintained at 37°C in 5% CO_2 and transfected with Lipofectamine 2000 (HEK293FT) or LTX (MDA-MB231; Invitrogen). Primary cortical neurons were prepared from E16 mice as described for E18 rats (Goslin and Banker, 1989). In brief: the cortices of E16 mouse embryos were dissected and incubated for 20 min in 0.25% Trypsin, HBSS-Hepes, washed 3× with 5 ml plating media, triturated 25× with a P1000 tip, and plated on poly-D-lysine–coated dishes in plating media (Neurobasal [Invitrogen], 5% FCS, 2% B27 [Invitrogen], L-glutamine, and penicillin/streptomycin) and maintained without FCS at 37°C in 5% CO_2 and lysed after 36 h.

Scratch, random migration, and cell spreading assays

Confluent control- or tamoxifen-treated Lpd MEFs or MDA-MB-231 cells were scratched with a P200 pipette tip and treated with mitomycin C, and the scratch area was measured at 0 and 24 h with ImageJ. Control- or tamoxifen-treated Lpd MEFs were plated onto fibronectin (10 µg/ml)-coated coverslips for 60 min (spreading) or in 12-well dishes for 12 h and imaged for 24 h every 5 min.

Quantification of cell migration speed and persistence

Cell track coordinates were reformatted into CEL format and imported into Mathematica for analysis using the Chemotaxis Analysis Notebook v1.5β by G. Dunn (King's College London, England, UK). Sample frequency at which speed measurements were taken and used to calculate mean track speed (MTS) was defined as the lowest time interval (dt) at which the persistence of the population of cells was stable. Because different populations and groups have different persistence profiles, it was necessary to select the lowest common dt that was applicable to all groups being compared. This interval was also used to calculate persistence, which is the total sum displacement over the straight-line distance for a fixed time ratio (TR). e.g., TR = 4 means that the straight-line distance from start of dt1 to the end point of dt4 was divided by the sum displacement of four consecutive dt intervals (dt1+ dt2 + dt3 + dt4). Tracks are generally long enough for multiple Sum[dt]/TR persistence measurements. The persistences for each track were therefore averaged to obtain mean track persistence (MTP), which is an accurate estimate for the persistence of a cell throughout the length of movies, and overcomes traditional persistence measurement obstacles of track length, sample frequency, and positional tracking error. MTS and MTP were averaged across each population of cells to obtain mean population speed (MPS) and mean population persistence (MPP) at designated dt and TR. The persistence profile of each population at increasing dt and fixed TR of four was plotted and used to determine the point at which each population's persistence profile plateaued, indicating, therefore, that the population persistence was stable. For MEF migration, the lowest common dt was 30 min. For the *Xenopus* MO migration experiments the lowest dt was 21 min. Persistences were compared at TR = 4 and TR = 2 for MEFs and *Xenopus*, respectively.

Immunofluorescence analysis and imaging

For immunofluorescence analysis, cells were plated on nitric acid–washed coverslips (Hecht Assistant) and fixed with 4% paraformaldehyde-PHEM (60 mM Pipes, 25 mM Hepes, 10 mM EGTA, 2 mM $MgCl_2$, and 0.12 M sucrose). Goat anti–rabbit or anti–mouse Alexa Fluor 488 or 568 (Invitrogen) secondary antibodies were used, and cells were mounted (Prolong Gold; Invitrogen). A microscope (IX 81 [Olympus], with filter wheels [Sutter], an ASI X-Y stage, Cascadell 512B camera [Photometrics], and 4× UPlanFL, 10× UPlanFL, 60× Plan-Apochromat NA 1.45, or 100× UPlan-Apochromat S NA 1.4 objective lenses) was used, and line scans were analyzed with MetaMorph software.

Immunoprecipitation, GST pull-downs, and Western blotting

Cells were harvested in lysis buffer (50 mM Tris HCL, 200 mM NaCl, 1% NP-40, 2 mM $MgCl_2$, 10% glycerol, pH 7.4, 1 mM Na_3VO_4, 10 mM NaF, and protease inhibitors [complete mini without EDTA]; Roche). Lysates were incubated on ice for 30 min and centrifuged at 17,000 *g* at 4°C for 15 min. Protein concentration was then determined (Pierce BCA protein assay kit; Thermo Fisher Scientific). Lysates were precleared with protein A beads (Thermo Fisher Scientific) and incubated with glutathione beads for GST pull-downs or with antibody or control IgG, followed by 1% BSA blocked protein A beads. Beads were washed with lysis buffer, separated on SDS-PAGE gels, transferred onto Immobilon-P membranes (EMD Millipore), blocked in 5% BSA, and probed with the indicated antibodies, followed by HRP secondary antibodies (Dako). Blots were developed with the ECL kit (Thermo Fischer Scientific) and x-ray film, or the Immun-Star WesternC ECL kit (Bio-Rad Laboratories) using the Bio-Rad Imager and ImageLab software.

Far-Western blot and peptide array

GST and MBP fusion proteins were purified from BL21 *E. coli* using glutathione (GE Healthcare) or amylose (New England Biolabs, Inc.) beads. Western blots of purified GST-Lpd fragments or custom-made peptide

Published November 18, 2013

arrays (Cancer Research UK services) were overlayed as described previously (Niebuhr et al., 1997) with purified MBP-Abi full-length or MBP-Abi-Δ-SH3, and MBP was detected with anti-MBP antibodies (New England Biolabs, Inc.).

Generation of Lpd conditional KO mice

All experiments were performed according to UK Home Office regulations. Lpd conditional KO mice were generated using C57BL6 ES cells (Taconic-Artemis GmbH) by flanking exon 4 with loxP sites (Fig. 5 A), and the selection cassette was removed by crossing to Flp mice and crossed to PGK-Cre (Lallemand et al., 1998; general deleter) C57BL6 (provided by A. Behrens, London Research Institute, Cancer Research UK, London, England, UK), β-actin-Cre (Lewandoski and Martin, 1997), or DCT-lacZ$^{tg/tg}$ (Mackenzie et al., 1997; provided by I. Jackson, Medical Research Council, Edinburgh, Scotland, UK) mice on a mixed genetic background.

Whole-mount β-galactosidase staining of embryos

DCT-lacZ$^{tg/tg}$;β-actin-Cre$^{tg/+}$;Lpd$^{flox/flox}$ and DCT-lacZ$^{tg/tg}$;β-actin-Cre$^{+/+}$;Lpd$^{flox/flox}$ embryos were used at E14, with time of gestation calculated using the day of detection of a vaginal plug as E1. Embryos were dissected in ice-cold PBS and fixed in 0.25% glutaraldehyde at 4°C for 40 min on a rolling platform. Fixed embryos were washed in ice-cold PBS for 15 min at 4°C on a rolling platform before incubating in permeabilization buffer (2 mM $MgCl_2$, 0.02% NP-40, and 0.01% sodium deoxycholate in PBS, without Ca^{2+} or Mg^{2+}) for 30 min and two further washes for 15 min at room temperature before staining with β-galactosidase substrate solution (2 mM $MgCl_2$, 0.02% NP-40, 0.01% sodium deoxycholate, 5 mM K_3Fe, 5 mM K_4Fe, and 0.4 mg/ml 5-bromo-4-chloro-3-indolyl β-D-galactosidase) for 24–48 h in darkness, at 4°C on a rolling platform. Embryos not fully stained after this time were transferred to 37°C or left at 4°C in stain solution until staining was completed. Embryos were post-fixed in 4% PFA for 2 h at 4°C and transferred into PBS.

Melanoblast quantification

Both left and right side trunk regions were imaged using a microscope (SMZ1500; Nikon) and camera (Exi Aqua; QImaging). Melanoblast numbers from whole-mount embryos were quantified using MetaMorph Integrated Morphometric Analysis software within three 1 mm × 1.5 mm boxes positioned at the middle of the trunk between the fore and hind limbs. The three boxes were aligned next to each other with the most distal box (from the somites) placed closest to the umbilical cord. Melanoblast numbers were quantified from the boxes by running an automated object count from the MetaMorph Integrated Morphometric Analysis software using automated thresholding of the images. Melanoblasts were identified as objects by screening for objects that are within 10–88 pixels to filter nonspecific staining of veins and other small artifacts.

Xenopus methods

NC culture. Vitelline membranes were peeled off from embryos at stage 15 using tweezers, and the embryos were left to recover. Around stage 18, the superficial pigmented layer was removed and NC cells were taken out using a hair mounted on a glass pipette. The NC explants were then cut is small pieces and transferred into a fibronectin-coated dish and cultured in modified Danilchick's medium at room temperature.

In situ hybridization. Embryos were fixed in MEMFA for 1 h at room temperature and washed several times in methanol. Embryos were then rehydrated by a series of methanol solutions of decreasing concentration, washed in PBS plus 0.1% Tween 20, and bleached in 5% H_2O_2 solution for a few minutes. A brief post-fixation in 3.7% in formaldehyde was performed, then embryos were washed in PBS and passed into a formamide-based hybridization buffer. Embryos were incubated overnight at 67°C in hybridization buffer containing a digoxigenin-labeled antisense probe (1 µg/ml). Probes are washed using formamide-based solutions, and PBS with 0.1% Tween 20. Embryos were passed into a blocking solution (TBS, 10% serum) and incubated overnight with an alkaline-phosphatase–coupled anti-digoxigenin antibody (1/3,000). Antibody was washed in TBS serum for one day and one night. Staining is performed in alkaline-phosphatase buffer containing NBT and BCIP (3 µl/ml). The mRNA probes used were Slug (Mayor et al., 1995) and Twist (Hopwood et al., 1989).

Time-lapse analysis. For cell tracking, NC cells were dissociated in low-calcium/magnesium Danilchik's medium and were cultured as single cells on fibronectin-coated glass coverslip monitored using a 10× objective lens on an inverted microscope (Axiovert; Carl Zeiss) equipped with a camera (Hamamatsu Photonics). Pictures were acquired every 3 min. Cell tracking was performed using ImageJ Manual Tracking plug-in and Imaris spot tracker software.

Cell protrusion analysis. NC cells were plated on plastic Petri dishes and monitored using a 63× water-immersion lens on an upright microscope (Leica). Protrusions were defined as the region devoid of vitelline platelets.

Drosophila methods

Analysis of fixed *Drosophila* egg chambers. Ovaries of 3-d-old females fed on fresh yeast were dissected in PBS and fixed with 4% paraformaldehyde, and stained with Alexa Fluor 633 Phalloidin (Invitrogen). At stage 9, the distance between the center of the border cell cluster and the anterior columnar follicle cells ("border cell position") was measured in ImageJ (http://rsb.info.nih.gov/ij/). For stage 10 egg chambers, the percentage of the total migration was calculated using the distance from the anterior edge of the egg chamber to the center of the cluster as a percentage of the total migration distance (to the anterior columnar follicle cells). Transgenic lines for RNAi knockdown of *pico* and *SCAR* were as described previously (Jonchere and Bennett, 2013). UAS-SCAR RNAi (VDRC 21908) was provided by Vienna Drosophila RNAi Center. Genotypes of fixed samples were as follows:

slbo-GAL4, UAS-GFP, his2A-RFP/+.

slbo-GAL4, UAS-GFP, his2A-RFP/ UAS-pico RNAi (line 9); UAS-pico RNAi (line 4)/+.

slbo-GAL4, UAS-GFP, his2A-RFP/+; UAS-pico/+.

slbo-GAL4, UAS-GFP, his2A-RFP/UAS-SCAR RNAi (VDRC 21908).

slbo-GAL4, UAS-GFP, his2A-RFP/UAS-SCAR RNAi (VDRC 21908); UAS-pico/+.

Live imaging of *Drosophila* egg chambers. Egg chambers from fattened ovaries (see "*Drosophila methods*") were dissected and cultured at 25°C in imaging media (Schneider's medium, 15% FBS, 1 µg/ml insulin, and 1 µg/ml streptomycin and penicillin) as described by Prasad et al. (2007), with minor modifications. In brief, ovaries were removed from the abdomen of fattened flies and separated into individual fresh droplets of media before dissection of single ovarioles. Egg chambers were placed between two coverslips in the center of a gas-permeable Lumox dish (Sigma-Aldrich). A third coverslip was placed on top to prevent movement while imaging and surrounded by halocarbon oil 27 (Sigma-Aldrich). Confocal stacks were taken at multiple positions using a confocal microscope (LSM 710; Carl Zeiss) equipped with a 488-nm argon ion laser, fitted to an inverted microscope with a 20× 0.75 NA Fluor objective. 2.5-µm-thick z sections (~10–15 images/stack) were taken at each position at 2-min intervals. If necessary, imaging was paused briefly during the time lapse to adjust the focus. The time lapses were cropped at 50% (early stage) for analysis. Maximum intensity projections were generated, and subsequent analysis was performed using a custom macro for ImageJ to analyze border cell migration behavior and protrusion dynamics, as described in Poukkula et al. (2011; provided by P. Rorth [National University of Singapore, Singapore] for custom macros). In brief, time-lapse movies were split into the relevant stages of migration, and processed into binary images after individual thresholding of each movie. Images of border cell clusters were segmented into cluster cell body and cellular protrusions. Protrusions were then categorized by position with respect to the leading cell: front, 315–45°; back, 135–225°; side, 45–135° or 225–315°. In addition to logging the protrusion behavior, the macro automatically tracked the movement of the cluster in xy, enabling information such as migration speed and directed movement to be calculated. Rate per frame was calculated based on the mean distance the cluster center had moved from one frame to the next. Early tumbling was calculated as the mean percentage of frames per time lapse movie that showed rounded clusters, exhibiting changes in the position of individual cells within the cluster for two or more consecutive frames in the first half of migration. Genotypes of time-lapse images were as follows (some of the fly strains were provided by B. Stramer [King's College London, London, UK], Denise Montell [Johns Hopkins University, Baltimore, MA], Vienna Drosophila RNAi Center, and Bloomington Drosophila Stock Center):

c306-GAL4/+; UAS-LifeAct-GFP/+.

c306-GAL4/+; UAS-LifeAct-GFP/UAS-pico RNAi (line 9); UAS-pico RNAi (line 4)/+.

c306-GAL4/+; UAS-LifeAct-GFP/+; UAS-pico/+.

c306-GAL4/+; UAS-LifeAct-GFP/UAS-SCAR RNAi (VDRC 21908).

c306-GAL4/+; UAS-LifeAct-GFP/+; UAS-Pvr^{DN}/+.

c306-GAL4/+; UAS-LifeAct-GFP/UAS-SCAR RNAi (VDRC 21908); UAS-pico/+.

Statistical analyses

Statistical analyses were performed using GraphPad Prism software (see figure legends).

Published November 18, 2013

Online supplemental material

Fig. S1 shows the colocalization of Lpd with Scar/WAVE1, Abi1, and Sra1 at the leading edge of the CAD neuronal cell line. Fig. S2 shows Western blots that indicate that Lpd can be in complex with both Abi1 and VASP, that the interaction between Lpd and the Scar/WAVE complex is positively regulated by active Rac, and that protein levels of RIAM, Mena, EVL, and VASP are not altered in Lpd KO MEFs. Fig. S3 shows that knocking down Lpd expression reduces cell migration in scratch wound healing experiments in Rat2 fibroblasts. Fig. S4 demonstrates the absence of Lpd expression in Lpd KO mice and the presence of Lpd expression in mouse melanoblasts in Western blots. Fig. S5 shows that overexpression or knockdown of Lpd has no effect on NC induction in *Xenopus*. Videos 1 and 2 show one of the Lpd KO MEF (1) and one of the Rat2 fibroblasts scratch wound healing assays (2) used for quantification in Fig. 5 (C and D) and Fig. S3. Video 3 demonstrates that GFP-Lpd localizes to the leading edge of *Xenopus* NC cells. Video 4 shows that Lpd overexpression increases lamellipodia size. Online supplemental material is available at http://www.jcb.org/cgi/content/full/jcb.201304051/DC1.

We thank Pernille Rorth for custom macros; Brian Stramer, Denise Montell, Vienna Drosophila RNAi Center, and Bloomington Drosophila Stock Center for *Drosophila* strains; Frank Gertler, John Scott, and Andreas Trumpp for sharing plasmids and antibodies; and Ian Jackson and Axel Behrens for sharing mice. We thank Elena Sviderskaya for the melb-a melanoblast stem cell line. We also thank Ang Li (Beatson Institute, Glasgow, Scotland, UK) for help with the β-galactosidase protocol.

L. Dodgson was supported by a Medical Research Council Capacity Building studentship. D. Soong is supported by a British Heart Foundation grant (RE/08/003). M. Kotini is supported by a PhD scholarship from the Latsis Public Benefit Foundation. E. Theveneau is supported by a Wellcome Trust Value in People award. M. Michael was supported by a Medical Research Council studentship. C. Navarro was supported by a European Molecular Biology Organization long-term fellowship. D. Bennett was supported by grants from Cancer Research UK (C20691/A11834; C20691/A6678), North West Cancer Research (CR847), and the Wellcome Trust (084659/Z/08/Z). R. Mayor is supported by grants from Medical Research Council UK (MR/J000655/1), Biotechnology and the Biological Sciences Research Council, and the Wellcome Trust. M. Krause is supported by grants from the Biotechnology and Biological Sciences Research Council (BB/G00319X/1; BB/F011431/1; BB/J000590/1) and the Wellcome Trust (077429/Z/05/Z; 082907/Z/07/Z).

Author contributions: A.-L. Law, C. Bodo, C. Navarro, and M. Krause performed the biochemistry; A. Vehlow, A.-L. Law, U. Perera, and C. Navarro performed the cell biology; and A.-L. Law, C. Bodo, and M. Krause performed the mouse experiments. D. Soong and A.-L. Law quantified cell migration and spreading. G.A. Dunn conceived and wrote the Mathematica notebook for analysis of cell migration. L. Dodgson and E. Taylor performed experiments on fixed *Drosophila* samples; L. Dodgson performed all *Drosophila* live imaging experiments and analyzed the data. D. Bennett conceived, designed, and analyzed the *Drosophila* data. M. Kotini and E. Theveneau performed all the *Xenopus* experiments; R. Mayor designed and analyzed the *Xenopus* data. M. Krause conceived, designed, and analyzed the mammalian experiments and wrote the manuscript. All authors contributed to the writing of the manuscript.

Submitted: 8 April 2013
Accepted: 21 October 2013

References

Bear, J.E., J.J. Loureiro, I. Libova, R. Fässler, J. Wehland, and F.B. Gertler. 2000. Negative regulation of fibroblast motility by Ena/VASP proteins. *Cell*. 101:717–728. http://dx.doi.org/10.1016/S0092-8674(00)80884-3

Bear, J.E., M. Krause, and F.B. Gertler. 2001. Regulating cellular actin assembly. *Curr. Opin. Cell Biol.* 13:158–166. http://dx.doi.org/10.1016/S0955-0674(00)00193-9

Bear, J.E., T.M. Svitkina, M. Krause, D.A. Schafer, J.J. Loureiro, G.A. Strasser, I.V. Maly, O.Y. Chaga, J.A. Cooper, G.G. Borisy, and F.B. Gertler. 2002. Antagonism between Ena/VASP proteins and actin filament capping regulates fibroblast motility. *Cell*. 109:509–521. http://dx.doi.org/10.1016/S0092-8674(02)00731-6

Bianco, A., M. Poukkula, A. Cliffe, J. Mathieu, C.M. Luque, T.A. Fulga, and P. Rørth. 2007. Two distinct modes of guidance signalling during collective migration of border cells. *Nature*. 448:362–365. http://dx.doi.org/10.1038/nature05965

Campellone, K.G., and M.D. Welch. 2010. A nucleator arms race: cellular control of actin assembly. *Nat. Rev. Mol. Cell Biol.* 11:237–251. http://dx.doi.org/10.1038/nrm2867

Carmona-Fontaine, C., H.K. Matthews, S. Kuriyama, M. Moreno, G.A. Dunn, M. Parsons, C.D. Stern, and R. Mayor. 2008. Contact inhibition of locomotion in vivo controls neural crest directional migration. *Nature*. 456:957–961. http://dx.doi.org/10.1038/nature07441

Friedl, P., and D. Gilmour. 2009. Collective cell migration in morphogenesis, regeneration and cancer. *Nat. Rev. Mol. Cell Biol.* 10:445–457. http://dx.doi.org/10.1038/nrm2720

Friedl, P., J. Locker, E. Sahai, and J.E. Segall. 2012. Classifying collective cancer cell invasion. *Nat. Cell Biol.* 14:777–783. http://dx.doi.org/10.1038/ncb2548

Goslin, K., and G. Banker. 1989. Experimental observations on the development of polarity by hippocampal neurons in culture. *J. Cell Biol.* 108:1507–1516. http://dx.doi.org/10.1083/jcb.108.4.1507

Hahne, P., A. Sechi, S. Benesch, and J.V. Small. 2001. Scar/WAVE is localised at the tips of protruding lamellipodia in living cells. *FEBS Lett.* 492:215–220. http://dx.doi.org/10.1016/S0014-5793(01)02239-6

Hanahan, D., and R.A. Weinberg. 2011. Hallmarks of cancer: the next generation. *Cell*. 144:646–674. http://dx.doi.org/10.1016/j.cell.2011.02.013

Hopwood, N.D., A. Pluck, and J.B. Gurdon. 1989. A *Xenopus* mRNA related to *Drosophila* twist is expressed in response to induction in the mesoderm and the neural crest. *Cell*. 59:893–903. http://dx.doi.org/10.1016/0092-8674(89)90612-0

Innocenti, M., A. Zucconi, A. Disanza, E. Frittoli, L.B. Areces, A. Steffen, T.E. Stradal, P.P. Di Fiore, M.F. Carlier, and G. Scita. 2004. Abi1 is essential for the formation and activation of a WAVE2 signalling complex. *Nat. Cell Biol.* 6:319–327. http://dx.doi.org/10.1038/ncb1105

Insall, R.H., and L.M. Machesky. 2009. Actin dynamics at the leading edge: from simple machinery to complex networks. *Dev. Cell*. 17:310–322. http://dx.doi.org/10.1016/j.devcel.2009.08.012

Jonchere, V., and D. Bennett. 2013. Validating RNAi phenotypes in *Drosophila* using a synthetic RNAi-resistant transgene. *PLoS ONE*. 8:e70489. http://dx.doi.org/10.1371/journal.pone.0070489

Krause, M., E.W. Dent, J.E. Bear, J.J. Loureiro, and F.B. Gertler. 2003. Ena/VASP proteins: regulators of the actin cytoskeleton and cell migration. *Annu. Rev. Cell Dev. Biol.* 19:541–564. http://dx.doi.org/10.1146/annurev.cellbio.19.050103.103356

Krause, M., J.D. Leslie, M. Stewart, E.M. Lafuente, F. Valderrama, R. Jagannathan, G.A. Strasser, D.A. Rubinson, H. Liu, M. Way, et al. 2004. Lamellipodin, an Ena/VASP ligand, is implicated in the regulation of lamellipodial dynamics. *Dev. Cell*. 7:571–583. http://dx.doi.org/10.1016/j.devcel.2004.07.024

Kunda, P., G. Craig, V. Dominguez, and B. Baum. 2003. Abi, Sra1, and Kette control the stability and localization of SCAR/WAVE to regulate the formation of actin-based protrusions. *Curr. Biol.* 13:1867–1875. http://dx.doi.org/10.1016/j.cub.2003.10.005

Lafuente, E.M., A.A. van Puijenbroek, M. Krause, C.V. Carman, G.J. Freeman, A. Berezovskaya, E. Constantine, T.A. Springer, F.B. Gertler, and V.A. Boussiotis. 2004. RIAM, an Ena/VASP and Profilin ligand, interacts with Rap1-GTP and mediates Rap1-induced adhesion. *Dev. Cell*. 7:585–595. http://dx.doi.org/10.1016/j.devcel.2004.07.021

Lallemand, Y., V. Luria, R. Haffner-Krausz, and P. Lonai. 1998. Maternally expressed PGK-Cre transgene as a tool for early and uniform activation of the Cre site-specific recombinase. *Transgenic Res.* 7:105–112. http://dx.doi.org/10.1023/A:1008868325009

Lanier, L.M., M.A. Gates, W. Witke, A.S. Menzies, A.M. Wehman, J.D. Macklis, D. Kwiatkowski, P. Soriano, and F.B. Gertler. 1999. Mena is required for neurulation and commissure formation. *Neuron*. 22:313–325. http://dx.doi.org/10.1016/S0896-6273(00)81092-2

Lebrand, C., E.W. Dent, G.A. Strasser, L.M. Lanier, M. Krause, T.M. Svitkina, G.G. Borisy, and F.B. Gertler. 2004. Critical role of Ena/VASP proteins for filopodia formation in neurons and in function downstream of netrin-1. *Neuron*. 42:37–49. http://dx.doi.org/10.1016/S0896-6273(04)00108-4

Lewandoski, M., and G.R. Martin. 1997. Cre-mediated chromosome loss in mice. *Nat. Genet.* 17:223–225. http://dx.doi.org/10.1038/ng1097-223

Li, A., Y. Ma, X. Yu, R.L. Mort, C.R. Lindsay, D. Stevenson, D. Strathdee, R.H. Insall, J. Chernoff, S.B. Snapper, et al. 2011. Rac1 drives melanoblast organization during mouse development by orchestrating pseudopod- driven motility and cell-cycle progression. *Dev. Cell*. 21:722–734. http://dx.doi.org/10.1016/j.devcel.2011.07.008

Lin, J.Y., and D.E. Fisher. 2007. Melanocyte biology and skin pigmentation. *Nature*. 445:843–850. http://dx.doi.org/10.1038/nature05660

Lyulcheva, E., E. Taylor, M. Michael, A. Vehlow, S. Tan, A. Fletcher, M. Krause, and D. Bennett. 2008. *Drosophila* pico and its mammalian ortholog lamellipodin activate serum response factor and promote cell proliferation. *Dev. Cell*. 15:680–690. http://dx.doi.org/10.1016/j.devcel.2008.09.020

Machesky, L.M., and R.H. Insall. 1998. Scar1 and the related Wiskott-Aldrich syndrome protein, WASP, regulate the actin cytoskeleton through the Arp2/3 complex. *Curr. Biol.* 8:1347–1356. http://dx.doi.org/10.1016/S0960-9822(98)00015-3

Mackenzie, M.A., S.A. Jordan, P.S. Budd, and I.J. Jackson. 1997. Activation of the receptor tyrosine kinase kit is required for the proliferation of melanoblasts in the mouse embryo. *Dev. Biol.* 192:99–107. http://dx.doi.org/10.1006/dbio.1997.8738

Matthews, H.K., L. Marchant, C. Carmona-Fontaine, S. Kuriyama, J. Larraín, M.R. Holt, M. Parsons, and R. Mayor. 2008. Directional migration of neural crest cells in vivo is regulated by Syndecan-4/Rac1 and non-canonical Wnt signaling/RhoA. *Development*. 135:1771–1780. http://dx.doi.org/10.1242/dev.017350

Mayor, R., R. Morgan, and M.G. Sargent. 1995. Induction of the prospective neural crest of *Xenopus*. *Development*. 121:767–777.

McShea, M.A., K.L. Schmidt, M.L. Dubuke, C.E. Baldiga, M.E. Sullender, A.L. Reis, S. Zhang, S.M. O'Toole, M.C. Jeffers, R.M. Warden, et al. 2013. Abelson interactor-1 (ABI-1) interacts with MRL adaptor protein MIG-10 and is required in guided cell migrations and process outgrowth in *C. elegans*. *Dev. Biol.* 373:1–13. http://dx.doi.org/10.1016/j.ydbio.2012.09.017

Michael, M., A. Vehlow, C. Navarro, and M. Krause. 2010. c-Abl, Lamellipodin, and Ena/VASP proteins cooperate in dorsal ruffling of fibroblasts and axonal morphogenesis. *Curr. Biol.* 20:783–791. http://dx.doi.org/10.1016/j.cub.2010.03.048

Miki, H., S. Suetsugu, and T. Takenawa. 1998. WAVE, a novel WASP-family protein involved in actin reorganization induced by Rac. *EMBO J.* 17:6932–6941. http://dx.doi.org/10.1093/emboj/17.23.6932

Niebuhr, K., F. Ebel, R. Frank, M. Reinhard, E. Domann, U.D. Carl, U. Walter, F.B. Gertler, J. Wehland, and T. Chakraborty. 1997. A novel proline-rich motif present in ActA of *Listeria monocytogenes* and cytoskeletal proteins is the ligand for the EVH1 domain, a protein module present in the Ena/VASP family. *EMBO J.* 16:5433–5444. http://dx.doi.org/10.1093/emboj/16.17.5433

Oskarsson, T., M.A. Essers, N. Dubois, S. Offner, C. Dubey, C. Roger, D. Metzger, P. Chambon, E. Hummler, P. Beard, and A. Trumpp. 2006. Skin epidermis lacking the c-Myc gene is resistant to Ras-driven tumorigenesis but can reacquire sensitivity upon additional loss of the p21Cip1 gene. *Genes Dev.* 20:2024–2029. http://dx.doi.org/10.1101/gad.381206

Poukkula, M., A. Cliffe, R. Changede, and P. Rørth. 2011. Cell behaviors regulated by guidance cues in collective migration of border cells. *J. Cell Biol.* 192:513–524. http://dx.doi.org/10.1083/jcb.201010003

Pula, G., and M. Krause. 2008. Role of Ena/VASP proteins in homeostasis and disease. *Handbook Exp. Pharmacol.* 186:39–65. http://dx.doi.org/10.1007/978-3-540-72843-6_3

Prasad, M., and D.J. Montell. 2007. Cellular and molecular mechanisms of border cell migration analyzed using time-lapse live-cell imaging. *Dev. Cell*. 12:997–1005. http://dx.doi.org/10.1016/j.devcel.2007.03.021

Prasad, M., A.C. Jang, M. Starz-Gaiano, M. Melani, and D.J. Montell. 2007. A protocol for culturing *Drosophila melanogaster* stage 9 egg chambers for live imaging. *Nat. Protoc.* 2:2467–2473. http://dx.doi.org/10.1038/nprot.2007.363

Quinn, C.C., D.S. Pfeil, and W.G. Wadsworth. 2008. CED-10/Rac1 mediates axon guidance by regulating the asymmetric distribution of MIG-10/lamellipodin. *Curr. Biol.* 18:808–813. http://dx.doi.org/10.1016/j.cub.2008.04.050

Rørth, P. 2012. Fellow travellers: emergent properties of collective cell migration. *EMBO Rep.* 13:984–991. http://dx.doi.org/10.1038/embor.2012.149

Stavoe, A.K., J.C. Nelson, L.A. Martínez-Velázquez, M. Klein, A.D. Samuel, and D.A. Colón-Ramos. 2012. Synaptic vesicle clustering requires a distinct MIG-10/Lamellipodin isoform and ABI-1 downstream from Netrin. *Genes Dev.* 26:2206–2221. http://dx.doi.org/10.1101/gad.193409.112

Steffen, A., K. Rottner, J. Ehinger, M. Innocenti, G. Scita, J. Wehland, and T.E. Stradal. 2004. Sra-1 and Nap1 link Rac to actin assembly driving lamellipodia formation. *EMBO J.* 23:749–759. http://dx.doi.org/10.1038/sj.emboj.7600084

Stradal, T., K.D. Courtney, K. Rottner, P. Hahne, J.V. Small, and A.M. Pendergast. 2001. The Abl interactor proteins localize to sites of actin polymerization at the tips of lamellipodia and filopodia. *Curr. Biol.* 11:891–895. http://dx.doi.org/10.1016/S0960-9822(01)00239-1

Suetsugu, S., D. Yamazaki, S. Kurisu, and T. Takenawa. 2003. Differential roles of WAVE1 and WAVE2 in dorsal and peripheral ruffle formation for fibroblast cell migration. *Dev. Cell*. 5:595–609. http://dx.doi.org/10.1016/S1534-5807(03)00297-1

Suraneni, P., B. Rubinstein, J.R. Unruh, M. Durnin, D. Hanein, and R. Li. 2012. The Arp2/3 complex is required for lamellipodia extension and directional fibroblast cell migration. *J. Cell Biol.* 197:239–251. http://dx.doi.org/10.1083/jcb.201112113

Sviderskaya, E.V., W.F. Wakeling, and D.C. Bennett. 1995. A cloned, immortal line of murine melanoblasts inducible to differentiate to melanocytes. *Development*. 121:1547–1557.

Theveneau, E., and R. Mayor. 2012. Neural crest delamination and migration: from epithelium-to-mesenchyme transition to collective cell migration. *Dev. Biol.* 366:34–54. http://dx.doi.org/10.1016/j.ydbio.2011.12.041

Theveneau, E., L. Marchant, S. Kuriyama, M. Gull, B. Moepps, M. Parsons, and R. Mayor. 2010. Collective chemotaxis requires contact-dependent cell polarity. *Dev. Cell*. 19:39–53. http://dx.doi.org/10.1016/j.devcel.2010.06.012

Todaro, G.J., and H. Green. 1963. Quantitative studies of the growth of mouse embryo cells in culture and their development into established lines. *J. Cell Biol.* 17:299–313. http://dx.doi.org/10.1083/jcb.17.2.299

Wehrle-Haller, B., M. Meller, and J.A. Weston. 2001. Analysis of melanocyte precursors in Nf1 mutants reveals that MGF/KIT signaling promotes directed cell migration independent of its function in cell survival. *Dev. Biol.* 232:471–483. http://dx.doi.org/10.1006/dbio.2001.0167

Wu, C., S.B. Asokan, M.E. Berginski, E.M. Haynes, N.E. Sharpless, J.D. Griffith, S.M. Gomez, and J.E. Bear. 2012. Arp2/3 is critical for lamellipodia and response to extracellular matrix cues but is dispensable for chemotaxis. *Cell*. 148:973–987. http://dx.doi.org/10.1016/j.cell.2011.12.034

Xu, Y., and C.C. Quinn. 2012. MIG-10 functions with ABI-1 to mediate the UNC-6 and SLT-1 axon guidance signaling pathways. *PLoS Genet.* 8:e1003054. http://dx.doi.org/10.1371/journal.pgen.1003054

Yan, C., N. Martinez-Quiles, S. Eden, T. Shibata, F. Takeshima, R. Shinkura, Y. Fujiwara, R. Bronson, S.B. Snapper, M.W. Kirschner, et al. 2003. WAVE2 deficiency reveals distinct roles in embryogenesis and Rac-mediated actin-based motility. *EMBO J.* 22:3602–3612. http://dx.doi.org/10.1093/emboj/cdg350